U.S. Department
of Transportation
**Federal Aviation
Administration**

Nitric Oxide Measurement Study:

Office of Environment
and Energy
Washington, D.C. 20591

Optical Calibration Volume I

Report Numbers:
FAA-EE-80-28
USAF ESL TR-80-12
NASA CR-159861
USN NAPC-PE-37C
EPA-460/3-80-013

MAY 1980
L.G. Dodge
M.B. Colket, III
M.F. Zabielski
J. Dusek
D.J. Seery

Technical Report Documentation Page

1. Report No.	2. Government Accession No.	3. Recipient's Catalog No.
FAA-EE-80-28		

4. Title and Subtitle	5. Report Date
Nitric Oxide Measurement Study: Optical Calibration - Volume I	October 18, 1979
	6. Performing Organization Code
7. Author(s) L. G. Dodge, M. B. Colket, III, M. F. Zabielski, J. Dusek, D. J. Seery	8. Performing Organization Report No. R79-994150-1
9. Performing Organization Name and Address United Technologies Research Center Silver Lane East Hartford, CT 06108	10. Work Unit No. (TRAIS)
	11. Contract or Grant No. DOT FA77WA-4081
	13. Type of Report and Period Covered
12. Sponsoring Agency Name and Address U.S. Department of Transportation Federal Aviation Administration Office of Environment and Energy Washington, DC 20591	14. Sponsoring Agency Code

15. Supplementary Notes Funding for this study was provided by an Interagency Committee. Contributing agencies and report nos. are: DOT-FAA (FAA-EE-80-28); USAF (ESL TR-80-12); NASA (CR-159861); USN (NAPC-PE-37C); and EPA (EPA-460/3-80-013).

16 Abstract

Calibration devices suitable for providing known amounts of nitic oxide (NO) at temperatures ranging from 300 K to 2000 K and pressures of 0.5 atm (50.7kPa) to 2.0 atm (203kPa) are described with their design considerations. Methods for confirming nitric oxide concentrations are given. The spectroscopic theory for the absorption of ultraviolet radiation in the $\gamma(0,0)$ band of nitric oxide is reviewed. Experimental values for oscillator strengths and broadening parameters for NO with various collision partners are provided. Experimental results confirming the adequacy of a computer spectral model and, hence, the calibration are presented along with the details of the model. Finally, the results of an empirical calibration of an infrared gas correlation spectrometer are given.

The Nitric Oxide Measurement Study is in three volumes:
Optical Calibration - Volume I;
Probe Methods - Volume II;
Comparison of Optical and Probe Methods - Volume III.

17. Key Words	18. Distribution Statement
Nitric oxide, ultraviolet spectroscopy, high temperature calibration, broadening parameters, oscillator strengths, spectroscopic model, infrared gas correlation spectrometer.	Document is available to public through the National Technical Information Service, Springfield, VA 22161

19. Security Classif. (of this report)	20. Security Classif. (of this page)	21. No. of Pages	22. Price
Unclassified	Unclassified	222	

ABSTRACT

Calibration devices suitable for providing known amounts of nitric oxide (NO) at temperatures ranging from 300 K to 2000 K and pressures of 0.5 atm (50.7kPa) to 2.0 atm (203kPa) are described with their design considerations. Methods for confirming nitric oxide concentrations are given. The spectroscopic theory for the absorption of ultraviolet radiation in the $\gamma(0,0)$ band of nitric oxide is reviewed. Experimental values for oscillator strengths and broadening parameters for NO with various collision partners are provided. Experimental results confirming the adequacy of a computer spectral model and, hence, the calibration are presented along with the details of the model. Finally, the results of an empirical calibration of an infrared gas correlation spectrometer are given.

ACKNOWLEDGMENTS

This contract was administered by the Federal Aviation Administration. Funding for this work was provided by an Interagency Committee representing the Federal Aviation Administration (FAA), Air Force, Navy, National Aeronautics and Space Administration (NASA), and the Environmental Protection Agency (EPA).

The assistance of Mr. D. Kocum, Mr. R. P. Smus, Mr. D. Santos, and Mr. R. L. Poitras during the experimental portions of this study is gratefully acknowledged. The authors also would like to acknowledge the contributions of the following UTRC staff: Dr. P. J. Marteney for his kinetics analysis during the calibration source design phase; Mr. L. Chiappetta, Jr. and Dr. R. N. Guile for aerodynamic analyses of the microprobes; Mr. M. D. Page and R. E. LeBarre for programming; Mr. R. Thornton and Mr. C. Ekstrom for electronic instrumentation and Mrs. Barbara Johnson for data reduction and report preparation. Our thanks are extended to A. Kondracki of the Standards Laboratory of Pratt and Whitney Aircraft for certifying gas mixtures used in this study.

In addition, we extend our thanks to Mr. J. Few and his colleagues at Arnold Research Organization for providing us with their spectral computer model and for their cooperation during their measurements made at UTRC. Finally, thanks are given to Dr. D. Gryvnak of Ford Aerospace for his infrared gas correlation measurements.

Nitric Oxide Measurement Study:
Task I
Optical Calibration

TABLE OF CONTENTS

LIST OF FIGURES

LIST OF FIGURES (Cont'd)

LIST OF TABLES

I. INTRODUCTION

Since Johnston (1971) and Crutzen (1970, 1972) independently suggested that the injection of nitric oxide (NO) into the upper atmosphere could significantly diminish the ozone (O_3) concentration, an accurate knowledge of the amount of NO emitted by jet aircraft has been a serious concern to those involved in environmental studies. This concern intensified when McGregor, Seiber, and Few (1972) reported that NO concentration measured by ultraviolet resonant spectroscopy were factors of 1.5 to 5.0 larger than those measured by extractive probe sampling with subsequent chemiluminescent analysis. These initial measurements were made on a YJ93-GE-3 engine as part of the Climatic Impact Assessment Program (CIAP) which was one of four studies (CIAP, NAS, COMASA, COVOS (see References)) commissioned to determine the possible environmental consequences of high altitude aircraft operation, especially supersonic aircraft. After those studies were initiated, economic factors strongly favored the production and operation of subsonic aircraft. Nevertheless, since the subsonic aircraft fleet is large and does operate as high as the lower stratosphere, interest in the causes of the discrepancies between the two NO measurement methods continued. Few, Bryson, McGregor, and Davis (1975, 1976, 1977) reported a second set of measurements on an experimental jet combustor (AVCO-Lycoming) where the spectroscopically determined NO concentrations were factors of 3.5 to 6.0 higher than those determined by the probe method. In this set of measurements, optical data were obtained not only across the exhaust plume but also in the sample line connecting the probe with the chemiluminescent analyzer. The sample line optical data seemed to agree with the chemiluminescent analyzer data; hence, it was suggested that the discrepancies were due to phenomena occurring in the probe. These results stimulated a third set of measurements involving ultraviolet spectroscopy (Few et al, 1976a, 1976b), infrared gas correlation spectroscopy (D. Gryvnak, 1976a, 1976b) and probe sampling on an Allison T-56 combustor. The measured ratios of the ultraviolet to the probe values typically ranged between 1.5 and 1.9 depending on the data reduction procedure. The ratios of the infrared to the probe values varied between 1.1 to 1.5 also depending on the method of data reduction. In addition to these engine and combustor data, evidence supportive of the accuracy of the ultraviolet spectroscopic method, i.e., calibration data and model predications, was presented by McGregor, Few, and Litton (1973); Davis, Few, McGregor and Glassman (1976); and Davis, McGregor, and Few (1976). Nevertheless, it was still not possible to make a judgment on the relative accuracy of the spectroscopic and probe methods. The most significant reasons for this were: the complexity of the spectroscopic theory and computer model required to infer concentration from optical transmission; the inadequate treatment of probe use; and the incomplete exhaust temperature and pressure data which are necessary for a valid comparison of the methods. Recently, Oliver et al (1977, 1978) as part of the High Altitude Pollution Program has ranked these discrepancies as a major and a continuing source of uncertainty in atmospheric model predictions.

The purpose of this investigation was to identify and determine the magnitude of

the systematic errors associated with both the optical and probe sampling techniques for measuring NO. To accomplish this, the study was divided into three parts. The first was devoted to calibrating the ultraviolet and infrared spectroscopic methods. This entailed developing procedures which could provide known concentrations of NO over a wide range of temperatures and pressures, and also reviewing and correcting the ultraviolet spectroscopic theory used in the engine and combustor measurements cited above. The second part of this study was focused on sample extraction, transfer, and analysis by chemiluminescent instrumentation. The sampling methods were used on three successively more complicated combustion systems starting with a flat flame burner and culminating with a jet combustor. The results are presented in TASK II Report: Probe Methods . In the third part of this study, optical measurements were made on the same three combustion systems operated at the same conditions used for the probe measurements. The results of the optical and probe measurements were compared and are given in TASK III Report: Comparison of Optical and Probe Methods.

This report, i.e, TASK I, covers the results of the first part of this study. As indicated above, the optical calibration entailed several steps which will be briefly described below.

The first was the selection and development of devices which would provide known concentrations of NO from room temperature to approximately 2000 K. Known concentrations at pressures from subatmosphere to two atmospheres were also required but not over the above temperature range. The selection of the devices was governed by the following criteria. NO decomposition through either hetero- or homogeneous processess was to be minimal ($\leq 10\%$) relative to the discrepancies cited above. Temperature and concentration distributions were to be known along the optical path and stable during the measurement. The optical path and the concentrations were to be such that unambiguous optical data would be obtained.

The second part of the calibration process started with the translation of a spectroscopic computer model developed and used at Arnold Research Organization (ARO) by the authors cited above (McGregor, Davis, Few. Glassman). This model was generously provided by J. D. Few and H. N. Glassman. After encountering serious deficiencies in that model (see Appendix B), a new model was developed which was used to process both resonant line and continuum source, ultravilet, spectroscopic data. In addition, broadening parameters and oscillator strengths were experimentally determined.

The third part of the calibration process was the actual verification of the new model over the temperature range given above using a hollow cathode resonant lamp. Measurements were also performed by ARO personnel with a capillary discharge lamp. These results are described in an internal report by Few, Lowry, McGregor and Keefer (1979). A review of that report is included in Section IV.

Finally, an empirical calibration of an infrared gas correlation spectrometer was performed. The results of that calibration are presented by D. Gryvnak of Ford Aerospace in Appendix A.

II. CALIBRATION DEVICES

A. Design Considerations

II.A.1 NO Decomposition, Equilibrium and Kinetic Considerations

The complexity of the problem of providing known concentrations of nitric oxide at elevated temperatures and given pressures may be demonstrated by the paradoxical predictions of equilibrium theory for the reaction

$$2NO \rightleftarrows N_2 + O_2 \qquad (1)$$

Assuming infinite time is available and an initial mixture of NO in nitrogen, equilibrium values of NO may be calculated using mass balance and the equilibrium constant $K_p^{eq} = p_{N_2} \times p_{O_2}/p^2_{NO} = 5.06 \times 10^{-2} \exp(+21{,}700/T)$ (determined from JANAF tables). In Figure 1, where ratios of equilibrium to initial values are plotted, it is shown that as temperature decreases from 2000K, the amount of decomposition becomes greater. Equilibrium data, in fact, predict that NO in N_2 mixtures successfully used in calibrating analytical instruments should not be useful. Clearly equilibrium information, by itself, is inadequate since kinetics play the dominant role. Indeed, the problem of decomposition is most severe at elevated temperatures.

Nevertheless, Figure 1 suggests that calibration procedures and apparatus must be selected carefully if problems caused by equilibrium conditions are to be avoided. Fortunately, the rate of destruction of NO is limited by chemical kinetics, which in turn is dependent on local temperature, pressure, and the presence of other reactive species and/or surfaces. In fact, at room temperature the homogeneous reaction rate is so slow that pure NO can be stored under pressure for indefinite periods with negligible conversion to N_2O, NO_2 and O_2. Alternatively, much NO can be lost in short periods of time in the presence of a catalyst or a reactive surface such as copper or even other gaseous species such as oxygen where NO may be lost via the reaction.

$$NO + NO + O_2 \rightarrow 2NO_2 \qquad (2)$$

Furthermore, it is clear that only through careful consideration of the rate of chemical kinetics (both homo- and heterogeneous) can wide variations of temperature and concentration conditions be provided for NO calibration. A literature review of both the homogeneous and heterogeneous reactions (e.g., Wise and Frech (1952), Yuan et al. (1959), McCullough (1975), Kaufman and Kelso (1955), Winter (1971), Shelef and Kummer (1969), and Fraser and Daniels (1958)), suggests three temperature regimes for the decomposition of NO at atmospheric pressure: (1) below 1000K, heterogeneous kinetics dominate, (2) above 1400K homogeneous reactions dominate, and (3) between 1000 and 1400K a transition region exists. The size, i.e., temperature window of the transition region for a given experiment depends, of course, on the reactivity and surface area of exposed walls, the concentration of NO, and the identity of any third body (diluent) if present.

EQUILIBRIUM VALUES OF NO AT VARIOUS INITIAL CONCENTRATIONS AND TEMPERATURES

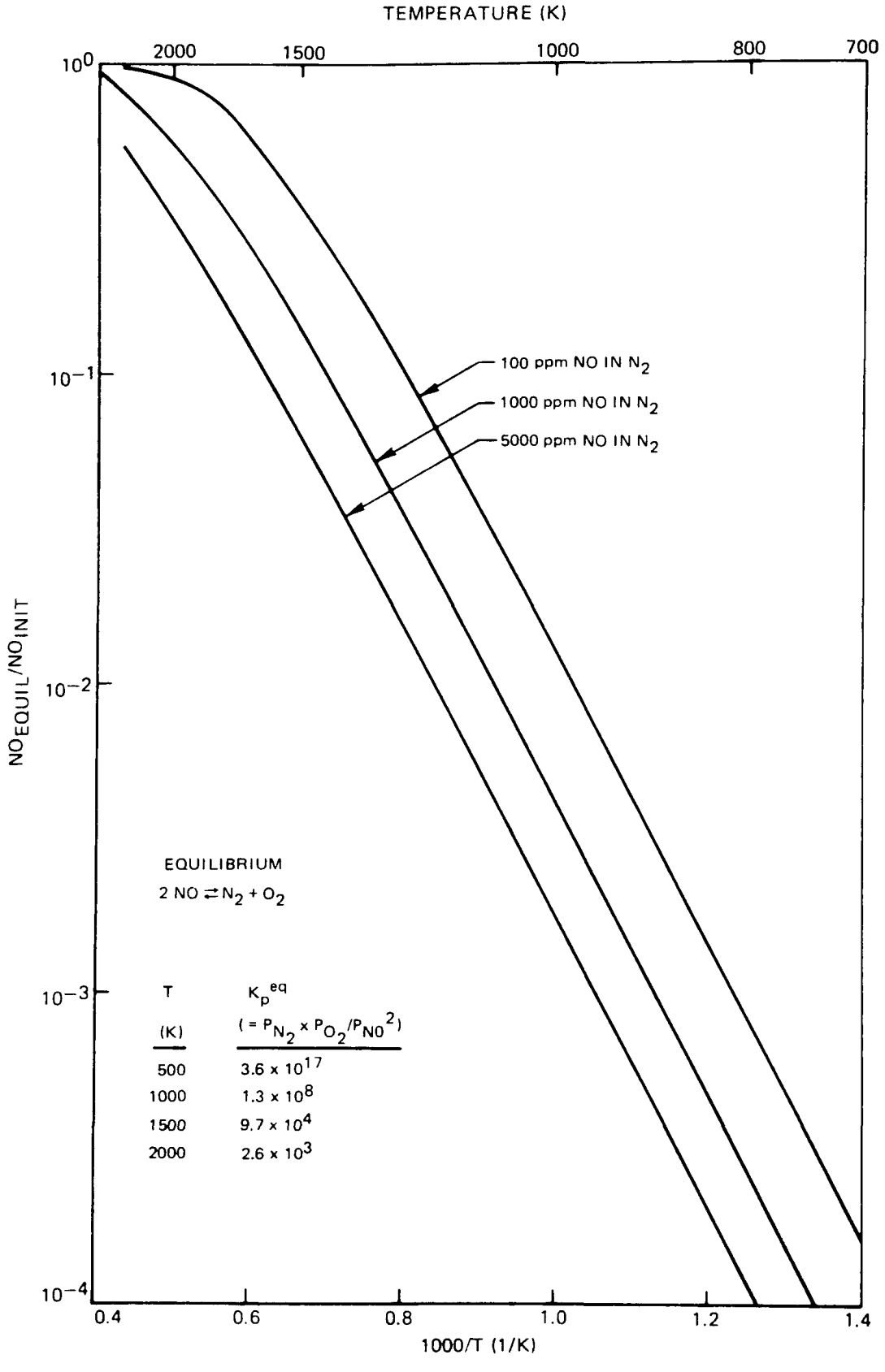

79-04-54-1

Of the several reports on the homogeneous (thermal) decomposition of NO, perhaps the most comprehensive is the recent work by McCullough (McCullough (1975), McCullough et al. (1977)). In this work, mixtures of NO in Ar (100 ppm - 5%) were passed through a packed ceramic flow reactor at temperatures between 1500 and 2100K at atmospheric pressure. In addition to presenting a detailed chain mechanism for the decomposition of NO, this work provides experimental data for NO thermal decomposition at the concentration levels of interest in the present study, i.e., 100-5000 ppm. Assuming that the effective dead volume in McCullough's reactor is 2.75 cm^3 (estimated from this published data and using McCullough's decomposition data), the time for 5% loss of the initial NO can be computed. The results are shown in Fig. 2 for several temperatures and concentration levels. A reduction of $\leq$ 10% during test time is considered to be the objective of the calibration system.

II.A.2. High Temperature Calibration

These data suggest that an apparatus capable of providing a calibrated source of nitric oxide up to 2000K must be able to heat the NO within several milliseconds and continually replace the decomposing NO with freshly heated NO. Otherwise, the stationary nitric oxide would undergo thermal decomposition during the period of calibration, which for the infrared (IR) system may be 5 to 10 minutes. Even for the ultraviolet (UV) measurements, a minute or so is required. Since a flow system appears necessary in order to continually replace the heated NO, a static heated cell would clearly be impractical. Several other calibration devices can immediately be eliminated for high temperature use. For example, NO can be premixed with an inert carrier and then heated by flowing it through a hot furnace or heat exchanger. This technique, unfortunately, is not feasible since the time required for heating of the gas will be on the order of seconds. Several methods of preheating the carrier gas and then injecting cold NO prior to the optical measurement were also considered, e.g., a plasma torch. However, in these cases characteristic times of diffusion, i.e., mixing, were found to be limiting. A shock tube has the advantage of elevating the gas temperature nearly instantaneously (microseconds) but insufficient time is available (only several hundred milliseconds) for calibration before a reflected or rarefraction wave changes the gas temperature and pressure.

The most viable alternative which would both heat the NO within several milliseconds and continually supply freshly heated NO is a lean $H_2/O_2/Ar$ flame seeded with NO. Argon rather than nitrogen is selected as the diluent since it would prevent additional formation of NO via the Zeldovich (1947) reactions.

This technique has, in fact, been used successfully at UTRC (Seery, et al (1979)) in 1/10th atmosphere flames using molecular beam sampling and by Kaskan and Hughes (1973). This previous work indicated that NO would not be lost in the reaction zone of a lean H_2/O_2 flame. To investigate the conservation of NO

TIME FOR 5% OF INITIAL NO CONCENTRATION TO DECOMPOSE

CURVES ESTIMATED FROM MCCULLOUGH (1975) DATA

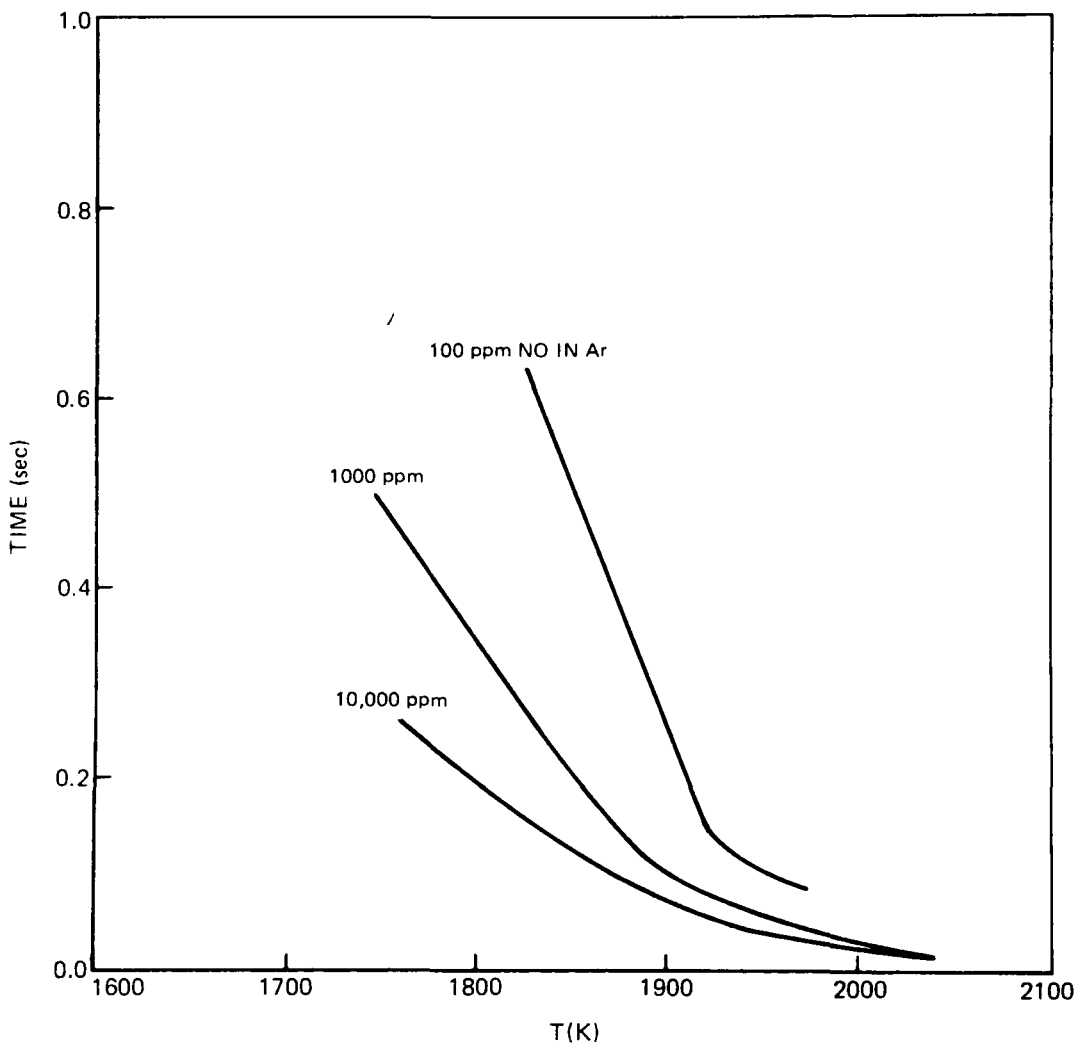

79-04-54-2

in a post flame region where optical measurements would be made, decomposition reactions and their rates were examined. These calculations predict that NO decomposition should be small immediately above a lean $H_2/O_2/Ar$ flame at atmospheric pressure. Due to the very wide flammability limits of a hydrogen/oxygen flame, it is expected that a flat flame burner could be used as a calibration device over the temperature range 1000-2000K. In addition, this device is particularly suitable since in Tasks II and III of this program, a flat flame burner using methane for fuel is needed.

II.A.3. Low Temperature Calibration

Given that a $H_2/O_2/Ar$ flat flame can be employed for NO calibration from 1000-2000K, the lower temperature range, 300-1000K with possibly some temperature overlap remains to be considered. A literature review indicates that heterogeneous reactions in the absence of high concentrations of reactive radicals dominate below 1100K. Unfortunately agreement on overall reaction rates and heterogeneous mechanisms is generally so poor that Shelef and Kummer (1969) remarked in their summary of catalytic reduction of NO,

> "It is truly so that catalysis is an art rather than a science and although those working in catalysis are impelled to offer plausible mechanisms for the catalytic process based on kinetic and other data, these attempts often fall very short of exact mechanistic descriptions of surface processes involved. We can indicate broadly those solid surfaces that will be of use in the catalytic reactions of NO but it will require many more experiments before we can hope to formulate the theory that will enable us to predict in advance the catalytic behavior of a given surface for these important reactions."

Conclusions generally differ, for example, with regard to the experimental reaction order for which values of zero (Yuan, et al (1959), and Fraser and Daniels (1958)), one (Winter (1971)), and two (Wise and Frech, (1952)) have been obtained. Here, the reaction order, n, is defined by the overall rate law.

$$\frac{d[NO]}{dt} = -k[NO]^n \qquad (3)$$

where k is the effective rate constant which in general depends on temperature, reaction order, surface material, and active or available surface sites. The reaction order, in turn, may depend on NO concentration, temperature, surface material, and available surface sites. For example, Wise and Frech (1952) show that, by doubling the surface to volume ratio, the overall decomposition rate doubles at 900K. [NO], in Eq. 3, represents the concentration of nitric oxide.

To reduce reaction rates, it is clear that total surface area should be minimized and that a relatively inactive surface should be used. Porous surfaces should be avoided due to relatively high total surface areas. One measurement (Fraser and Daniels, (1958) using nitrogen absorption and the Brunauer, Emmett and Teller (BET) theory (Brunauer, et al (1938)), indicates that the total surface area of typical metal oxides are approximately thirty times their macroscopic surface areas. Polished quartz or glazed ceramic, of course, would provide ideal surfaces due to their smooth surfaces and well-known low catalytic activity. Considerable experimental data are available on ceramic materials such as alumina (Al_2O_3) or zirconia (ZrO_2); however, the surfaces are not glazed and NO pressures are typically much higher (approximately 10-500 torr) than the pressures of interest in this work (1000 ppm of NO in one atmosphere of N_2 is equivalent to .76 torr). Extrapolation of this decomposition data to the desired conditions of the present work, i.e., low initial NO concentrations and small surface areas must be questionable, especially in light of the comments by Shelef and Kummer. In fact, direct application of their equations (Fraser and Daniels (1958), Mori, at al. (1973), and Yuan, et al. (1959)) to the proposed conditions would predict loss of essentially all NO within a matter of seconds.

Wise and Frech (1951) measured the decomposition of NO in a quartz tube at high NO concentrations. They assumed two competing mechanisms, homogeneous and heterogeneous, for which they determined a reaction order of two for both mechanisms. Their overall equation may be written

$$\frac{d[NO]}{dt} = -(k_1 + k_2)\,[NO]^2 \qquad (4)$$

where

$$k_1 = 1.4 \times 10^4 \exp(-10770/T)\ cm^3\text{-}mole^{-1}\text{-}sec^{-1}$$

$$k_2 = 3.1 \times 10^{15} \exp(-41270/T)\ cm^3\text{-}mole^{-1}\text{-}sec^{-1}$$

and where [NO] represents the NO concentration in moles/cc. k_1 and k_2 are the hetero- and homogeneous rate constants, respectively, for a quartz vessel having a surface to volume ratio of 0.49 cm^{-1}. These equations suggest that it takes approximately one day at 1200 K and 5½ years at 800K to decompose 5% of an initial NO concentration of 1000 ppm. However, one must be very hesitant in accepting these conclusions at face value. For example, Wise and Frech performed their experiments at the equivalent of 250,000 to 750,000 ppm NO in one atm (101 kPa of N_2), two and one-half orders of magnitude higher than the concentrations of interest in this work. In addition, these authors do not report sufficient information on their experimental technique or sufficient experimental data to have confidence in their results (see Appendix C). Finally, no other experimental results on NO decomposition over quartz were found in the literature to confirm or contradict these results.

If Wise and Frech's conclusions are accepted, then a static quartz cell could be used up to 1100 K only, of course, if extreme care is taken so as to avoid exposure to any other materials within the heated cell and no gaseous impurities such as oxygen are present. Since the previously published report is in question, a simple alternative might be to construct a heated quartz cell and flow mixtures of NO in a carrier through the cell. Although this approach was considered, it was decided that uncertainties in temperature profiles (radial and axial) and difficulties in probing together make this approach undesirable.

Several other systems were considered where the carrier gas is preheated and then the NO injected in a mixing zone just upstream of the optical measurement. All of these designs, however, were subject to limitations by characteristic diffusional rates and, therefore, could not be recommended. An alternative system was conceived in which the nitric oxide and carrier gas is premixed and then heated prior to the optical measurement up to the temperatures of interest. The gas is heated using a quartz bed heat exchanger. Quartz is used to minimize catalytic activity. This concept appeared to have several advantages. First, uniform mixing of NO with the carrier would not be a problem. Second, a design could be selected to be compatible with the flat flame burner and, consequently, much of their support facilities would be identical and could be used for either configuration. Furthermore, the flowing gas would be easily accessible to probe measurements of concentration, and temperature. This calibration device, entitled the flowing gas heater (FGH), seemed to be most practical for the lower temperature range (300-1000 K). Details of design and operating characteristics are described in a following section.

At room temperature, a static cell should also be used. With this device, concentration and temperature profiles are well-defined and a variety of experiments can be performed including broadening measurements using several different gases, and comparison of results from certified gas mixtures and from mixtures made on site. This device is described in Section III.A.1.

In summary, the approach for calibration of the optical measurement for nitric oxide includes the use of three devices: 1) a static cell at room temperature, 2) a flowing gas heater for the temperature range 300-1000 K, and 3) a flat flame burner with a $H_2/O_2/Ar$ flame useful in the temperature range 1000-2000 K. Items two and three were constructed with similar geometry so that either could be installed in a central facility which allows for optical, thermocouple, and probe access. This facility is provided with a gas handling system.

B. Description of Devices and Performance

II.B.1. Central Gas Facility

The central facility includes a gas-handling system and a water-cooled shroud to contain the gas flow. The former consists of necessary plumbing that blends various mixtures of gases for feeding both the flat flames and the flowing gas heater. Separate blending facilities were constructed for the main and buffer gas flows. The stainless steel shroud has mounts for thermocouple and gas sampling probes and provides for optical access.

A diagram of the gas handling system is depicted in Fig. 3. The gases used in these experiments were argon (Ar), nitrogen (N_2), oxygen (O_2), methane (CH_4), hydrogen (H_2), carbon dioxide (CO_2), nitric oxide (NO), and two mixtures of nitric oxide and argon. The mixtures were approximately 10 percent NO, 90 percent Ar, and 25 percent NO, 75 percent Ar. For each mix ratio, several bottles were purchased and, for each bottle, the vendor (Scientific Gas Co.) specified the ratio and certified the percentages to within $\pm$ 2 percent of their stated values. The concentrations were verified to within approximately 3 percent, using both mass spectrometric (MS) and chemiluminescent analysis (CA). In the latter case, since NO concentrations of 10 percent and 25 percent cannot be easily measured using a standard CA, the mix ratios were verified by diluting the gas using the gas-handling system and comparing results using the same analysis techniques with gravimetrically-prepared mixtures of NO in Ar (Scott) and with mixtures prepared from pure NO and Ar.

Flow rates of gases were controlled by using orifices, metering valves, and 0-150 psig pressure gauges. The gauges are 8½" diameter gauges from Wallace and Tiernan and are accurate to within $\pm$ 0.15 psi. The orifices were all operated at critical flow and ranged in diameter from 0.0015" to .050". The combination of orifices, pressure gauges, and metering valves allowed the accurate control of flows ranging from 8×10^{-4} to 3.5 grams/sec of N_2. The stability of the flow system was enhanced by using two stage regulators upstream of the metering valves. Although pressures and temperatures were continuously monitored, only occasional adjustment of the metering valves was required.

Orifices less than .025" size were all jeweled orifices (Swiss Jewel Co. and Brockton Jewel Co.), mounted in brass and aluminum discs and the discs were mounted in 1/2-in. stainless steel fittings. Larger orifices were machined and placed in fittings. Flow calibrations were made using a 3-liter wet test meter (CGA/Precision Scientific) for flows less than 0.3 grams/sec (N_2). A calibrated volume was used for larger flow rates and for hazardous gases. Typical calibration curves are shown in Fig. 4. Although most of the calibrations were performed using nitrogen, several measurements were made using each of the other gases in

SCHEMATIC OF GAS HANDLING SYSTEM

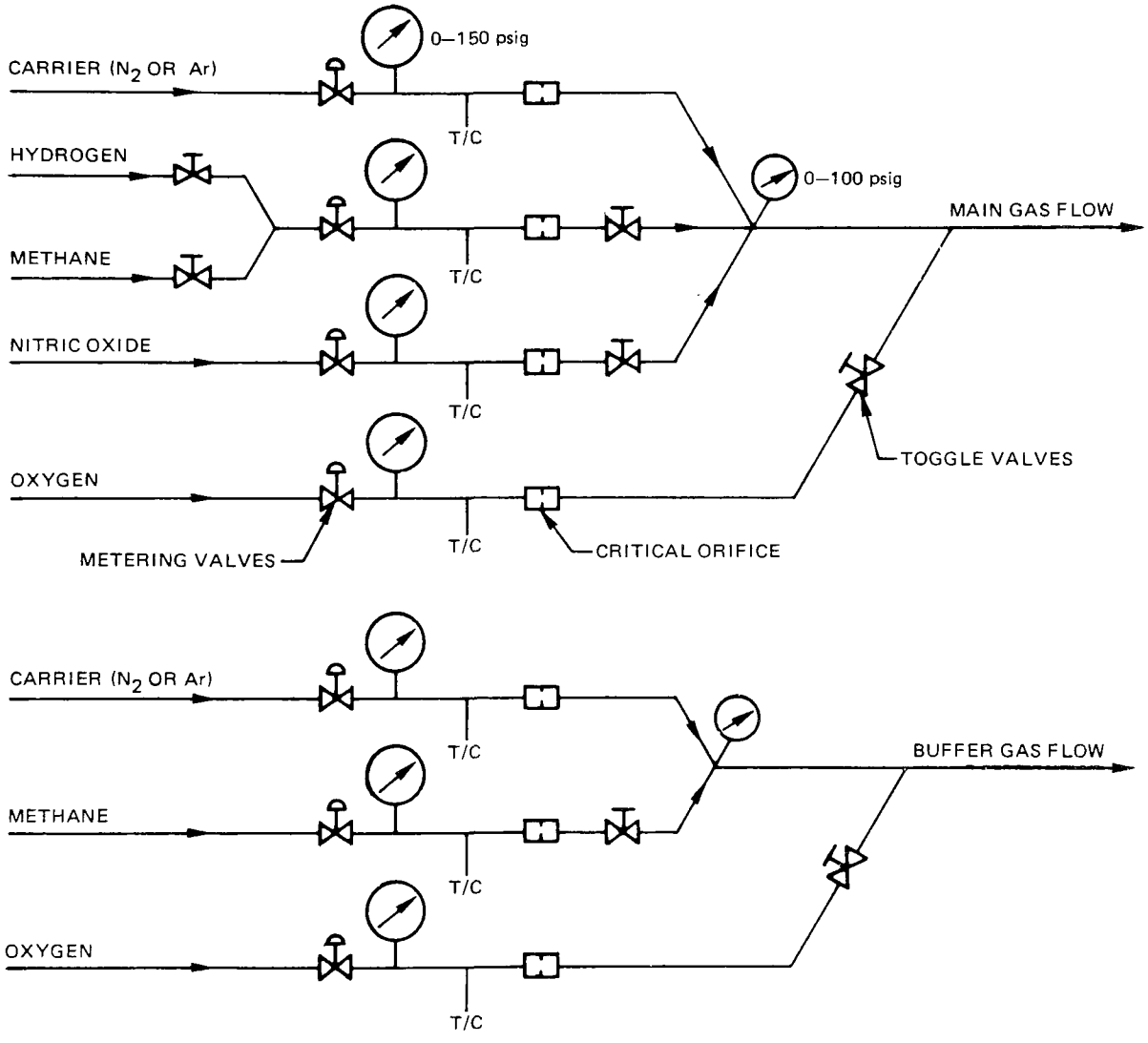

79–04–54–18

TYPICAL CALIBRATION CURVES FOR CRITICAL ORIFICES

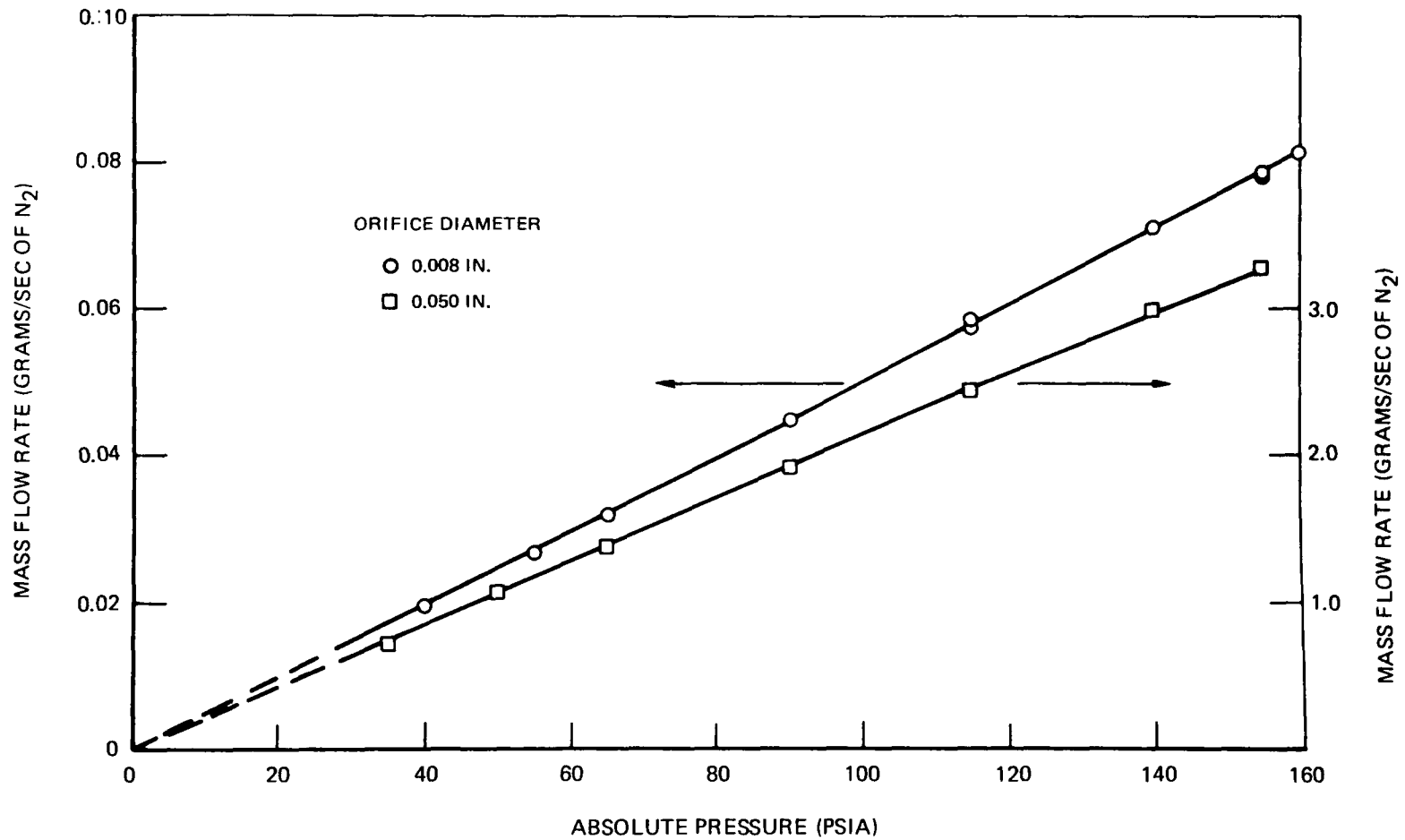

79-04-54-16

FIG. 4

these experiments. Correction factors between N_2 and other gases for a given orifice were within 3 percent of those predicted by the equation (derived from Shapiro, 1953),

$$\frac{\dot{m}_x}{\dot{m}_{N_2}} = \sqrt{\frac{\gamma_x MW_x}{\gamma_{N_2} MW_{N_2}}} \frac{\left(\frac{2}{\gamma_x + 1}\right)^{\frac{\gamma_x + 1}{2(\gamma_x - 1)}}}{\left(\frac{2}{\gamma_{N_2} + 1}\right)^{\frac{\gamma_{N_2} + 1}{2(\gamma_{N_2} - 1)}}} \tag{5}$$

where the subscripts x and N_2 refer to the two gases of interest; $\dot{m}$ is the mass flow rate; γ is the ratio of specific heats; and MW is the molecular weight. This equation was used when experimental data for a given gas and orifice were unavailable. Discharge coefficients were assumed to be similar.

Pressures downstream of the orifices were continually monitored to ensure that the orifices, indeed, were choked. Pressure ratios ($P_{upstream}/P_{downstream}$) were always 3.0 or greater while approximately 2.0 is required to maintain choked flow.

Calibration curves were repeatable to within 2% (usually to within less than 1%) for measurements using either the wet test meter or the calibrated volume. Measurements using both techniques for the same orifice were within 3%. The uncertainty associated with blending a mixture was primarily dependent on the uncertanties in the orifice calibrations (~3%), pressure readings (~0.5%) and the vendor certified and cross-checked Ar/NO mixture (<3%).

For the nitric oxide feed lines, the tubing, fittings, and valves were constructed of stainless steel to minimize corrosion of the lines and loss of NO to surface reactions.

Once the gases mixed, their transit time to the test rigs was less than one-half second. Oxygen was added just prior to the flat flame burner to minimize the total volume of a combustible gas mixture and to reduce the effect of the reaction.

$$NO + NO + O_2 \longrightarrow 2NO_2 \tag{2}$$

The shroud and other support facilities are depicted in Fig. 5. Its purpose is to contain the gas flow and to prevent outside air currents from disturbing the flow. It is essentially a rectangular box constructed of stainless steel, is open at both ends, and has internal dimensions of 22 cm long, 14 cm wide, and 26 cm high. Copper tubing is silver soldered on the outside for water cooling. A large (12.5 x 5 cm) port covered by quartz is installed on one side to view the quartz bed and flames. A top view is shown in Fig. 6.

STAINLESS STEEL SHROUD AND ASSEMBLY

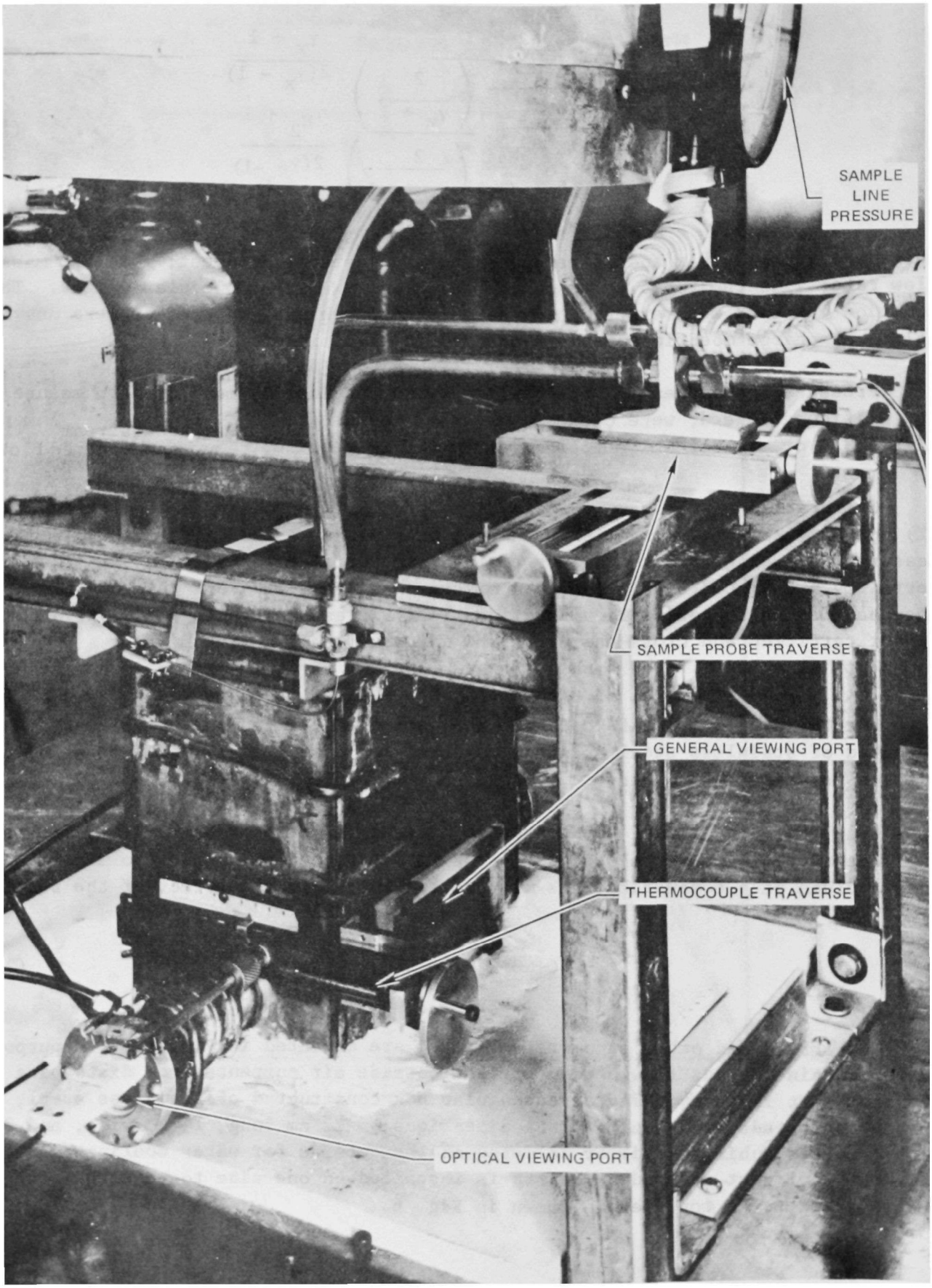

79-04-54-20

CALIBRATION ASSEMBLY (TOP VIEW)

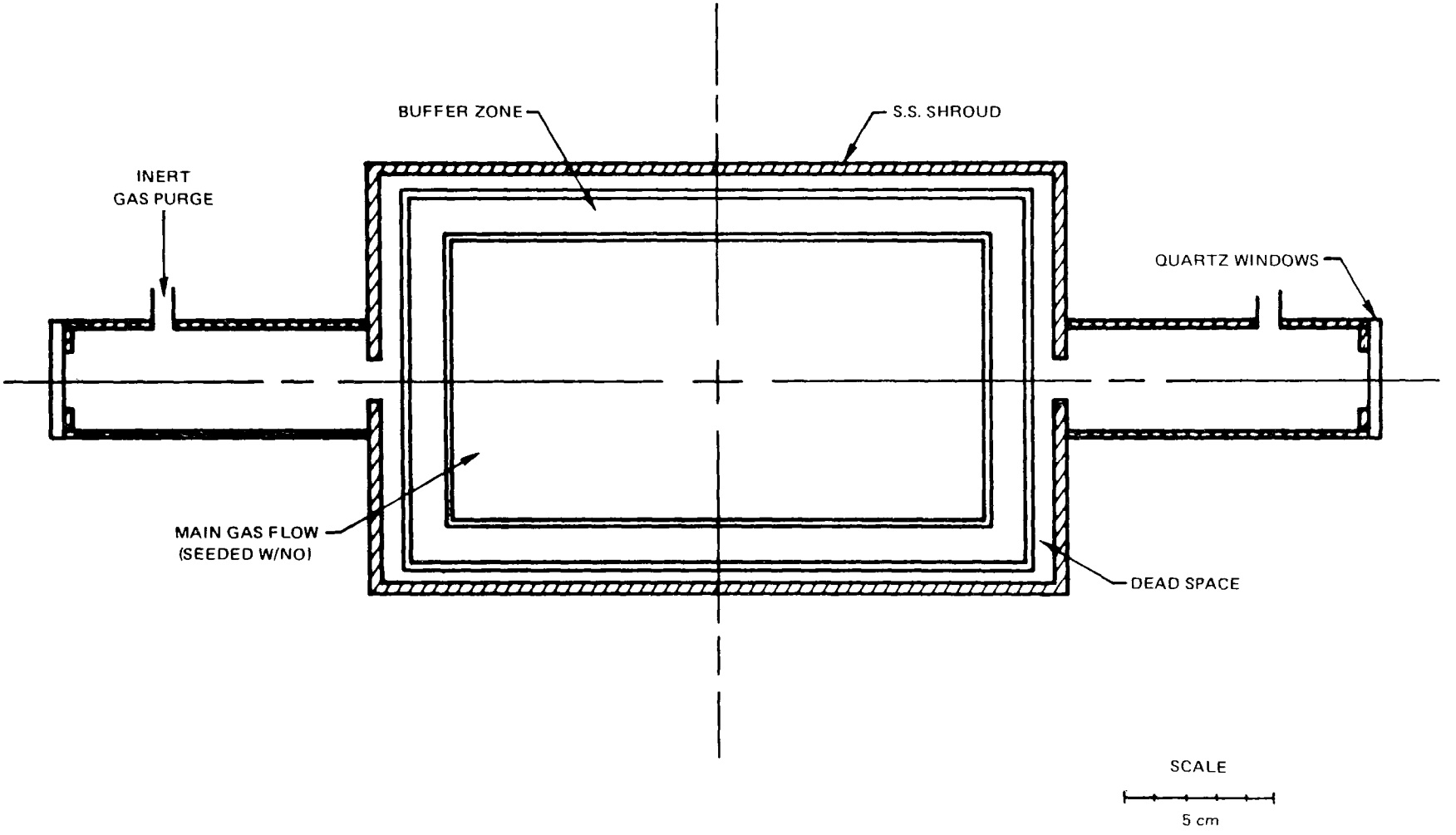

FIG. 6

79-04-54-3

Tubes (3.4 cm i.d.) are welded on opposite ends of the shroud to mount the optical windows and to protect the optical grade quartz or salts flats from the flame environment. Purge ports were attached to these tubes to flush out any residual nitric oxide and to prevent gaseous diffusion of NO into these colder regions. The gas exit from these tubes was 1.3 cm in diameter.

A thermocouple mount and traversing mechanism were attached to the outside wall of the shroud directly above one of the tubes. The thermocouple bead could be placed at the same height as the optical beam. The traversing mechanism allowed for free movement (x + y translation) throughout a given horizantal plane. Accuracy of positioning in both the x and y directions was approximately $\pm$ 1 mm relative and $\pm$ 4 mm absolute.

The probe mount and traversing mechanism for the gas sample probes were mounted outside the shroud. The probe mount could be adjusted vertically approximately 1 cm. This movement was sufficient to position the probe tip at the height of the optical axis. A traversing mechanism was purchased which allowed for x-y movement throughout a given vertical plane and with a relative accuracy of $\pm$ 0.1 mm. Probes were positioned with $\pm$ 3 mm absolute accuracy.

II.B.2. Flowing Gas Heater

A cut-away view of the flowing gas heater is shown in Fig. 7. As previously mentioned, the FGH was designed to be a low temperature calibration device with a quartz heat exchanger. Ceramic heaters (Electro-Applications), which are capable of reaching 1480 K, heat the quartz bed primarily by radiative heat transfer. The quartz bed is contained by a long, rectangular quartz tube (17.4 x 9.2 x 255 cm) open at the top and necked down to a 2.5 cm diameter tube at the bottom. Inside are cylindrical quartz tubes ranging in diameter from 5 to 15 mm o.d. with the largest at the bottom and with their sizes gradually decreasing to the top. From the bottom of the heat exchanger, two chromel-alumel thermocouples in alumina sleeves were inserted to monitor internal bed temperatures. Several other Cr-Al thermocouples were mounted on the outside of the quartz wall using a ceramic paste.

The buffer zone was between the quartz wall and the internal sides of the ceramic heaters. Its equivalent area was 84 cm^2. A buffer zone was designed to provide a region that would have similar gas temperature as the main flow yet be void of nitric oxide. The gas flowing through the buffer zone was always the same as the carrier gas in the main stream. The buffer region was sealed on the bottom by a horizontal quartz plate. Four vertical ceramic heaters were cemented in place and were surrounded by a stainless steel heat shield (reflector) and approximately 10 cm of insulation.

Due to its bulk and to material constraints the flowing gas heater could not be raised or lowered once in position. All profiles (temperature and concentration)

FLOWING GAS HEATER

FIG. 7

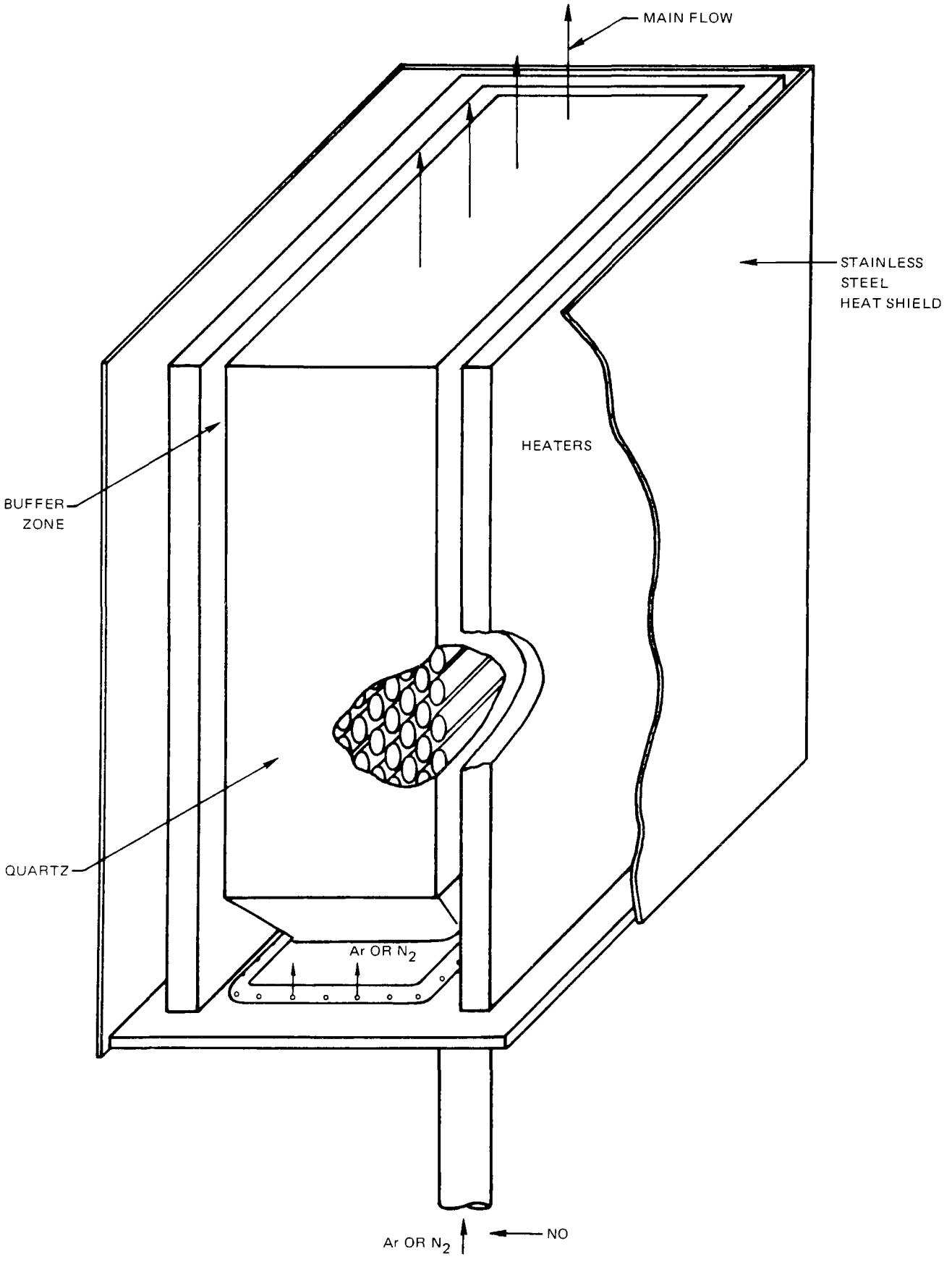

79-04-54-4

were obtained at a fixed location above the gas exit of the quartz heat exchanger. This distance (6.5 cm) was at the height of the optical axis.

II.B.2.a. Probe Measurements

Several probes of differing design were made in order to access various portions of the optical path above the flowing gas heater. These uncooled probes are described briefly in Table II-A; where applicable, figures that show profiles of NO concentrations also indicate the probe(s) used to obtain the data.

The extracted gas samples were analyzed either with a mass spectrometer or a chemiluminescence analyzer. Details of these analyses systems and the corresponding sampling trains are given at the end of this section.

II.B.2.b. Temperature Measurements

Gas temperatures above the flowing gas heater were measured using a chromel-alumel thermocouple. Wires were 0.010 inches in diameter while the diameter of the junction is approximately 0.015 inches. Lead wires pass through an alumina rod approximately 30 cm long mounted on the traversing mechanism at the side wall of the shroud. The thermocouple bead was supported 3.0 cm below the ceramic rod. Millivolt outputs were measured using a Data Precision Model 3500 DVM with a room temperature junction. Radiation corrections were calculated and found to be insignificant.

II.B.2.c. Experimental Results

Tests were made to investigate NO conservation at room temperature and NO profiles across the length of the optical axis. A typical profile is shown in Fig. 8. The loss of approximately 8 percent NO from the seed value, which is calculated from relative flow rates, is apparently due to a small percentage of intermixing of the buffer and main flows. For these profiles and for all data presented in this report, the window purge was on at a flow rate of .0109 moles/sec (.0043 moles/sec/cm^2) of nitrogen. For all calibration experiments, the molar flow rate of the carrier and buffer zones were held constant at .109 and .0164 moles/sec (6.8×10^{-4} and 1.95×10^{-4} moles/sec/cm^2) respectively. These values are independent of molecular weight of the carrier gas or exit temperature of the quartz bed. Under these conditions, the gas residence time within the quartz heat exchanger is approximately three seconds.

Elevated gas temperatures were achieved by applying power to the ceramic heaters. Periodically, the flow rate of the carrier would be increased to the desired flow conditions for comparison of the actual gas temperatures to the desired test conditions. Two hours were generally required to reach peak operating temperatures due to the large mass and, therefore, large thermal

TABLE II-A

Description of Sampling Probes Used Over
The Flowing Gas Heater and The Flat Flame Burner

Probe	Material	Internal Diameter (mm)	Water Cooled	Orifice Diameter inches	(microns)
A	Quartz	5	Yes	.025	(635)
B(1)	Quartz	5	Yes	.006	(150)
C	Quartz	4	No	.012	(305)
D	Quartz	5	No	.035	(890)
E(2)	Stainless Steel	1.2	No	.047	(1200)
F(3)	Stainless Steel	1.2	No	.047	(1200)

(1) Photographs in Figs. 12 and 13.

(2) Probe inserted horizontally into the sampling region through the optical ports which had their windows replaced with aluminum plates with a small hole for the probe.

(3) Probe inserted vertically down the center of the shroud but had a right angle bend at the height of the optical axis.

NORMALIZED CONCENTRATION PROFILES ALONG OPTICAL AXIS OVER FLOWING GAS HEATER

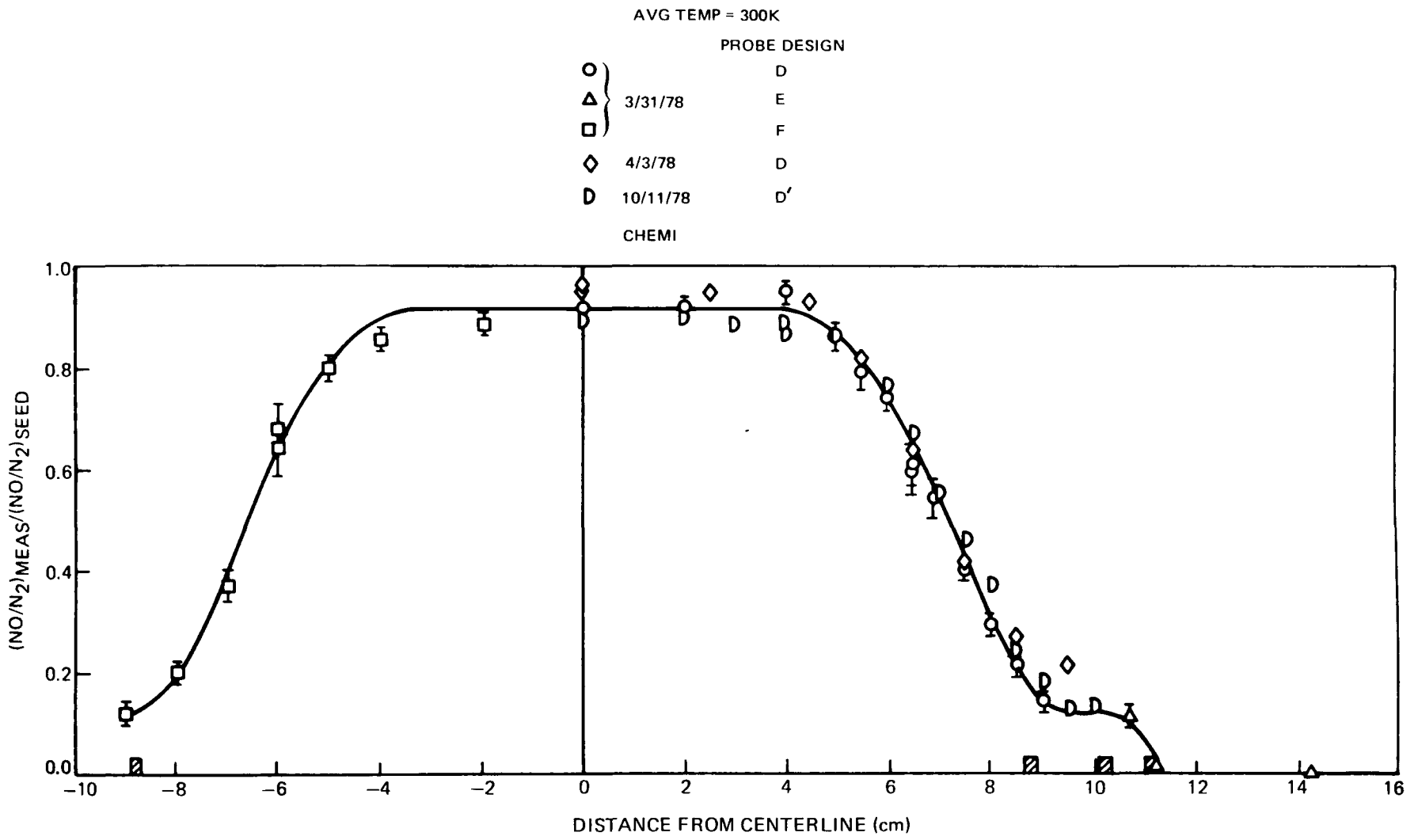

79-04-54-7

FIG. 8

inertia of the heaters and surrounding insulation. Peak gas temperatures that were achieved were slightly above 850 K. Higher temperatures were prevented primarily by local hot spots in the ceramic heaters which underwent thermal runaway before other portions of the heaters had reached their peak temperatures. The cause of the runaway was most likely due to nonuniformities (bends or connections) in the alloy heating wires.

Normalized concentration profiles of nitric oxide at low and at elevated temperatures are compared in Fig. 9. Two prominent features are apparent. First of all, nitric oxide is conserved within the quartz heat exchanger. Although these data were obtained using the chemiluminescence analysis system, similar results were obtained with the mass spectrometer and its sampling system. Secondly, the wings (8.5 to 11 cm from the centerline) contain noticeably less nitric oxide at elevated temperature than at room temperature. This difference appears to be real since profiles obtained at many different dates exhibit this phenomena. It is believed that the difference in the wings is due primarily to a reduction in the available time for mixing of the main and buffer flows at elevated temperatures. The reduction is due to a velocity increase that is proportional to temperature.

When heated to gas temperatures above 500 K, it was found that power input to the quartz bed was insufficient to maintain constant temperatures. This problem existed in spite of the fact that even at 1/2 power (2.4 kW), the ceramic heaters provided sufficient power, in theory, to elevate the gas from room temperature to 800 K. Consequently stable temperature profiles above 500 K could only be maintained for 10-15 minutes. Furthermore, "temperature waves" could be observed within the quartz bed itself, depending on the immediate history of heating and/or cooling cycles. Consequently, temperature profiles were obtained for each set of experiments performed at elevated temperatures. A typical profile is shown in Fig. 10.

II.B.3. Flat Flame Burner

A photograph of the flat flame burner is shown in Fig. 11. Its surface is sintered copper constructed by Thermit, Inc. Otherwise the burner is made of sheet copper with two separate zones: the main, NO-seeded zone and the buffer zone. Imbedded in the 5/8" thick sintered surface are copper coils for water cooling. The inside dimensions for the region of the main gas flow was 17.5 x 9.2 cm or 161 cm^2. The buffer zone is slightly smaller than for the flowing gas heater with an effective area of 76 cm^2. The flow systems feeding both the buffer and main zones at the bottom of the burner were described earlier.

II.B.3.a. Probe Measurements

For gas sampling over the flat flame, water cooled quartz probes were used. Similar designs were used both for the MS analysis and for detection via CA.

NO PROFILES OVER FLOWING GAS HEATER AT DIFFERENT TEMPERATURES

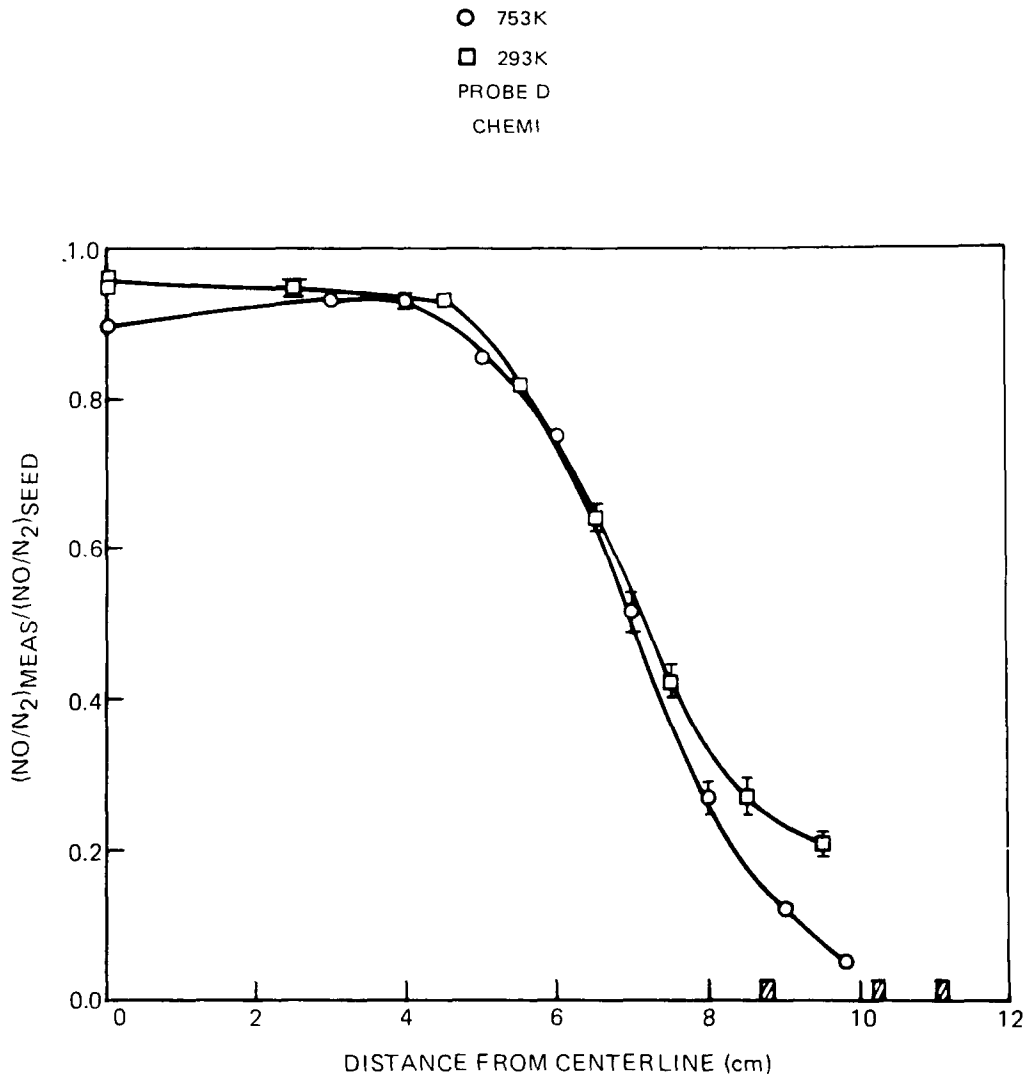

79-04-54-5

TYPICAL TEMPERATURE PROFILES OVER FLOWING GAS HEATER AT ELEVATED TEMPERATURE AND ALONG OPTICAL AXIS

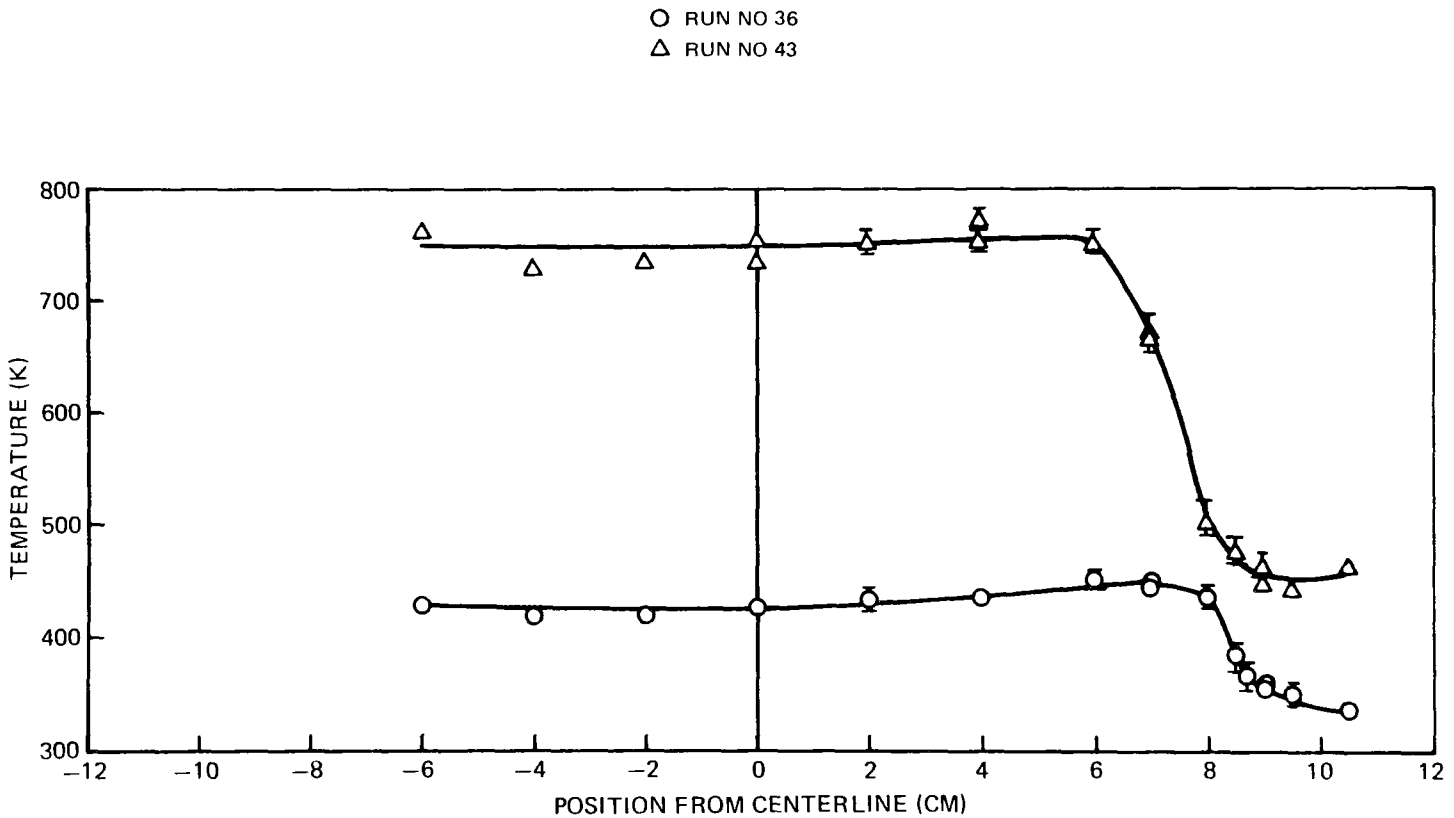

79-04-54-19

FIG. 10

FIG. 11

FLAT FLAME BURNER

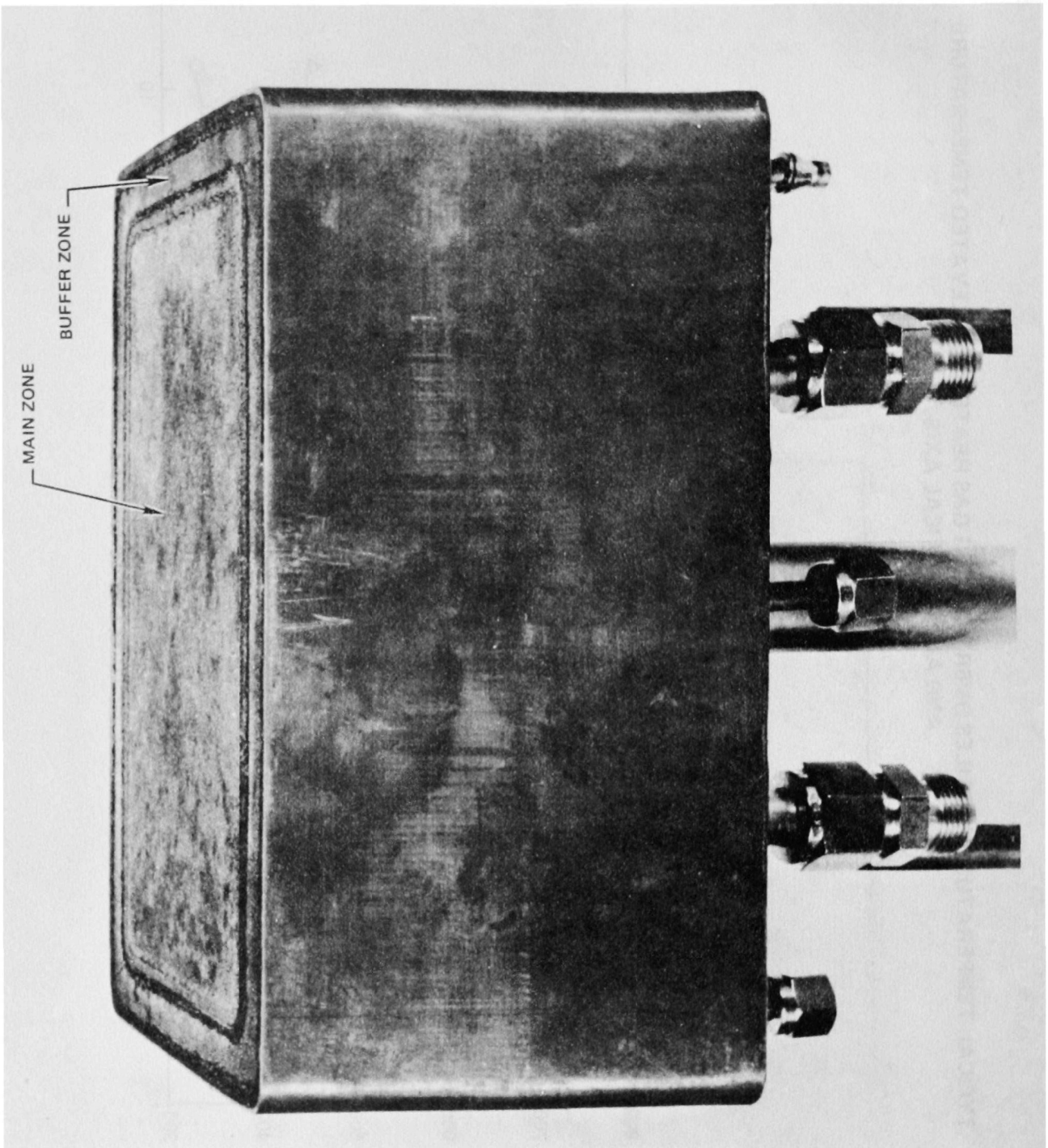

79-04-54-21

The primary difference was the orifice size. To feed the mass spectrometer, both low sampling pressure and very little sample volume are required. For mass spectrometric analysis, probe tips were small, approximately 150 microns in diameter (several tips were made due to occasional breakage and/or devitrification). A typical probe and tip (probe B in Table II-A) are shown in Figs. 12 and 13, respectively. (Although Figure 13 presents an illusion, the water-in tube is indeed placed to one side of the gas sample tube). The CA required much larger flow rates and a tip opening of 635 microns in diameter was used.

The large diameter of the water cooled probes prevented sampling of the flame closer than 1.5 cm from the wall of the shroud. To sample the gas in this region close to the wall an uncooled quartz probe (C) of 6 mm o.d. was constructed. This probe was only used on a low temperature flame so that catalytic activity on the hot quartz wall and divitrification of the quartz would both be minimized.

It should be pointed out that calculations using the UTRC probe deck were performed for the quartz probes. Although details of the program will be described in the Task II report, it is worthwhile mentioning an important prediction. For the microprobes, of approximately 150 microns in diameter, aerodynamic quenching of the gas sample is impossible, even at back pressures of $\sim$ 10 torr used in this work. The limiting factor is the growth of the boundary layer which prevents the flow from accelerating supersonically. [Although plans are being made to test this prediction on an atmospheric pressure flame, limited measurements made in a flame at 76 torr (Seery, unpublished, 1978) suggest that the mass flow rate varies with back pressure even down to a pressure ratio of 10]. This pressure ratio should be compared with the ratio of 2 to 1, which is normally believed to be sufficient to choke the flow. These conclusions may have practical implications to many flame researchers who have believed previously that their microprobes were aerodynamically quenched even with pressure ratios as low as 2 or 3 to 1.

II.B.3.b. Temperature Measurements

For the flat flame burner, temperatures were monitored with a buttwelded Ir/60% Ir-40% Rh thermocouple (.003" wires) coated with a mixture of 10% beryllium oxide and 90% yttrium oxide. Kent (1970), has found that a mixture of these metal oxides provides a good non-catalytic coating for thermocouples above 2000 K. The bead with its coating had a total diameter of .0035" $\pm$ .0005" and was approximately 1.2 cm away from either lead/support wire (.010" diameter).

Photographs of the thermocouple assembly and a close up of the yoke are shown in Figs. 14 and 15. Millivolt output was measured using a DVM and converted to temperatures uncorrected for radiation using published tables (Blackburn and Caldwell, 1962).

Estimates of radiation corrections were calculated by equating the heat transfer from the gas stream to total radiation

WATER–COOLED QUARTZ MICROPROBE

FIG. 12

79–04–54–22

TIP OF QUARTZ MICROPROBE

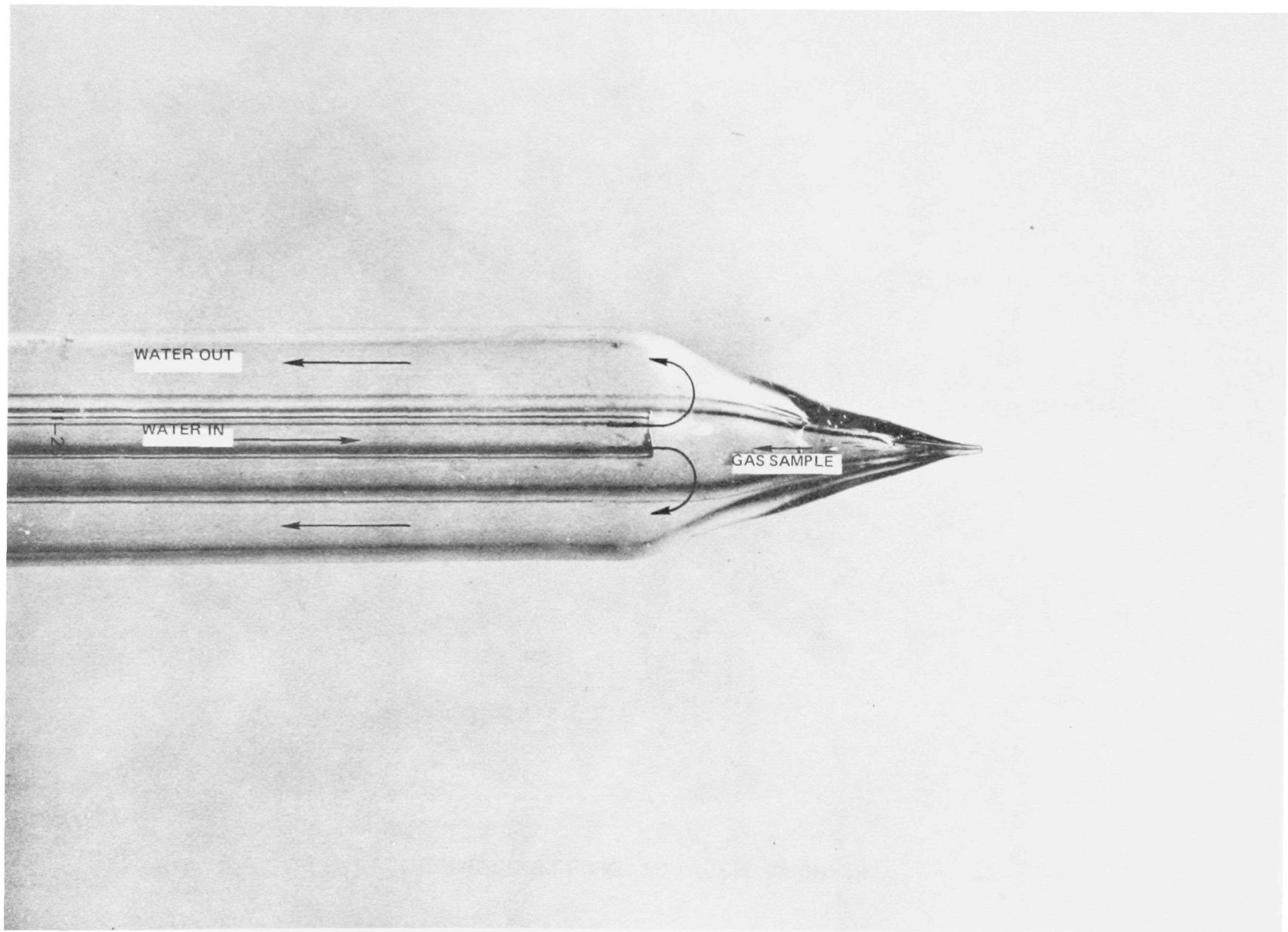

79-04-54-23

FIG. 13

THERMOCOUPLE AND TRAVERSE MECHANISM

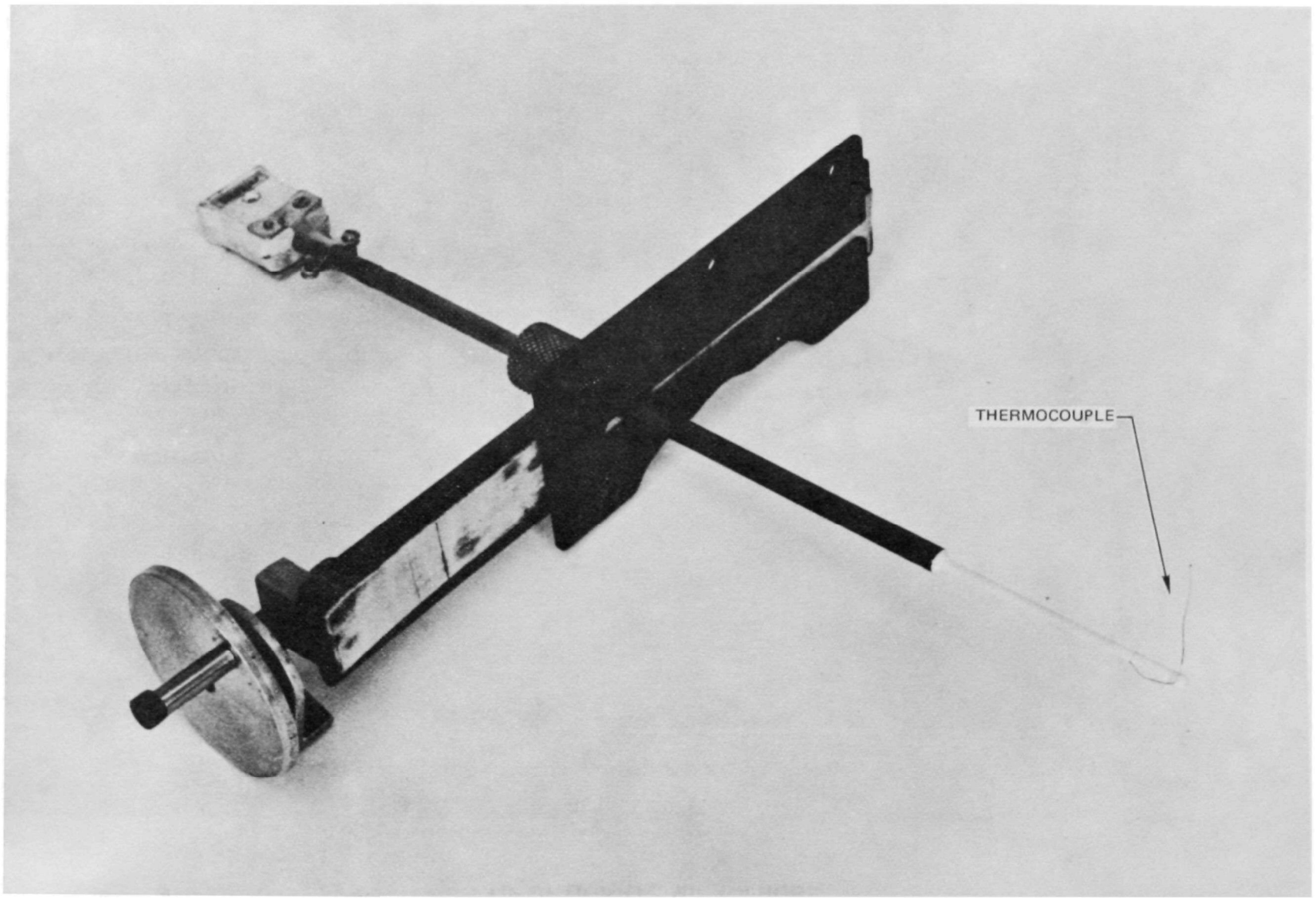

FIG. 14

Ir/Ir–40%Rh THERMOCOUPLE AND SUPPORT WIRE

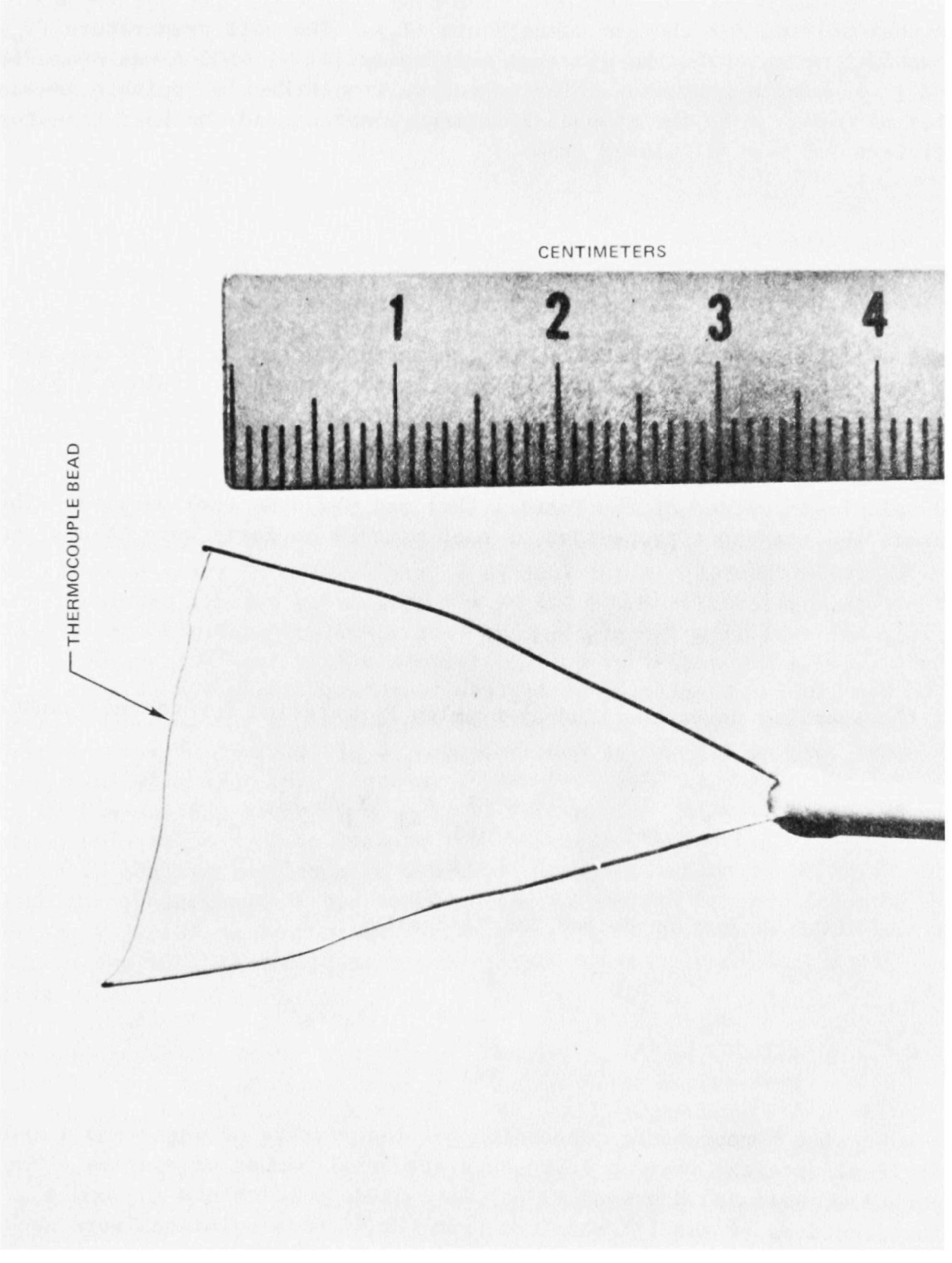

79–04–54–25

$$h\,(T_g - T_{T.C.}) = \varepsilon\,\sigma\,(T_{T.C.}^4 - T_w^4) \tag{6}$$

and then solving for the gas temperature (T_g). The wall temperature (T_w) was assumed to be zero and the spectral emissivity (ε) at 6500 A was measured to be $0.62 \pm .1$ using a pyrometer which agreed well with Kent's (private communication) value of 0.64. σ is the Stephan-Boltzmann constant and the heat transfer coefficient (h) was calculated from

$$Nu = \frac{hd}{\lambda} \tag{7}$$

where d is the bead diameter, λ, the thermal conductivity of the gas, and where the Nusselt Number (Nu) was determined from the expression (Hinze, 1959)

$$Nu = .42Pr^{.2} + .57Pr^{.33}Re^{0.5} \tag{8}$$

and calculated values of the Prandtl (Pr) and Reynolds (Re) numbers. Thermodynamic and transport properties of each mixture of gases were calculated using

$$C_{pm} = \sum_{i=1}^{n} X_i\, C_{pi} \tag{9}$$

for the specific heat, the Lindsay-Bromley Formulation for thermal conductivity.

$$\lambda_m = \sum_{i=1}^{n} \lambda_i/[1 + \sum_{\substack{j=1 \\ j\neq i}}^{n} A_{ij}\,(X_j/X_i)], \tag{10}$$

and the Wilke Estimation Method for viscosity

$$\mu_m = \sum_{i=1}^{n} \mu_i/[1 + \sum_{\substack{j=1 \\ j\neq 1}}^{n} \phi_{ij}\,(X_j/X_i)]. \tag{11}$$

The subscript m represents properties for the mixture of gases and i and j for individual species, where n represents the total number of species. The expressions reported in Reid and Sherwood (1966) were used to calculate A_{ij} and ϕ_{ij}. The molar fractions of gas (X) obtained from the flow calculations were used in the above determinations.

Properties of the individual gases were obtained from JANAF tables (C_p), Hanley (1973) (μ and λ for Ar) and Svehla (1962) (μ and λ for all other gases).

Due to the uncertainties in the emissivity calculation of transport properties of mixtures, and bead diameter, it is estimated that the calculation of ΔT ($= T_g - T_{T.C.}$) is accurate to within 20-25 percent.

II.B.3.c. Exhaust Analyzer

The Scott Model 119 Exhaust Analyzer used in this present investigation provides for the simultaneous analysis of CO, CO_2, NO or NO_2, O_2 and total hydrocarbons (THC). The analyzer is an integrated system, with flow controls for sample, zero and calibration gases conveniently located on the control panel. The incoming gas sample passes through a refrigeration condenser ($\sim$275K), to remove residual water vapor. As the sample passes from the condenser, it is filtered to remove particulate matter. The system is comprised of five different analytical instruments. Beckman Model 315B Non-Dispersive Infrared (NDIR) Analyzers are used to measure the CO and CO_2 concentrations in the gas sample. Concentration ranges available on the CO analyzer were from 0-200 ppm to 0-15% on several scales. Concentration ranges available on the CO_2 analyzer were 0-4% and 0-16%. The accuracy of the NDIR analyzers is nominally $\pm$ 1% of full scale. A Scott Model 125 Chemiluminescence Analyzer is used to measure the NO and NO_2 concentrations in the gas sample. Concentration ranges available with this instrument were from 0-1 ppm to 0-10,000 ppm on several scales, with a nominal $\pm$ 1% of full scale accuracy. The thermal converter used in the chemiluminescent analyzer was stainless steel, and was operated at a temperature of approximately 1000 K. A Scott Model 150 Paramagnetic Analyzer is used to measure the O_2 concentration in the gas sample. Concentration ranges available with this instrument were from 0-1% to 0-25% on several scales, with a nominal accuracy of $\pm$ 1% of full scale. A Scott Model 116 Total Hydrocarbon Analyzer is used to measure the hydrocarbon concentration in the gas sample. This analyzer utilizes an unheated flame ionization detection system to provide for measurement of hydrocarbons (as carbon) in concentration ranges from 0-1 ppm to 0-10%, with a nominal accuracy of $\pm$ 1% of full scale. Output signals from the various analyzers are displayed on chart recorders and a digital display.

For those flows in which Ar was the bulk or carrier gas, the chemiluminescent analyzer was calibrated with a gravimetrically prepared NO in Ar standard.. This instrument can also be calibrated with NO in N_2 standards; however a correction factor of 1.20 must be applied to the indicated reading. This difference in calibration is primarily due to viscous effects in the instrument sample capillary and varying quenching efficiencies between Ar and N_2. These effects have been recently analyzed (Dodge, et al. 1979).

Gas samples were transferred to the SCOTT analysis instruments through a four meter (13 feet) sampling line purchased from Technical Heaters, Inc. This sampling line was constructed with an electrical heater including thermocouple and had a TFE teflon core of .48 cm (3/16 in.) internal diameter. For measurements over the flowing gas heater, samples were extracted using an uncooled quartz probe (D) with an orifice diameter of 890 microns (0.035 in.). Typical sampling line pressures and temperatures were 500 torr ($\sim$2/3 atm) and 300 K respectively. Under these conditions, the calculated residence time in the sampling line is approximately 3/4 seconds (mass flow is assumed to be 50 percent of choked flow). For sampling from the flame, probe A was used with an orifice of 635 microns (0.025 in.). Using lower pressures and elevated temperatures of 380 torr (1/2 atm) and 110°C in the sampling line, respectively, the calculated residence time is similar, approximately one second. Although these times are well within the required residence times required by the Federal Register (1976), it should be pointed out that a gas sample typically undergoes much longer transit times as it passes through the remainder of the sampling train prior to analysis. For example, after the heated sample line, the sample travels through refrigerators, metal bellows pumps, filters, sample bypass, flow valves, all connecting lines and finally the chemilumenescence detector. Altogether these components increase the sample transit time (from probe tip to detector) by a factor of 15 to 20 from what is calculated in the sample line alone. The increase is due not only to an increase in total line length but also to a pressure rise (via the pumps) and the sample bypass, both of which act to drastically reduce the gas velocity. The overall effect of the sample bypass is favorable, since it provides a technique to continually flush the sample lines and to increase the flow rate and velocity through the first part of the sampling train. Ideally, the bypass should be located immediately upstream of the analytical instruments. These comments are particularly pertinent to analysis of gas samples containing high concentrations of nitric oxide due to the reaction

$$NO + NO + O_2 \rightarrow 2NO_2 \qquad (2)$$

which is second order in NO and third order in total pressure. In the case of the gas correlation measurements, NO concentrations of nearly 10,000 ppm were required. With an oxygen rich environment, measurements in this laboratory demonstrated that as much as 7 percent of the NO was converted to NO_2 via Reaction 2. Indeed, kinetic measurements performed in this sampling system produced an evaluation of the rate constant k_2 which was within 25 percent of the accepted value (Hampson and Garvin, 1978) and were consistent with the fractional conversion to NO_2 observed during the IR measurements. Therefore, any NO_2 (NO_x minus NO) was assumed to be formed in the sampling line (and are reported as NO) for these series of tests where nitric oxide concentrations were exceptionally high.

II.B.3.d Mass Spectral Analysis

The calibration was conducted with mixtures of NO in Ar for the lower temperatures (T < 900 K) and by seeding NO into lean $H_2/O_2/Ar$ flame at the higher temperatures (900 K < T < 2000 K). Standard instrumentation used for emission measurements is not suitable for determining H_2 and Ar. In addition, since the calibration of the chemiluminescent analyzer is dependent on the bulk or carrier gas, interpreting NO measurements in the region of the buffer and shroud is not straightforward.

Mass spectrometry is a method that with proper sampling technique can readily measure homonuclear molecules (H_2, O_2, N_2), inert gases, and nitric oxide. Moreover, proper sampling is more easily achieved since the mass spectrometer inlet and sampling line can be operated at pressures of 10 torr (1.3 kPa). This ensures a rapid reduction of the sampled gas temperature and pressure and minimizes sample transfer time. Since only small mass flows are required to make a measurement, the probe orifice can be made smaller than that used if a standard analytical instrument train is employed.

The instrument used in these measurements is a one-meter, time-of-flight mass spectrometer operated at a source pressure of 5×10^{-6} torr (6.6×10^{-4} Pa). Residual gas pressure is typically less than 1×10^{-8} torr (1.33×10^{-6} Pa). The master clock for the instrument is crystal controlled at 10 kHz; hence, 10^4 spectra per second are obtained. Through the use of ion sampling, the high frequency real-time output is converted into a lower frequency suitable for a data acquisition system. This acquisition system was a Northern Scientific NS 575 signal averager and NS 408 F tape interface with a Wang Mod 7 digital tape transport. For the data reported here, 8 to 32 low frequency spectra were averaged to improve the precision of the data. The mass spectrometer inlet was maintained at 8 torr (1.06 kPa). The sample line was heated 3/8" stainless steel which was held at a temperature no greater than 390 K. The terminal pressure of the sample line when capped was 1.5×10^{-2} torr (2.0 Pa). Sample transfer time was less than 0.5 sec for He.

The procedure used to reduce the data depended on the calibration device. For the flowing gas heater, the procedure consisted of measuring the intensities at masses 28 (N_2), 30 (NO), 36 (Ar), 40 (Ar). ^{36}Ar isotope was used as a monitor on instrument performance. The sensitivity factors for these constituents were empirically determined from gas standards and from mixes of gases prepared with the critical flow gas system. These sensitivity factors are used to take into account viscous effects in the mass spectrometer gas inlet, ion source pumping speed, ionization cross section, ion gate transmission, and ion detector mass

discrimination. The sensitivity factors used relative to Ar, i.e., $S_{Ar}^{Ar} = 1.0$, were $S_{N2}^{Ar} = 1.16$ and $S_{NO}^{Ar} = 1.03$. Mole fraction of NO was obtained from

$$X_{NO} = S_{NO}^{Ar} \cdot I(30)/\{S_{N_2}^{Ar} \cdot I(28) + S_{NO}^{Ar} \cdot I(30) + I(40)\} \tag{12}$$

For the flat flame burner, the procedure is made complicated by the difficulty in making an accurate H_2O measurement. The standard method employed in emission measurements is to dry the sample in a low temperature trap. Such a drying procedure is not required for these mass spectral measurements since the total molar flow rate of Ar is known. A further complication is introduced by the mixing of gas from the three zones of the apparatus. This latter problem can be treated by using the knowledge that the N_2 originates only from the window purge and the CO_2 comes only from the buffer zone flame.

The composition of the flow at any point can be described by

$$X_M + X_B + X_{N_2} = 1 \tag{13}$$

where X_M is the fraction from the main burner flow, X_B is the fraction from the buffer flow, and X_{N_2} is the fraction from the window purge. Using N_2 and CO_2 as tracers, the local intensity ratios of N_2 and CO_2 to Ar are

$$\frac{I(28)}{I(40)} = \frac{1}{S_{N_2}^{Ar}} \left\{ \frac{X_{N2}}{X_M M_{Ar} + X_B B_{Ar}} \right\} \tag{14}$$

and

$$\frac{I(44)}{I(40)} = \frac{1}{S_{CO_2}^{Ar}} \left\{ \frac{X_B B_{CO_2}}{X_M M_{Ar} + X_B B_{Ar}} \right\} \tag{15}$$

where M_{Ar} is the mole fraction of Ar in the main burner flow; B_{Ar} is the mole fraction in the buffer flow; I(44) is the CO_2 intensity; $S_{CO_2}^{Ar}$ is the CO_2 sensitivity; and B_{CO_2} is the mole fraction of CO_2 produced in the buffer flame. M_{Ar} and B_{Ar} are known from the calibrated flow system. B_{CO_2} is known from the equilibrium value of CO_2 for the buffer flame. Solving for X_{N_2} and X_B yields

$$X_{N2} = \left[\left(\frac{S_{CO_2}^{Ar} \, I(44)}{S_{N_2}^{Ar} \, I(28)} \right) \left(1 - \frac{B_{Ar}}{M_{Ar}} \right) \frac{1}{B_{CO_2}} + \frac{1}{M_{Ar}} \left(\frac{I(40)}{I(28)} \right) + 1 \right]^{-1} \tag{16}$$

$$X_B = X_{N_2} \left(\frac{S^{Ar}_{CO_2} \; I(44)}{S^{Ar}_{N_2} \; I(28)} \right) \frac{1}{B_{CO_2}} \tag{17}$$

The results of equations (16) and (17) can be inserted into equation (13) which then can be solved for X_M.

Given these expressions, the local water to argon expression can be calculated from

$$\frac{I(18)}{I(40)} = \frac{B_{H_2O} \; X_B + M_{H_2O} \; X_M}{B_{Ar} \; X_B + M_{Ar} \; X_M} \tag{18}$$

where B_{H_2O} and M_{H_2O} are known from the equilibrium value of H_2O for the buffer and main flames, respectively. The mole fraction at any point for a given ith molecule is

$$X_i = \frac{I(i)/I(40)}{T} \tag{19}$$

where

$$T = 1 + \frac{1}{I(40)} \left\{ S^{Ar}_{CO_2} . I(44) + S^{Ar}_{N_2} . \; I(28) + S^{Ar}_{NO} . \; I(30) + S^{Ar}_{O_2} . \; (32) + I(18) \right\} \tag{20}$$

All terms are measured values with the exception of the I(18)/I(40) ratio which is calculated. Also, for the buffer region and a small region on either side of it, corrections are made for the contributions of CO(30) isotope to the nitric oxide intensity and for the contributions of CO(28) from the flame and ion fragmentation of CO_2 to the nitrogen intensity.

II.B.3.e. Experimental Results

Initial tests of several flame conditions indicated a flow instability several centimeters above the burner surface. To dampen these flow fluctuations a three level tier of screens was constructed and hung from the side walls of the shroud. The lowest screen was 7 cm above the optical axis. Slots were cut at appropriate positions for movement of the probes along the optical axis. Although not mentioned previously, this set of screens was used in all measurements above the flat flame burner and flowing gas heater.

TABLE II-B

FLOW CONDITIONS FOR OPTICAL MEASUREMENTS
OVER FLAT FLAME BURNER

Uncorrected Thermocouple Temperature (K)	Mole Fraction			Equivalence Ratio	Distance of optical axis above burner (cm)	Total Molar flow rate (moles/sec)
	H_2	O_2	Ar			
950	0.073	0.102	0.825	0.36	2.0	0.128
1220	0.116	0.114	0.770	0.51	1.5	0.134
1400	0.169	0.116	0.715	0.73	1.5	0.145
1600	0.330	0.170	0.491	0.92	1.0	0.194

After selecting several flame conditions (listed in Table II-B), initial gas sampling was made with probe B (Table II-A) and analysis was made with the mass spectrometer. Typical profiles of nitric oxide along the optical axis are shown in Fig. 16. Flow conditions for the $H_2/O_2/Ar$ flames are given in Table II-B. The observed scatter is characteristic of a statistical analysis for the operating conditions of the mass spectrometer. This scatter could be reduced by additional averaging of spectra. It is apparent that nitric oxide is conserved through the flame front at least for the low temperature flames. Similar data demonstrates conservation at higher temperatures.

A typical thermocouple profile with radiation corrections is reproduced in Fig. 17. The profile shows near symmetry around the centerline. The slight temperature rise near the edges (around 8 cm from the center) is probably due to a separation by the sintered copper and the copper plate between the main and the buffer flows. Resultant gas velocities are higher which push the flame away from the burner and decrease the local heat loss to the burner.

At approximately 8.5 centimeters from the center of the burner, the temperature drops drastically. This fall-off seems surprising considering the existence of the buffer flame out to 10.2 centimeters and is caused by the strong nitrogen purge exiting from the window tubes. The effect of the purge at the selected flow rates is quite noticeable on both the temperature and NO profiles. Although this perturbation is undesirable, its presence does not affect the ability to make the optical measurements since probe measurements provide sufficient data to reduce results using multiple zones. Probe measurements indicated that lower flow rates were ineffective in flushing out cold NO from the optical arms. Additional experimental data on both the flowing gas heater and flat flame burner are presented in the following chapter.

NO HORIZONTAL PROFILES OVER FLAT FLAME BURNER

$H_2/O_2/Ar$

		THERMOCOUPLE TEMPERATURES (K)	NO SEED LEVELS (WET) ppm	
MASS SPEC	○	1220	1995	PROBE B
	△	950	2030	
	□	950	2030	
CHEMI	◹	950	2030	PROBE C

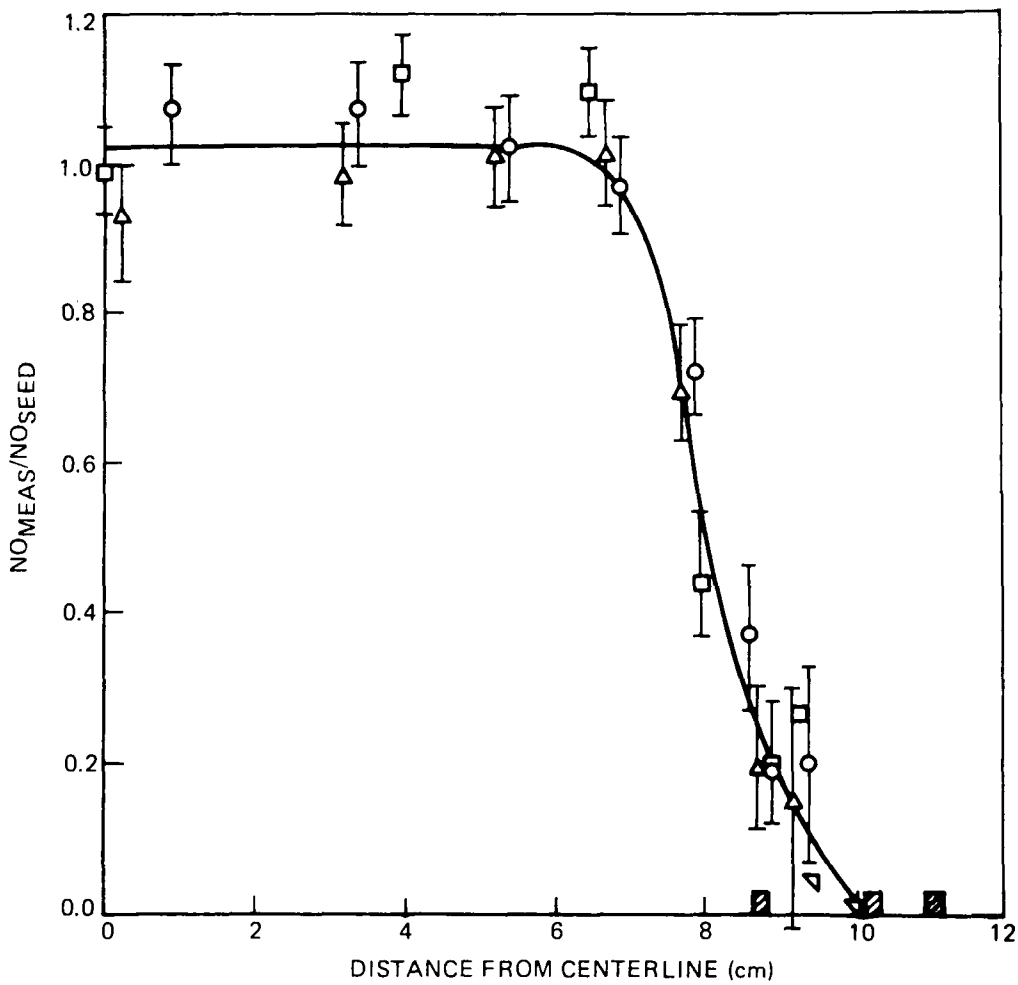

79-04-54-8

HORIZONTAL TEMPERATURE PROFILES OVER FLAT FLAME BURNER

$H_2/O_2/Ar$

UNCORRECTED TEMPERATURE = 1400K

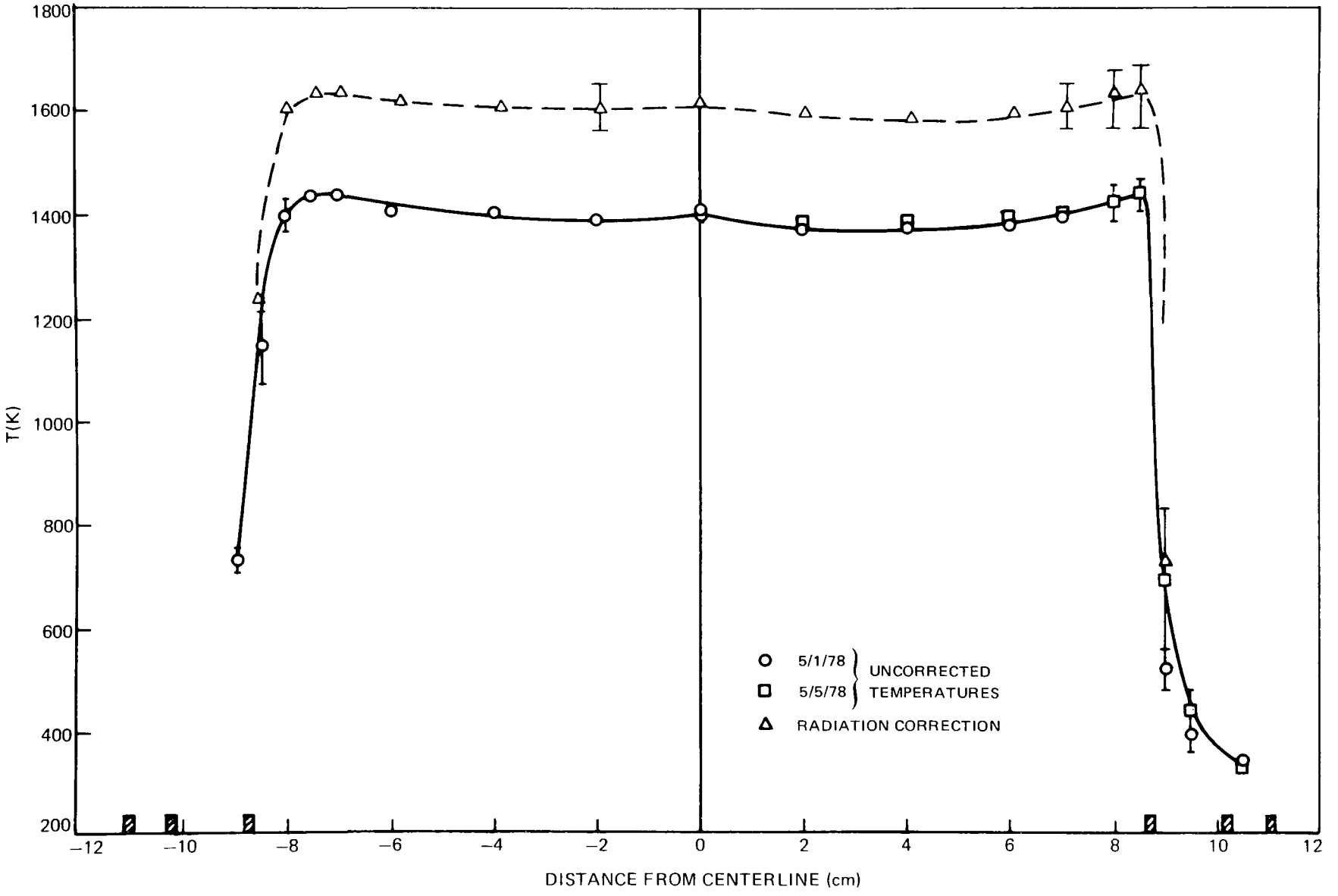

79-04-54-14

FIG. 17

III. ULTRAVIOLET ABSORPTION

A. Apparatus

III.A.1. Gas Mixing System for Static Cell Optical Measurement

The majority of static cell calibration data were obtained by mixing gases using the system shown in Fig. 18. The system was evacuated below 25 x 10^{-3} torr (3.3 Pa.) and then filled with a calibration gas to the desired pressure. If it was desired to raise the pressure of the diluent gas further without adding more NO, the valve to the static cell was closed, the system evacuated, and then filled with the diluent gas by slowly raising the regulator pressure until the final desired pressure was reached. The valve to the static cell was opened so that the pressure in the rest of the system dropped and then quickly recovered via the regulator to the desired final pressure and the valve was closed.

Pressures were monitored with three gauges. A thermocouple gauge was used to verify the vacuum integrity of the system. A Barocell Datametrics capacitance manometer (model 570 A sensor and model 1173 readout) with full scale ranges from 0 - 0.1 torr (0 - 13.3 Pa.) to 0 - 1000 torr (0 - 133.3 kPa.) was used along with a Wallace and Tiernan 0 - 150 psia (0 - 1.034 MPa.) pressure gauge to determine pressures.

For the broadening and oscillator strength study, cylinders of NO diluted to about 2000 ppm in N_2, Ar, CO_2, and CH_4 were obtained from Scott Environmental Technology along with the highest purity diluent gases commercially available. The specifications for these gases are given in Table III-A. The NO/ N_2 concentration was independently verified; but, the other cylinders were accepted as labeled based on gravimetric blending by the vendor and vendor analysis.

III.A.2. Light Sources

Two distinct types of light sources were used. One lamp was a low pressure hollow cathode lamp which produced discrete emission lines in the γ (0,0), γ (1,1), and γ (2,2) bands of NO. The other lamp was a high pressure Xe lamp which produced continuum radiation in the region of interest.

III.A.2.a. Narrow-Line Lamp

The hollow cathode lamp was operated with a dc discharge in flowing air and produced emission lines from principally NO molecules, N_2 molecules and ions, and Ar atoms. The spectral lines used in this study were in the γ (0,0), γ (1,1), and γ (2,2) bands ($A^2\Sigma^+ - X^2\pi$) of NO.

ARRANGEMENT OF APPARATUS FOR OPTICAL MEASUREMENTS

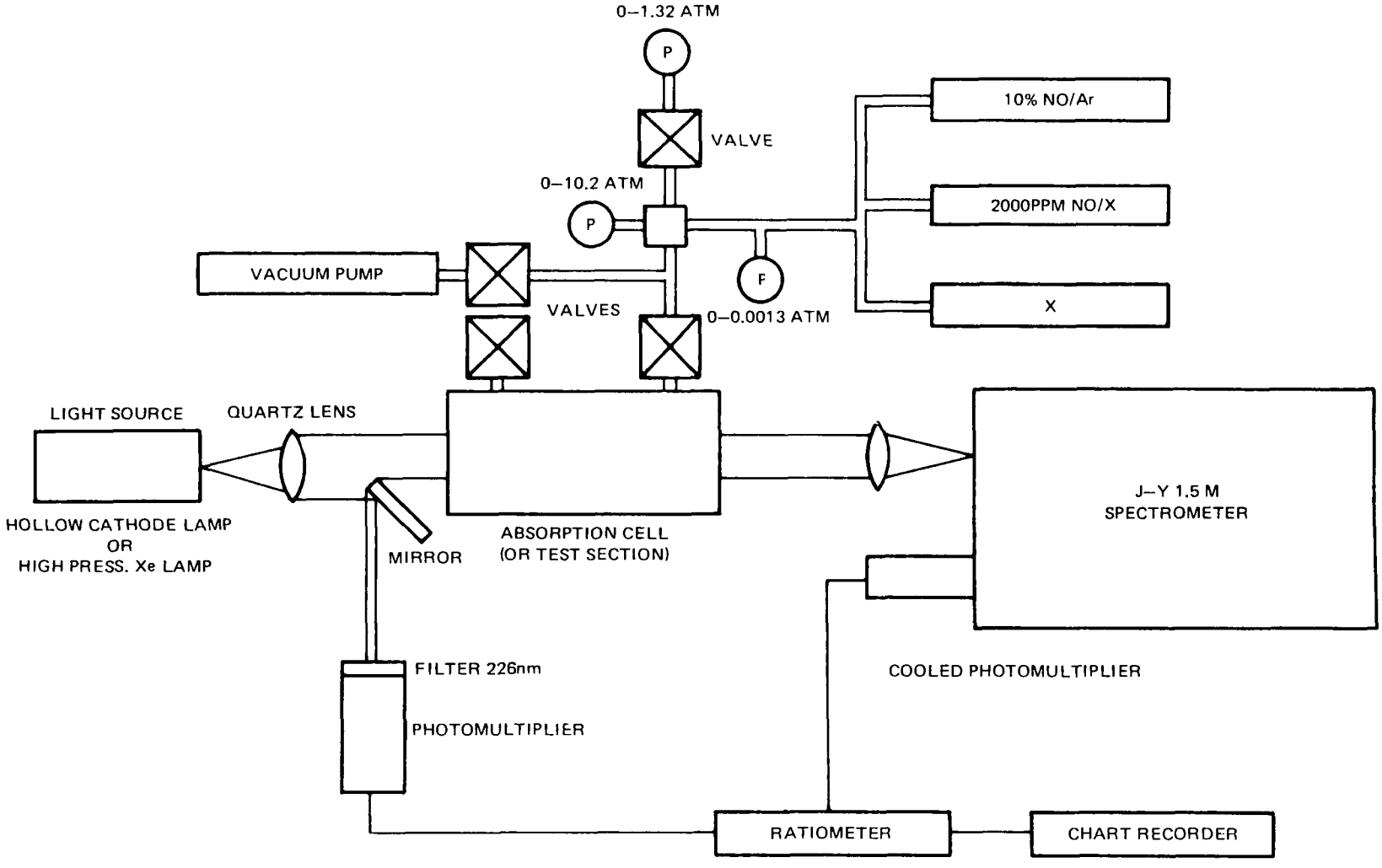

FIG. 18

TABLE III-A

Specifications for Gases

Gas Blends of NO

Diluent Gas	Concentration of NO (ppm)	Vendor Analysis Accuracy
Ar	1980	±1%
CO_2	2030	±1%
CH_4	2000	±1%
N_2	2080	±2%

Pure Gases

Diluent Gas	Purity	Maximum O_2
N_2	99.998%	5 ppm
CO_2	99.99%	5 ppm
CO	99.99%	5 ppm
CH_4	99.99%	5 ppm
Ar	99.999%	2 ppm

The design of the water-cooled hollow cathode lamp is shown in Fig. 19 and followed that of Meinel (1975), who generously provided a drawing of his lamp. The operating characteristics are similar to those described by Meinel (1975). The lamp was operated on flowing air at a pressure of 2 torr and a current of 25 mA (0.1% electronic stability over eight hours). The ballast resistors were combined for a net resistance of 1.67K and the operating voltage was about 600V. At constant pressure, the intensity stability of the lamp was excellent (<.5% drift) over several hours.

The possible steps leading to the production of NO in an excited state from air in the discharge are discussed by Meinel (1975). It is clear from the emission spectra that the excited NO molecules are not in rotational or vibrational thermal equilibrium. The population distribution of the $^2\Sigma(v'=0)$ level is shown in Fig. 20, where the points represent resolved spectral lines. The lines drawn through the points were used as an input to the computer program to determine the strengths of unresolved lines, as explained in the description of the computer program.

There is a small amount of light in the NO γ (0,0) band which appears to be from some molecule(s) other than NO. The NO lines may be readily located, but there are some weaker spectral features between the lines which have not been identified, as shown in Fig. 21. These extra lines are not absorbed like the other NO lines as shown in Fig. 22. The effect that this "extra-light" has on the measured f-values is discussed in the section describing the oscillator strength measurements.

III.A.2.b Continuum Lamp

The lamp used to obtain a continuum output was a 1000 watt high pressure Xe arc lamp (Canrad-Hanovia 976C-0010) mounted in an Oriel housing and using an Oriel power supply. The lamp exhibited a moderate amount of intensity drift (3% over 10 min), and the lamp housing had to be vented to the outside because of the significant quantity of ozone produced.

III.A.2.c Spectrometer and Associated Electronics

A 1.5-m focal length J-Y spectrometer in a temperature controlled box with a 2400 g/mm holographic grating (110 x 110 mm), aperture of f/12, and Fastie curved slits was employed for all measurements. Typical slit function, full width at half maximum (FWHM), was observed to be .0018 nm with 7 μm slit settings for the 226 nm NO lines observed in the 2nd order of the grating. Most of the spectra were recorded with a Hamamatsu R166 solar blind (Cs-Te photocathode) photomultiplier tube cooled to -30°C in a Products for Research TE-177 thermoelectrically cooled housing. Some measurements were also made with an EMI 9659QB photomultiplier (extended S-20 photocathode) cooled to -78°C with dry ice.

WATER COOLED HOLLOW CATHODE LAMP

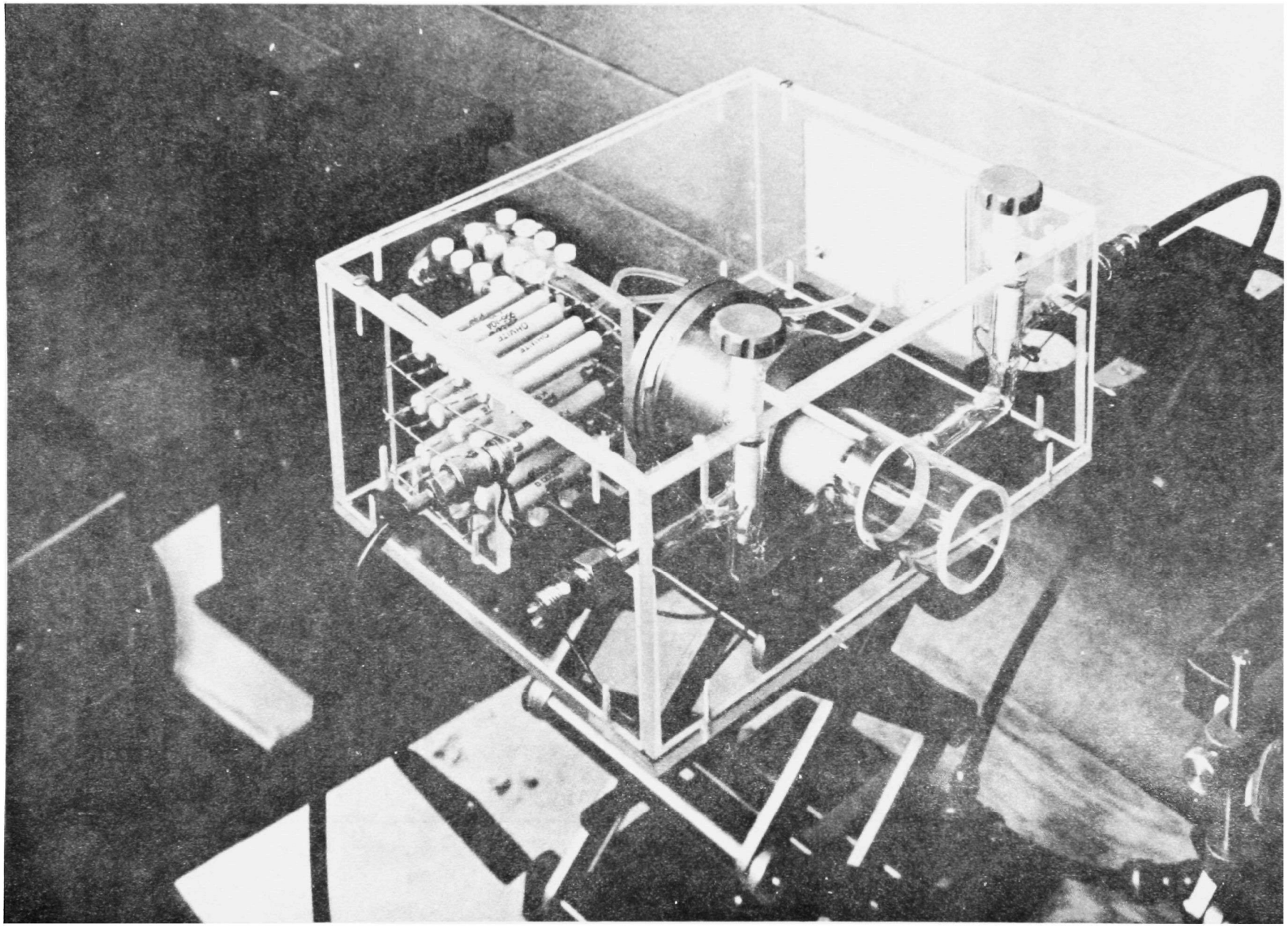

FIG. 19.

INTENSITY DISTRIBUTION IN NARROW–LINE LAMP

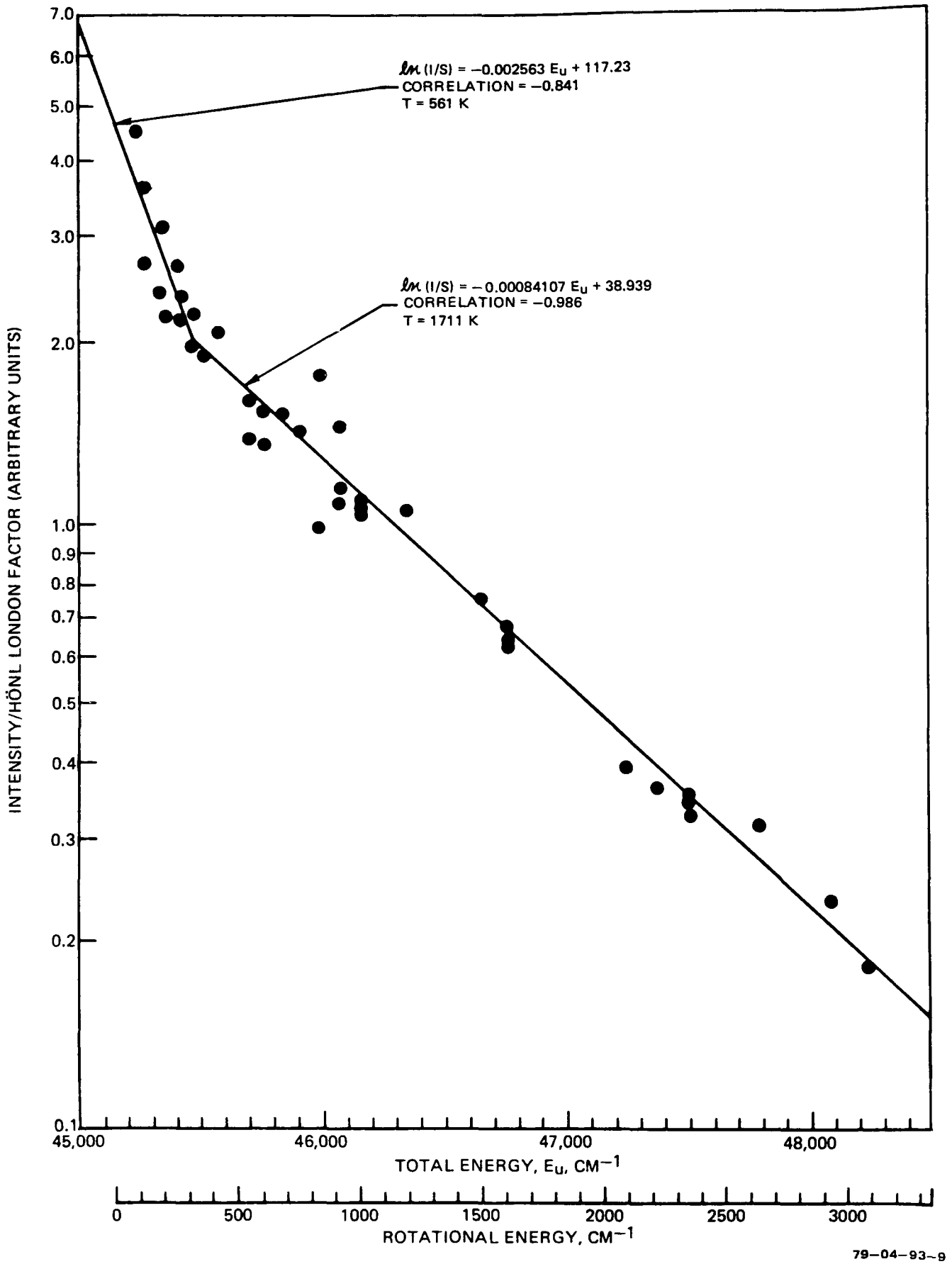

NARROW–LINE LAMP EMISSION

1. P_{11} (6.5) + P_{11} (11.5)
2. P_{11} (7.5) + P_{11}(10.5) + P_{22} (22.5) + Q_{12} (22.5)
3. P_{11} (8.5) + P_{11} (9.5)
4. Q_{22} (14.5) + R_{12} (14.5) + R_{22} (9.5) + P_{12} (31.5)
5. P_{22} (21.5) + Q_{12} (21.5)

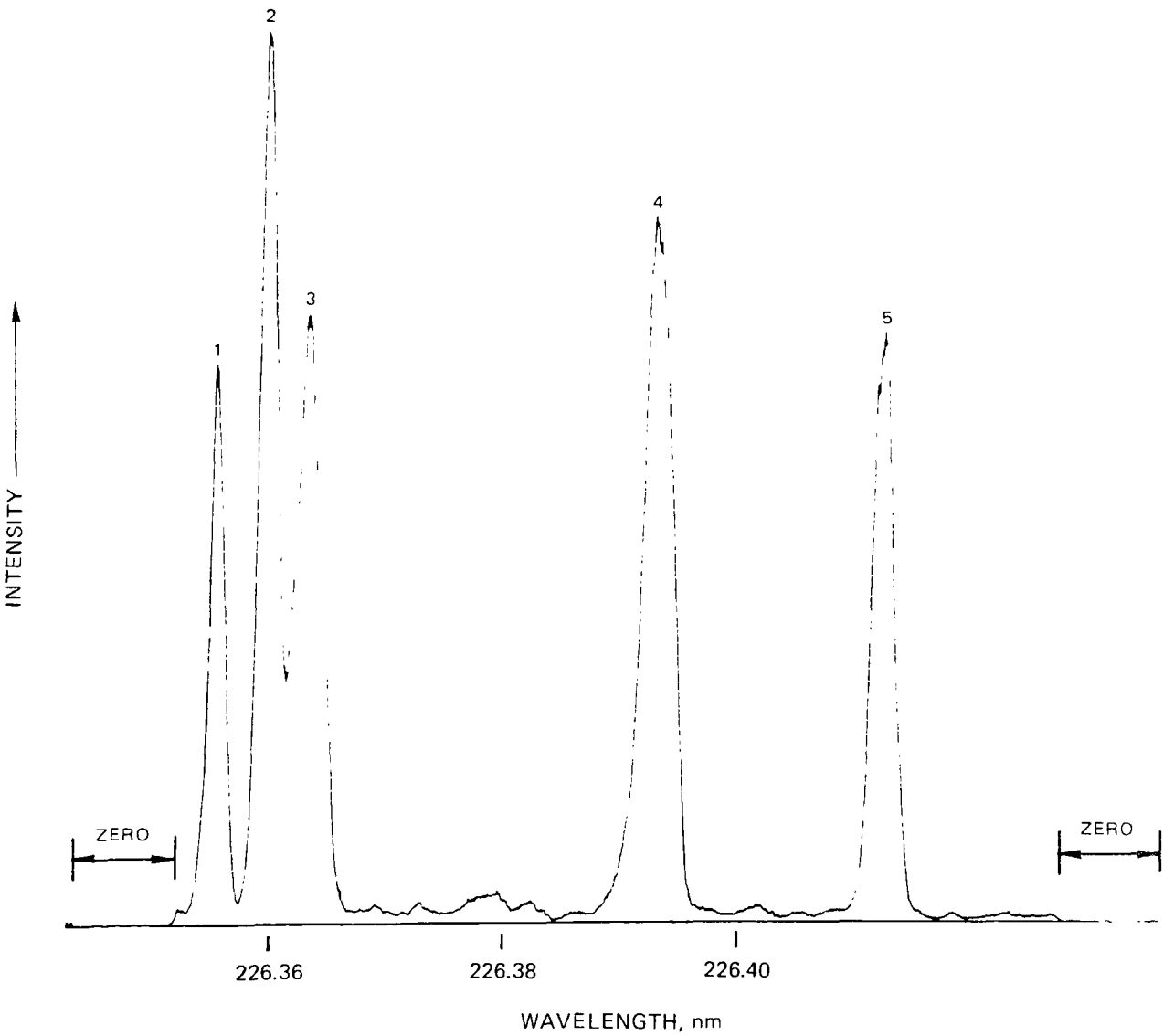

79–02–155–1

EMISSION FROM FIG. 21 AFTER ABSORPTION BY 5 TORR 10% NO/AR OVER PATH LENGTH OF 18.6 cm

1. P_{11} (6.5) + P_{11} (11.5)
2. P_{11} (7.5) + P_{11} (10.5) + P_{22} (22.5) + Q_{12} (22.5)
3. P_{11} (8.5) + P_{11} (9.5)
4. Q_{22} (14.5) + R_{12} (14.5) + R_{22} (9.5)
5. P_{22} (21.5) + Q_{12} (21.5)

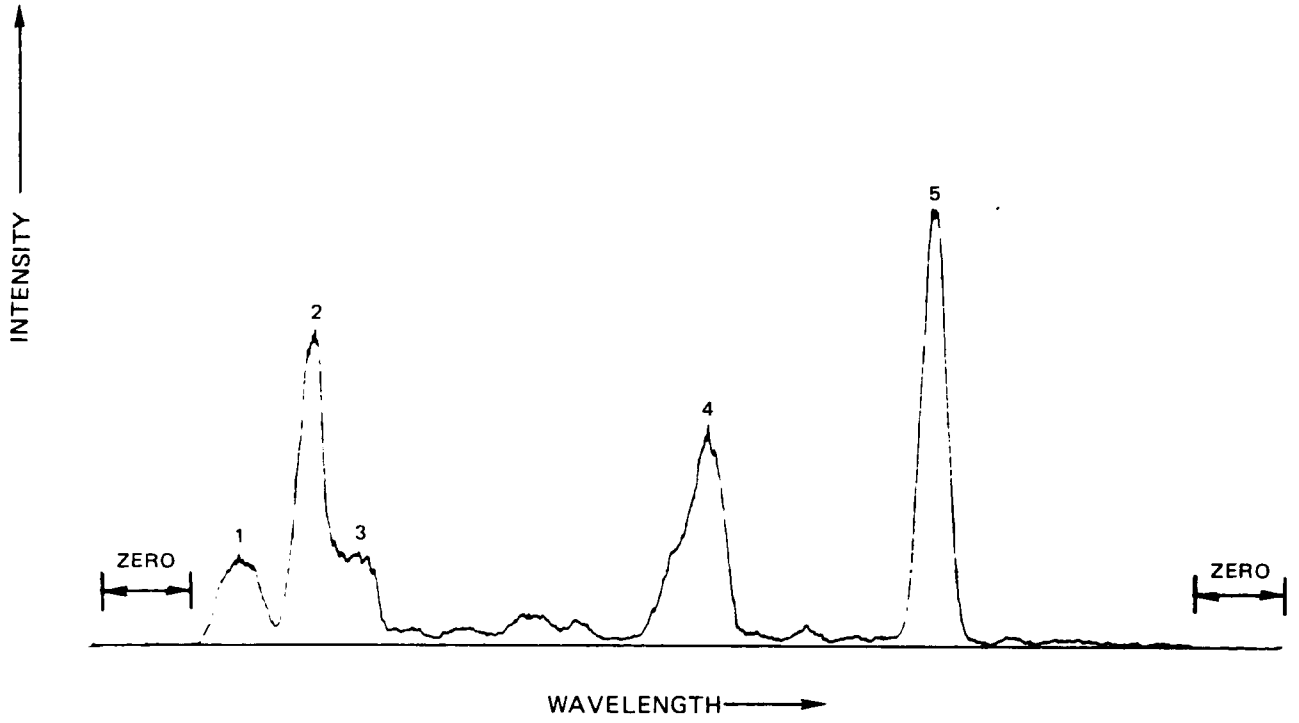

79-02-155-2

The signal from the photomultiplier was amplified with an Analog Devices AD310K used in the electrometer mode with feedback components of R_f = 100 M and C_f = 5000pf. The scan rate was $3.95 \cdot 10^{-4}$ nm/sec. The resulting spectra were recorded with a Hewlett-Packard 7100B strip chart recorder. In the case of the continuum lamp, some of the spectra were corrected for lamp drift by a ratiometric technique. This involved a reference measurement of the source lamp prior to any absorption, and was accomplished by placing a flat mirror slightly off the beam directed through the calibration apparatus which reflected light through a 226 nm filter and onto an EMI 9601B photomultiplier tube. The signal from the spectrometer was divided by this reference signal in an Ithaco model 3512 ratiometer and this resultant ratio was recorded on the strip chart recorder. This ratiometric technique reduced but did not eliminate baseline drift in the recorded spectra while using the continuum lamp.

The ultraviolet radiation from the source lamp was collimated and directed through the 12.7 mm diameter apertures in the FGH/FFB shroud, across the FGH/FFB, and then imaged on the spectrometer slit using fused silica lenses.

The spectrometer was operated in high resolution and low resolution. The slits were set at about 5 to 10 μm for the high resolution work, corresponding to slit functions with FWHM of about .0015 nm to .0025 nm. The slits were set at 1380 μm for the low resolution studies, with a FWHM value of 0.146 nm.

III.A.3 Static Cell

The static cell is a room temperature absorption cell made of stainless steel with valves toward each end and UV grade fused silica windows. The cell was leaked checked at 10^{-6} torr ($1.33 \cdot 10^{-4}$ Pa.) and 115 psig (791 kPa.). The cell i.d. is 22 mm and the optical path is 18.6 cm.

B. Theoretical Development of Ultraviolet Absorption

III.B.1. Necessity for Theoretical Model

A detailed theoretical model has been developed to describe the absorption of ultraviolet radiation by nitric oxide in the (0,0) band. It would not be unreasonable to question the necessity for such a first principles model, when the possibility exists for an empirical calibration technique. But how well can known concentrations of NO be generated over a temperature range of 300 K to 2000 K and a pressure range of 0.5 to 1.5 atm? The answer is that it is difficult and expensive to generate a complete range of conditions necessary for repetitive empirical calibration. The approach adopted in this work was to start with a theoretical model and then verify that model by testing it over a range of conditions, similar to the approach used by Davis et al. (1976a) but with additional information from high resolution continuum absorption data.

An additional problem with empirical models is that they are often instrument dependent and quite difficult to transfer from a given instrument at one laboratory to instruments in general. An example for this particular experiment would be that a strictly empirical calibration would depend on the characteristics of the narrow-line source (rotational distribution) and the spectrometer (PM tube response and slit function) which would make duplication of results at various laboratories difficult. The theoretical model does include some empirical "adjustments," as will be discussed, and several experimentally determined input parameters, but the absorption process is modeled from basic principles.

III.B.2. Transmission Formulas, Narrow-Line Source

The general problem of relating measured absorptions in the $\gamma(0,0)$ band to molecular densities of NO may be summarized as follows. In order to predict low resolution absorption profiles in the $\gamma(0,0)$ band, it is necessary to model on the order of 500 lines whose relative intensities change with temperature, and whose shape changes with temperature, pressure, and gas composition. These lines are so closely spaced that even when recorded with a high resolution instrument, many of the lines overlap.

The theory for the transmission of a group of Doppler broadened NO source lines through an absorbing gas with both Doppler and collision broadened lines has been developed by Davis et al. (1976). We will use the results of Eqs. (1) through (14) of Davis et al. (1976), which can be summarized as follows. The total transmitted intensity for the jth emission line ($\bar{T}_j$) due to absorption by many lines is related to the line center source intensity of the jth line ($I^{o}_{\nu j}{}^{o}$), the Doppler width of the source $(\Delta_s \nu_j)_D$, the line center Doppler absorption coefficient of the gas (k_{ν_i}), the broadening parameter (a'), and the path length (ℓ) by,

$$\bar{T}_j = I^{\circ}_{\nu_j} \int_{\circ}^{\infty} \exp\left\{ -\left[\frac{2(\nu - \nu_j^{\circ})}{(\Delta_s \nu_j)_D} \sqrt{\ln 2} \right]^2 \right\} \cdot \exp\left\{ -\frac{\ell}{\pi} \sum_i k_{\nu_i}^{\circ} \int_{-\infty}^{\infty} \frac{a' e^{-y^2} dy}{a'^2 + (\omega_i - y)^2} \right\} d\nu \tag{20}$$

where a' is related to the Lorentz full width at half maximum (FWHM) in the absorbing gas $(\Delta_a \nu_i)_L$ and the corresponding FWHM of the Doppler component $(\Delta_a \nu_i)_D$ by

$$a' = \frac{(\Delta_a \nu_i)_L}{(\Delta_a \nu_i)_D} \sqrt{\ln 2} \tag{21}$$

and where

$$\omega_i = \frac{2(\nu_i - \nu_i^{\circ})}{(\Delta_a \nu_i)_D} \sqrt{\ln 2} \tag{22}$$

The Doppler widths (FWHM) of the source and absorbing line are given by

$$(\Delta \nu_j)_D = \nu_j^{\circ} \frac{2}{c} \sqrt{\frac{2(\ln 2) k T}{m}} = \nu_j^{\circ} \frac{2}{c} \sqrt{\frac{2(\ln 2) RT}{M}} \tag{23}$$

where ν_i° is the wavenumber of line center, c is the speed of light, k is Boltzmann's constant, T is the appropriate temperature (either source or absorber), m is the molecular mass in grams of the emitting or absorbing molecule, R is the universal gas constant, and M is the molecular weight in grams per mole. The Lorentz FWHM due to collisions is given by,

$$(\Delta_a \nu)_L = \frac{Z_L}{\pi c} = \frac{1}{\pi \tau c} \tag{24}$$

where Z_L is the frequency of collisions between an absorbing molecule and the perturbing molecules, and τ is $1/Z_L$ or the mean time between collisions.

It should be noted that this development assumes that the collision process and line broadening can be accurately explained by the Lorentz collision theory, an assumption which is discussed in detail later in this report. The use of the Lorentz theory to examine experimental results is certainly the usual assumption, but deviations from Lorentz-theory behavior have been observed in numerous instances (see Section III.B.5 on broadening theory).

It is worthwhile considering the factors in Eq. (20) which must be known or determined in order to predict the transmission. The relative intensities of the source lines at line center must be measured for the narrow-line lamp, and intensities of lines that cannot be measured directly must be interpolated from a Boltzmann plot such as shown in Fig. 20. The Doppler FWHM ($(\Delta\nu_j)_D$) may easily be calculated from Eq. (23). The path length (ℓ) is easily determined. The broadening parameter (a') must be determined experimentally because theoretical computation of the Lorentz FWHM ($(\Delta_a\nu_i)_L$), which is necessary to determine a' through Eq. (21) is not feasible. The experimental technique used to determine a' is described in a later section. The final parameter which must be determined to solve Eq. (20) for the transmission is the absorption coefficient at line center for a Doppler broadened line ($k^o_{\nu_i}$). The relation between $k^o_{\nu_i}$ and the density of molecules in the initial state and the oscillator strength is described below.

II.B.3 Computation of Doppler Absorption Coefficient

The line center absorption coefficient for a Doppler broadened line ($k^o_{\nu_i}$) is given by Mitchell and Zemansky (1971),

$$k^o_{\nu_i} = \frac{2\,e^2}{m_e\,c^2}\sqrt{\frac{\pi\ \ln 2}{}}\quad \frac{N(n''v''\ \Sigma\ ''J''\ p'')\quad f_{v'v''\ J'J''}}{(\Delta_a\nu_i)_D} \tag{25}$$

where e is the electron charge, m_e is the electron mass, c is the speed of light, $f_{v'v''J'J''}$ is the oscillator strength of the line, and N(n''v''Σ''J''p'') is the population of the initial energy state. The single and double primes refer to upper and lower electronic state parameters, respectively.

The Doppler FWHM ($(\Delta_a\nu_i)_D$) can be calculated from Eq. (23). The oscillator strength for a line ($f_{v'v''J'J''K'K''p''}$) is related to the oscillator strength for a band ($f_{v'v''}$) by (Thorne (1974)),

$$f_{v'v''J'J''K'K''p''} = \frac{S_{J'J''K'K''p''}}{2J'' + 1}\quad f_{v'v''} \tag{26}$$

where $S_{J'J''K'K''p''}$ is the Hönl-London factor and J'' is the rotational quantum number in the lower electronic state. The band oscillator strength ($f_{v'v''}$) for the NO γ(0,0) band has been measured previously and another determination is reported in this work (see experimental results section). The Hönl-London factors may be computed from equations given by Earls (1935), but with an adjustment factor for proper normalization (multiply Earls values by 4). It is important to note that the summation convention for the Hönl-London factors suggested by Tatum (1967) has been adopted here, that is:

$$\sum_{\text{sub-levels}} \quad \sum_{J'} S_{J'J''} = (2-\delta_{o,\Lambda''})\ (2S + 1)\ (2J'' + 1) \tag{27}$$

where the summation over sub-levels includes both spin splitting levels (the 2S + 1 factor) and Λ doubling levels (the $2-\delta_{o,\Lambda}$ factor). The value $\delta_{o,\Lambda}$ is unity for $\Lambda = 0$, but zero otherwise. For the NO $\gamma(0,0)$ band, the summation convention for the Honl-London factor becomes

$$\sum_{\text{sub-levels}} \quad \sum_{J'} S_{J'J''} = 4\ (2J'' + 1) \tag{28}$$

from the fact that $(2S + 1) = 2$, and $(2-\delta_{o,\Lambda''}) = 2$ (see later section on the spectroscopy of NO for an explanation of quantum numbers).

The remaining factor in Eq. (25) which must be determined in order to solve for $k^{o}_{\nu_i}$ is represented by the somewhat awkward but definitive notation $N(n''v''\ \Sigma''J''p'')$, which is the population of the energy level of interest for a molecule obeying Hund's case (a). The more often used symbol $N_{J''}$ is sometimes ambiguous in that it may or may not include the factor of 1/2 for the Λ doubled levels. Thus $N(n''v''\Sigma''J''p'')$ represents the number of molecules in the electronic state n", vibrational state v", spin state Σ", rotational level J", and with specified parity p" (+ or -). The fraction of the total number of molecules which are in a given level is represented by $N(n''v''\Sigma''J''p'')/N$, and can be determined for the NO $2\pi_{1/2}$ and $2\pi_{3/2}$ sublevels of the ground state as follows.

The ground state of the NO molecule is intermediate between Hund's cases (a) and (b), but to a close approximation follows Hund's case (a). Following Tatum's (1967) convention and notation for Hund's case (a) for the $2\pi_{1/2}$ state (all terms are for the lower electronic state and, hence, should have double primes),

$$\frac{N(nv\Sigma Jp)}{N} = \left[\frac{2(2S + 1)\ \exp\ ((-hc/kT)\ T_o)}{\sum_{\text{all states}} 2(2S+1)\ \exp((-hc/kT)T_o)}\right] x \left[\frac{\exp\ ((-hc/kT)\ G(v))}{\Sigma_v\ \exp\ ((-hc/kT)\ G(v))}\right]$$

$$x \left[\frac{\exp\ ((-hc/kT)\ (-A/2))}{\exp\ ((-hc/kT)\ (-A/2)) + \exp\ ((-hc/kT)\ (A/2))}\right]$$

$$x \left[\frac{(2J + 1)\ \exp\ ((-hc/kT)\ F(J))}{\Sigma_J\ (2J + 1)\ \exp\ ((-hc/kT)\ F(J))}\right] x \left[\frac{1}{2}\right] \tag{29}$$

where S is the electron spin quantum number, h is Planck's constant, T_o is the electronic term value when spin is neglected, G(v) is the vibrational term value, A is the spin splitting constant, and F(J) is the rotational term value. The equivalent expression for the $2\pi_{3/2}$ state is identical except that the numerator in the third term in brackets becomes exp ((-hc/kT)(A/2)).

The first term in brackets in Eq. (29) is the fractional population of a given electronic level, N(n)/N, and differs from that given by Tatum in that we have used the "average" electronic term value T_o (or electronic term value when spin is ignored) rather than Tatum's T_e where $T_e = T_o + A\Lambda\Sigma$ (for $^2\pi_{1/2}$, $T_e = T_o-(A/2)$; for $^2\pi_{3/2}$, $T_e = T_o + (A/2)$). The use of T_e in place of T_o would produce (for the NOγ(0,0) band), a term essentially* identical to the third term in brackets in Eq. (29), but following Tatum's guidelines, the fractional populations of the spin-split levels are to be calculated separately and explicitly as N(nvΣ)/N(nv), the third term in brackets. Thus, it would appear that Tatum has accounted for the fractional populations of the spin-split levels twice, which we have avoided by using T_o in Eq. (29). For the electronic term value, as expressed in Eq. (29), the first term in brackets is unity.

The second term in brackets in Eq. (29) is the fractional population of a given vibrational level, N(nv)/N(n), which for the v" = 0 level is close to unity at 300 K but decreases to about 0.74 at 2000 K. The third term in brackets in Eq. (29) determines the fractional population N(nvΣ)/N(nv) of the spin-split $^2\pi_{1/2}$ and $^2\pi_{3/2}$ levels. The fourth term in brackets represents the fractional population of a given rotational level N(nvΣJ)/N(nvΣ). By employing the usual approximations (Herzberg (1950)), the sum in the denominator of the fourth term in brackets may be written as kT/hcB. The fifth term, symbolically written N(nvΣJp)/N(nvΣJ), accounts for the Λ-type doubling of the rotational levels of the $^2\pi$ state into two sublevels of parity + and -. Because the upper electronic state being considered is a $^2\Sigma$ state, only one of the two sublevels is active for a transition to a specified upper state rotational level (Herzberg (1950)).

* This assumes that exp ((-hc/kT)T_e) << 1 for all electronic states higher than the ground state ($^2\pi$), which is true for the NO molecule even at high temperature.

Thus, Eq. (29) for the $^2\pi_{1/2}$ state may be rewritten:

$$\frac{N(nv\Sigma Jp)}{N} \simeq \left[\frac{\exp((-hc/kT)G(v))}{\Sigma_v \exp((-hc/kT)G(v))}\right] \times \left[\frac{\exp((-hc/kT)\ (-A/2))}{\exp((-hc/kT)(-A/2)) + \exp((-hc/kT)(A/2))}\right] \times \left[\frac{hcB}{2kT}\ (2J+1)\ \exp\ ((-hc/kT)\ F\ (J))\right] \tag{30}$$

The equivalent expression for the $^2\pi_{3/2}$ state is:

$$\frac{N(nv\Sigma Jp)}{N} \simeq \left[\frac{\exp((-hc/kT)G(v))}{\Sigma_v \exp((-hc/kT)G(v))}\right] \times \left[\frac{\exp((-hc/kT)\ (A/2))}{\exp((-hc/kT)\ (-A/2)) + \exp((-hc/kT)(A/2))}\right] \times \left[\frac{hcB}{2kT}\ (2J+1)\ \exp\ ((-hc/kT)\ F\ (J))\right] \tag{31}$$

These expressions may be modified intermediate to Hund's case (a) and (b) by absorbing the spin-splitting term into the expression for F(J) (Hill and Van Vleck (1928)) and dropping the third term in brackets on the right-hand side of Eq. (29). When this is done, however, the rotational partition function may no longer (in general) be approximated as kT/hcB. Assuming that the spin-splitting energy is absorbed into F(J) and the resultant is labeled $F_i(J)$, with i = 1 for the $^2\pi_{1/2}$ state and i = 2 for the $^2\pi_{3/2}$ state, then instead of Eqs. (30) and (31), one gets,

$$\frac{N(nv(\Sigma J)p)}{N} = \left[\frac{\exp((-hc/kT)\ G(v))}{\Sigma_v \exp((-hc/kT)\ G(v))}\right] \times \left[\frac{(2J+1)\ \exp\ ((-hc/kT)\ F_i\ (J)}{\Sigma_{i\,=\,1,\,2} \quad \Sigma_J\ (2J+1)\ \exp\ ((-hc/kT)\,F_i\ (J))}\right] \times \left[\frac{1}{2}\right] \tag{32}$$

For the NO molecule, we have determined that the rotational partition function can be approximated with high accuracy ($\pm$ 0.3% for 300 K < T < 2000 K) as almost Hund's case (a),

$$\Sigma_{i=1,2}\Sigma_J (2J+1)\exp((-hc/kT)F_i(J)) \tilde{=} (kT/hcB)\left[\exp((-hc/kT)(-A+2B)/2) + \exp(-hc/kT)(A-2B)/2)\right] \quad (33)$$

for the energy equations and constants as given by Engleman, et al (1970). This approximation was subsequently verified by D. Keefer. Thus, Eq. (32) for the intermediate Hund's case between (a) and (b) becomes,

$$\frac{N(nv(\Sigma J)p)}{N} \tilde{=} \left[\frac{\exp((-hc/kT)G(v))}{\Sigma_v \exp((-hc/kT)G(v))}\right] x \left[\frac{1}{\exp((-hc/kT)(-A+2B)/2) + \exp((-hc/kT)(A-2B)/2}\right] x \left[\frac{hcB}{2kT}(2J+1)\exp((-hc/kT)F_i(J)\right] \quad (34)$$

If Eqs. 23, 26, and 34 are substituted into Eq. (25), the result is

$$k\nu_i^\circ = \frac{e^2 hB}{2m_e \nu_i^o k}\sqrt{\frac{\pi m_a}{2k}} \frac{1}{T_a}3/2 \; f_{v'v''} S_{J'J''} N \quad (35)$$

$$x\left(\frac{\exp((-hc/kT_a)G(v''))}{\Sigma_{v''}\exp((-hc/kT_a)G(v''))}\right) \quad x \quad \left(\frac{1}{\exp((-hc/kT_a)(-A+2B)/2)+\exp((-hc/kT_a)(A-2B)/2)}\right)$$

$$x \quad \exp((-hc/kT_a)F_i(J''))$$

or, substituting for the constants,

$$k\nu_i^\circ = \frac{1.755\cdot 10^{-10}}{T_a^{3/2}} f_{v'v''} S_{J'J''} N \left(\frac{\exp(-1.4388G(v'')/T_a)}{\Sigma_{v''}\exp(-1.4388G(v'')/T_a)}\right) x \left(\frac{1}{\exp(86.18/T_a)+\exp(-86.18/T_a)}\right) (\exp(-1.4388F F_i(J'')/T_a)) \quad (36)$$

With Eq. (36) for $k_{\nu_i}^\circ$, all terms necessary to calculate the transmission ($\bar{T}_j$) using Eq. (20) have been determined except for the broadening parameter a' and a confirmation of the band oscillator strength $f_{v'v''}$.

III.B.4. Transmission Formulas, Continuum Source

The development of the transmission formulas for continuum radiation is very similar to that used for the narrow-line case given in Eq. (20). The source function is much simplified to just I(ν), which is a very slowly varying and easily measured function. The transmitted intensities must be recorded continuously as

a function of wavenumber rather than as discrete intensities at the line center of emission lines, as is done for the narrow-line source. The transmission at any wavenumber ν is,

$$T(\nu) = I(\nu)\exp\left\{-\frac{\ell}{\pi}\sum_i k_{\nu_i}^{o}\int_{-\infty}^{\infty}\frac{a' e^{-y^2}dy}{a'^2+(\omega_i-y)^2}\right\} \tag{37}$$

where the symbols are the same as explained previously for Eq. (20).

III.B.5 Broadening Theory

There is no lack of theoretical models available to treat pressure broadening. The theories of pressure broadening are discussed in some detail by Breene (1957), Hindmarsh and Farr (1972), and Mitchell and Zemansky (1971). Thorne (1974) discusses the subject with less depth but good clarity. An often quoted work for microwave and infra-red regions is the paper by Anderson (1949).

In spite of the number of theoretical models available, experimentalists tend to use the standard Lorentz theory and label discrepancies as deviations from the Lorentz theory, rather than attempting to use other models. In this report, results from the Lorentz theory and Weisskopf theory are used, but the reader is referred to the previous references for the details of these theories.

The Lorentz model assumes that the optical collision diameter is independent of the relative velocities of the two colliding molecules (or atoms). From the Lorentz theory the FWHM due to collisions, $\Delta\nu_L$, is given by Mitchell and Zemansky (1971),

$$\Delta\nu_L = \frac{Z_L}{\pi c} \tag{38}$$

where Z_L is the collision frequency of a single molecule, c is the velocity of light, and $\Delta\nu_L$ is in wavenumbers. It should be noted that this is true only for collisions between molecules of different types. If the molecules are all of the same type then Eq. (38) is multiplied by a factor of 2. This is due to the fact that each collision terminates one mean free path if the collision is between the gas being studied and a foreign gas, but it terminates two mean free paths if the collision is between two molecules of the same type. The interest here is in collisions between a minor species and foreign gases, so Eq. (38) applies.

The total number of collisions per second between molecules of type 1 and type 2 with number densities n_1 and n_2 and molecular weights (molar) M_1 and M_2 is given by Mitchell and Zemansky (1971) as,

$$Y = 2n_1n_2d_{1-2}^2\sqrt{2\pi RT\left(\frac{1}{M_1}+\frac{1}{M_2}\right)} \tag{39}$$

where d is the hard sphere collision diameter ($d = r_1 + r_2$, where r is the radius), R is the universal gas constant, and T the absolute temperature. The collision frequency per molecule of a given type is,

$$Z_L = \frac{Y}{n_1} = 2n_2 d_{1-2}^2 \sqrt{2\pi RT \left(\frac{1}{M_1} + \frac{1}{M_2}\right)} \tag{40}$$

Combining Eqs. (38), (40), (21)

$$a_2' = \frac{1}{\nu\sqrt{\pi}} \; n_2 d_{1-2}^2 \sqrt{1 + \frac{M_1}{M_2}} \tag{41}$$

where ν is the wavenumber. Expressing n_2 in terms of the partial pressure (atm) of the foreign gas and temperature (K), d in cm, and ν in cm^{-1}

$$a_2' = \frac{4.14 \cdot 10^{21}}{\nu} \; d_{1-2}^2 \sqrt{1 + \frac{M_1}{M_2}} \; \frac{P_2}{T} \tag{42}$$

or

$$a_2' = C_2 \frac{P_2}{T} \tag{43}$$

If more than one foreign gas is active in broadening, Z_L is summed over all the species and a_i' for each species is,

$$a_i' = C_i \frac{P_i}{T} \tag{45}$$

where P_i is the partial pressure of the ith species. The total a' is the sum of the a_i's.

An important point must be made regarding the collision diameter and the effective collision cross-section. The effective optical collision diameter is given by d in the equations above. References in the field of kinetic theory, such as Reif (1965), and Hirschfelder et al (1954), call πd^2 the effective cross-section, while Mitchell and Zemansky, Davis et al (1976), and others drop the π and refer to d^2 as the effective cross-section. Thus, caution must be exercised in comparing effective cross-sections given by different authors. We define cross-section as πd^2 in this report.

According to the Lorentz theory, at constant pressure, $\Delta\nu_L$ is proportional to $T^{-0.5}$ and a' is proportional to $T.^{-1.0}$. There is a significant amount of evidence to indicate that the temperature dependence is stronger than this. Hence, the temperature dependence of $\Delta\nu_L$ should be between $T^{-0.5}$ and $T^{-1.0}$ and that of a' between $T^{-1.0}$ and $T^{-1.5}$. Among the evidence for a stronger temperature dependence for neutral atoms or molecules is work by Hansen (1978), Townes and Schawlow (1955), Engleman (1969), Cann et al (1979), Planet et al (1978), and Breene (1967).

The Weisskopf theory gives a stronger temperature dependence in agreement with a significant amount of experimental work (Thorne (1974)). Weisskopf developed a collision theory which includes the effect of collision time in computation of the cross-section. For collisions between neutral atoms or molecules, the Weisskopf theory, for a constant pressure, gives the collision width as $\Delta\nu_w$ proportional to $T^{-0.7}$ and a' proportional to $T.^{-1.2}$ This is in almost exact agreement with the result reported by Hansen (1978) of $\Delta\nu$ proportional to $T^{-0.73}$ for CO broadening over a wide range of temperatures. The evidence from the flame measurements reported here indicates that the temperature dependence of the Weisskopf theory seems to fit the experimental data for NO broadening better than the Lorentz theory.

III.B.6. Spectroscopic Details of the Nitric Oxide Ultraviolet γ (0,0) Band

III.B.6.a. Band Systems of NO

The electronic transitions of the NO molecule are observed in the ultraviolet and vacuum ultraviolet spectral regions. The lower energy transitions involving the ground ($X^2\pi$) state are labeled as follows (Pearse and Gaydon (1965)).

Transition Type	Label
$A^2\Sigma^+ - X^2\pi$	γ system
$B^2\pi - X^2\pi$	β system
$C^2\pi - X^2\pi$	δ system
$D^2\Sigma^+ - X^2\pi$	ε bands

The excited electronic states are labeled in order of increasing energy by A, B, C, etc., and therefore the lowest energy (longest wavelength) transitions are in the γ system, which makes that system the most easily accessible for absorption measurement of NO.

The bandheads for some of the lower vibrational levels are shown in Table III-B. For determining NO concentrations from spectroscopic absorption measurements at temperatures below 1000 K, it is only necessary to consider those states originating from a ground vibrational level (v" = 0). The longest wavelength transition of this type is the γ (v'=0, v"=0) band at ~226 nm. A number of experimental problems become more severe at wavelengths shorter than this: (1) the transmission of quartz decreases, (2) hot CO_2 and O_2 bands absorb more strongly at flame temperatures (3) the chance of interfering absorptions by other species increases, (4) intense continuum sources such as high pressure Xe and Hg-Xe lamps decrease rapidly in intensity, and (5) scattering by soot particles generally increases. Thus, the γ (0,0) band is the most reasonable band selection for the measurement of NO over the temperature range from 300 K to 2000 K.

TABLE III-B

Bandheads in the γ -System of Nitric Oxide
(Pearse and Gaydon (1965))

Double bandheads are given for each band

(nm)	v',v"
247.87	0,2
247.11	
244.70	1,3
244.00	
237.02	0,1
236.33	
231.63	2,3
230.95	
228.98	3,4
228.41	
226.94	0,0
226.28	
224.54	1,1
223.94	
222.24	2,2
221.63	
219.96	3,3
219.40	
215.49	1,0
214.91	

The γ (0,0) band represents transitions between the zeroth vibrational levels of the excited state $A^2\Sigma^+$ and the ground state $X^2\pi$. The ground electronic energy level of the NO molecule is split into two sub-levels, the lower energy $^2\pi_{1/2}$ state and the higher energy $^2\pi_{3/2}$ state, which are widely split in energy (~120 cm^{-1}). Because of the considerable difference in energy of the two sublevels, the $^2\pi$ state of NO is usually treated as following Hund's case (a), but is actually intermediate to cases (a) and (b), approximating case (a) for small rotational velocities, but undergoing some spin uncoupling at higher rotational rates. The upper $A^2\Sigma^+$ electronic state belongs strictly to case (b) coupling, as do all Σ states.

III.B.6.b. Energy Levels

The equations and constants used here to determine the energy for various rotational levels in both upper and lower electronic states are almost exclusively from Engleman, et al. (1970). Energy levels of a molecule (exclusive of translation) may be approximated as the sum of the rotational (E_r), vibrational (F_v), and electronic energies (E_e),

$$E = E_e + E_v + E_r \tag{46}$$

It is common practice to express the molecular energies as term values, which are energy values divided by hc, and have units of cm^{-1}. Using the term value notation, Eq. (46) becomes,

$$T = T_e + G(v) + F(J) \tag{47}$$

In an electronic transition the wave number (cm^{-1}) of a spectral line is given by the difference of the term value in the upper electronic state (T') and the lower electronic state (T"),

$$\upsilon = T' - T'' = (T_e' - T_e'') + (G'(v') - G''(v'')) + (F_v'(J') - F_v''(J'')) \tag{48}$$

III.B.6.c Energy Level Equations for the $X^2\pi$ State of NO

For the $^2\pi$ state of NO, the electronic energy and rotational energy are slightly coupled so that T_e and F(J) are not independent. The term value energy equation is modified so that $F_i(J)$ contains not only the rotational energy, but also the energy associated with the spin splitting in the $^2\pi$ state, and T_o contains the electronic energy exclusive of spin-splitting,

$$T'' = T_o'' + G''(v'') + F_i''(J'') \tag{49}$$

where the vibrational term value G(v) is,

$$G(v) = \omega_e (v+0.5) - \omega_e X_e (v+0.5)^2 \tag{50}$$

and the rotational term $F_i(J)$ is,

$$F_i(J) = B_v((J+0.5)^2-1)-D_v((J+0.5)^4-(J+0.5)^2+1)\mp B_v \sqrt{\alpha} \tag{51}$$

$$\alpha = \frac{(Y_v-2)^2}{4} + ((J+0.5)^2-1)\left[1+2\mu(2(J+0.5)^2-\lambda)+\mu^2\left((2(J+0.5)^2-1)^2-1\right)\right] \tag{52}$$

$$Y_v = \left[A + C(J-0.5)^2\right]/B_v \tag{53}$$

$$\mu = D_v/B_v \tag{54}$$

The minus (-) sign is for the $^2\pi_{1/2}$ state in which J = K + 0.5 and i = 1, while the plus (+) sign is for the $^2\pi_{3/2}$ state in which J = K - 0.5 and i = 2. It should be noted that our equation for $F_i(J)$ includes a term "$-B_v$" not found in Engleman, et al. (1970), but which should be included following the derivations from the original papers cited by Engleman. We have adjusted the upper state electronic energy given by Engleman, et al. accordingly. We have likewise added to the equation for α a term "μ^2," but this is numerically inconsequential. There also appears to be a typographical error in the sign convention given by Engleman, et al.

In addition to the spin-orbit splitting of the $^2\pi$ state, each of the levels is subject to a slight perturbation by Λ-type doubling due to the interaction between the rotation of the nuclei and the electronic orbital angular momentum L (Herzberg (1950)). The magnitude of this shift is given by ϕ, where,

$$\phi = 0.5\ (J+0.5)\left[\left(\frac{2-Y_v}{2\sqrt{\alpha}} \mp 1\right)\left(\frac{P}{2} + Q\right) + \frac{Q}{\sqrt{\alpha}}\left((J+0.5)^2-1\right)\right] \tag{55}$$

and the sign convention is the same as above. Because of Λ-type doubling, each rotational level is split into two components, but for a given transition only one of the components is active. The reason for this is that the two components are of opposite parity (+ and -). Because of the selection rule $+ \leftrightarrow -$, only one of the components may interact with an upper state with specified parity (the upper state is not Λ-type doubled). The Λ-type doubling has an influence on the spectral line locations as follows,

$$\begin{aligned} F_{ic} &= F_i - \phi \\ F_{id} &= F_i + \phi \end{aligned} \tag{56}$$

where F_{ic} is the energy of the $^2\pi$ state (exclusive of vibrational energy) for the transitions P_{11}, P_{22}, Q_{12}, Q_{21}, R_{11}, and R_{22}, and F_{id} is the $^2\pi$ state energy for transitions P_{12}, P_{21}, Q_{11}, Q_{22}, R_{12}, and R_{21}.

The zero-point energy of a molecule is arbitrary in that only energy differances have significance. For the constants given by Engleman et al., if the vibrational and rotational (but not spin-splitting) energies are set to zero, the level of zero electronic energy is midway between the energies of the two spin split states ($^2\pi_{1/2}$ and $^2\pi_{3/2}$). If, in addition, the spin splitting term A approached zero, the two spin split states would collapse into one energy level defined as the zero electronic energy for this system. However, we have shifted this zero point energy by A/2 to correspond approximately to the zero level energy of the lower $^2\pi_{1/2}$ state. Thus $T_o = A/2$, and Eq. (49) becomes

$$T'' = \frac{A}{2} + G''(v'') + \begin{cases} F''_{ic}(J'') \\ F''_{id}(J'') \end{cases} \qquad (57)$$

and the upper electronic state energy given by Engleman et al. is increased by A/2.

The constants which describe the lower electronic state are given in Table III-C. The Λ doubling constant P has a different sign in Engleman et al.'s Tables VII and XI. We have chosen the negative sign because it gives better agreement between the experimental and theoretical line locations.

III.B.6.d Energy Level Equations for the $A^2\Sigma^+$ State of NO

The energy levels of the upper electronic state ($A^2\Sigma^+$) are described by the general Eq. (47)

$$T' = T'_e + G(v') + F'(J') \qquad (58)$$

where T_e is a constant, G(v) is given by Eq. (50), and F(J) is given by Engleman et al. as,

$$F_1(J) = B_v(J+0.5)(J-0.5) - D_v(J+0.5)^2(J-0.5)^2 + 0.5\gamma(J-0.5) \qquad (59a)$$

$$F_2(J) = B_v(J+0.5)(J+1.5) - D_v(J+0.5)^2(J+1.5)^2 - 0.5\gamma(J+1.5) \qquad (59b)$$

where $F_1(J)$ is for states with J = K + 1/2 and $F_2(J)$ is for states with J = K - 1/2. Of course, all values of J, K, and v are for the upper electronic state and would have single primes if any were indicated. The γ is a small spin splitting constant and the value used was determined by Bergeman and Zare (1972) from an rf resonance study. The constants used to describe the upper state are given in Table III-D.

TABLE III-C

$X^2\pi$ State Constants for NO
(from Engleman, et al. (1970))

T_o = 61.595 cm^{-1}* (=A/2)

A = 123.19 cm^{-1}

C = $-5.8 \cdot 10^{-4}$ cm^{-1}

ω_e = 1904.405 cm^{-1}

$\omega_e x_e$ = 14.1870 cm^{-1}

B_v = 1.69568 cm^{-1}

D_v = $4.5 \cdot 10^{-6}$ cm^{-1}

P = $-1.17 \cdot 10^{-2}$ cm^{-1}*

Q = $7.8 \cdot 10^{-5}$ cm^{-1}

*see text

TABLE III-D

$A^2\Sigma$ State Constants for NO
(from Engleman, et al. (1970) except as noted)

T_e = 43966.2643 cm^{-1}+

ω_e = 2374.307 cm^{-1}

$\omega_e x_e$ = 16.106 cm^{-1}

B_v = 1.98576 cm^{-1}

D_v = $4.6 \cdot 10^{-6}$ cm^{-1}

γ = .00276 cm^{-1}*

+adjusted for different zero references from Engleman, et al.

*from Bergeman and Zare (1972).

III.B.6.e. NO γ (0,0) Band Structure

For cases where the $^2\pi_{1/2}$ and $^2\pi_{3/2}$ energy levels are noticeably separated (Hund's case (a)), the band structure of a $^2\Sigma - ^2\pi$ transition is usually considered as two sub-bands, $^2\Sigma - ^2\pi_{1/2}$ and $^2\Sigma - ^2\pi_{3/2}$, which are separated from each other by the amount of doublet splitting of the $^2\pi$ state. There are six branches possible for each of two sub-bands, making a total of twelve branches. Because of the small spin splitting in the $^2\Sigma$ state of NO, only eight distinct branches are resolved, but in this study the spin splitting in the $^2\Sigma$ state has been included based on the value given by Bergeman and Zare (1972).

The selection rules which determine which upper and lower electronic states are involved in transitions are explained in detail by Herzberg (1950), and may be summarized as follows. For changes in vibrational energy, $\Delta v = v' - v'' = 0, \pm 1, \pm 2, \pm 3...$, with the relative strengths determined by the overlap of the potential energy curves. These relative strengths are given by the Franck-Condon factors. Concerning rotational levels, only states of opposite parity may interact, $+ \leftrightarrow -$, $+ \not\leftrightarrow +$, $- \not\leftrightarrow -$. This has an effect on which of the Λ-type doubled levels in the $^2\pi$ state may interact with given upper state levels. The total angular momentum J is restricted such that $\Delta J = J' - J'' = 0, \pm 1$. Since the $^2\pi$ state is intermediate between Hund's cases (a) and (b), the selection rule $\Delta N = N' - N'' = 0, \pm 1$ (older notation $\Delta K = K' - K''$) applies, but $\Delta N = \pm 2$ can appear subject to $\Delta J = \pm 1$, although the intensity is much reduced. Branches for which $\Delta J \neq \Delta N$ will generally be weaker.

These selection rules imply that there are twelve branches and the labeling of those branches is shown in Table III-E. The notation is the same as that used by McGregor et al. (1973), and there are additional diagrams in that report explaining the notation. The following line pairs are overlapped due to the small spin splitting in the upper state: P_{22} and Q_{12}; Q_{11} and P_{21}; Q_{22} and R_{12}; and R_{11} and Q_{21}.

TABLE III-E

Notation for Transitions of NO

Transition		Rotational Upper State		Rotational Lower State	$\Delta J=J'-J''$	$\Delta N=N'-N''$ (or $\Delta K=K'-K''$)+
$P_{12}(J'')$	=	$F_1'(J''-1)$	-	$F''_{2d}(J'')$	-1	-2
$P_{11}(J'')$	=	$F_1'(J''-1)$	-	$F''_{1c}(J'')$	-1	-1
$P_{22}(J'')$	=	$F_2'(J''-1)$	-	$F''_{2c}(J'')$	-1	-1
$P_{21}(J'')$	=	$F_2'(J''-1)$	-	$F''_{1d}(J'')$	-1	0
$Q_{12}(J'')$	=	$F_1'(J'')$	-	$F''_{2c}(J'')$	0	-1
$Q_{11}(J'')$	=	$F_1'(J'')$	-	$F''_{1d}(J'')$	0	0
$Q_{22}(J'')$	=	$F_2'(J'')$	-	$F''_{2d}(J'')$	0	0
$Q_{21}(J'')$	=	$F_2'(J'')$	-	$F''_{1c}(J'')$	0	+1
$R_{12}(J'')$	=	$F_1'(J''+1)$	-	$F''_{2d}(J'')$	+1	0
$R_{11}(J'')$	=	$F_1'(J''+1)$	-	$F''_{1c}(J'')$	+1	+1
$R_{22}(J'')$	=	$F_2'(J''+1)$	-	$F''_{2c}(J'')$	+1	+1
$R_{21}(J'')$	=	$F_2'(J''+1)$	-	$F''_{1d}(J'')$	+1	+2

+the newer notation replaces K with N.

C Experimental Results - Spectroscopic Measurements

III.C.1. Determination of Broadening Parameters

III.C.1.a. Background

In the discussion of the development of transmission formulas, it was shown that all quantities necessary to calculate the transmission have been determined except for the broadening parameter a' and the oscillator strength $f_{v'v''}$. Reasonable literature values exist for the oscillator strength, but there is no concensus for the broadening parameters.

There are several techniques for studying pressure broadening. When the rotational lines are closely spaced, as is the case for the NO γ (0,0) band, direct line shape measurements are difficult. A curve of growth technique may be used at various pressures and, with a knowledge of the oscillator strength, the broadening may be determined. This technique was used by Thorson and Badger (1957) to determine a collision diameter for NO broadening in the γ (0,0) band by N_2. A similar analysis was performed more recently by Tajime et al. (1978), but serious deficiencies in their theoretical model were pointed out by Dodge and Dusek (1979). Davis et al. (1976) utilized a narrow-line absorption technique to study NO broadening by N_2 but, again, serious problems in their theoretical model were pointed out by Dodge and Dusek (1978). Hadeishi et al. (1976) used a Zeeman tuned Cd lamp to determine the profile of a single NO line in the γ (1,0) band. (They report measurements of the 0-1 vibrational band of NO at 214.438 nm, but the γ (0,1) band is at about 236 nm, so we assume the measurements were for the γ (1,0) band.) The results of Tajime et al. (1978) and Davis et al. (1976) are in question because of the theoretical problems, but the measurements by Thorson and Badger (1957) and Hadeishi et al. (1976) may be in reasonable agreement. Unfortunately (or significantly), the results reported here are substantially different than in those two papers.

A number of measurements of the NO γ (0,0) band oscillator strength have been made, and, in contrast with the broadening measurements, there is reasonable agreement for most of the literature values. The results reported here are similar to published values. The problems associated with different techniques used to measure oscillator strengths are discussed by Thorne (1974).

III.C.1.b. Procedure

The technique used in this study for the oscillator strength and broadening measurements of the NO γ (0,0) band was unique in that the rotational structure of the band was resolved and actual individual line shapes and strengths were determined photometrically. This requires a resolution of about 130,000 at 225 nm. With the additional ability to scan a spectrum with photoelectric detection, it is possible to avoid the nonlinear response of photographic plates.

Commercial instruments with these specifications have only recently become available. In addition, a sophisticated computer model developed jointly at Arnold Engineering Development Center (AEDC) and this laboratory was required for reducing the data.

The individual line profiles were recorded mostly in the spectral region between the P_{11} and P_{22} bandheads where the lines were separated most clearly. All of these lines originated in the $^2\pi_{3/2}$ ground state. A few measurements were recorded in the P_{11} bandhead region to examine lines originating in the in the $^2\pi_{1/2}$ ground state.

All room temperature broadening measurements were made with the high pressure Xe DC arc lamp (continuum source), the static cell and associated gas mixing apparatus, and the high resolution spectrometer which were previously described. The ratiometric electronics were used for recording some spectra while others were recorded directly (Fig. 18).

The cell was first filled with about 5 torr (6.7 Pa) of 10% NO diluted in Ar and a scan was taken to determine the slit function of the instrument, along with a small contribution from the Doppler broadened gas. The slit function varied slightly in shape and width over several hours while data were being recorded, but the best fit to the experimental values could be obtained with a Gaussian. Our slit function was slightly wider near the base than a Gaussian, but it did not possess the wings characteristic of a Lorentzian. A more complicated slit function such as given by Kusch et al. (1977) did not seem warranted. The effect of convolving a slit function with the actual spectral shape is discussed by Thorne (1974), Kusch et al. (1977), and Sulzmann et al (1976). The convolution technique used here is described in the computer program description (Appendix D) The measured FWHM for the slit function was typically 0.0018 nm while the Doppler FWHM was 0.00051 nm. This slit function was monitored several times during each data set. For Gaussians, the half widths combine as $(\Delta\nu)^2 = (\Delta\nu_1)^2 + (\Delta\nu_2)^2 + \ldots$ (Thorne (1974)), and since both the slit function and Doppler shape are Gaussians, the actual slit function FWHM was typically .00173 nm. In comparison, the range of FWHM for N_2 for which broadening data were reduced was 0.00562 to 0.00965 nm, so slight variations in the slit function ($\pm$0.0002 nm) had negligible effect on the measured profiles. An example spectrum at low pressures is shown in Fig. 23.

After the slit function was determined, the gases were blended to arrive at a constant NO number density for a given final pressure, independent of diluent gas. Spectra were recorded at total pressures of 0.50 atm (50.7 kPa), 0.75 atm (76.0 kPa), 1.00 atm (101 kPa), 1.50 atm (152 kPa), and 2.00 atm (203 kPa). Experimentally recorded spectra for NO broadening by N_2 over this range of pressures are shown in Figs. 24-28. Similar spectra were obtained for NO diluted in CO_2, CO, Ar, and CH_4. These experimental spectra were compared with computer generated spectra such as those shown in Figs. 29-31, which correspond to N_2 broadening at

DOPPLER BROADENING (0.0005nm) AND SLIT FUNCTION (0.0015nm)

P_T = 0.0076 ATM

$P_{NO}\ell \cong 3.5\ 10^{17}\ CM^{-2}$

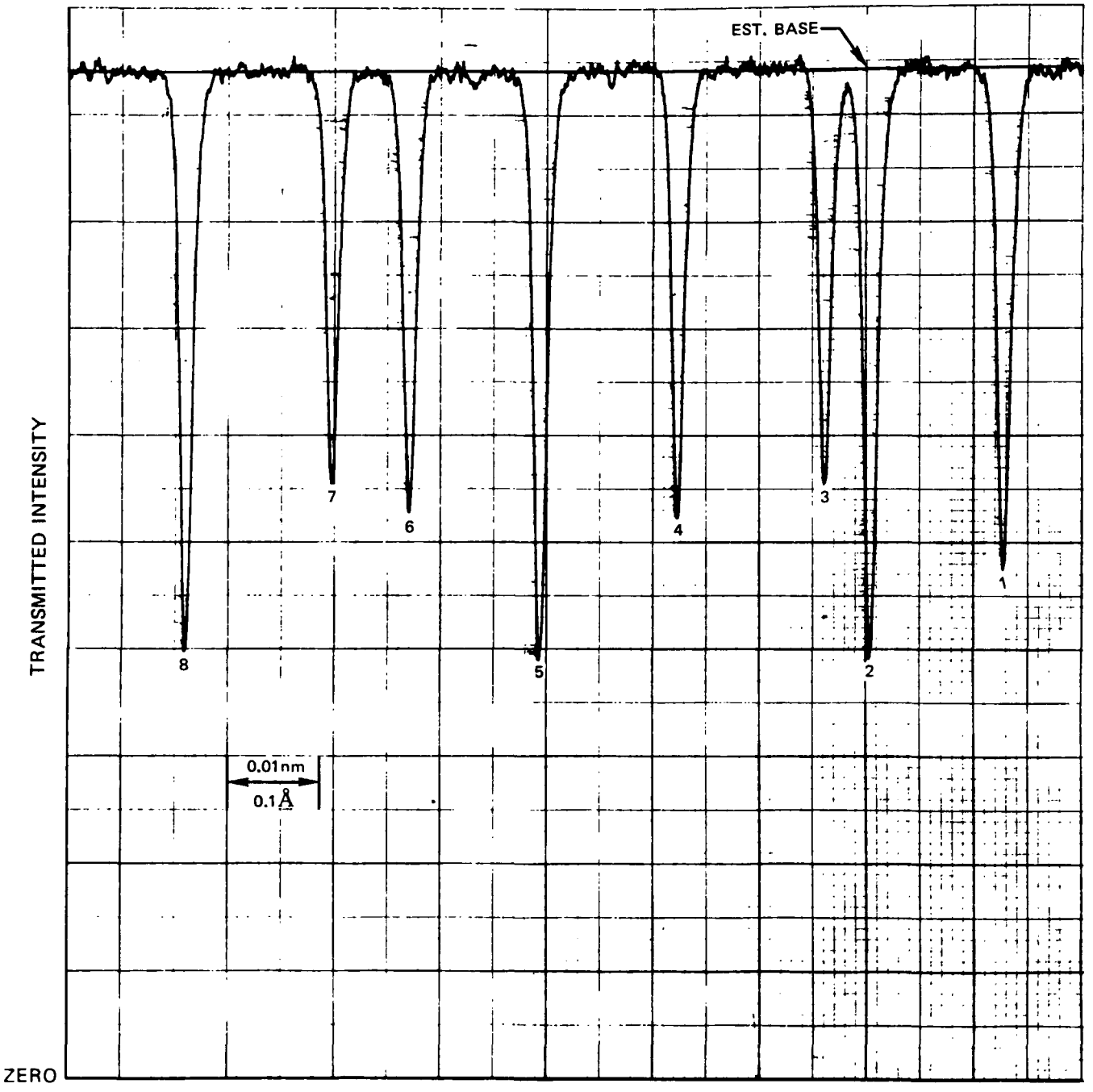

79-04-93-15

NO ABSORPTION SPECTRUM

P_T = 0.50 ATM

$P_{NO}\ell = 2.59 \cdot 10^{17}$ CM^{-2}

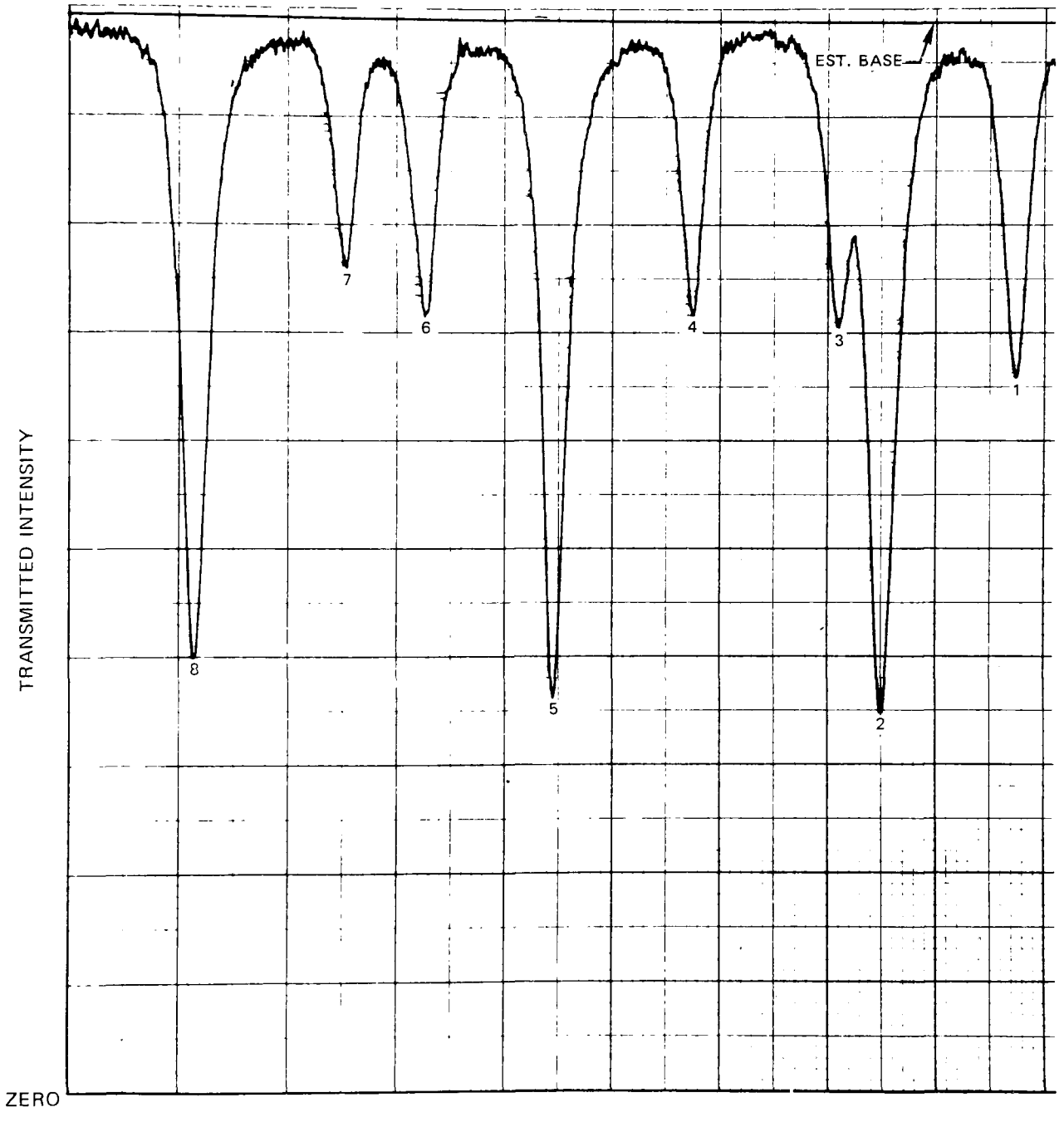

79-04-93-16

NO ABSORPTION SPECTRUM

P_T = 0.75 ATM

$P_{NO}\ell = 3.89 \cdot 10^{17}$ CM^{-2}

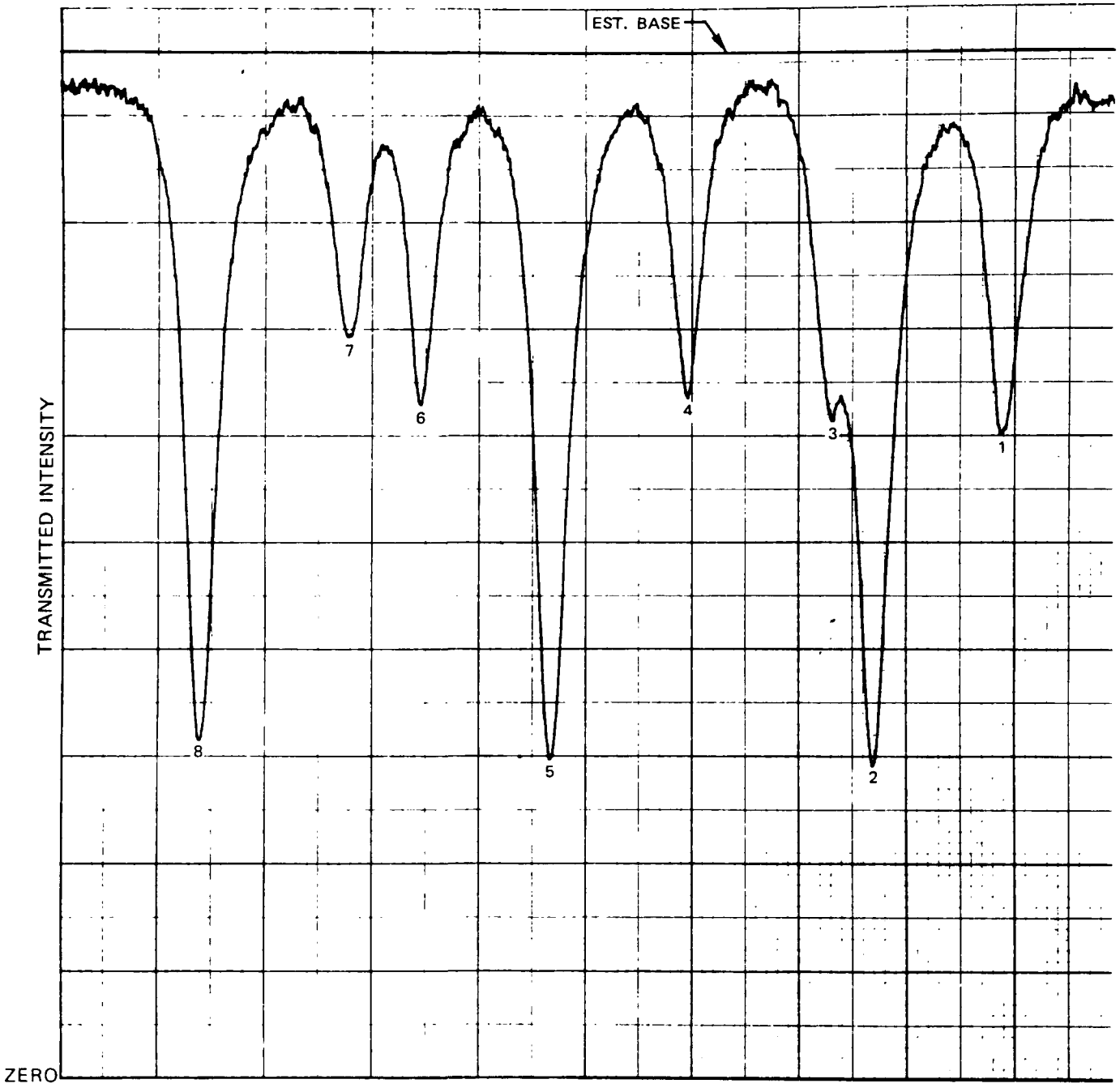

79-04-93-17

NO ABSORPTION SPECTRUM

P_T - 1.00 ATM

$P_{NO}\ell = 5.18 \cdot 10^{17}$ CM^{-2}

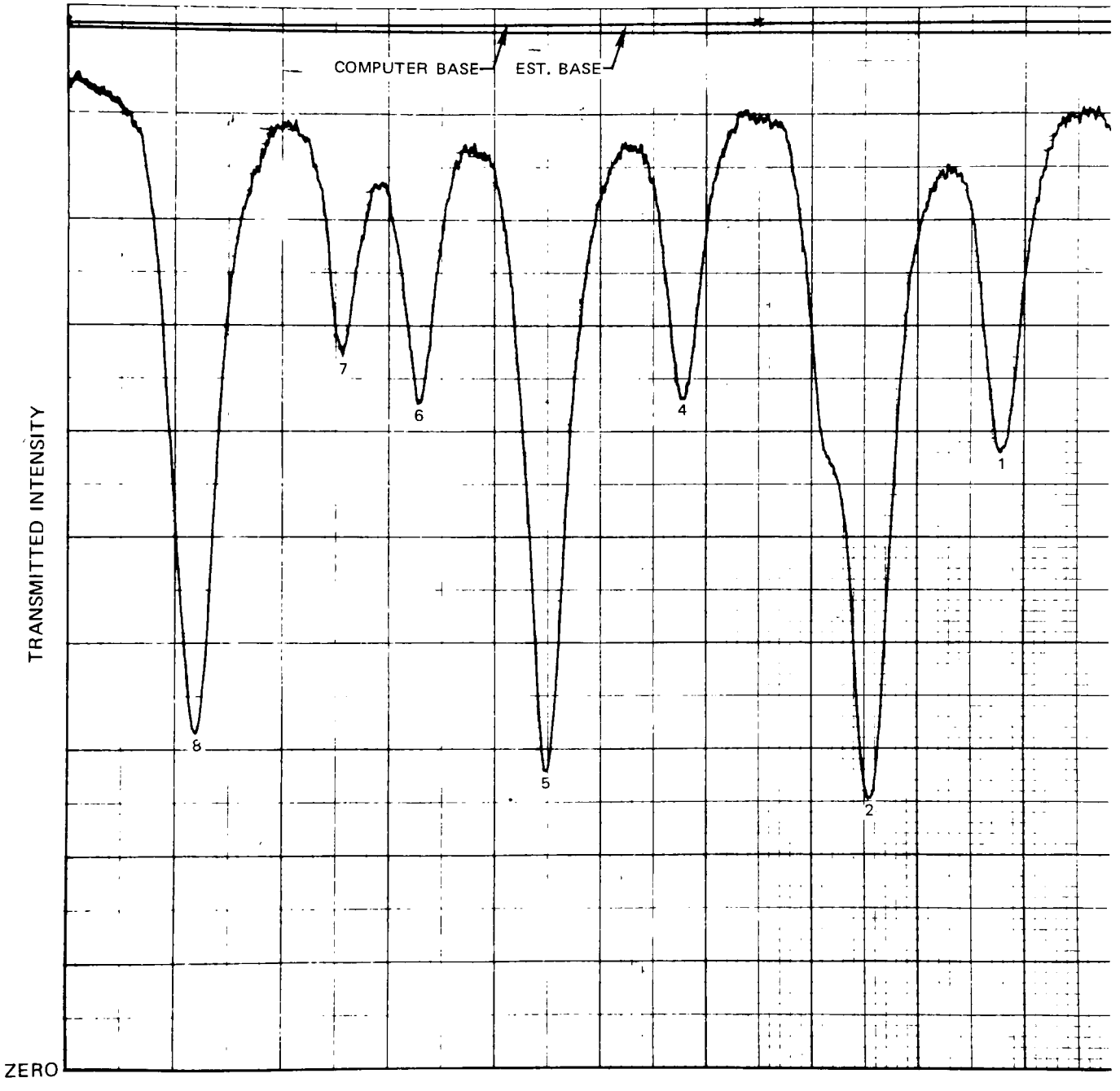

79-04-93-18

NO ABSORPTION SPECTRUM

P_T = 1.50 ATM

$P_{NO}\ell = 5.18 \cdot 10^{17}$ CM^{-2}

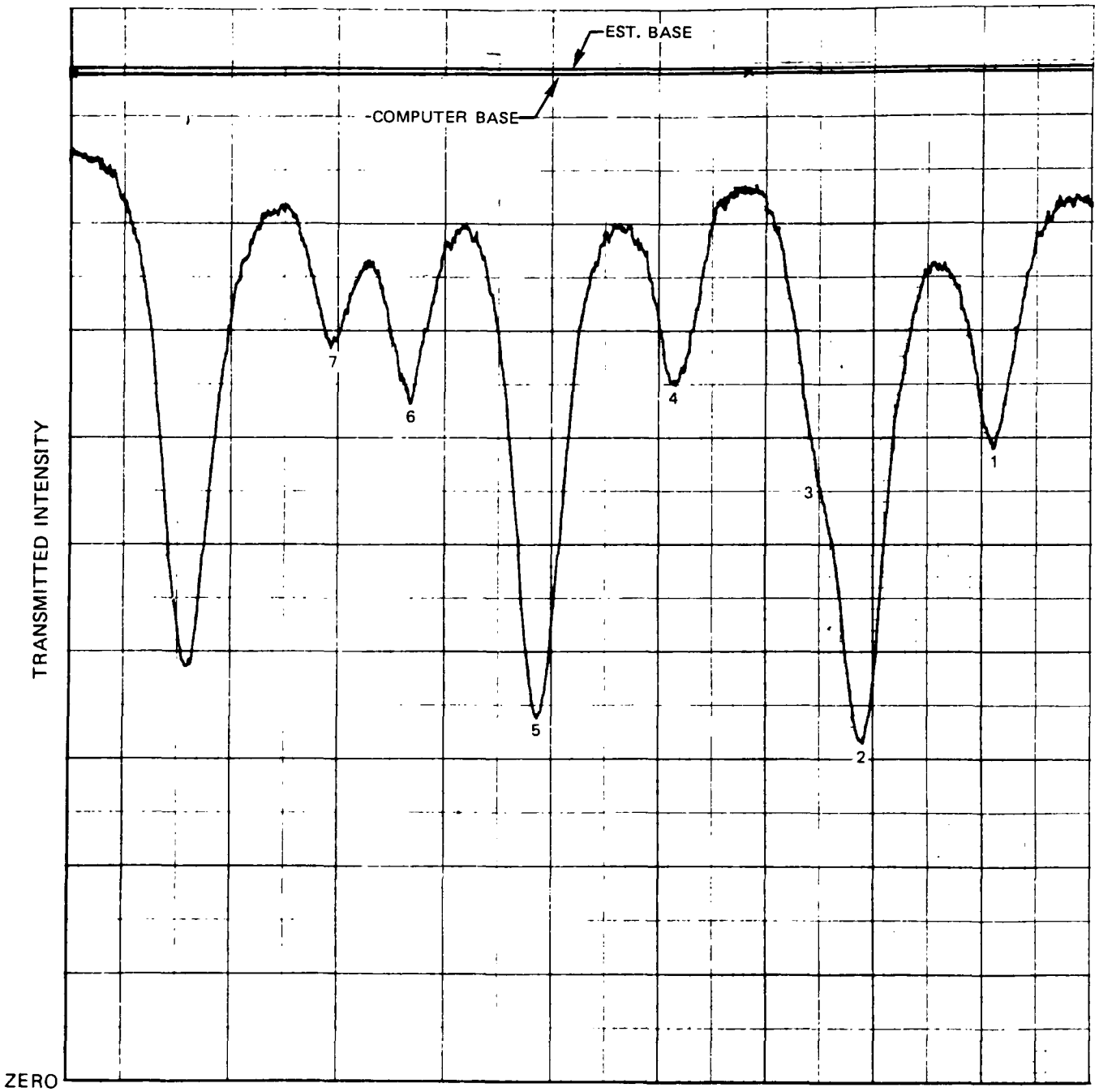

79-04-93-19

NO ABSORPTION SPECTRUM

P_T = 2.00 ATM

$P_{NO}\ell = 5.18 \cdot 10^{17}$ CM^{-2}

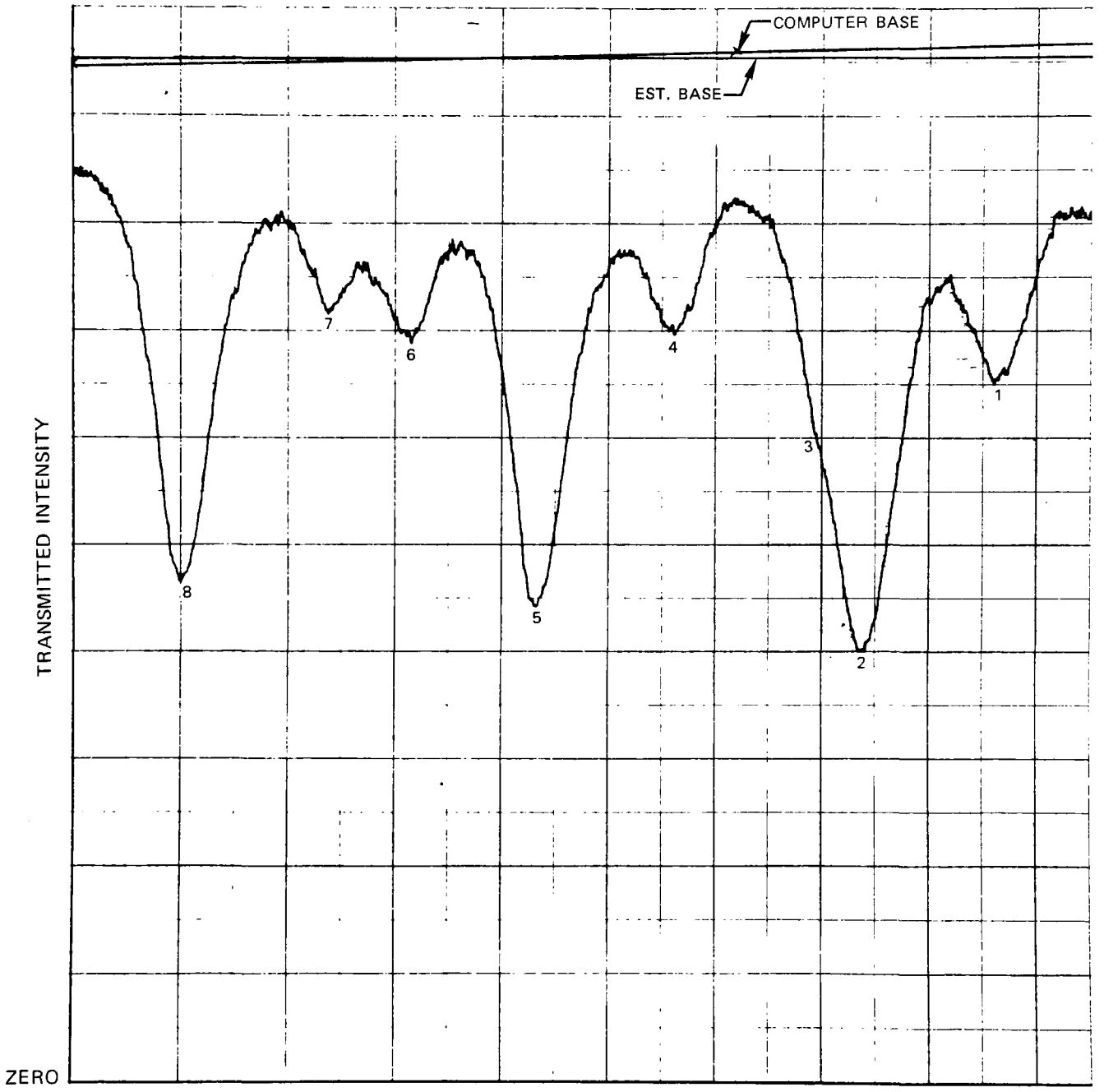

79-04-93-20

COMPUTER SPECTRUM

P_T = 0.75ATM

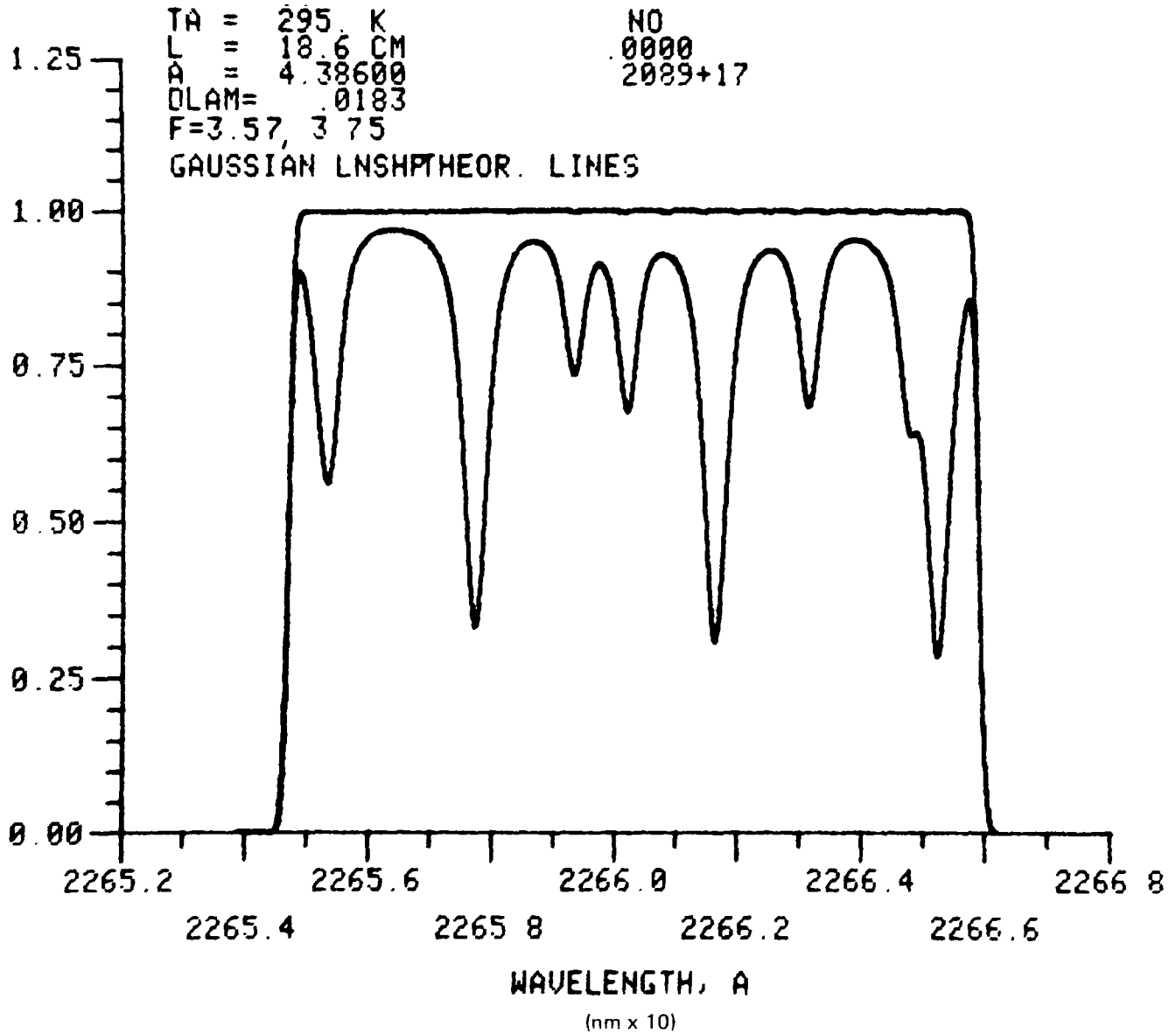

79-04-93-14

FIG. 29

COMPUTER SPECTRUM

P_T = 1.00ATM

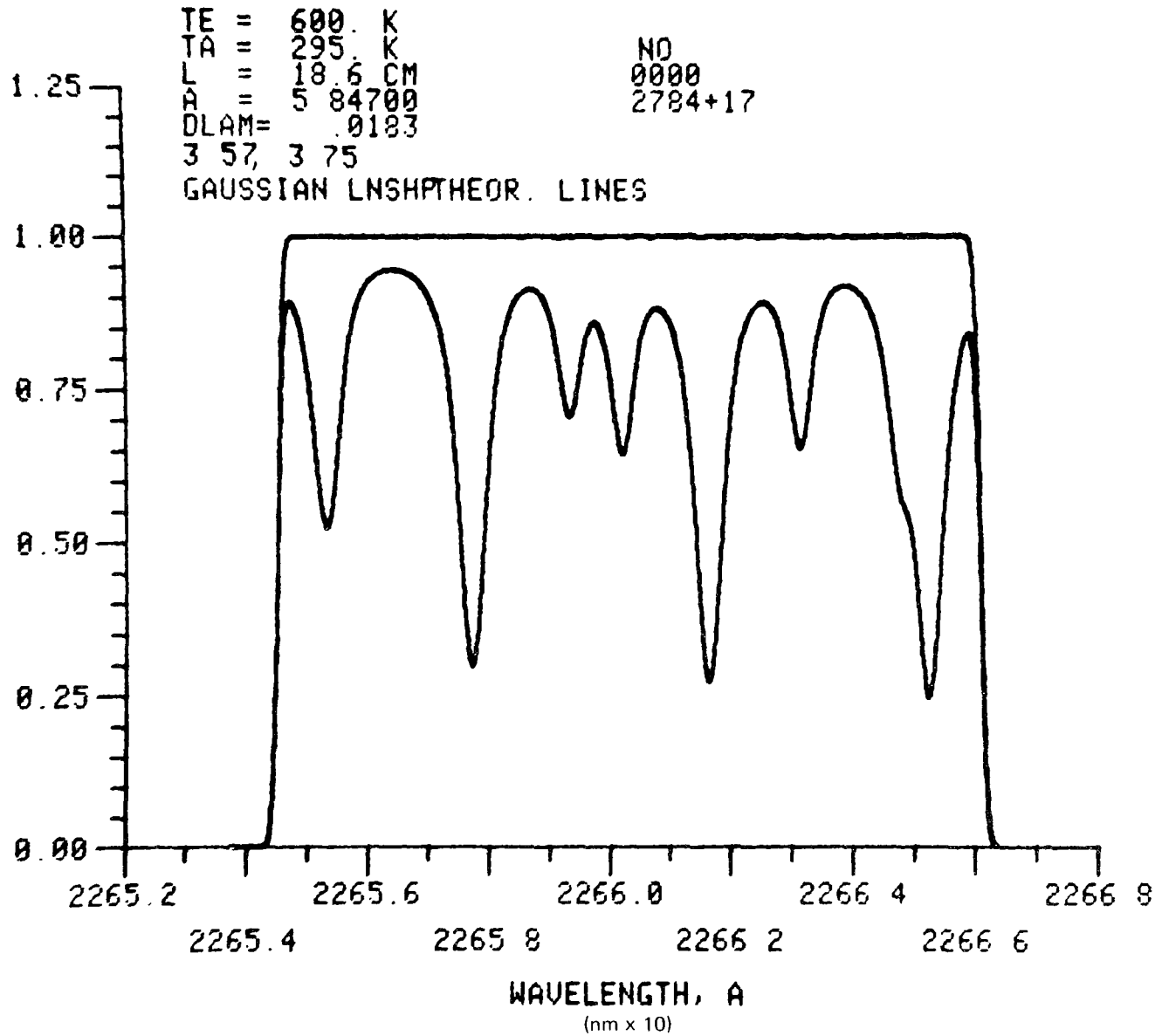

79-04-93-13

FIG. 30

COMPUTER SPECTRUM

P_T = 1.50ATM

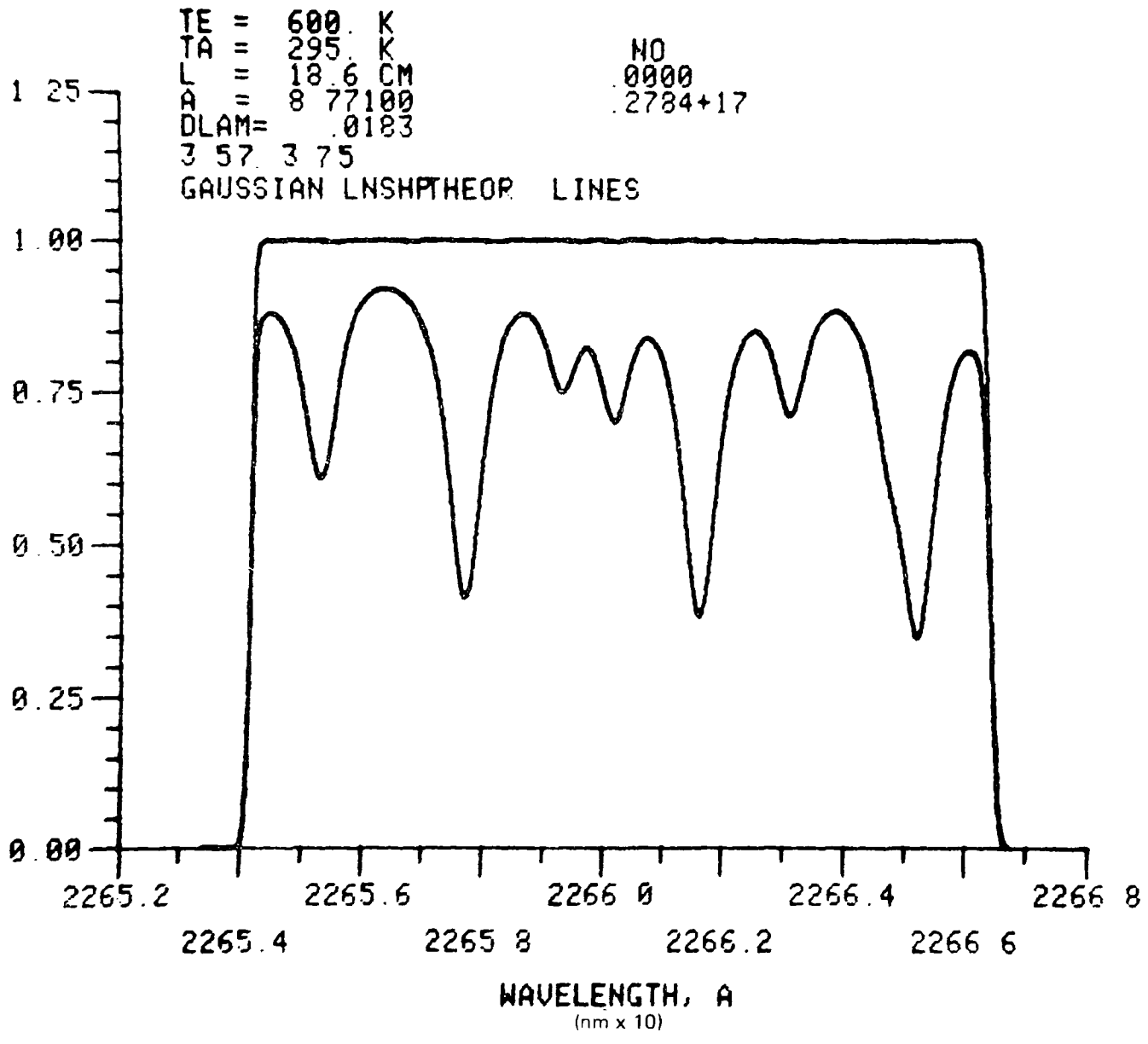

79-04-93-12

FIG. 31

pressures of 0.75 atm (76.0 kPa), 1.00 atm (101 kPa), and 1.50 atm (152 kPa). The spectral lines in Figs. 24-28 are identified in Table III-F.

At these NO densities, there is significant absorption between even the most widely spaced lines over most of the pressure range studied. Thus the zero absorption baseline must be determined. Even with the dual-beam ratiometric electronics small amounts of drift occurred in the zero absorption signal. The baseline was determined in two ways. First, the zero absorption signals before and after the runs were averaged and called the estimated baseline (EST. BASE. in Figs. 24-28). Second, for the higher pressure cases, the computer spectra were used to estimate a baseline and called computer baseline (COMPUTER BASE. in Figs. 24-28). These agreed very well for the N_2 and Ar data. The CO_2 and CH_4 generally showed somewhat more absorption in the wings than predicted by the computer model, and thus, the estimated baseline was as much as 5 percent higher than the computer baseline relative to zero transmission for the worst case at 2 atm (203 kPa) condition. Such a comparison for CO could not be made easily because pure CO gas absorbed significantly in the region of interest as shown in Fig. 32. None of the other gases showed any absorption in this region. All data were reduced relative to the computer baseline.

Reported data are only for the Q_{22} (9.5) + R_{12} (9.5) line pair and the Q_{22} (10.5) + R_{12} (10.5) line pair and for the pressure range of 1.00 atm (101 kPa) to 2.00 atm (203 kPa). This pressure was selected to reduce uncertainties from changes in the slit function. However, at the lower pressures where half widths could be measured for all lines, the widths were consistent, and independent of J value within experimental precision. At all pressures there was excellent agreement between the computer predicted spectral shape and the observed profiles. The same pressure broadening value gave an excellent match between experimental and computed spectra for transitions originating in the $^2\pi_{1/2}$ state for the pressures 0.75 atm (76.0 kPa), 1.00 atm (101 kPa), and 1.32 atm (133 kPa), as shown in Figs. 33 and 34.

III.C.1.c Low Temperature Broadening Data and Discussion

A listing of the typical experimental results for the broadening of NO by N_2, CO_2, CO, CH_4, and Ar is given in Table III-G. This table gives an indication of scatter in the data. All error bands in Table III-G are 1σ of the experimental data and do not reflect systematic errors. It is estimated that the broadening parameters C and K are accurate to within 15 percent.

As discussed in the section on broadening theory, the Lorentz theory gives the temperature dependence of a' as $a' = CP/T$, while the Weisskopf theory results in $a' = KP/T^{1.2}$ (Thorne (1974)). The optical collision diameter d is also shown. As discussed previously, collision cross-sections are defined as either d^2 or πd^2.

TABLE III-F

SPECTRAL LINES USED FOR BROADENING MEASUREMENTS

Group Number	Line Identification	Wavelength[+] (nm) or (Å/10)	Wavenumber[+] (cm^{-1})
1	$P_{22}(15.5)$	226.66669	44117.642
	$Q_{12}(15.5)$	226.66647	44117.685
2	$Q_{22}(8.5)$	226.65247	44120.410
	$R_{12}(8.5)$	226.65234	44120.436
	$P_{12}(26.5)$	226.65156	44120.587
3	$R_{22}(4.5)$	226.64758	44121.363
4	$P_{22}(16.5)$	226.63137	44124.519
	$Q_{12}(16.5)$	226.63113	44124.564
5	$Q_{22}(9.5)$	226.61623	44127.466
	$R_{12}(9.5)$	226.61608	44127.496
6	$R_{22}(5.5)$	226.60194	44130.248
7	$P_{22}(17.5)$	226.59325	44131.941
	$Q_{22}(17.5)$	226.59300	44131.989
8	$Q_{22}(10.5)$	226.57724	44135.060
	$R_{12}(10.5)$	226.57708	44135.091

+Theoretically determined (difference in upper and lower energies). These are slightly different if experimental line locations by Engleman et al. (1970) or Deezsi (1958) are used.

ABSORPTION BY CO COINCIDENT WITH $\gamma(0,0)$ BAND OF NO

$$\sigma = \frac{1}{P\ell} \text{LOG}_e\ (I^o/I)$$

P... PARTIAL PRESSURE, ATM

ℓ... PATH LENGTH, CM

I^o/I... 1/TRANSMISSION

T = 296K

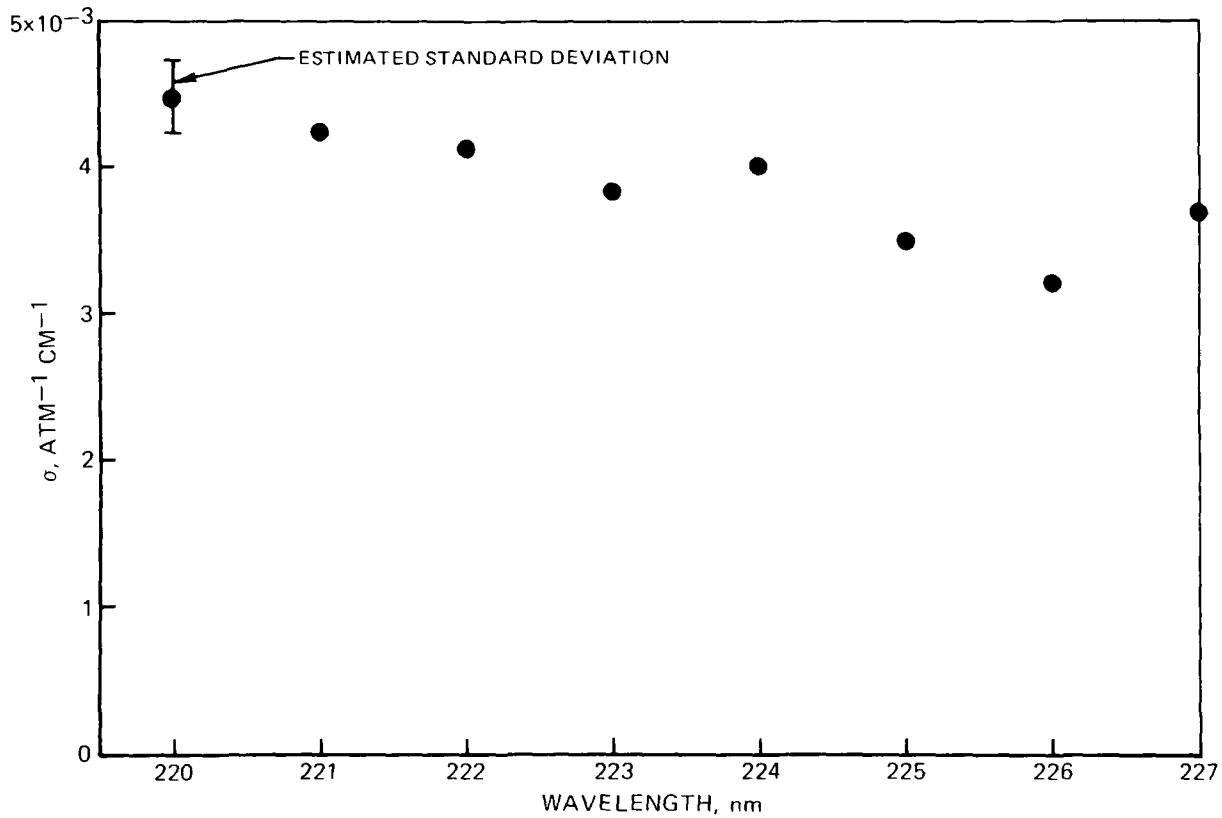

79-04-93-10

FIG. 32

SPECTRUM NEAR P_{11} BANDHEAD

P_T = 1 ATM

$P_{NO}\ell = 1.82 \cdot 10^{17}$ CM^{-2}

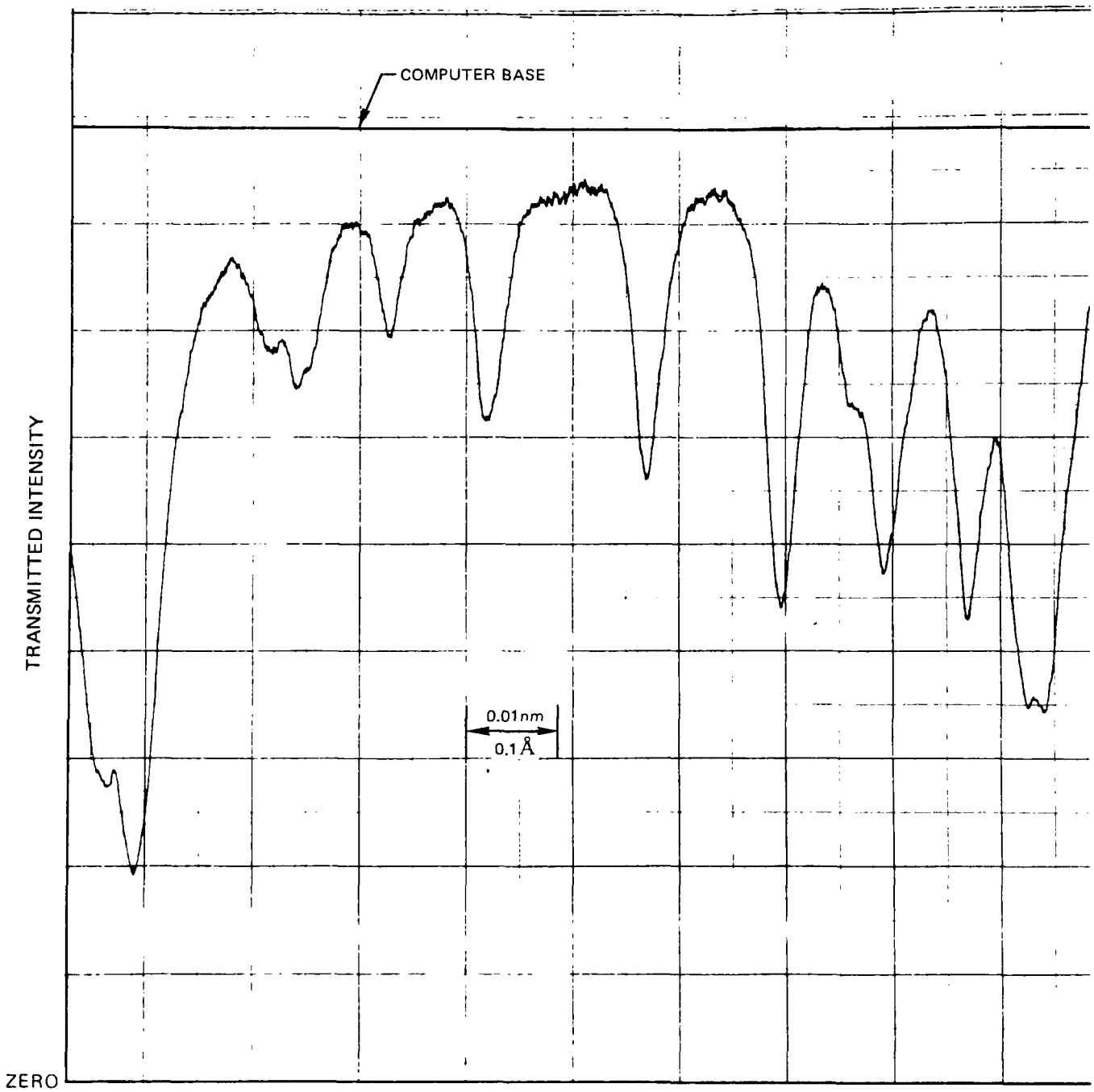

79-04-93-22

COMPUTER SPECTRUM NEAR P_{11} BANDHEAD

P_T = 1ATM, $P_{NO}\ell = 1.82 \cdot 10^{17}$ CM^{-2}

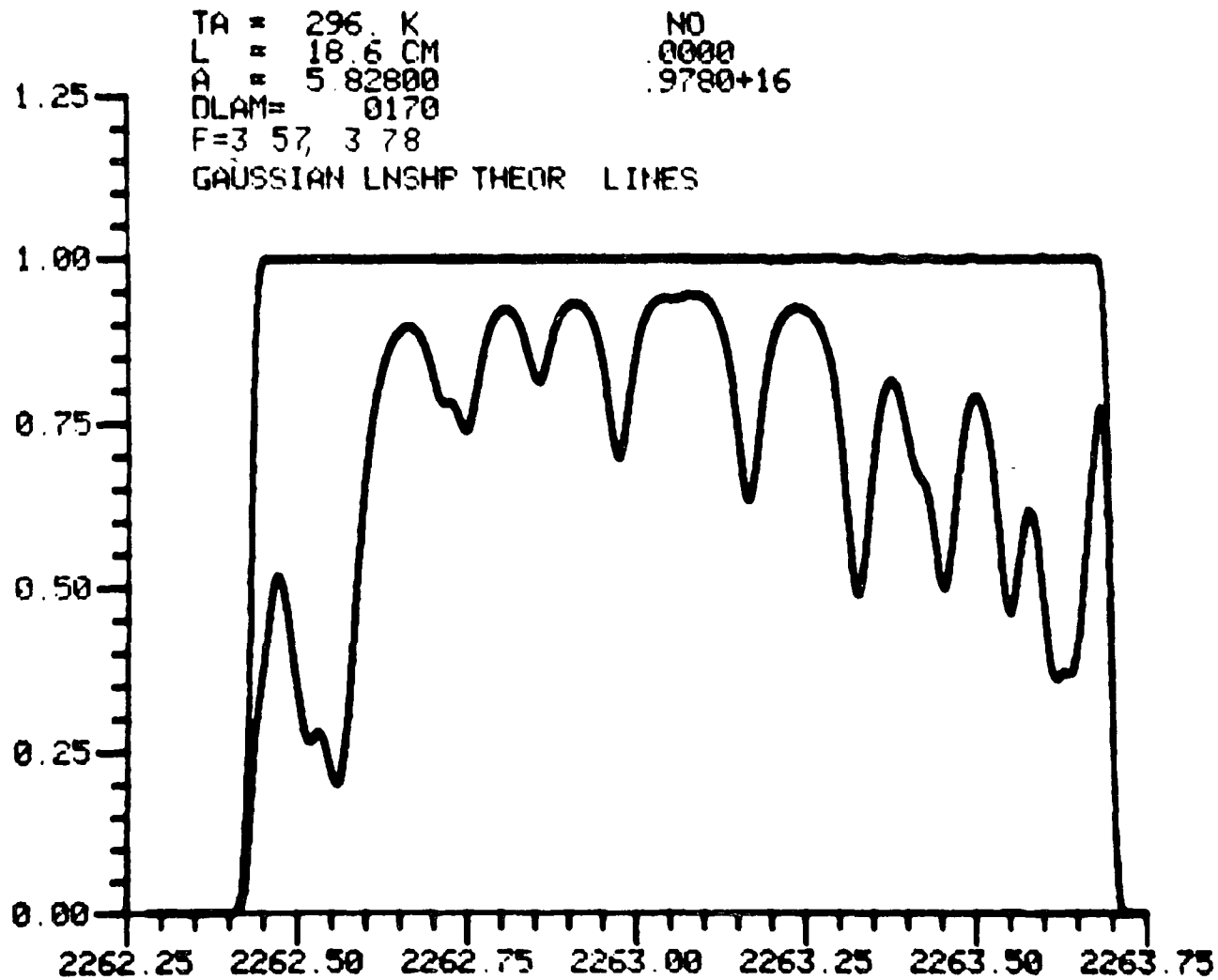

79-04-93-21

FIG. 34

TABLE III-G

BROADENING PARAMETERS FOR NO $\gamma(0,0)$
($A^2\Sigma$-$X^2\pi$) TRANSITIONS (ALL TOLERANCES ARE $\pm$ 1σ OF MEASURED DATA)

Gas	Pressure (atm)	FWHM (nm)	Slit Function (nm)	a'	C atm^{-1} K	K atm^{-1} $K^{1.2}$	d (nm)
N_2	1.00	.00562	.00176	6.04	1800		
N_2	1.50	.00743		8.50	1689		
N_2	2.00	.00965		11.31	1685		
N_2	AVG				1725	5383	1.13
CO_2	1.00	.00565	.00191	5.75	1705		
CO_2	1.50	.00720 $\pm$.00040		8.12	1605		
CO_2	2.00	.00961 $\pm$.00035		11.17	1656		
CO_2	AVG.				1655	5165	1.17
CO	1.00	.00580 $\pm$.00013	.00148	6.02	1782		
CO	1.50	.00747 $\pm$.00050		8.47	1671		
CO	2.00	.01038 $\pm$.00010		12.10	1791		
CO	AVG.				1748	5455	1.15
CH_4	1.00	.00635 $\pm$.00033	.00160	6.90	2046		
CH_4	1.50	.00836 $\pm$.00013		9.63	1904		
CH_4	2.00	.01041		10.41	1803		
CH_4	AVG				1918	5986	1.10
Ar	1.00	.00490 $\pm$.00029	.00181	4.25	1258		
Ar	1.50	.00638 $\pm$.00016		6.95	1371		
Ar	2.00	.00803 $\pm$.00040		9.22	1365		
Ar	AVG				1331	4154	1.04

There are two items of note in Table III-G. First, the collision parameters for the gases shown are very nearly the same with the exception of argon which is only a minor constituent of air fed combustion except in some research-type flames. This implies that the calibration for NO absorption will be relatively unaffected for various proportions of the gases shown assuming the gases have the same relative collision efficiency at elevated temperatures. Absent from Table III-G are two major species, H_2O and O_2. Water vapor measurements could not be made with a room temperature cell, although data were extracted from broadening measurements in $H_2/O_2/Ar$ flames as will be discussed. An effort was made to measure broadening by O_2, but the oxidation of NO to NO_2 in the presence of strong ultraviolet light was too rapid to make precise measurements. However, it was estimated from the recorded spectra that the broadening parameter for O_2 was not significantly different from the other gases tested and that its value was between that of Ar and N_2. Because of the similarity in molecular size, calculations for flames were made assuming that N_2 and O_2 have the same collision parameter. The convenience of a calibration almost independent of the gas composition should be contrasted with the extreme dependence shown for NO measurements by fluorescence (Schwarz, 1975). It should be noted that the data in Table III-G are for a constant NO density independent of pressure, so anomalously large self-broadening by NO cannot explain the relative independence of molecular type on the broadening parameter.

The magnitude of the collision cross-sections shown in Table III-G are much larger than previously reported, and may revive an argument that has existed in literature for some time. It was reported by Lambrey (1929, 1930) and by Naude (1930) that the γ system of NO showed abnormally large pressure broadening. An explanation offered by Moore, Wulf, and Badger (1953) was that this might be due to induced predisssociation. The suggestion of abnormally large broadening was opposed by Gaydon and Fairbairn (1954) and Thorson and Badger (1957). All of these measurements were made with photographic plates, which present a much more difficult problem for reducing line widths than the photometric data recorded in this study. It is not clear what constitutes abnormally large broadening, but our results are in conflict with those of the latter two references. For a partial pressure of NO (P_{NO}) of 2 torr (267 Pa) and a path length (ℓ) of 15 cm, and a total pressure with N_2 of 1 atm (101 kPa), Gaydon and Fairbairn (1954) estimate the true half-breadth or -width of a line is less than .025 $\mathring{A}$ (.0025 nm). In this study, the corresponding value is .00562 nm including the slit function and ~.0050 nm after deconvolving the slit function. Here, the optical depth was less, i.e., P_{NO} = .85 torr (113 Pa) and ℓ = 18.6 cm. Since the total pressure was the same, narrower lines rather than broader lines should have been observed. Similarly, collision cross-sections of this study are significantly greater than those of Thorson and Badger (1957) for γ (0,0) lines and those of Hadeishi et al. (1976) for γ (1,0) lines as shown in Table III-H. Included in the table are collision diameters from viscosity data, although it is not

TABLE III-H

Comparison of Collision Diameters for
Broadening of NO γ (0,0) Lines

Foreign Gas	Optical Collision Diameter (nm) This Study	Thorson & Badger	Hadeishi et al	Tajime et al	Diameter from Viscosity‡ (nm)
N_2	1.13	.38	.32+	.66*	.37
CO_2	1.17				.39
CO	1.15				.36
CH_4	1.10				.38
Ar	1.04				.34

+Assuming their collision cross-section of $1.0 \cdot 10^{-15}$ cm^2 is defined as d^2 in agreement with their references of Mitchell and Zemansky (1961).

*Based on incorrect theoretical model (see Dodge and Dusek (1979)), but Tajime et al. maintain that results will probably not drastically change.

‡Hirschfelder, Curtiss, and Bird (1954)

unusual for optical collision diameters to be larger than those from viscosity data (Engleman (1969), Townes and Schawlow (1955), Mitchell and Zemansky (1971)).

III.C.1.d. High Temperature Broadening Data and Discussion

The same procedure was used to measure the actual line profiles in the $H_2/O_2/Ar$ flames. However, the relative precision of these measurements was less than that for the room temperature static cell data because the line widths were much narrower. A FWHM of about 0.0031 nm was typical with a slit function FWHM of about 0.0018 nm. Thus, the actual line width without the instrument function was about 0.0024 nm which is not significantly larger than the slit function. The measured a' values are shown in Fig. 35 for four $H_2/O_2/Ar$ flames. Data are also shown for three $CH_4/O_2/N_2$ flames, which are quite similar. The solid line is for an a' given by the Weisskopf theory and the dotted line for the Lorentz theory. However, values of the broadening parameters C and K were estimated for both H_2O and O_2. Oxygen was assumed to be as efficient as N_2 as a broadener, which is probably reasonable. Water vapor is not similar to any of the molecules tested, but was assumed to be an efficient broadener slightly stronger than CH_4, which has a similar molecular weight. For these assumptions, the Weiskopf model fit the measured data within experimental precision. Perhaps more significantly, actual line profiles were determined at flame temperatures independent of any extrapolations from room temperature, albeit with some uncertainty.

III.C.2. Determination of Oscillator Strength

III.C.2.a. Continuum Lamp, Procedure and Results

The oscillator strength was determined from the same experimental data used for the broadening measurements. The procedure was to measure the peak absorptions on the same line pairs over the same pressure range and to compare that data with results from the computer model. Peak heights rather than areas were used to reduce the errors due to baseline uncertainty, and to simplify data reduction. For the region between the P_{11} and P_{22} bandheads used for the broadening measurements, all absorption lines are due to transitions connected with the $^2\pi_{3/2}$ level. Since Spindler et al. (1970) suggested that the strengths of the transitions connected with the $^2\pi_{1/2}$ state are about 6 percent larger than those for the $^2\pi_{3/2}$ state, separate measurement of the oscillator strength was made near the P_{11} bandhead region for transitions originating in the $^2\pi_{1/2}$ state, as shown in Fig 33. The results are given in Table III-I. Data are shown for NO mixtures in various diluent gases, but, of course, the oscillator strength must be independent of the diluent gas. Since the NO/N_2 mixture was confirmed independently of the gas vendor, the oscillator strength values for that mixture were used. The uncertainty in these values is estimated to be $\pm$ 10 percent.

MEASURED NO BROADENING PARAMETER IN FLAMES

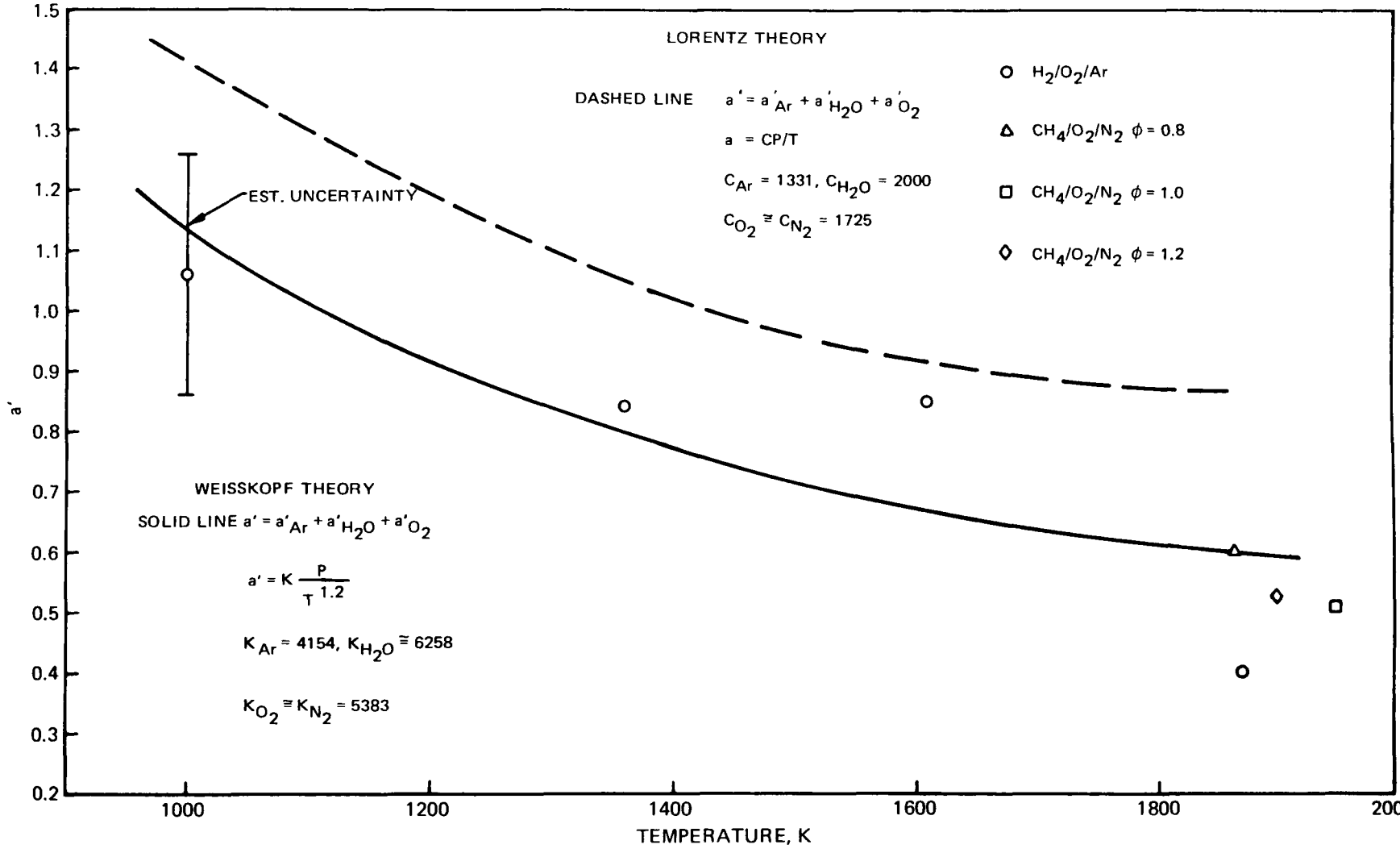

79-04-93-11

FIG. 35

TABLE III-I

OSCILLATOR STRENGTHS FOR THE NO $\gamma(0,0)$ ($A^2\Sigma^+ - X^2\pi$) BAND FOR DIFFERENT GASES*

	$f_{0,0} \times 10^4$	
NO Diluted In	$A^2\Sigma^+ - X^2\pi_{3/2}$	$A^2\Sigma^+ - X^2\pi_{1/2}$
N_2	3.57 ± 0.06†	$3.72 \pm .23$
CO_2	3.54 ± 0.004	
CH_4	3.51 ± 0.02	
Ar	3.27 ± 0.06	

*The oscillator strength must be independent of diluent gas, so the variation in values is indicative of the experimental error.

† $\pm 1\sigma$

TABLE III-J

OSCILLATOR STRENGTHS ($f_{0,0}$) FOR THE NO $\gamma(0,0)$ BAND:
LITERATURE SUMMARY

Author	Interpreted By	$f_{0,0} \times 10^4$
Weber & Penner (1957)	Pery-Thorne & Banfield (1970)	4.1 ± 0.8
Bethke (1959)	Pery-Thorne & Banfield (1970)	3.99 ± 0.4
Antropov, et al. (1964)	Pery-Thorne & Banfield (1970)	3.9 ± 0.8
Pery-Thorne & Banfield (1970)	Pery-Thorne & Banfield (1970)	$3.64 \pm .05$
Jeunehomme (1966)	Pery-Thorne & Banfield (1970)	3.0
Jeunehomme (1966)	Jeunehomme (1966)	3.8 ± 0.3
Farmer, Hasson, Nicholls (1972)	Farmer, et al. (1972)	$4.01 \pm .2$
Hasson, Farmer, Nicholls, Anketell (1972)	Hasson, et al. (1972)	$4.09 \pm .1$ $4.33 \pm .2$
Average		3.87
Huber and Herzberg (1979) Recommended Value		3.8
This Study ($^2\pi_{1/2}$)		3.72 ± 0.4

These results are compared with some previous values in Table III-J. The value for the $^2\pi_{1/2}$ state was chosen for comparison as it is the more heavily populated state (by a factor of 1.8) at room temperature. The oscillator strength determined in this study agrees well with the previous results, but appears to be slightly lower than the most reliable values. However, this study is unique in that the oscillator strength has been measured directly from individual lines in high resolution. We are not familiar with any previous work which provides such a direct measure of individual line strengths.

III.C.2.b. Narrow-Line Lamp, Procedure and Results

The broadening data determined by the continuum lamp were used in the model to predict transmission by the narrow-line lamp. The oscillator strengths were adjusted from those determined by the continuum lamp in order to match experimental data obtained with the narrow-line lamp. The oscillator strength should be same for both models, but several sources of error can cause small differences.

The narrow-line lamp contains a small amount of radiation not accounted for in the model. This can be seen by comparing Figs. 21 and 22 which display output from the narrow-line lamp before and after absorption by a low pressure NO sample. The major peaks denoted 1-5 show absorption as predicted by the model, but the low level light between the peaks is not absorbed by the NO. This tends to decrease the f value required to fit experimental data. An estimate of the effect of the "extra-light" on f value is shown in Table III-K along with the values determined for the narrow-line lamp before correction. There may be other factors associated with this difference in f values, such as a shift in frequency for the emission lines due to the strong electric fields in the lamp, but these have not been investigated.

III.C.3 Summary of Hot Calibration Device Data

III.C.3.a Flowing Gas Heater: Summary of Concentration and Temperature Data

The carrier flow rate through the flowing gas heater was held constant at 0.109 moles/sec for all temperatures and gases. Typical concentration and temperature profiles are depicted in Figs. 8-10 and 36. Various concentrations of nitric oxide were added to the main gas flow at each temperature, and for each condition gas samples were extracted from the center of the optical axis and analyzed using the chemiluminescence detector. Although measured values were nearly always lower than the calculated seed level, the two values were usually within 7%. Predicted nitric oxide concentrations from the optical measurements are compared to the average of the seed and measured values.

TABLE III-K

OSCILLATOR STRENGTHS ($f_{0,0}$) FOR NO $\gamma(0,0)$ BAND: A COMPARISON

	$f_{0,0} \times 10^4$		
Transition	Continuum Lamp	Narrow-Line Lamp	Narrow-Line Lamp With "Extra-Light" Correction
$^2\Sigma-^2\pi_{1/2}$	3.72	3.53	3.76
$^2\Sigma-^2\pi_{3/2}$	3.57	3.20	3.43

NITRIC OXIDE PROFILES OVER FLOWING GAS HEATER AT ELEVATED TEMPERATURES

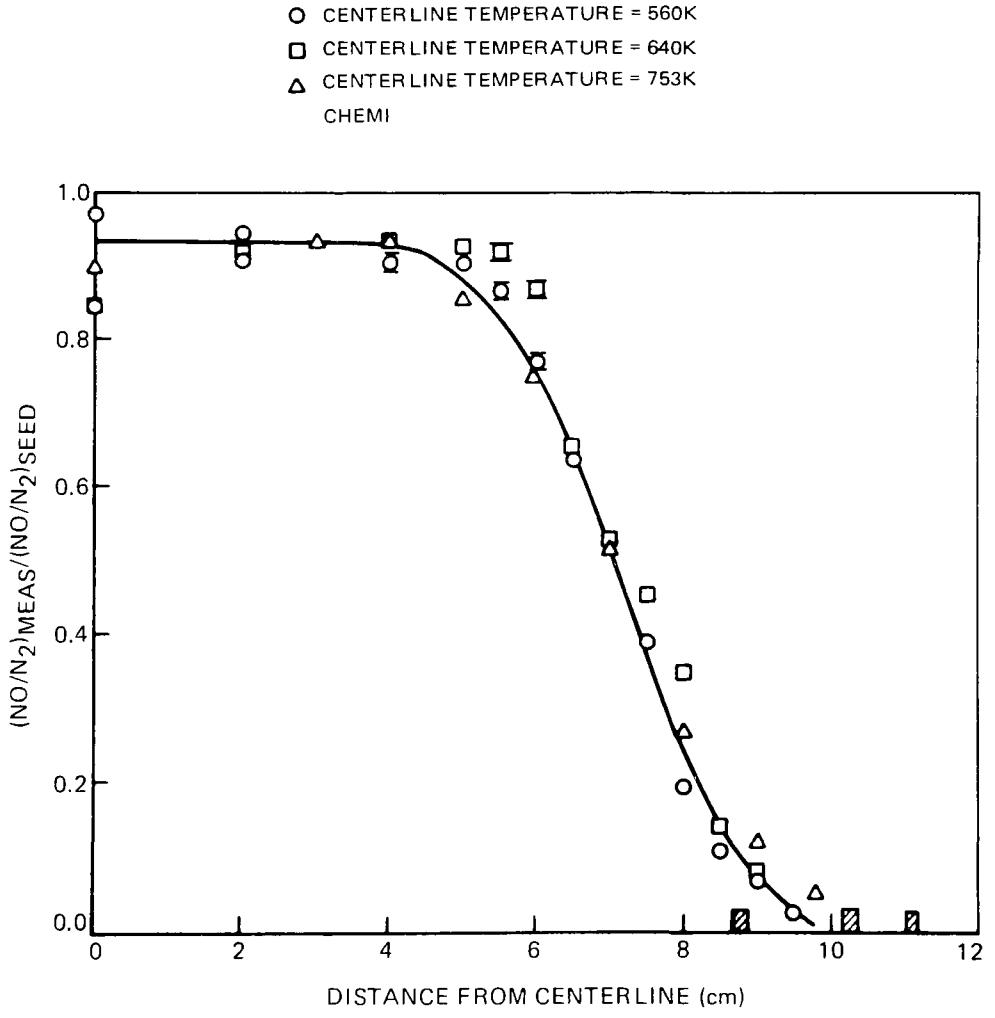

79-04-54-6

III.C.3.b Flat Flame Burner: Summary of Concentration and Temperature Data

For the optical measurements of NO, four flame conditions were selected. The thermocouple temperatures (uncorrected for radiation) at the centerline were 950, 1220, 1400 and 1600 K. The flow conditions for these flames are listed in Table II-B. Profiles of thermocouple temperatures and radiation corrections are shown in Figs. 17 and 37-39. Various NO concentrations were introduced into the unburned gas for all four flame conditions. Concentration profiles (normalized) are shown in Fig. 16. Except for a few high seed levels of NO during the gas correlation experiments, all nitric oxide was introduced using the 10% NO and 90% Ar mixtures. The excess argon associated with the added NO is not included in the tables and typically amounts to 1 to 2% of the total gas flow. For several of the gas correlation experiments, the 25% NO, 75% Ar mixtures were used to reduce the effect of the added argon. Once conservation of nitric oxide had been confirmed using mass spectrometric analysis, it was not necessary to repeat these measurements for all tests. During the UTRC optical measurements, therefore, only cold flow measurements of NO in Ar were made before and after each set of experiments. These measurements were made to verify orifice calibrations and to ensure that leaks or other problems did not develop in the gas handling system. Concentrations of nitric oxide during flame conditions were determined using calculated flow rates and assuming complete combustion to water. Since the total concentration of other species such as H_2, H_2O_2 and radicals is rather small, this later assumption provides a good and simple approximation. According to techniques outlined in Section II.B.3.d, the mass spectrometric data were reduced to provide the profiles of other species within the flame. These data are reproduced in Figs. 40 and 41 for two flame conditions.

Profiles of nitric oxide and optical measurements over the burner assembly were also made at room temperature for comparison with the FGH and the static cell. The profile data is reproduced in Fig. 42.

III.C.4 Narrow-Line Calibration Study

As previously mentioned, one of the principal goals of the first phase of this contract was the development of a model for predicting the transmission of narrow-line NO radiation through a gas containing NO molecules at temperature range from 300K to 2000K. The validity of the model would be certainly established if an agreement of approximately $\pm$ 10% in NO concentration between theoretical prediction and measurement was achieved. The bulk of the data presented in this section are within the specified tolerance. Those data that are not within this tolerance reflect some of the experimental difficulties associated with NO chemistry and measurement.

HORIZONTAL TEMPERATURE PROFILES OVER FLAT FLAME BURNER

$H_2/O_2/Ar$

UNCORRECTED TEMPERATURE = 950K

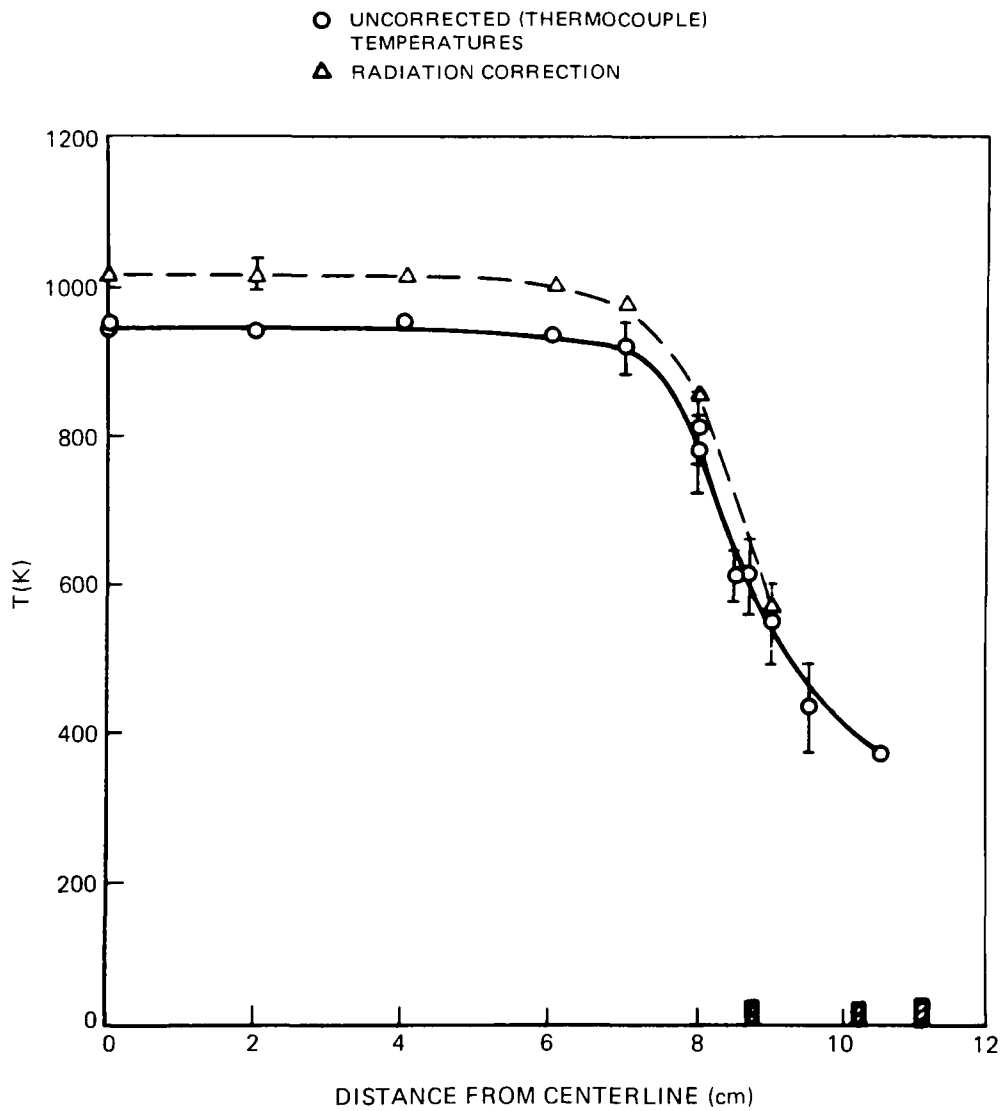

79-04-54-12

HORIZONTAL TEMPERATURE PROFILES OVER FLAT FLAME BURNER

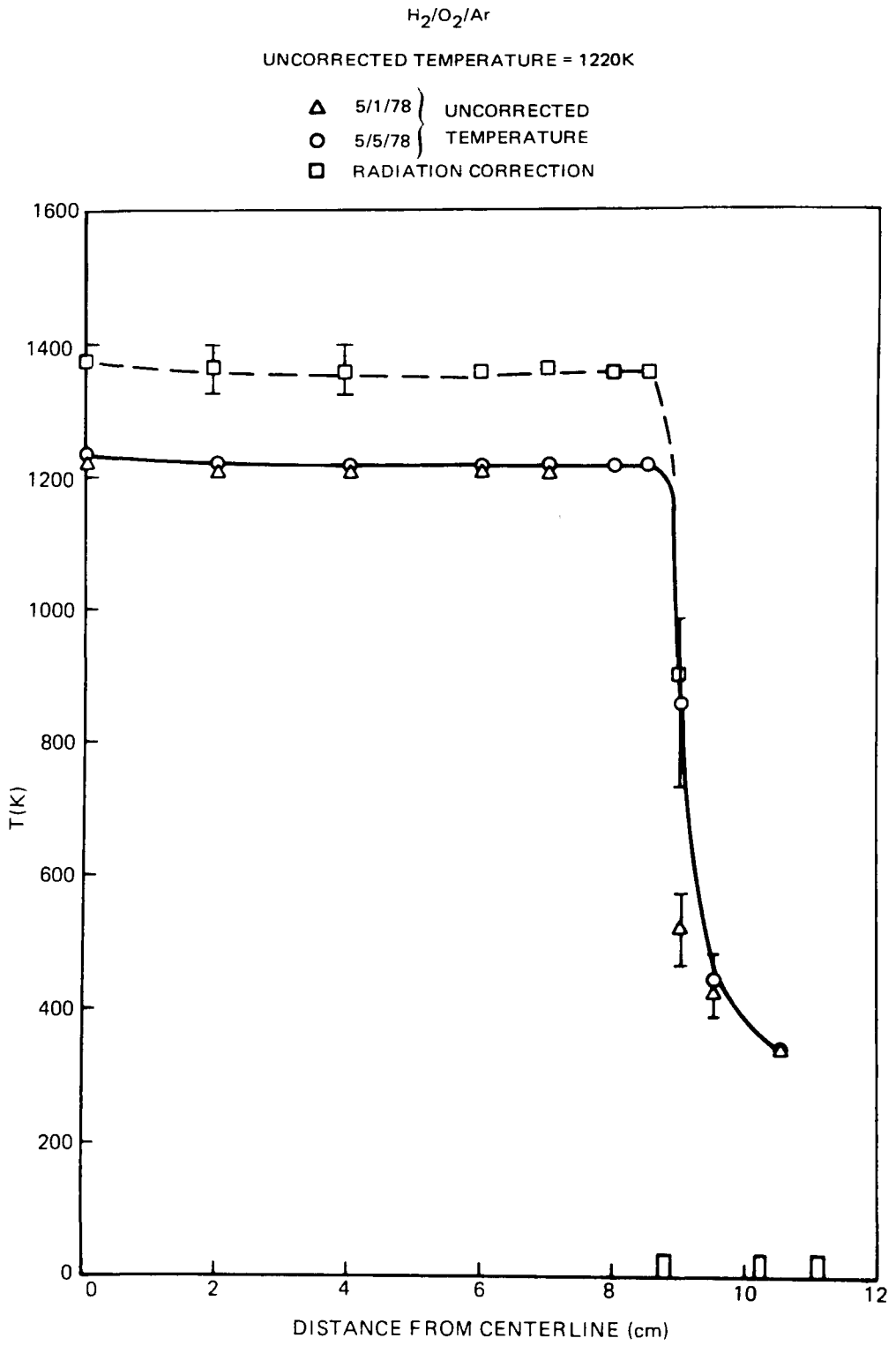

79-04-54-13

HORIZONTAL TEMPERATURE PROFILES OVER FLAT FLAME BURNER

$H_2/O_2/Ar$

UNCORRECTED TEMPERATURE = 1600K

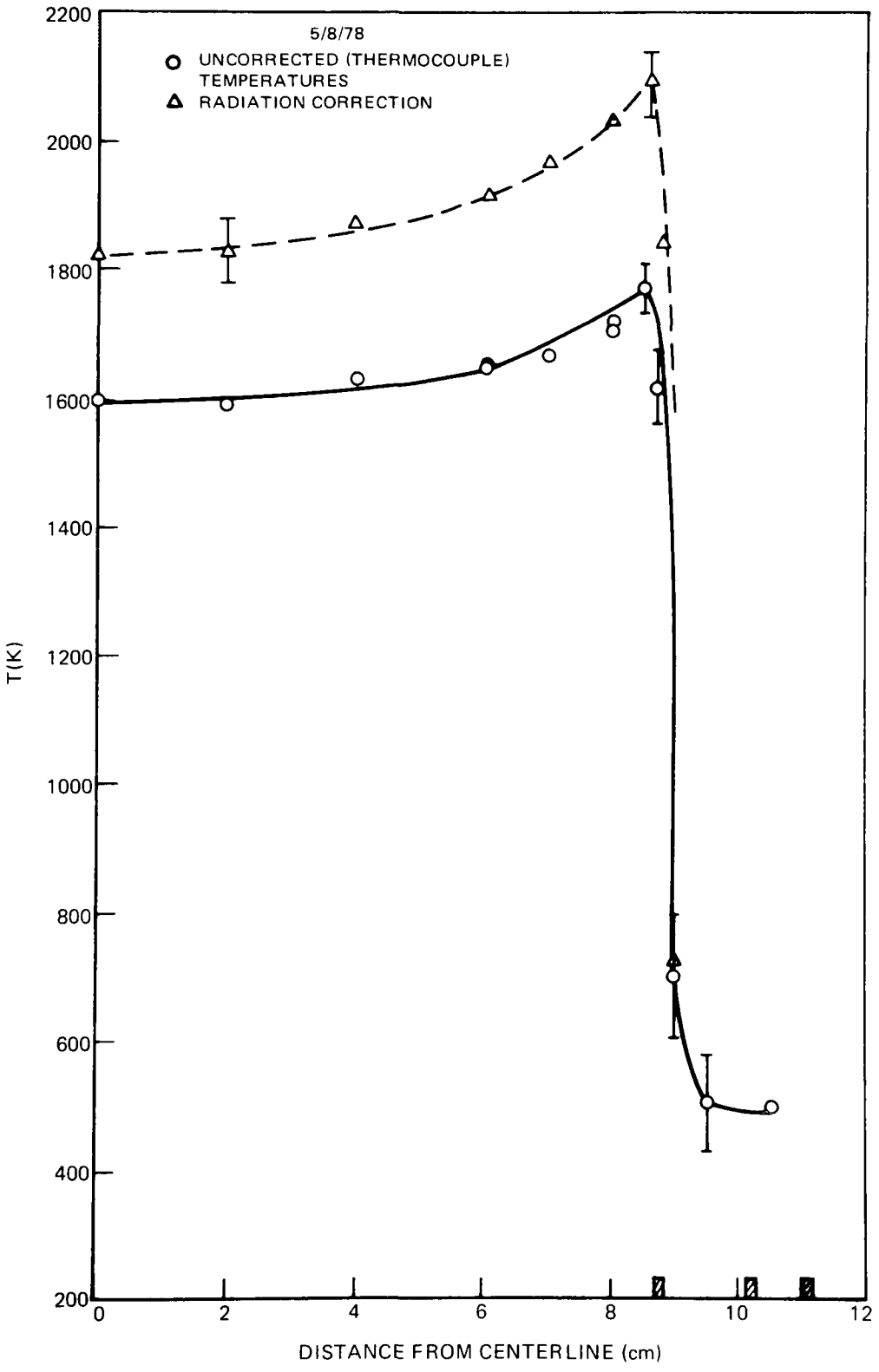

79-04-54-15

HORIZONTAL PROFILES OF MAJOR SPECIES OVER FLAT FLAME BURNER

$H_2/O_2/Ar$

UNCORRECTED TEMPERATURE = 950 K

MASS SPEC ANALYSIS

T = 950K (UNCORRECTED)

PROBE B

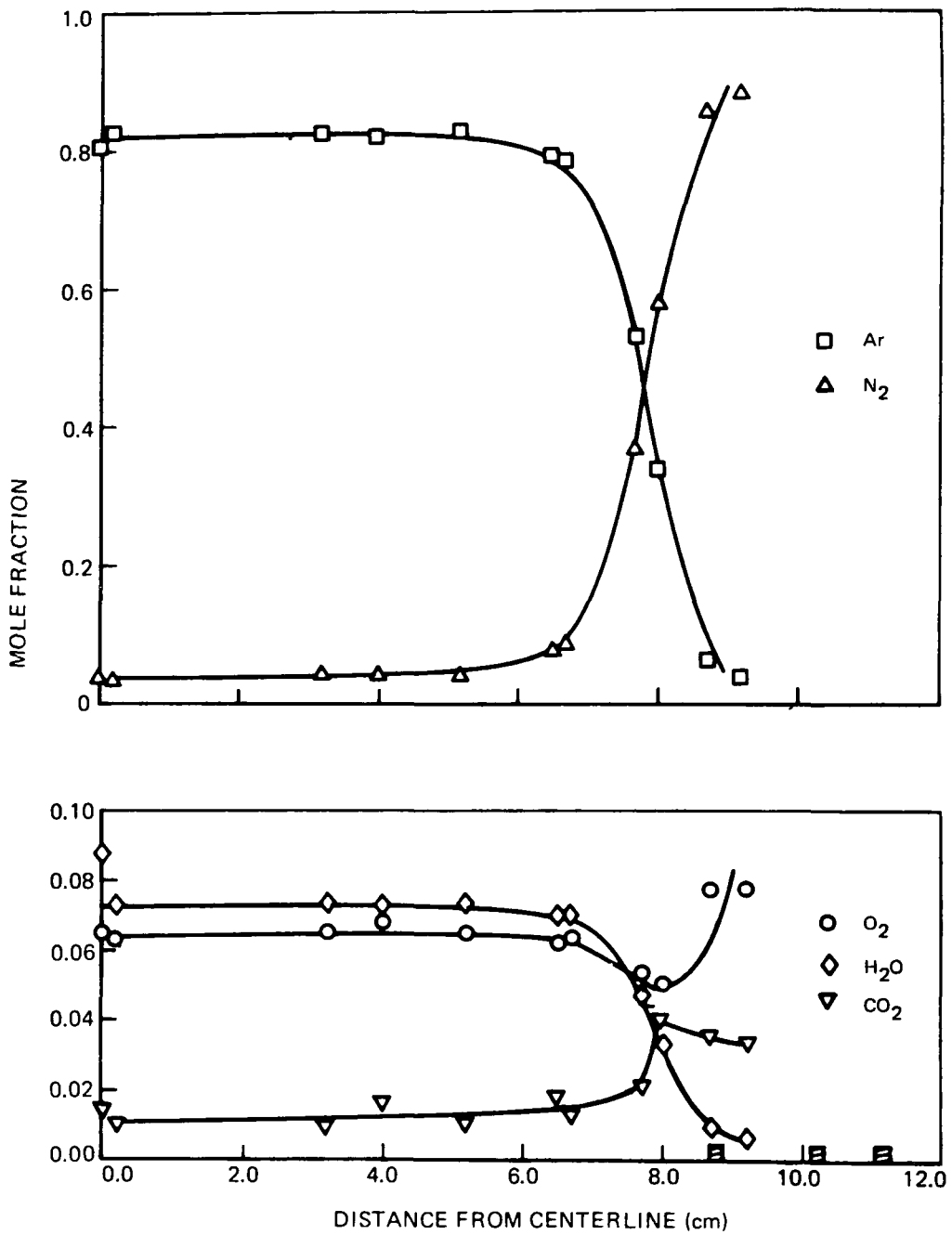

79-04-54-10

HORIZONTAL PROFILES OF MAJOR SPECIES OVER FLAT FLAME BURNER

$H_2/O_2/Ar$

UNCORRECTED TEMPERATURE = 1220K

MASS SPEC ANALYSIS

T = 1220K (UNCORRECTED)

PROBE B

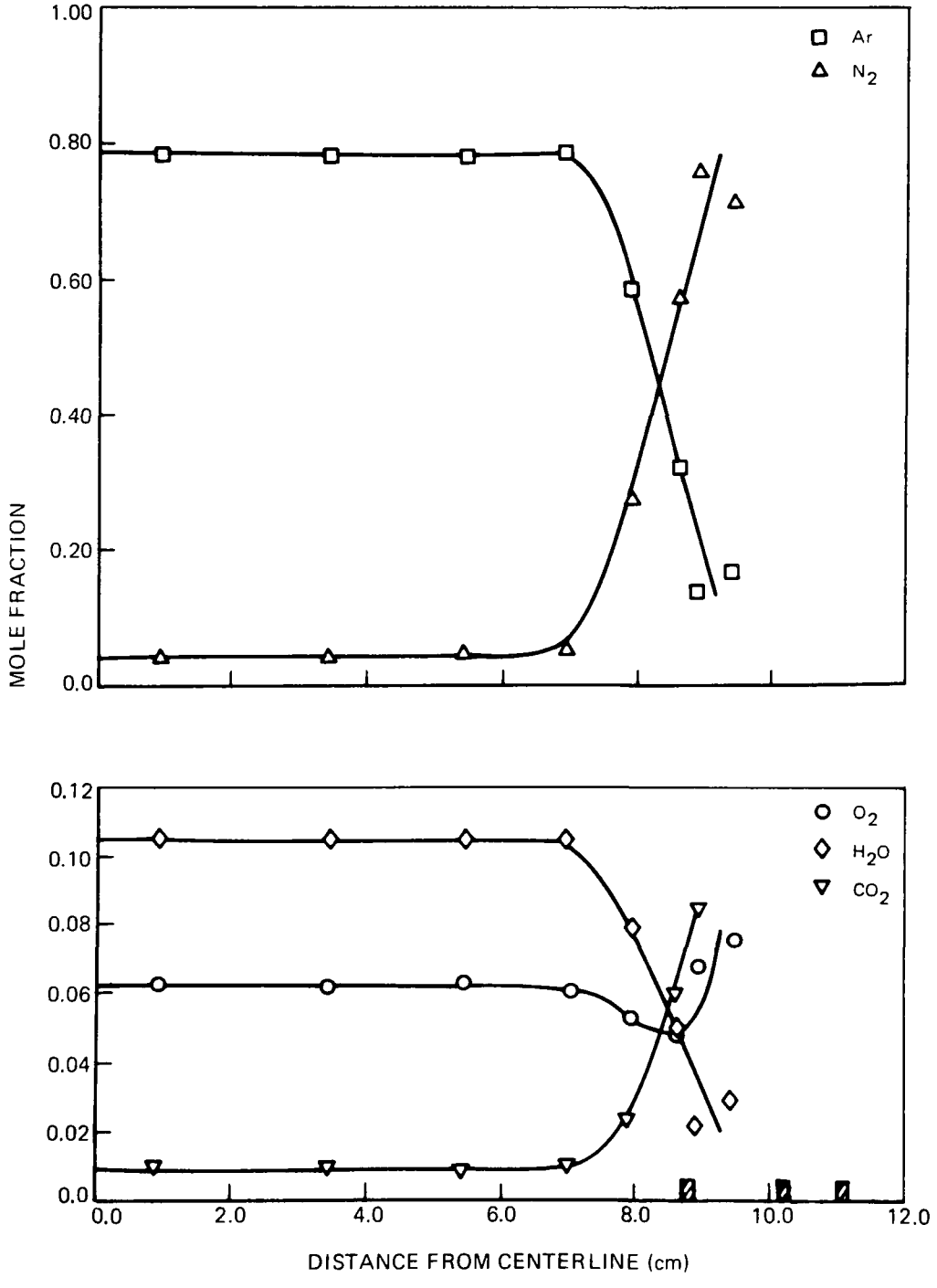

79-04-54-11

NO HORIZONTAL PROFILE OVER FLAT FLAME BURNER (COLD FLOW)

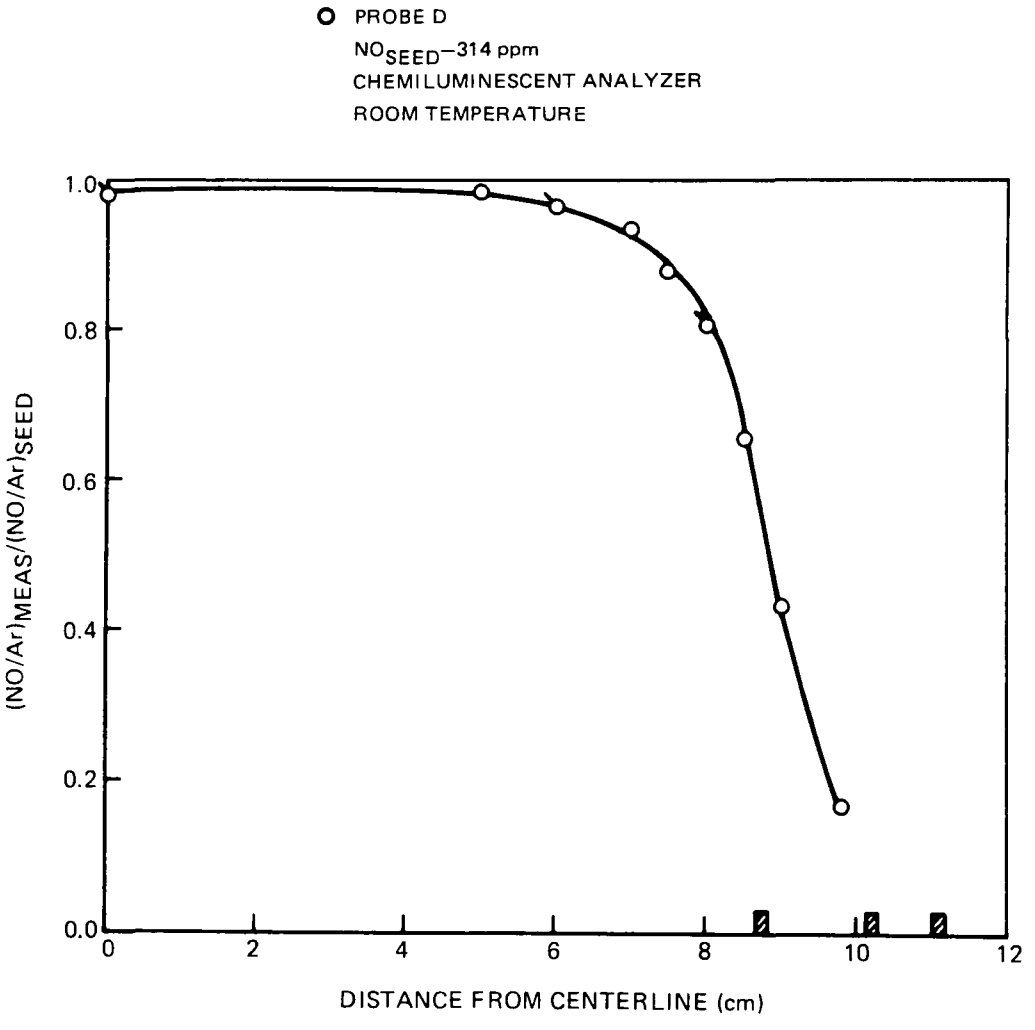

79-04-54-9

III.C.4.a Static Cell Optical Measurements

A number of tests were performed in an 18.6 cm long static cell at room temperature. Tests were performed in high resolution on single line pairs and in low resolution (.146 nm FWHM) using gases blended with the gas mixing system and gas mixtures obtained from vendors. Data were obtained for a pressure range of .0627 atm (6.35 kPa) to 1.32 atm (134 kPa). Some of these data for low resolution scans with gases (NO diluted in N_2) checked against National Bureau of Standards reference gases and used without dilution are shown in Table III-L. The table lists the cylinder concentration (NO in N_2 by volume), total pressure, optical depth, and the measured transmission for the two bandheads which are displayed for a spectra at this resolution in Fig. D-8. The first bandhead is located at about 226.8 nm and the second is located at about 226.15 nm. Also given in Table III-L is the transmission as predicted by the computer model, and an estimate of the error that would be incurred in predicting the NO concentration in the static cell from the measured transmission and the computer model. Since the NO concentration is approximately proportional to ln T, where T is the transmission, the error E is defined by $E = 1 - (\ln T_{PRED}/\ln T_{MEAS.})$, which is multiplied by 100 to convert a percent error. Thus, if the known NO concentration is multiplied by the factor (1 + E), the predicted and measured transmission values will agree. This same definition is used for the flowing gas heater and flat flame burner, except than the factor (1 + E) is multiplied by the probe determined NO profile for agreement between predicted and measured transmissions.

These tests were used to obtain an estimate of the apparent line width of the narrow-line source, and the effective oscillator strength. The line width in the source could not be measured directly, but could be inferred from measurements in the static cell over a range of pressures. At the higher pressures, the absorption is almost independent of the source line width, and the absorption data at these pressures were used to determine the effective oscillator strength when using the narrow-line lamp. The oscillator strength determined in this manner resulted in a slightly smaller value than that determined with the continuum source as shown in Table III-K, with the difference attributable (at least partly) to the "extra light" in the narrow-line lamp, as discussed previously. At the lower pressures, the emission line width from the lamp becomes comparable with the absorption line width, and the transmittance at these pressures depends on the value assumed for the source line width. The best fit to the static cell data were obtained for a source Doppler width with a temperature of 600 K. This compares favorably with the value of 561 K for the lower temperature part of the Boltzmann plot for the line strengths in the narrow-line lamp (Fig. 20). Meinel (1975) has suggested that this low temperature part of the Boltzmann plot should give a measure of the translational temperature of the lamp, which, in turn, determines the Doppler width of the emitted lines. This agreement may be fortuitous, because the "extra light" phenomena should also affect the apparent lamp line width.

TABLE III-L

Static Cell Calibration Data (NO in N2)

Cylinder Concentration (ppm)	Total Pressure (atm)	Optical Depth (cm^{-2})	1st Bandhead Trans. Meas.	1st Bandhead Trans. Pred.	Error in Pred. NO Conc. (%)†	2nd Bandhead Trans. Meas.	2nd Bandhead Trans. Pred.	Error in Pred. NO Conc. (%)†
93.3	1.315	$5.679 \cdot 10^{16}$	.896	.890	-6.5	.824	.821	-1.9
93.3	1.000	$4.317 \cdot 10^{16}$	.900	.900	-0.2	.843	.842	-0.8
93.3	.751	$3.240 \cdot 10^{16}$	.912	.909	-3.2	.864	.859	-3.5
93.3	.500	$2.159 \cdot 10^{16}$	.917	.920	+3.1	.879	.879	-0.1
93.3	.474	$2.044 \cdot 10^{16}$	.918	.921	+4.4	.880	.881	+0.9
93.3	.250	$1.079 \cdot 10^{16}$	.934	.939	+9.2	.906	.909	+3.1
93.3	.125	$5.405 \cdot 10^{15}$	.956	.959	+5.7	.938	.938	+1.3
470	1.001	$2.176 \cdot 10^{17}$	.627	.625	-0.7	.465	.469	+1.2
470	.751	$1.633 \cdot 10^{17}$	.646	.633	-4.5	.513	.498	-4.6
470	.503	$1.093 \cdot 10^{17}$	.674	.666	-2.9	.568	.555	-4.2
470	.249	$5.426 \cdot 10^{16}$	.738	.734	-1.5	.668	.651	-6.2
470	.125	$2.721 \cdot 10^{16}$	.816	.812	-2,4	.762	.748	-6.8
470	.0627	$1.363 \cdot 10^{16}$	.887	.882	-4.2	.846	.835	-7.5

† These errors are based on more significant figures than shown in this table. See discussion in Section III.C.4.a for definition of error.

III.C.4.b Flowing Gas Heater (FGH) Optical Measurements

Calibration tests were performed with the flowing gas heater for NO diluted in pure N_2 and pure Ar at a total pressure of 1 atm (101 kPa) and over a temperature range from 295K to 825K. All of these absorption spectra were obtained in low resolution (FWHM = .146 nm = 1.46 Å), and transmission data were reduced for the first bandhead, located at about 226.8 nm and the second bandhead, located at about 226.15 nm. A comparison of the computer model prediction versus measured transmission is shown in Table III-M. The values from the computer model were based on an NO concentration which was the average of the measured value (chemiluminescent analyzer) and the value computed from flow calculations for the critical orifices. The ratio of the measured NO concentration to that predicted by the flow system was $\sim$ 0.96, which was less than unity because of diffusion of purge gas into the main stream and, possibly, calibration errors. The actual temperature and NO concentration profiles were approximated as two or three zones of constant temperature for computer predicted transmissions. The data were reduced assuming Lorentz broadening, that is $a' = CP/T$. For comparison with the data reduction procedure used for the flat flame burner, the Weisskopf dependence ($a' = KP/T^{1.2}$) could have been employed for the FGH. At room temperature the Weisskopf theory would give the same result as the Lorentz theory, but, at the highest temperatures in the FGH, the Weisskopf theory would systematically reduce the predicted transmissions as shown for Run 43 in Table III-M. At these temperatures the predicted absorptance (-ln T) is increased about 11 percent, so that the numbers in column "Error in Pred. NO Conc." would be reduced by about 11 percent. The overall errors would probably be slightly reduced by this procedure.

III.C.4.c Flat Flame Burner (H_2/O_2/Ar/NO) Optical Measurements

Optical calibration for NO absorption was performed for H_2/O_2/Ar/NO flames at 1 atm (101 kPa) over a temperature range from 1000K to 1860K. Data were obtained independently for the continuum lamp and the narrow-line lamp.

The continuum lamp data were used principally to determine the line widths in the flames, but the transmission information was also available, and since this high resolution technique was used on some of the $CH_4/N_2/O_2$/NO flames of Task III, data were reduced for the H_2/O_2/Ar/NO flames to determine its applicability. Transmission data for three flames at 1000K, 1360K and 1610K are compared with computer model predicted transmissions in Table III-N. These were reduced based on NO centerline levels computed from flow calculations for the critical orifices, which were checked in cold flow, and profile data as shown in Fig. 16. Two or three zones of constant temperature were assumed.

The narrow-line lamp data were obtained for four different flame temperatures with at least two NO concentrations at each temperature. The computed and actual transmissions for the two bandheads observed in the low resolution spectra are

TABLE III-M

Flowing Gas Heater (FGH) Optical Measurements

Run Number	Temp (Centerline) (K)	NO Conc. (Centerline) (ppmV)	Diluent Gas	1st Bandhead Trans. Meas.	1st Bandhead Trans. Pred.	Error in Pred. NO Conc. (%)†	2nd Bandhead Trans. Meas.	2nd Bandhead Trans. Pred.	Error in Pred. NO Conc. (%)†
31	295.8	287	Ar	.735	.752	+7.9	.609	.643	+12.3
32	295.8	112	Ar	.882	.895	+13.3	.818	.841	+16.3
33	295.8	108	N_2	.904	.912	+9.1	.848	.861	+9.9
34	295.8	280	N_2	.779	.790	+6.2	.661	.684	+9.2
35	493.	112	Ar	.926	.930	+6.4	.899	.903	+4.7
36	453.	293	Ar	.793	.815	+13.3	.726	.750	+11.4
37	524.	111	N_2	.945	.944	−2.6	.920	.920	+0.4
38	452.	280	N_2	.823	.843	+14.4	.764	.783	+10.1
39	825.	110	Ar	.962	.961	-2.6	.947	.946	-0.6
40	788.	287	Ar	.891	.896	+5.0	.854	.859	+3.5
41	768.	284	N_2	.907	.908	+1.9	.869	.873	+3.1
42	793.	109	N_2	.962	.965	+11.8	.949	.951	+4.9
43	756.	430	N_2	.856	.862	+5.2	.805	.811	+3.6
44	738.	521	Ar	.791	.809	+10.7	.733	.747	+6.2
43§	756	430	N_2	.856	.847	- 6.8	.805	.794	-6.1

† These errors are based on more significant figures than shown in this table. See discussion in Section III.C.4.a for definition of error.

§Test case for a′ determined from Weisskopf theory. See text.

TABLE III-N

CONTINUUM LAMP TRANSMISSIONS FOR
$H_2/O_2/Ar/NO$ FLAT FLAMES

Spectral Lines	1000K Flame		1360K Flame		1610K Flame	
	Meas.	Computer Model (a'=1.10)	Meas.	Computer Model (a'=0.8)	Meas.	Computer Model (a'=0.8)
$P_{22}(15.5)+Q_{12}(15.5)$	.643	.628	.694	.702	.751	.759
$Q_{22}(8.5)+R_{12}(8.5)$ $+P_{12}(26.5)$	.597	.599	.702	.709	.744	.760
$P_{22}(16.5)+Q_{12}(16.5)$	.607	.634	.690	.688	.738	.757
$Q_{22}(9.5)+R_{12}(9.5)$	.620	.598	.695	.702	.754	.764
$R_{22}(5.5)$	.879	.886	.920	.924	.940	.941
$P_{22}(17.5)+Q_{12}(17.5)$	.666	.647	.688	.700	.748	.761
$Q_{22}(10.5)+R_{12}(10.5)$	.554	.586	.672	.705	.751	.753
AVG. ERROR IN PREDICTING NO FROM MODEL (%)†		+1.2		+4.7		+4.9
ACTUAL NO CONCENTRATION (PPMV)	1466		1690		1867	

†See discussion in Section III.C.4.a for definition of error.

shown in Table III-0. The computed transmissions were based on a centerline value which was the average of calculated levels for the critical orifices and chemiluminescent measurements (corrected for Ar response), and profile data as shown in Fig. 16. Two or three zones of constant temperature were assumed. The a' values used to generate the computer spectra were taken from the solid line in Fig. 35. An estimate of the error in predicted transmission due to the uncertainty in the a' values is also shown in Table III-0 for the highest temperature flame. The uncertainty in a' of 0.6 $\pm$ 0.2 results in a variation of predicted NO of $\pm$ 9.7 percent.

The overall agreement between predicted and measured values was within $\pm$ 16 percent for the flame data, which was slightly greater than the original goal of $\pm$ 10%, but was reasonable given the experimental uncertainties and relative to the previously reported discrepancies. It should be noted that the overall errors result from the summation of errors in the model, scatter in the experimental spectra, uncertainties in the broadening parameter a', uncertainties in the flame profiles for temperature and NO, and errors in the gas blending procedure.

TABLE III-O

FLAT FLAME BURNER RESULTS
(H_2/O_2/Ar/NO FLAMES)

Temp (K)	Conc. (Centerline) (ppmV)	Run#	a' (Centerline)	1st Bandhead Trans. Meas.	1st Bandhead Trans. Pred.	Error In Pred. NO Conc. (%)†	2nd Bandhead Trans. Meas.	2nd Bandhead Trans. Pred.	Error In Pred. NO Conc. (%)†	Avg. Error (%)†
1000	653	2	1.14	.824	.811	-8.2	.790	.750	-22.0	-15.1
1000	1027	1	1.14	.743	.720	-10.6	.690	.635	-22.3	-16.4
1360	999	3	0.80	.822	.835	+ 8.0	.777	.776	- 0.5	+ 3.6
1360	1194	6	0.80	.790	.809	+10.1	.729	.738	+ 3.9	+ 7.0
1610	1092	4	0.67	.852	.864	+ 8.7	.807	.811	+ 2.3	+ 5.5
1610	1575	5	0.67	.793	.811	+ 9.7	.734	.741	+ 3.1	+ 6.4
1610	1988	11	0.67	.740	.768	+12.3	.672	.687	+ 5.5	+ 8.9
1870	1231	7	0.60	.866	.889	+18.2	.824	.842	+11.2	+14.7
1870	2324	9	0.60	.769	.802	+16.0	.718	.726	+ 3.3	+ 9.6
§1870	2324	9	0.40	.769	.781	+ 6.2	.718	.702	- 6.4	- 0.1

†See discussion in Section III.C.4a for definition of error.

§Test case for sensitivity to a'. See text.

IV. DISCUSSION

A. Introduction

The computer model that was developed by W. K. McGregor, M. Davis, J. D. Few and their colleagues at Arnold Research Organization (ARO) was one of the starting points of this study. Initially, it was thought that the model rested on a sound theoretical basis and was supported by strong experimental evidence. However, experimental data obtained with the static cell, i.e., under the most ideal conditions, were not in agreement with the predictions of the model. A thorough examination of the program for errors in translation onto the UTRC UNIVAC 1110 computer revealed no such errors. Additional verification of proper translation was obtained when the results of test computations made at both UTRC and ARO were in agreement. An intense review of gas standards, mixing procedure, optical and electronic instrumentation did not yield the cause of the disagreement. Consequently, the theoretical basis of the model was studied and found deficient. The errors that were discovered are reported in Appendix B. These errors appear in reports published since 1973; however, a precise knowledge of the various forms of the model from 1973 through 1977 is not known. Suggested refinements to the model delivered to UTRC are also noted in Appendix B. A new model was developed on the theory presented in Section III of this report. A description of the new model is given in Appendix D. A major subroutine entitled NO·Spect (Appendix D) was also provided to ARO in July 1978. This subroutine can be used to interpret only resonant lamp data.

B. Comments on ARO AEDC TMR-79-P7

As part of this study, measurements were made on the UTRC calibration devices by ARO personnel using a capillary discharge lamp. The results of those measurements are contained in an internal ARO Report (AEDC TMR-79-P7) by Few, McGregor, and Keefer (1979). This report will be published externally at a later date.

In order to prevent further confusion in the literature stemming from the errors contained in the reports listed in Appendix B and problems contained in AEDC TMR-79-P7, it seemed necessary and was requested by the FAA that the content of this latest report be discussed here. That report has four major sections each of which will be considered below.

IV.B.1. TMR Introduction

The last part of this section should be expanded to include a statement that the agreement of the optical measurements with the calculated input of NO concentration in conjunction with the probe profiles are generally within the uncertainties of the probe and optical measurements. As written it could be inferred that the uncertainties rest only in the probe measurements. Such an interpretation would not be accurate as will be indicated later in this review.

IV.B.2 TMR Review of Model

In subsection A which is on the spectroscopic theory, it is stated that the Hönl-London factors are those of Earls as previously defined in a report by Davis, McGregor, and Few (AEDC-TR-76-12, February 1976). Unfortunately some of the Hönl-London factors included in that report are in error. In subsection B on model parameters, the authors state that the oscillator strength value of $4.09 \pm 0.1 \times 10^{-4}$ Hasson et al) appears to be the most reliable. The author's judgment is neither in agreement with Huber and Herzberg (1979) who prefer 3.8×10^{-4} nor with 3.7×10^{-4} determined by UTRC. With regard to source temperature, it should be remembered that 950 ± 25 K is a factor of 3 higher than that previously reported (e.g. McGregor, Few. Litton (1973), Few Bryson and McGregor (1976)). Moreover, the broadening parameters reported are a function of both the oscillator strength that was selected from the literature and the source temperature, and, hence, are inferred and not directly determined.

IV.B.3 TMR Optical Results

In the description of the calibration facility, it is incorrectly stated that the majority of the sampling measurements on the flowing gas heater were made with the mass spectrometer. In fact, the bulk of these measurements was made with the chemiluminescent analyzer. It is also incorrectly stated that the buffer flame of the flat flame burner was lean burning $H_2/O_2/Ar$. The buffer flame was actually a lean $CH_4/O_2/Ar$ flame. Figures 5 and 6 give respectively concentration and temperature profiles over the flowing gas heater. In these figures, the uncertainty is listed as unknown. These uncertainties are given in Figures 9 and 10 in the main body of the Task I Report. Similarly, Figures 7 and 8 of the ARO report give concentration profiles with "unknown" uncertainties. See Figures 42 and 16 of the Task I Report. Also, in Figure 11 of the ARO report, the 40% uncertainty refers only to the radiation correction factor and is not the uncertainty of the temperature measurement itself. It is not clear why, as in the Introduction, the implication is given that the uncertainties in the experimental data reside only in probe, thermocouple, and calibration device performance. Indeed, this is an incomplete assessment of the uncertainties. A complete assessment of the errors should also include variations in lamp intensity, drift in system electronics, trigger and grating scan uncertainties and their influence on the signal averaging process used by ARO. These experimental uncertainties were readily identifiable during the ARO measurements made at UTRC.

With regard to data treatment, the new model developed by ARO is briefly described. This new model does not employ a Beer's Law zonal treatment of temperature and concentration inhomogeneities encountered in combustion systems. Instead, the new model keeps a detailed knowledge of the emission line shape from zone to zone. Figure 17 illustrates in an exaggerated manner the importance of a problem which can occur when the absorber line is narrower than the source line. Such a situation, it is stated, would be encountered for a jet engine exhaust under altitude conditions. This statement is extremely vague and in the context of this study is misleading. No information is given on what altitude such a condition may occur. Moreover, no data were obtained

in this study that required consideration of this phenomena. In addition, if the ICAO standard atmosphere is used to provide temperature and pressure as a function of altitude and if 600 K is assumed to be a typical static temperature of a jet exhaust, then the absorbing lines at 35,000 feet are still considerably wider than the emission lines. Even at 65,000 feet, significant transmitted line center "burnout" is not expected.

Equation (17) $[\Delta c = \{(\ell n\, \tau_{meas}/\ell n\, \tau_{cal})-1\} \cdot 100]$ that was used to compute the percent error in concentration given in Tables 3, 4, and 5 is not the same expression used in Task I Report Tables III-L, III-M, and III-O. The expression used in Task I Report was

$$\Delta c = \left(1 - \frac{\ell n\, \tau_{cal}}{\ell n\, \tau_{meas}}\right) \cdot 100$$

Using equation (17), the root-mean square average departures of the calculated NO concentration is reported in the TMR as $\pm 9\%$ for the absorption cell, $\pm 18\%$ for the flowing gas heater, and $\pm 21\%$ for the flat flame burner. This method of summarizing the errors obscures the fact that the errors indicated in Tables 4 and 5, which respectively contain data from the flowing gas heater and flat flame burner are not really random but systematic. In fact, for the bulk of the data reported in those Tables, the error is positive and, generally, increases with temperature. The average error for all the ARO tests from room temperature to the highest temperatures was equivalent to an overprediction of NO using the optical technique by + 15%, but at the highest temperature the overprediction was + 29%. This systematic error is most likely due to deviations from Lorentz broadening theory. This deviation is discussed in Section III of Task I Report. Moreover, the errors (-15% to +4.8) listed in Table III for the absorption cell give an indication of the errors associated with the optical measurement system used by ARO.

IV.B.4 TMR Summary

With regard to the broadening study results, it is suggested that the broadening due to H_2O is the same as that of N_2, Ar, and CO_2. The basis for this suggestion is that the broadening cross sections for N_2, Ar, and CO_2 are similar. This suggestion cannot be accepted because of the evidence presented in Figure of Task I Report. Furthermore, H_2O is a polar molecule while N_2, Ar, and CO_2 are not.

It is restated in this summary that the ARO procedure avoids the incorrect assumption of Beer's law which is reasonable for this data where the absorber lines are considerably wider than the source lines. Furthermore, serious difficulty with Beer's law would be expected during measurement on turbine engine exhausts at simulated altitudes. However, there is no evidence presented in this ARO report that supports these statements. In fact, for all the measurements made in this study, the Beer's law assumption is valid. Moreover, it is also a valid assumption for those altitudes in which the majority of the jet aircraft fleets operate.

Finally, the ARO report concludes with a statement that a 20% projected uncertainty can be expected by the use of the ARO UV resonance line absorption technique based on the results obtained with uncertain temperature and concentration profiles

in the calibration devices. It must be reiterated that uncertainties also arise from the performance of the optical systems as indicated by errors in the static cell measurements which were obtained under the most ideal conditions.

C. Comparison of Hollow Cathode and Capillary Discharge Performance

Although these lamps are very different in design, the emission characteristics are quite similar as opposed to the statement made in TMR-79-P7. Overall, the transmission characteristics through media containing NO at various temperatures can be seen to be comparable from the data in Table IV-A.

D. Comparison of the UTRC and ARO Computer Programs

Except for input data, e.g., lamp temperature,broadening coefficients, etc., the main body of the present ARO computer program appears to be substantially similar to the version developed by UTRC from the 1977 ARO model (Davis et al (1976a)). At room temperature, the predictions of the ARO model agree with those of the UTRC model. However, the predictions diverge significantly at elevated temperature due to the different temperature dependence for the broadening parameter a'. The ARO model employs Lorentz theory while the UTRC model employs Weisskopf theory. The ARO model will systematically predict more nitric oxide than the UTRC model for a given transmission, pressure, and elevated temperature distribution. As stated in Section IV.B.3, the different broadening dependence is the probable cause for the systematic overprediction of NO by the ARO model at the high temperatures in the flat flame burner tests at UTRC.

Moreover, it should be noted that the data reported in Table III-N on the continuum lamp transmissions for the flat flames was reduced using a model which stored the line shape for each zone. For a continuum lamp measurement, this procedure is necessary. However, for a resonant lamp, such a procedure was not necessary for this study. At typical commercial jet exhaust temperatures and operating altitudes ($H \leq$ 40,000 ft) this procedure is not necessary. Moreover, even at 65,000 ft, the resonant line sources will have lines which are narrower than the exhaust absorber lines.

E. Comment on Gas Correlation Measurements

As stated in Appendix A, this instrument was designed to measure several pollutant molecules emitted from smokestacks, NO being one of those molecules. For that application, this instrument has considerable merit. However, for measurements in this study, this instrument in its present configuration was not well suited for several reasons. The first was related to the failure of the detector that was used in the Wright-Patterson measurements. The active area of the original detector was circular (1.3 mm dia) while the replacement has a rectangular area (4 mm x 0.4 mm). This geometric mismatch is considerable. The second was that the intrinsic noise of the replacement detector was higher than that of the original detector. These two items alone were most likely responsible for a factor of four increase in the noise equivalent NO. A third reason was due to the lines chosen for correlation.

For temperatures up to 900K, this selection of lines was such to produce a temperature independent calibration curve. Above 900K, however, the selection is no longer optimum; hence, the sensitivity decreases by almost a factor of three at the highest temperatures of this study.

The center-line concentrations necessary for adequate signal-noise ratios for the infrared measurements were typically factors of 2 to 10 greater than those used in the ultraviolet measurements. Because of the loss in sensitivity, a side-by-side comparison data is not possible.

TABLE IV-A

COMPARISON OF TRANSMISSION DATA
ARO LAMP VERSUS UTRC LAMP

	TRANSMISSION			
	1st BH		2nd BH	
	ARO	UTRC	ARO	UTRC
STATIC CELL				
93.3 ppm	.892	.905	.835	.850
	.901	.899	.849	.843
470 ppm	.621	.628	.482	.504
		.627		.497
FGH				
280,ppm 452 K		.823		.764
288ppm, 448 K	.817		.753	
FFB				
999 ppm, 1360 K		.822 ($\sigma=1.96\cdot10^{-4}$)		.777 ($\sigma=2.53\cdot10^{-4}$)
1066 ppm, 1360 K	.811 ($\sigma=1.97\cdot10^{-4}$)		.747 ($\sigma=2.74\cdot10^{-4}$)	

V. SUMMARY AND CONCLUSIONS

Methods for providing known amounts of NO from room temperature to 2000 K were developed. At room temperature, a stainless steel, static cell was used. This cell, which was 18.6 cm long and 2.2 cm in diameter, was leak checked at 1 x 10^{-6} torr (1.33 x 10^{-4} Pa) and could be pressurized to 115 psia (792 kPa). Its windows were ultraviolet grade fused silica. The cell was attached to a precision mixing apparatus and used in obtaining the majority of the broadening and oscillator strength information presented in this report. For temperatures up to 850 K, a quartz-bed heat exchanger, through which mixtures of NO in N_2 and Ar were flowed, served as a calibration device. NO decomposition in the bed was not significant (< 10%). NO concentrations, measured with both uncooled quartz and metallic probes at and near the centerline, were in close agreement with NO concentrations calculated for a gas mixing apparatus which employed critical flow orifices. The NO determinations were made with both chemiluminescent analysis and mass spectrometry. For those cases where Ar was the bulk gas, proper account of viscosity and quenching phenomena was taken in the calibration of the chemiluminescent analyzer. Kinetic analysis indicated that substantial decomposition would not occur in this exchanger up to 1000 K. Thermal runaway of the electrical heating elements, however, prevented its use at that temperature. For temperatures of 1000 K to 2000 K, a lean $H_2/O_2/Ar$ flat flame seeded with NO was used. The burner surface was constructed of water-cooled, sintered copper with two zones: a main, NO-seeded zone and an unseeded buffer zone. Measurements made with water-cooled quartz probes indicated downstream conservation of NO in flames whose stoichiometries were varied from 0.36 to 0.92. Ar was used as a bulk gas instead of N_2 to preclude the formation of thermal NO. The data confirm that water-cooled quartz probes can be used in measuring NO in lean $H_2/O_2/Ar$ flames. Detailed concentration and temperature distributions were obtained along the optical path for both high temperature devices. These distributions had to be available for the reduction of the optical data and their comparison with probe results. The temperature measurements were made with thermocouples. For the quartz-bed heat exchanger measurements, uncoated chromel-alumel was used. In the flame measurements, Ir/60%Ir-40%Rh wires (76μm) coated with 10% beryllium oxide and 90% yttrium oxide were employed. The purpose for the coating was to minimize catalysis on the wires. Corrections for radiation losses were applied to the data obtained on the flames.

Two distinct ultraviolet sources were used in this study. The first was a hollow cathode lamp. A dc discharge in air at low pressure (2 Torr; 266 Pa) produced emission lines mainly from NO molecules, N_2 molecules and ions, and Ar atoms. The spectral lines used in this study were in the $\gamma(0,0)$, $\gamma(1,1)$ and $\gamma(2,2)$ bands ($A^2\Sigma^+ - X^2\pi$) of NO. The second source was a high pressure Xe lamp which produced radiation of the continuum type through the above spectral region.

A detailed review of the previously developed spectroscopic theory and computer model, which was supplied to these authors at the beginning of this study by ARO, Inc., revealed several significant errors (Appendix B). The accuracy of the optical results published by the originators of that theory and model is, hence, in doubt. Due to the complex history of the computer model, inconsistencies in calibration data and the unavailability of the original raw data, it is not possible to comment with certainty on the accuracy of the optical data existing in the literature. Where possible, some reanalysis of the original data will be included in TASK III Report.

Because of these difficulties, the spectral theory used in the previously published model was corrected, and the computer model was expanded so that not only data from resonant line sources can be analyzed but also that from continuum sources (Appendix D). Experimental data were obtained at low and elevated temperatures using these significantly different spectral sources. A comparison of these data showed excellent agreement; hence, the validity of the theory and model were established.

In order to use this model, a knowledge of the broadening of NO spectral lines in foreign gases was necessary. Data on broadening in Ar, N_2, CO_2, CO and CH_4 were obtained by the direct observation in high resolution of isolated lines using the continuum source. If Lorentz theory is assumed, i.e., a'=CP/T, the following values of C were obtained: C(Ar) = 1331 atm^{-1} K; C(N_2) = 1725 atm^{-1} K; C(CO_2) = 1655 atm^{-1} K; C(CO) = 1748 atm^{-1} K; and C(CH_4) = 1918 atm^{-1} K. If Weisskopf theory is assumed, i.e., a' = K'P/$T^{1.2}$, then the same experimental data yield: K' (Ar) = 4154 $atm^{-1}K^{1.2}$; K' (N_2) = 5383 $atm^{-1}K^{1.2}$; K' (CO_2) = 5165 $atm^{-1}K^{1.2}$; K'(CO) = 5455 $atm^{-1}K^{1.2}$; and K (CH_4) = 5986 $atm^{-1}K^{1.2}$. These data were also reduced to determine the following collision diameters: d(Ar) = 1.04 nm; d(N_2) = 1.13 nm; d(CO_2) = 1.17 nm; d(CO) = 1.15 nm; and d(CH_4) = 1.10 nm. Because of the oxidation of NO to NO_2 by O_2, precise measurement of the broadening parameter for O_2 was not possible. However, for the data obtained, it was estimated that the broadening parameter for O_2 has a value which lies between that of Ar and N_2. Data taken on the flames indicated that at elevated temperature Weisskopf theory seemed to provide a better fit to the data. If that theory is used and if it is assumed that O_2 is as efficient a broadener as N_2, then the broadening parameter for H_2O is 6260 atm^{-1} $K^{1.2}$.

Oscillator strengths were determined from data obtained with both radiation sources. From the continuum lamp data, the oscillator strengths for the NO $\gamma(0,0)$ $A^2\Sigma^+ - X^2\pi_{3/2}$ band when NO is diluted in N_2, CO_2, CH_4, and Ar were $3.57 \pm 0.06 \times 10^{-4}$, $3.54 \pm 0.004 \times 10^{-4}$, $3.51 \pm 0.02 \times 10^{-4}$, $3.27 \pm 0.06 \times 10^{-4}$, respectively. A measurement of the $A^2\Sigma^+ - X^2\pi_{1/2}$ band with N_2 as the diluent yielded an oscillator strength of $3.72 \pm 0.23 \times 10^{-4}$. This value was chosen for comparison with values in the literature because the $^2\pi_{1/2}$ state is more heavily populated at room temperature than the $^2\pi_{3/2}$ state. The agreement is good but slightly lower that those considered to be the most reliable. However, it should be noted that this study is unique since the oscillator strengths were measured directly from individual lines in high resolution.

With the use of the broadening data obtained with the continuum lamp, the oscillator strengths in the model were adjusted so that transmissions predicted by the model agreed with the experimental data obtained with the hollow cathode lamp. The values for the $^2\pi_{1/2}$ and $^2\pi_{3/2}$ were 3.53×10^{-4} and 3.20×10^{-4} respectively. These values were low relative to the continuum values because of the presence of radiation in the hollow cathode lamp due to species other than NO. If an estimate is made of the effect of this excess radiation, the oscillator strengths for these transitions are 3.76×10^{-4} ($^2\pi_{1/2}$) and 3.43×10^{-4} ($^2\pi_{3/2}$). The source temperature used in this and all calculations involving the hollow cathode lamp was 600 K.

Sufficient measurements were conducted and compared with model predictions of transmission that the optical system, based on a hollow cathode lamp and associated spectral model, can be considered calibrated to measure NO. If accurate temperature and pressure data are available and if the NO absorption is large relative to the noise, then measurements with accuracies of at least $\pm$ 20% are possible.

Similarly, if a proper model is used, the capillary discharge lamp (see Section IV.D.) can also be considered calibrated.

In order to reach this conclusion for the hollow cathode lamp, data were obtained and processed in the following manner. Two concentrations of NO in N_2 (93.3 ppm and 470 ppm, independently certified) were introduced into the static cell at pressures ranging from 47 Torr (6.3 kPa) to 1000 Torr (133 kPa). The first and second bandhead transmissions of the $\gamma(0,0)$ transitions were measured and compared with model predictions. The averaged errors in concentration between predicted and measured were -0.3% and -2.23% for the first and second bandhead data sets, respectively. For the quartz-bed heat exchanger and the flat flame, the temperature and concentration profiles were divided into zones, and the transmissions through each zone were calculated using the average temperature and concentration in each zone. For the quartz-bed heat exchanger, the averaged errors in concentration for the total data set based on first and second bandhead transmissions were +7.14% and +6.79%, respectively. Similarly, for the flat flame data, the averaged errors for the data sets were +7.04% and -2.19%, respectively. The maximum error encountered for any single measurements was 22.3%. Finally, for the high resolution continuum measurements, the averaged error of the set was +3.6% in concentration. It must be noted that these errors reflect the errors associated with the optical measurements, model predictions, and the temperature and probe concentration measurements.

Finally, an empirical calibration of the infrared gas correlation spectrometer was performed (Appendix A). Because this instrument was originally designed for stack monitoring, i.e., low temperatures and high densities, it was not well-suited for the measurements of interest here. The low temperature data indicated that the instrument was 20% more sensitive relative to the calibration previously used in jet combustor measurements. This variation is attributed to changes in grating alignment. A dependence of the calibration on broadening gas was observed and determined. For temperatures up to 900 K, the calibration, within the scatter of the instrument output,

remained constant. Above 900 K, a significant decrease in sensitivity was observed. This dependence is most likely due to significant changes in the populations of the lines selected by the grating assembly. However, sufficient data were obtained to allow measurements to be made at high temperatures if high NO seeding of the media is used.

REFERENCES

Abramowitz, M. and I. A. Stegun: Handbook of Mathematical Functions, Dover, N.Y. (1965).

Anderson, P. W.: Phys. Rev., 76, 647 (1949).

Antropov, E. T., N. N. Sobolev and V. P. Cheremisinov: Opt. Spectrosc. 16, 115 (1964).

Blackburn, G. F. and F. R. Caldwell: J. Research, NBS-C Engineering and Instrumentation 66C, 1 (1962).

Bergeman, T. H., and R. N. Zare: Bull. Am. Phys. Soc., 17, 149 (1972).

Bethke, G. W.: J. Chem. Phys., 31, 662 (1959).

Breene, R. G., Jr.: Rev. Mod. Phys., 29, 94 (1957)

Brunauer, S., P. H. Emmett and E. Teller: J. Am. Chem. Soc. 60, 309 (1938).

Cann, M. W. P., R. W. Nicholls, W. F. J. Evans, J. L. Kohl, R. Kurucz, W. H. Parkinson, and E. M. Reeves: Appl. Opt., 18, 964 (1979).

CIAP (Climatic Impact Assessment Program) DOT-TST-75-51, 52 (1975).

COMESA (Committee on Meteorological Effects of Stratospheric Aircraft) U.K.. Meteorological Office, Bracknell (1975).

COVOS (Comite d'Etudes sur les Consequences des Vols Stratospheriques) Societe Meteorologique de France, Boulogne (1976).

Crutzen, P. J.: Quart. J. Royal Met. Soc., 96, 320 (1970).

Crutzen, P. J.: Ambio, 1, 41 (1972).

Davis, M. G., W. K. McGregor and J. D. Few: Arnold Engineering Development Center Report AEDC-TR-74-124 (AD-A004105), (1976 a)

Davis, M. G., J. D. Few and W. K. McGregor: Arnold Engineering Development Center Report AEDC-TR-76-12 (ADA021061), (1976 b)

Davis, M. G., W. K. McGregor and J. D. Few: J. Quant. Spectrosc. Radiat. Transfer, 16, 1109 (1976).

Deezsi, I: Acta Phys. 9, 125 (1958).

Dodge, L. G., and J. Dusek: Private Communication (1978).

Dodge, L. G., and J. Dusek: Appl. Opt. 18, 419 (1979).

Dodge, L. G., M. F. Zabielski, L. M. Chiappetta and D. J. Seery: To be submitted to Env. Sci. & Tech. (1979).

Earls, L. T.: Phys. Rev., 48, 423 (1935).

Engleman, R., Jr.: J. Quant. Spectrosc. Radiat. Transfer, 9, 391 (1969).

Engleman, R., Jr., P. E. Rouse, H. M. Peek and V. D. Baiamonte: Los Alamos Scientific Laboratory Report LA-4364, (1970).

Farmer, A. J. D., V. Hasson and R. W. Nicholls: J. Quant. Spectrosc. Radiat. Transfer, 12, 627 (1972).

Federal Register, Vol. 41, No. 181, Part 87 - Control of Air Pollution from Aircraft and Aircraft Engines, September 16, 1976.

Few, J. D., R. J. Bryson, W. K. McGregor, and M. G. Davis, in Proc. Intl. Conf. Environmental Sensing and Assessment, Las Vegas, Nev. (Sept. 1975).

Few, J. D., R. J. Bryson, and W. K. McGregor: Arnold Engineering Development Center Report AEDC-TR-76-180 (1977).

Fraser, J. M. and Daniels, F.: J. Phys. Chem. 62, 215-220 (1958).

Gaydon, A. G., and A. R. Fairbairn: Proc. Phys. Soc. (London), A67, 474 (1954).

Hadeishi, T., Y. Agarwall, R. D. McLaughlin, and F. Robben: Lawrence Berkeley Laboratory Report, LBL No. 5213 (1976).

Hanley, H. J. M.: J. Phys. Chem. Ref. Data, 2, 619 (1973).

Hanson, R. K.: in Shock Tube and Shock Wave Research, Ed. B. Ahlborn, A. Hertzberg, D. Russell, p. 432, Univ. of Washington Press, Seattle (1978).

Hasson, V., A. J. D. Farmer, R. W. Nicholls and J. Anketell: J. Phys. B, Atom. Molec. Phys., 5, 1248 (1972).

Herzberg, G.: Molecular Spectra and Molecular Structure, I. Spectra of Diatomic Molecules, 2nd Ed., Van Nostrand Reinhold, New York (1939).

Hill, E., and J. H. VanVleck: Phys. Rev., 32, 250 (1928).

Hindmarsh, W. R., and J. M. Farr: Prog. in Quant. Electronics, 2, 143 (1972).

Hinze, J. O.: Turbulence, McGraw-Hill, London, 1959, p. 76.

Hirschfelder, J. O., C. F. Curtiss, and R. B. Bird: Molecular Theory of Gases and Liquids, p. 10, John Wiley, New York (1954).

Huber, K. P., and G. Herzberg: Molecular Spectra and Molecular Structure, Vol. IV. Constants of Diatomic Molecules, Van Nostrand Reinhold, New York (1979).

Jeunehomme, M.: J. Chem. Phys. 45, 4433 (1966).

Johnston, H. S.: Science, 173, 517.

Kaskan, W. E. and D. E. Hughes: Combustion and Flame 20, 381-388 (1973).

Kaufman, F. and J. R. Kelso: J. Chem. Phys. 23, 1702-1707 (1955).

Kent, J. H.: Combustion and Flame 14, 279 (1970).

Kent, J. H.: Private Communication.

Kusch, H. J., G. Rondigs and K. Wendt: J. Quant. Spectrosc. Radiat. Transfer, 17, 53 (1977).

Lambrey, M.: Compt. Rend. 189, 574 (1929); 190, 261 (1930).

Lambrey, M.: Compt. Rend., Ann. Phys. 14, 95 (1930).

McCullough, R. W.: "Measurement of Critical Rate Constants for Nitric Oxide Decomposition". HTGL Report No. 1, Mechanical Engineering Department, Stanford University, Stanford, Calif. August 1975.

McCullough, R. W., C. H. Kruger and R. K. Hanson: Comb. Sci. Tech. 15, 213-223 (1977).

McGregor, W. K., J. D. Few and C. D. Litton: Arnold Engineering Development Center Report AEDC-TR-73-182, AD-771 642 (1973).

McGregor, W. K., B. L. Seiber and J. D. Few: in Proc. Second Conf. Climatic Impact Assessment Program, Cambridge, Mass. (Nov., 1972).

Meinel, H.: Z. Naturforsch., 30a, 323 (1975).

Mitchell, A. C. G. and M. W. Zemansky: Resonance Radiation and Excited Atoms, Cambridge Univ. Press (1971).

Mori, Y. and K. Ohtake: Comb. Sci. Tech. 16, 11-20 (1977).

Mori, Y., K. Ohtake and T. Taira: Proceedings of 13th Symposium on Engineering Aspects of Magnetohydrodynamics, VII.3.1 (1973).

Mulliken, R. S. and A. Christy: Phys. Rev., 38, 87 (1931).

Naude, S. M.: Phys. Rev. 36, 333 (1930).

NAS (National Academy of Science), "Environmental Impact of Stratospheric Flight", Climatic Impact Committee (1975).

Oliver, R. C., E. Baver and Wasylkiwskyj: DOT-FAA Rpt. FAA-AEE-78-24.

Oliver, R. C., E. Baver, H. Hidalgo, K. A. Gardner and Wasylkiwskyj: DOT-FAA Rpt. FAA-EQ-77-3 (1977).

Pearse, R. W. B. and A. G. Gaydon: The Identification of Molecular Spectra, Chapman and Hall, London (1965).

Pery-Thorne, A. and F. P. Banfield: J. Phys. B.: Atom. Molec. Phys., 3, 1011 (1970).

Planet, W. G., G. L. Tettemer, and J. S. Knoll: J. Quant. Spectrosc. Radiat. Transfer, 20, 547 (1978).

Reid, R. C. and T. K. Sherwood: The Properties of Gases and Liquids, McGraw-Hill, Inc. 2nd Edition, 1966; p. 420-1, 483-4.

Reif, F.: Fundamentals of Statistical and Thermal Physics, P. 469, McGraw-Hill, New York (1964).

Schwarz, F. P. and H. Okabe: Anal. Chem., 47, 703 (1975).

Seery, D. J.: Private Communication 1978.

Seery, D. J., M. Zabielski and G. L. Dodge: E.P.A. Report to be published, 1979.

Shapiro, A. H.: The Dynamics and Thermodynamics of Compressible Fluid Flow, Volume 1, p. 84, Ronald Press Company, New York 1953.

Shelef, M. and J. T. Kummer: "The Behaviour of Nitric Oxide in Heterogenous Catalytic Reactions" presented in Symposium on Important Chemical Reactions in Air Pollution Control, Part II. 62nd Annual Meeting of AIChE, Washington, D.C., November 16-20, 1969.

Spindler, R. J., Jr., L. Isaacson and T. Wentink, Jr.: J. Quant. Spectrosc. Radiat. Transfer, 10, 621 (1970).

Svehla, R. A.: "Estimated Viscoscities and Thermal Conductivites of Gases at High Temperatures". NASA-TRR-132, 1962.

Sulzmann, K. G. P., G. E. Parks and S. S. Penner: J. Quant. Spectrosc. Radiat. Transfer, 16, 97 (1976).

Tajime, T., T. Saheki and K. Ito: Appl. Opt. 17, 1290 (1978).

Tatum, J. B.: Astrophys. J. Suppl. 14, 21 (1967).

Thorne, A. P.: Spectrophysics, John Wiley & Sons, New York (1974).

Thorson, W. R. and R. M. Badger: J. Chem. Phys., 27, 609 (1957).

Townes, C. H. and Schawlow: Microwave Spectroscopy, p. 368, Mc Graw Hill, New York (1955).

Weber, D. and S. S. Penner: J. Chem. Phys., 26, 860 (1957).

Winter, E. R. S.: J. Catalysis, 22, 158-170 (1971).

Wise, H. and M. F. Frech: J. Chem. Phys. 20, 22-24 (1952).

Yuan, E. L., J. I. Slaughter, W. E. Koerner and F. Daniels: J. Phys. Chem. 63, 952-956 (1959).

Zeldovitch, Ya. B., P. Ya. Sadovnikov, and D. A. Frank-Kamenetskii: Oxidation of Nitrogen in Combustion" (Transl. by M. Shelef) Academy of Sciences of USSR, Institute of Chemical Physics, Moscow-Leningrad (1947).

APPENDIX A

MEASURING NO IN AIRCRAFT JET EXHAUSTS BY GAS-FILTER CORRELATION TECHNIQUES, TASK I.

David A. Gryvnak

Ford Aerospace and Communications Corp.
Aeronutronic Division
Ford Road
Newport Beach, California 92663

November 1978*

Submitted to:
United Technologies Research Center P.O. 82126

FINAL REPORT TASK I

*Revised Version Received 4/12/79

INTRODUCTION AND SUMMARY

As a result of tests performed at Wright Patterson Air Force Base[1] the EPA Smokestack Instrument[2] was requested to be used on additional jet exhaust tests under controlled conditions. Tests were performed using a flat flame burner, flowing gas heater and in the future, will be made on a jet burner and a modified combustor can from a Pratt and Whitney FT12 combustor. This phase of the tests deals with the calibration procedures used for the flat flame burner and flowing gas heater conducted at United Technology Research Center (UTRC).

The EPA Instrument is a laboratory instrument designed to detect SO_2, CO, HCL, HF or NO contaminants being emitted from a smokestack. The details of the instruments are well documented[1,2] and are not repeated here. The instrument uses the principle of gas correlation to detect small amounts of contaminant gases and reduce or eliminate the effect of other gases such as H_2O, CO_2 etc. For this series of tests it is being used to detect NO in the exhaust aircraft jet engines for temperatures up to approximately 2000K.

Three different types of tests were performed. Static cell tests were performed using a sample cell to contain the gas at room temperature. At UTRC a glass cell 10 cm long with NaCl windows was filled with NO premixed with either Ar or N_2. At Ford two cells were used, each with a 20 cm path length. One cell with Al_2O_3 window, the other a glass cell with Al_2O_3 windows. The samples were NO premixed with N_2. The Flowing Gas Heater tests at UTRC consisted of flowing a carrier gas of either N_2 or Ar through a heater unit into a sample area that is 17 by 9.2 cm. Known amounts of NO were seeded into the carrier gas at temperatures up to 800K. Buffer gases surrounded and contained the sample gases and flooded the remainder of the sample area. NaCl windows allowed the light beam

to traverse the sample area while confining the gases. The Flat Flame Burner tests at UTRC consisted of flowing an argon carrier gas containing H_2 and O_2. The $H_2 + O_2$ was burned at the proper ratio and flow rates to create the desired temperatures from 1000K up to 1600K. The argon was seeded with known amounts of NO. The same buffering system and external housing used for the flowing gas heater were used for the flat flame burner.

Because of the versatility designed into the EPA instrument, it is not optimized for any particular gas contaminant, physical pathlength, particular environment or temperature. It was designed to be relatively insensitive to NO sample temperature changes up to 900K. This was achieved by selecting a spectral bandpass that contains NO absorption lines that will increase in strength and some that will decrease as the sample temperature increases. This results in the sum of the strengths of the lines remaining relatively constant for the temperature range from 300 to 900K. Above 900K the response of the instrument decreases with increasing temperature. The present tests were performed to calibrate the instrument and to determine if an empirical relationship could be formulated to account for the temperature effect. A curve has been determined to relate the original calibration to the higher temperatures. The instrument was found to be more responsive by 15 to 20% to samples pressurized with N_2 under static conditions at room temperature than when used at Wright Patterson Air Force Base. This is due primarily to a shift in the bandpasses of the grating box. The instrument was also found to be more responsive to samples diluted with Ar than to samples pressurized with N_2.

Differences of as much as 28% occurs for room temperature samples between static cell tests and flowing gas heater tests. These differences are most likely due to improper purge flow.

INSTRUMENT REFURBISHING

The instrument was received from EPA with no apparent damage in shipment. A few mirrors that were broken, previous to shipment, were replaced with mirrors of similar optical quality. The instrument was originally designed to be used on a smokestack, with an across-stack path using a retro-reflector to doublepass the sample area. With the type of test conducted at United Technology Research Center we could not doublepass the beam because of the physical dimensions of the apparatus involved. Consequently, a source section was built to be placed on the opposite side of the sample section to direct the beam through the sample area to the main instrument. This is similar to the technique used at Wright Patterson Air Force Base when the same instrument was used for NO measurements on a simulated jet aircraft engine. The source optics consisted of some focusing mirrors and an electronic reference that was actuated by the 435 Hz chopper that also chopped the light beam from a Nernst source. The main instrument was checked for optical alignment. The transfer optics had to be adjusted when the grating box was placed into the instrument. The mask on the transfer optics was removed in order to increase the throughput of the instrument.

The grating box is the same one used for the Air Force Wright Patterson experiment. The grating box passes three spectral intervals where NO absorption lines occur. Figure 1 shows three spectral curves over the spectral interval of interest. The upper panel shows the water vapor absorption by laboratory air at room temperature. The middle panel shows the spectral bandpasses of the grating box, and the third panel shows the absorption by NO in those bandpasses. As can be seen by the middle panel, the spectral bandpasses mask out the strongly absorbing H_2O lines. In the spectral interval between 1925 and 1940 cm^{-1} the

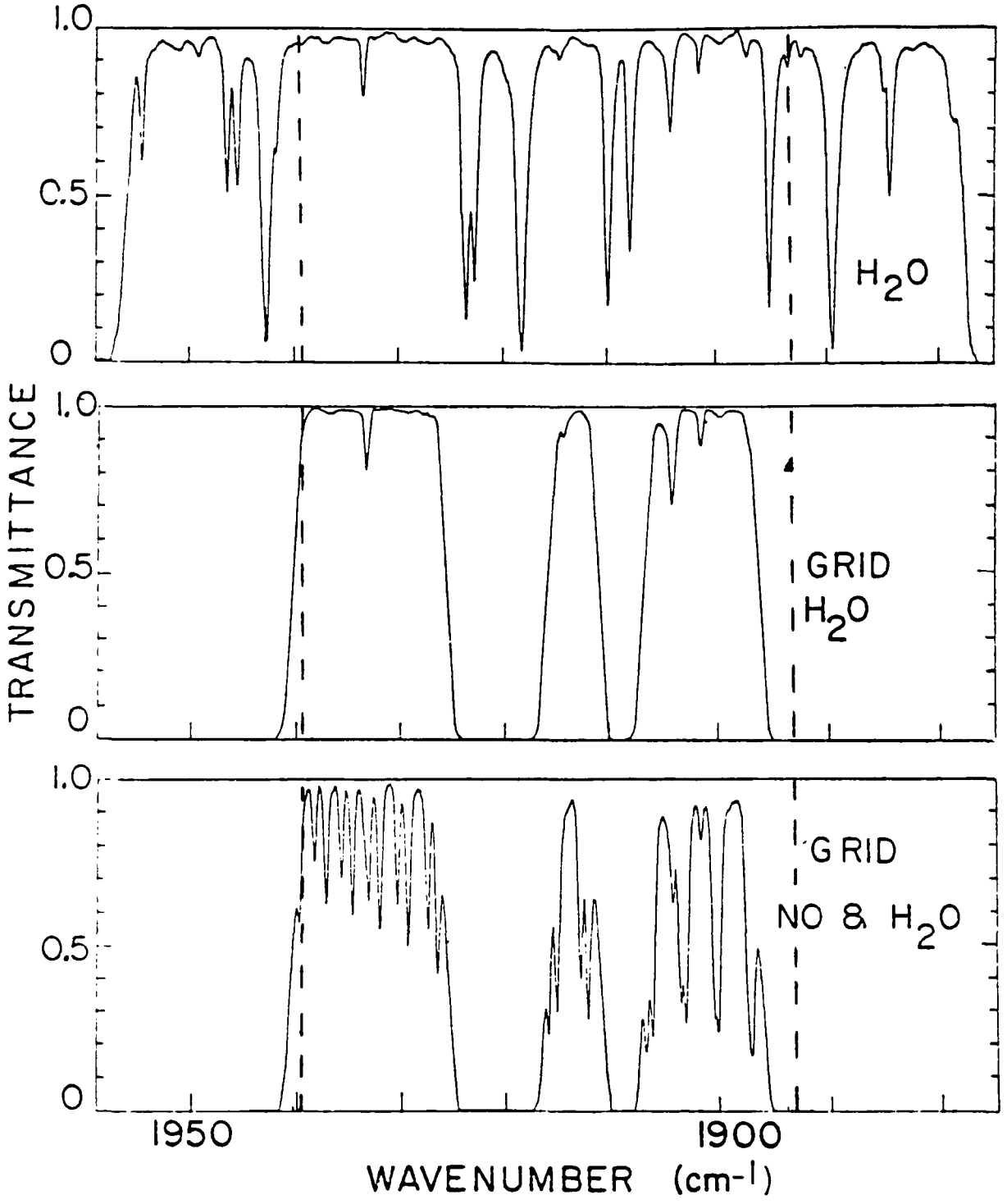

Figure 1. Spectral transmittance curves over the spectral interval passed by the NO grid assembly. The upper panel shows the H_2O absorption by laboratory air at room temperature. The middle panel shows the spectral bandpasses of the grid. The lower panel shows the absorp- by NO in the bandpasses of the grid. The dotted lines indicate the bandpass shift.

the NO absorption lines increase in strength as the temperature increases. In the spectral interval between 1895 and 1920 cm^{-1} the NO absorption lines decrease in strength as the temperature increases. The total absorption tends to remain constant as the temperature changes in the range from 300 to 900K. The grating box was placed into the instrument and optically checked.

The InSb detector was installed, however, the dewar had leaked causing the window of the detector to frost with water condensation. Our detector department attempted to reevacuate the dewar. The pins had epoxy deposited around them to stop the leak that was created by the cracks in the glass near the pins. The dewar was tubulated, evacuated and pumped for about four days, then the tubulation was sealed. The dewar subsequently was tested and found to hold liquid nitrogen for four hours. However, because the dewar was filled with liguid N_2 to the top the epoxy cracked and allowed the dewar to leak again.

A replacement detector, that was not optically suited for the instrument because of its element size, was installed in the instrument. The area of the element of this detector is 4 mm x 0.4 mm , whereas the area of the original detector element was 1.3 mm in diameter. The original preamps of the instrument were found to be defective in that two of the operational amplifiers had to be replaced. A new preamp was used with the replacement detector. The rest of the electronics were found to be functioning very well.

Because of the late arrival of the instrument and the length of time that it took to resolve the electronic and detector problems, limited time was

available to check out the instrument and make the needed repairs. The grating box was installed in the instrument and the transmittance of the correlation cell was checked. This was done by comparing the carrier signal when the correlation cell was not in the beam to the carrier signal when the correlation cell was in the beam. We found that the transmittance of the correlation cell was 57%, which was the same as when used on the Wright Patterson Air Force tests. This test seemed to be a good indicator that the correlation cell and the grating box were in good spectral alignment and that the correlation cell had probably not changed its spectral characteristics.

A calibration test was then performed to check the previous calibration. The calibration curve used at Wright Patterson is shown in Figure 2. A sample of 1000 ppm in a 20 cm sample cell produced a V' of 68×10^{-4}. From the previous calibration this V' would represent an absorber thickness of 2.1×10^{-2} atm cm_{STP}. Whereas the sample in the sample cell was 1.8×10^{-2} atm cm_{STP}. The instrument was indicating approximately 15% higher than the sample in the sample cell. The short term noise-equivalent V' was 4×10^{-4}, which gave a noise-equivalent u of 1.1×10^{-3} atm cm_{STP}.

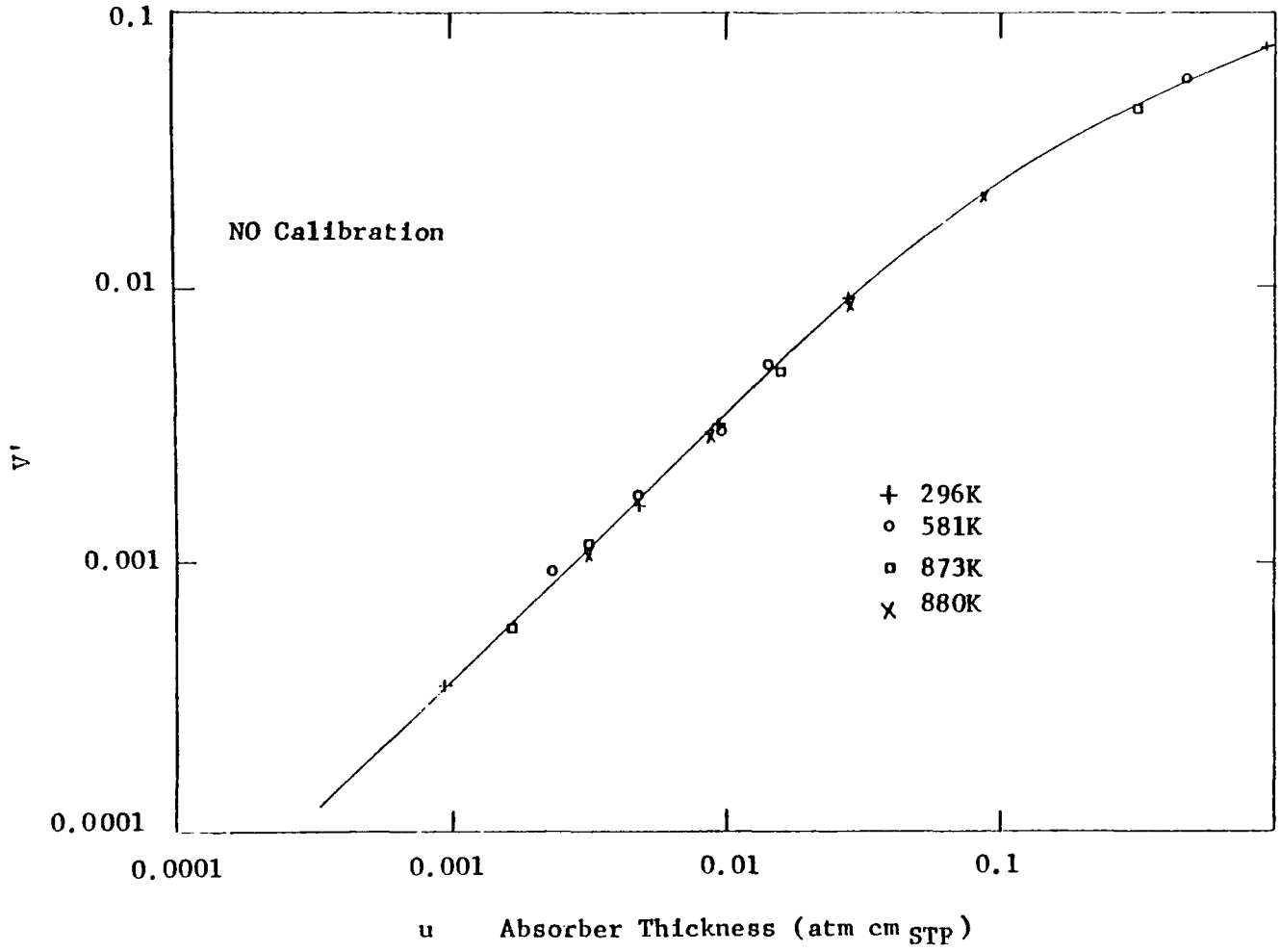

Figure 2. Calibration curve for NO used at Wright Patterson Air Force Base, instrument response V' vs absorber thickness u.

TEST AT UTRC

The instrument arrived at UTRC in Connecticut in very good shape, with no damage during shipment. The optics were set up, and mirrors had to be cut to accommodate some of the thermocouple connectors that were sticking out of the chimney.

Figure 3. shows an optical diagram of the equipment. Sodium chloride windows were used on the flat flame burner, and an image of the Nernst was formed in the center of the flat flame burner. Mirror M5 then focused the image on to mirror X1 of the EPA Instrument. A glass cell with sodium chloride windows could be inserted on the source side of the flat flame burner in order to test the instrument under static sample conditions. A burner with a sintered copper top produced a flat flame by burning $H_2 + O_2$ in an Ar carrier. The flat flame burner was replaced with a flowing gas heater wherein hot gases as high as 900K could be introduced into the infrared monitoring beam.

Tests using the static cell were done by first evacuating the cell in order to record a zero and then filling it with a sample. Two types of samples were used, one with argon gas as a broadener and the other with nitrogen gas as a broadener. After the sample was introduced into the cell and the signal recorded on the recorder, the cell was evacuated to record another zero. The two zeros on the chart were used to determine the zero position for the instrument when the gas was in the sample cell. If any drift had occurred it could be compensated for by drawing a line through the two zeros. Typical shifts were less than 1×10^{-4} for V' and 0.3×10^{-3} atm cm for u.

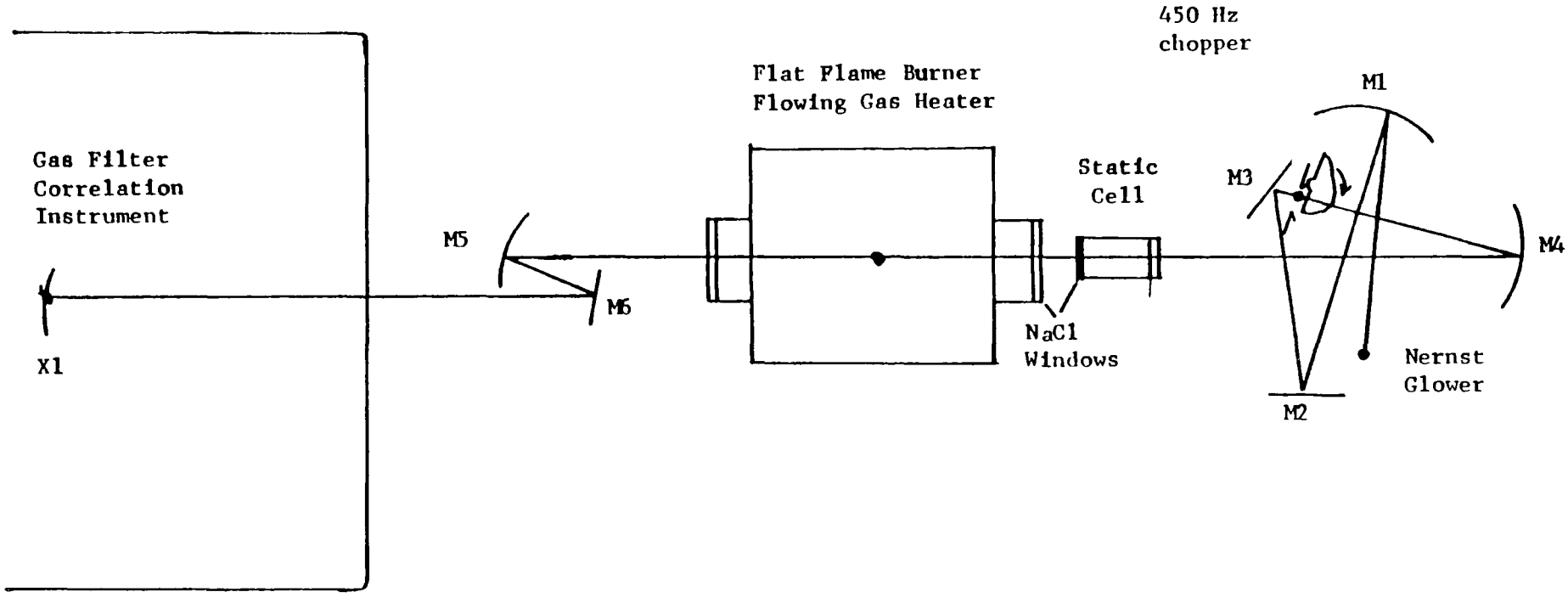

Figure 3. Optical diagram of source optics and sample area. The static cell was removed when the Flat Flame Burner or the Flowing Gas Heater was used.

A similar procedure was used for the flowing gas heater and the flat flame burner. The flowing gas heater was heated up to the temperature desired with either Ar or N_2 as a carrier gas; the temperature of the center of the flowing gas heater sample section was measured and recorded. A zero level was recorded on the chart, then the sample was seeded with NO to a predetermined amount and the NO concentration at the center of the sample area was determined by UTRC using quartz probe techniques. The signal was recorded on the recorder chart paper and the NO gas was turned off. The instrument then gave another zero level. The two zeros on either side of the signal recorded for the sample were used in order to determine the zero when the NO sample was in the sample section. A similar procedure was used for the flat flame burner. The burner was brought up to temperature, heating the argon carrier gas. Two zero levels were recorded, one before and one after the carrier gas was seeded with NO. In the flowing gas heater and the static cell tests both nitrogen and argon were used as a carrier gas. The nitrogen was not used for the flat flame burner for fear of creating other NO or NO_x products which would contaminate the sample area.

RESULTS

The techniques used to reduce the data are very similar to the one used for the tests conducted at Wright Patterson Air Force Base. The details of the data reduction can be found in their report (2). Only a brief description will be given here.

The signal, V', from the EPA instrument is proportional to the NO absorber thickness for small samples at constant temperature and concentrations. For

the samples encountered in these tests, $u = 2 \times 10^{-3}$ atm cm STP, the response of the instrument is linear as can be seen from the calibration curve in Figure 2. When the sample has temperature and concentration gradients, the sample path can be considered to be divided into small increments such that each incremental path is at a constant temperature and concentration. The absorber thicknesses for each increment can be determined and because of the linear response of the instrument their sum will give the total absorber thickness in the sample path. In order to compare the results of the instrument with the actual sample, the temperature and concentration gradients must be known. A computer program was created to calculate the absorber thicknessess of the samples at the elevated temperatures.

To determine the absorber thickness, values of temperature and concentration were determined from gradient and mole fraction gradient curves supplied by UTRC. For the flowing gas heater tests, four temperature profiles were supplied and shown in Figure 4. Each curve is flat for a distance out to approximately 4 or 5 cm from the centerline of the burner. The actual centerline temperatures of the samples are listed above the curves for which they were used. These profiles were determined within an hour from the tests using the EPA instrument were performed. The profiles are a result of probe measurements made by the UTRC staff on samples whose temperatures and concentrations were similar to those used when making the measurements with the EPA instrument. From the curves in Figure 4, the actual centerline temperatures of the NO sample can be off as much as 10% from the centerline temperature of the curve that was used to determine the sample absorber thickness. Figure 5 shows the mole fraction profile for three different temperatures. The 300K

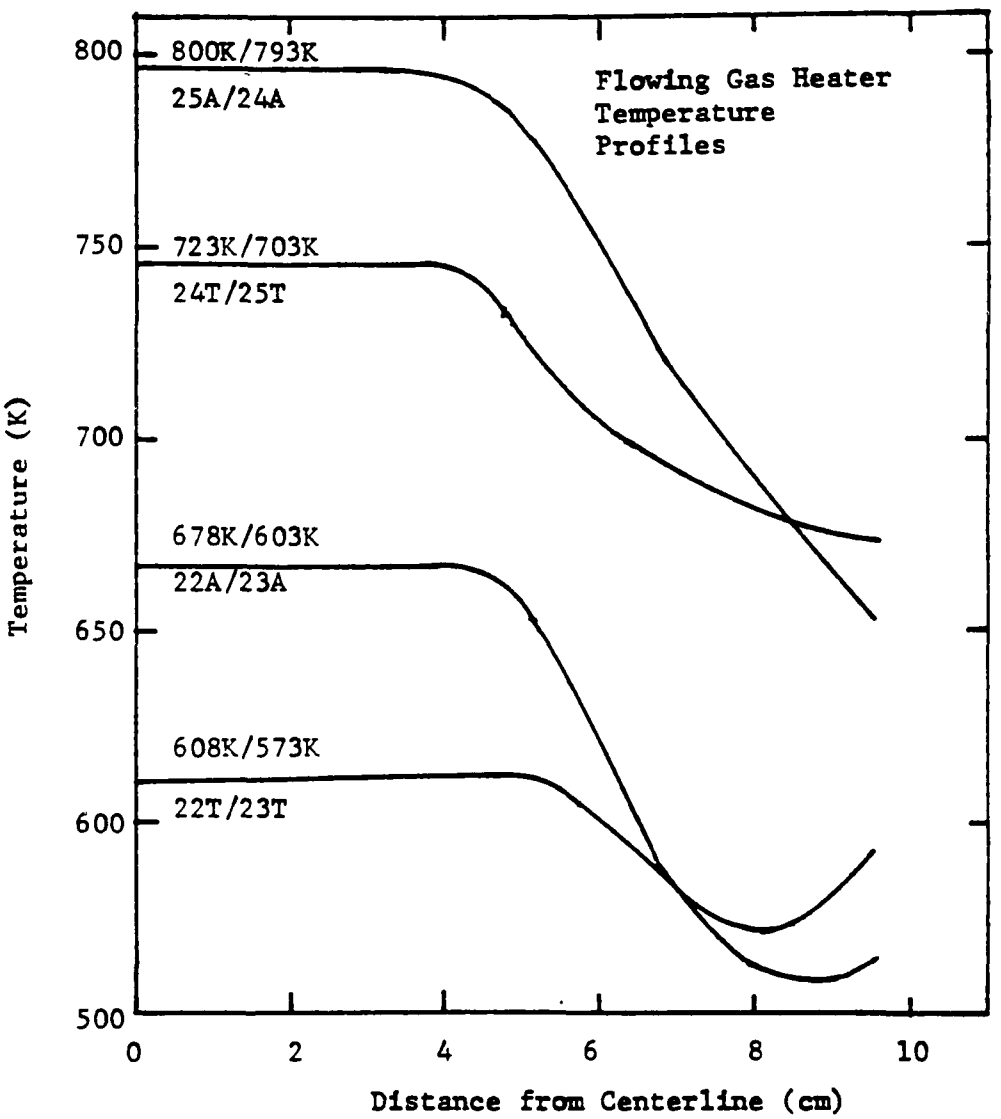

Figure 4. Temperature Profiles for the Flowing Gas Heater. The sample numbers for which the curves were used are written below each curve. The temperature at the center of the sample is listed above each curve.

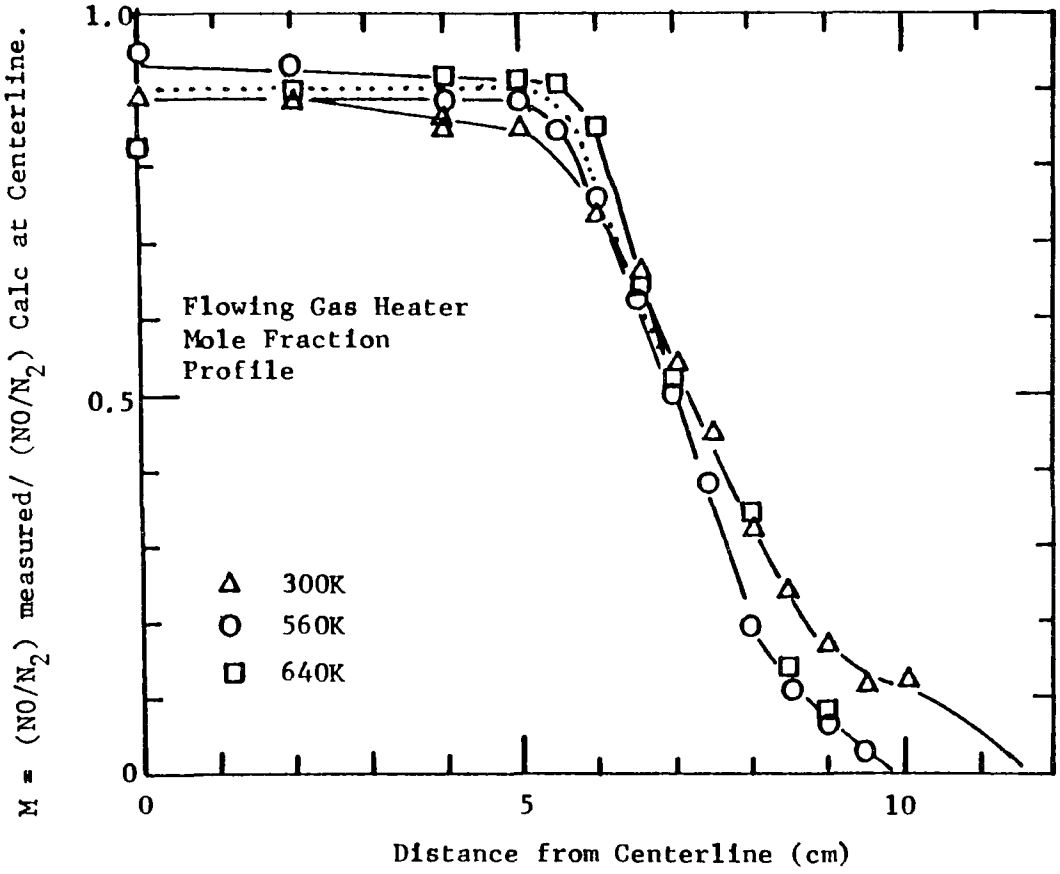

Figure 5. Mole Fraction Profile for the Flowing Gas Heater. The dotted curve was used for the elevated temperatures.

curve was used for the room temperature samples and the dotted curve was used for the elevated temperatures.

The absorber thickness, u, for a sample of constant temperature and concentration can be determined from the UTRC data from

$$u(\text{atm cm}_{STP}) = p(\text{atm})\ L(\text{cm})\ \frac{273}{\theta(K)} \qquad (1)$$

where

u = Absorber thickness in atm cm $_{STP}$

p = Absorber pressure in atm = $c(\text{ppm}) \times 10^{-6}$

c = Absorber concentration in ppm

L = Path length in cm

θ = Temperature in K (2)

However, if the concentration and temperature varys over the sample path, then the absorber thickness for a small incremental path length ΔL_i is given by

$$u_i = p_i \Delta L_i \frac{273}{\theta_i}$$

then the total absorber thickness for the path can be found by summing over the entire path.

$$u = \sum_i u_i = \sum_i p_i\ \Delta L_i \frac{273}{\theta_i} \qquad (4a)$$

and if the path is divided into equal increments, ΔL,

$$u = \Delta L\ 273 \times 10^{-6} \sum_i \frac{c_i}{\theta_i}$$

The concentration can be found from the mole fraction normalized concentration profile, M, and the centerline concentration, C, from the following expression.

$$c_i = M_i C \tag{5}$$

Therefore

$$uc = \Delta LC\ 273 \times 10^{-6} \sum_i \frac{M_i}{\theta_i}$$

where uc denotes the calculated absorber thickness. The values used in the calculations were determined at 0.5 cm increments from Figures 4 and 5. Integration was done from the center of the sample through 10 cm. The results were doubled on the assumption that the profile is symmetrical about the center line. Some of the representative curves of previous data indicate that this might not be an accurate assumption. Asymmetry might cause errors as large as 8%.

Because the calibration curve for the EPA instrument has been determined for temperatures in the range of 300K to 900K it is not expected to give absolute results for samples pressurized with Ar or for samples whose temperatures are higher than 900K. In addition it has previously been shown that the EPA instrument is giving values that are 15% higher than the original calibration curve. The signal, V', from the EPA Instrument will be used to determine a measured equivalent absorber thickness, um, from the original calibration curve. These measured equivalent absorber thicknesses will be compared to the calculated absorber thicknesses to determine an empirical temperature relationship between the instrument response and the calculated values for samples diluted with Ar.

Table 1 lists the results of the static cell tests. The first column lists the broadening gas. The second columns lists the results of the EPA instrument. The third column lists the calculated absorber thickness and the fourth column lists the ratios of um/uc. The noise equivalent u is approximately 2×10^{-3}. The values obtained for the fifth and sixth samples in Table 1 are for small samples diluted with N_2. The noise equivalent u represents a larger percentage error than for the samples for higher concentrations. The first three samples listed on Table 1, consequently would give the more accurate result. This indicates the EPA instrument is giving values of about 20% higher which agrees with the results that we obtained at Ford prior to the UTRC tests. The seventh and eighth samples are for the calibration test performed at Ford prior to and after the UTRC tests, respectively. The last two samples are for argon as a broadener gas and the values of um/uc are larger by about 35%. It has been shown (3) that the broadening abilities of Ar and N_2 on CO are different and a similar effect on NO might explain the observed effect above.

The results from the flowing gas heater tests are shown in Table 2. The upper portion of the table shows the nitrogen carrier data, the lower portion the argon carrier data. The left hand column list the test number; some of the tests were repeated at a later date and consequently given the same test number. The third column lists the temperature at the centerline of the sample. The next column lists the centerline temperature of the curve that was used in the calculation. The next column lists the centerline concentrations supplied by UTRC. The next column lists the measured equivalent absorber thickness, um, in atm cm_{STP}, as determined with the EPA instrument. Next column gives the calculated absorber thickness based on the probe curves given by UTRC. The last column gives the ratio of um/uc. The lower portion of the table lists the results when argon is used as a carrier gas.

TABLE 1

Static Cell Results

Broadener Gas	um (atm cm^3 STP $x10^3$)	uc (atm cm^3 STP $x10^3$)	um/uc
N_2	24.0	19.2	1.25
N_2	23.5	19.2	1.22
N_2	23.6	19.2	1.22
N_2	4.2	3.64	1.15
N_2	8.5	7.56	1.12
N_2	21.2	18.5	1.15
N_2	21.2	18.5	1.15
Ar	24.5	18.3	1.34
Ar	24.5	18.3	1.34

TABLE 2

Flowing Gas Heater Results

Test #	Carrier Gas	θ(K) Measured	θ(K) Curve	C ppm	um atm cm STP x10^3	uc atm cm STP x10^3	um/uc
20 T	N_2	296		669	12.0	9.22	1.30
21 T	N_2	296		1315	24.5	18.1	1.35
22 T	N_2	608	611	1025	7.5	6.69	1.12
23 T	N_2	573	611	1850	16.6	13.3	1.25
24 T	N_2	723	746	1580	8.9	8.53	1.04
25 T	N_2	703	746	2220	14.6	11.9	1.23
20 T	N_2	296		650	11.8	8.97	1.32
20 T	N_2	296		668	12.1	8.97	1.35
22A	Ar	678	667	1018	7.4	6.11	1.21
23A	Ar	603	667	2047	18.0	12.3	1.47
24A	Ar	793	796	1585	8.8	8.06	1.09
25A	Ar	800	796	2200	13.9	11.2	1.24
20A	Ar	295			15.6	9.07	1.72*
20A	Ar	295			15.2	9.07	1.68*

* Window purge was most likely improperly set.

The last column indicates a tendency for the ratio to decrease as the temperature increases. The ratio for the room temperature samples are much larger than the ratio for the samples at the elevated temperatures. The calculated results for sample 25T may be reduced if the temperature curve, 746K were corrected to the temperature of the centerline of the sample, 703K. It would cause the ratio to decrease coming closer to the results of sample 24T. The values obtained for the nitrogen samples tend to be lower than the samples with argon as the carrier gas in agreement with the tests on the static cell. The ratio for the argon sample tests also tend to get smaller as the temperature is increased.

For the flat flame burner tests, similar type calculations were carried out. However, the temperatures given at the centerline of the sample are not the true temperatures of gas but the temperature of the thermocouple. These temperatures have to be corrected because the thermocouples are radiating thereby decreasing their temperature giving a result that is lower then the actual gas temperature. The temperatures that were used were determined from curves given to us by UTRC. They are shown in Figure 6. Four different temperature profiles are represented. Listed above each curve is the corrected centerline temperature.

These curves were determined for similar sample conditions in the flat flame burner. However they were obtained prior to May 1978, six months before the tests with the EPA instrument. It was assumed that they would give a true representation of the temperature profile of the sample conditions of the present tests. The Centerline temperatures for the present samples were slightly

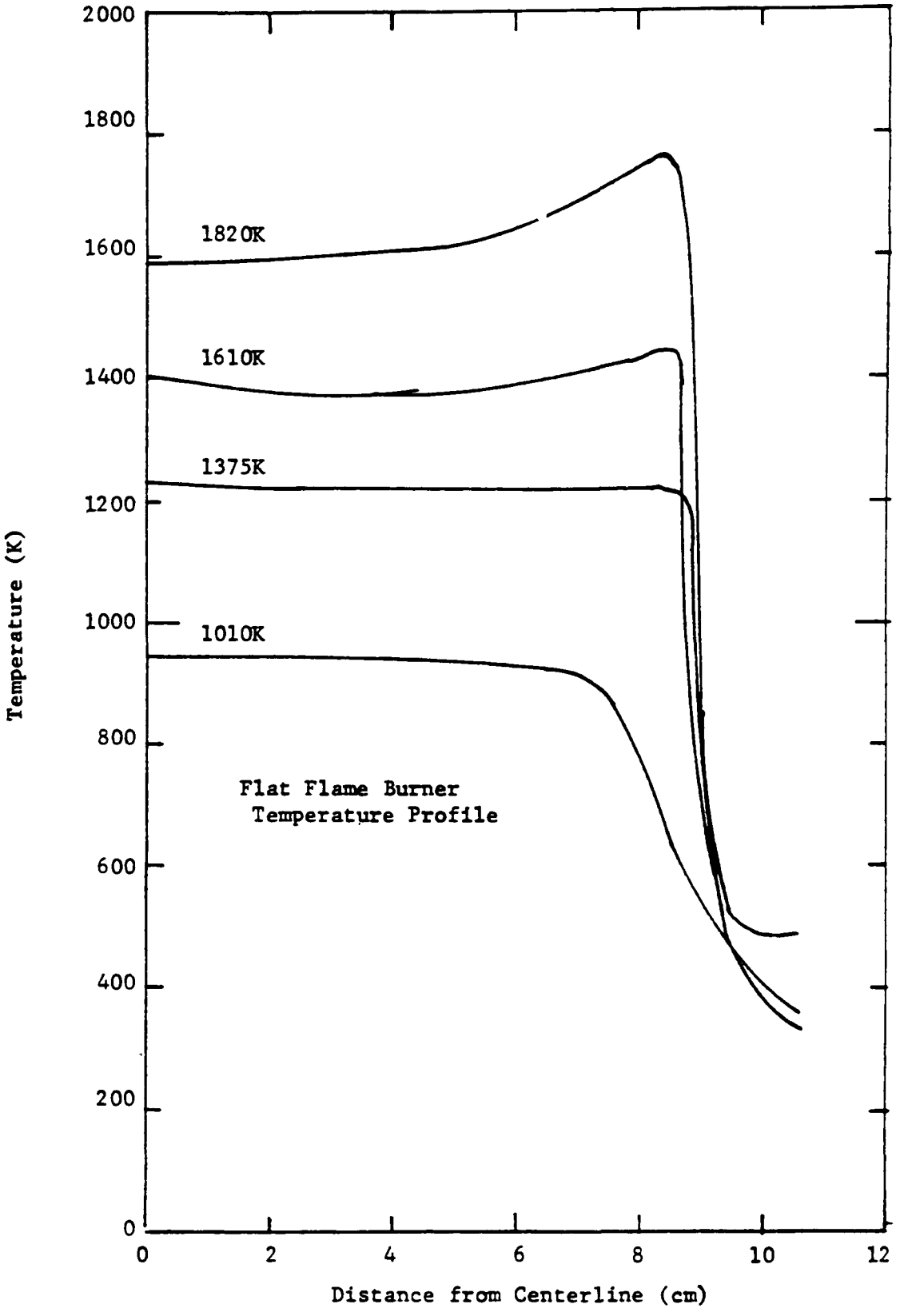

Figure 6. Temperature profile for the Flat Flame Burner
The centerline radiation temperature is listed for each curve

different. However, corrections to these temperature curves were made to get representative temperature profiles. We have interpolated between the curves for the different samples using a linear interpolation from 296°K to the calibration curve. The radiation correction was done in the following matter: The correction was assumed to follow the centerline temperature of the sample raised to some power, probably near the third power. The temperature corrections for the four different curves shown were plotted against the recorded centerline temperature on log-log paper. The slope of the curve gave the exponent for the following equation:

$$\ln \Delta\theta = \ln B + \ln(\theta)^n. \qquad (6)$$

From the slope of the curve, n was found to be 2.94 and by using the values that were used to determine the curve, B was found to be 1.24×10^{-7}. With the use of this equation the intermediate temperatures were corrected. Then with the use of the computer we determined the values of the integrated u, for the different samples. Figure 7 shows the curve determined using probe techniques prior to May 1978 that was used for the mole fraction profile for the flat flame burner calculations.

Table 3 lists the results for the flat flame burner tests. The second column in Table 3 shows the uncorrected centerline temperature; the third column lists the corrected center line temperature. The fourth column lists the value of the measured equivalent absorber thickness as measured by the EPA instrument, the sixth list the calculated values and the seventh column gives the ratio of um/uc. As can be seen from Table 3 the data are grouped into three different temperatures regions. As the temperature increases, the tendency for the ratio is to decrease, similar to the flowing gas heater results.

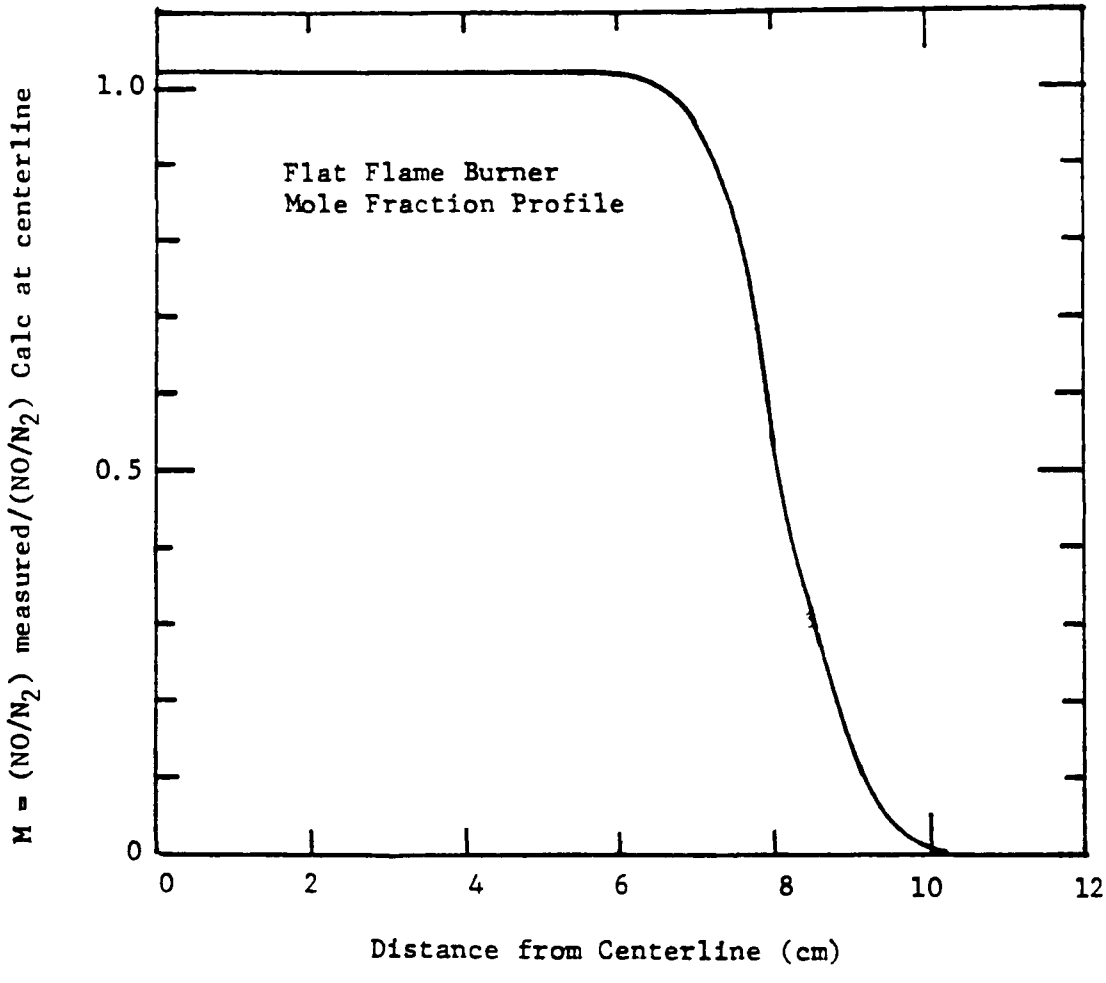

Figure 7. Mole fraction profile for the Flat Flame Burner

TABLE 3

Flat Flame Burner Results

Test #	θ(K) Uncorrected	θ(K) Corrected	C ppm	um atm cm^{3}STP x10^3	uc atm cm^{3}STP x10^3	um/uc
20F	940	1008	1389	5.8	6.41	0.905
21F	935	1002	1954	7.8	9.08	0.859
20FA	934	1001	2392	7.2	11.1	0.647
21FA	939	1007	3775	12.0	17.5	0.688
20FB	919	983	3248	13.0	15.4	0.846
21FB	919	983	2293	8.2	10.9	0.756
21FC	919	983	3606	16.0	17.1	0.937
22FA	1189	1325	3089	6.0	10.7	0.562
23FA	1180	1313	4246	8.5	14.8	0.574
26FA	1227	1377	4018	5.8	13.4	0.434
27FA	1227	1377	6074	8.5	20.2	0.420
27FA	1189	1325	6074	7.2	20.2	0.356
22FA	1189	1325	3089	8.4	10.7	0.787
23FA	1189	1325	4246	10.8	14.7	0.736
24FA	1393	1600	4136	5.1	12.0	0.425
25FA	1396	1615	6125	8.5	17.7	0.480
24FA	1381	1593	4136	7.5	12.1	0.618
25FA	1381	1593	6125	10.6	20.2	0.524
25FA	1381	1593	6125	11.8	20.2	0.584
25FB	1381	1593	6125	11.5	20.2	0.569

TESTS AT FORD

After the tests at UTRC, additional tests were performed at Ford that were not done prior because of time limitations. Also tests were performed to help explain some of the effects that were observed.

The grating box was tested by directing a beam of light through it and into a grating spectrometer. The spectral transmittance curve of the grating box was displayed on a chart recorder. The spectral bandpasses of the grating box were compared to the previous spectral bandpasses and found to have been displaced approximately 2 cm^{-1} toward lower wavenumber. The displacement of the spectral bandpasses probably resulted in the calibration shift. It could have changed the response of the instrument to H_2O; however, during our tests at UTRC, when the $H_2 + O_2$ burner was fired creating H_2O, no change in signal was observed, indicating that the instrument still had good H_2O rejection. Additional calibration tests were performed at the Ford facility confirming the previous shift of 15% in the calibration curve from the earlier data. The spectral transmittance curve of the correlation cell was obtained and compared to its previous transmittance curve, and no observable difference was noted.

There is a noticeable effect when Ar is used as a carrier or broadening gas as compared to N_2. We have observed a similar effect [3] between Ar and N_2 with CO as an absorbing gas. N_2 broadens the CO lines more than Ar. The wings of the broadened lines would have more absorption that the wings of less broadened lines. Because cylinders of Ar were not available to check the effect of the broadening ability of Ar on NO, a test was performed to

determine the effect of broadening the NO lines with N_2. A sample of NO at two different pressures near 1 atm was tested. A 1000 ppm NO in N_2 sample at 0.7 atm in a 20 cm cell was pressurized with N_2 to 1.0 atm and the signal, V', decreased from 55×10^{-4} to 51.5×10^{-4}. A decrease would be expected because the wings of the absorption lines contribute to V' as a negative correlation, when the lines are broadened the wing absorption is increased, thereby reducing the signal. Because Ar is not expected to broaden as much as N_2, the wings of the lines will absorb less for Ar-broadening thereby increasing the signal.

CONCLUSIONS

There is a calibration shift of approximately 15 to 20% higher from the calibration used for the Wright Patterson Air Force tests in 1975. This is probably due to the spectral shift of the gratin g box bandpasses of 2 cm^{-1} toward lower wavenumber. The N_2-broadened NO lines are broadened more than the Ar-broadened NO lines and consequently absorb more in the wings of the lines. However more absorption in the wings of the lines will cause a decrease in the signal, therefore the samples diluted by Ar give larger signals than samples pressurized by N_2.

The ratio um/uc for the flowing gas heater tests are considerably higher than for the static cell tests when Ar is used as the broadening gas. This is very clear when the ratio um/uc is compared in Table 1 and Table 2 for room temperature samples. The ratio is 1.34 for the static cell tests and 1.7 for the flowing gas heater. Personnel at UTRC indicate that the window purge was improperly set. The difference is not as great for the samples pressurized with N_2. The N_2 results are within experimental error.

Figure 8 shows a plot of the results for samples that are pressurized with Ar. The ratio um/uc is plotted against temperature. The large difference in the static cell tests and the flowing gas heater results is obvious. There is a large amount of scatter in the data. The noise-equivalent u was approximately 1×10^{-3} atm cm_{STP}, 5 to 10% of the observed signal, and accounts for some of the scatter. The use of standardized temperature and concentration profiles rather than using a profile for each sample could add 5 to 10% to the scatter. As can be seen from Tables 2 and 3 the centerline temperatures varied by as much

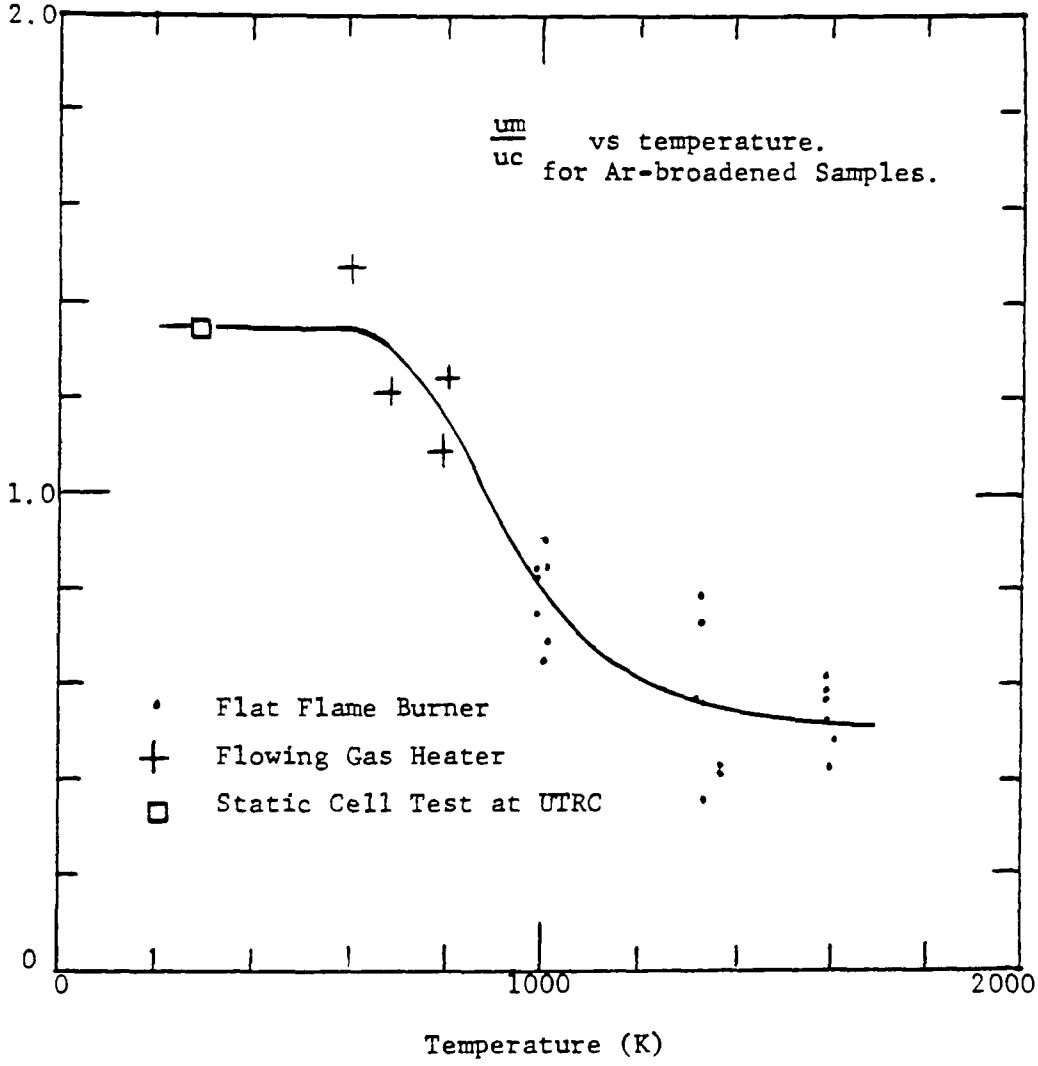

Figure 8. Plot of um/uc vs Temperature for Ar-broadened samples.

as 10% from the centerline temperatures of the profile curves used in the calculation. Another source of error that could add up to 7 to 10% is the assumption that the profiles are symmetrical. Previous data supplied by UTRC indicate that the profiles may not be symmetrical.

A smooth curve was drawn through the points in Figure 8. The curve shows the decrease in um/uc as the temperature increases. This apparent change in calibration was not observed for temperatures below 900K in the previous tests done in 1975. As can be seen in Figure 2 for temperatures up to 900K, under static conditions, a single calibration curve could be used. The absorption lines used in the detection of NO tend to account for temperature changes because some of the absorption lines increase in strength and and some decrease in strength with increasing temperature. The total strength of the sum of the lines would then tend to remain constant over the temperature range of interest. However as the temperature increases above 1000K the strengths of the lines all start to decrease and the response of the instrument falls off. For the subsequent tests on this contract the calibration curve should be modified by a factor determined from the curve from Figure 8.

A similar plot for N_2-broadened samples is shown in Figure 9. The differences between the static cell tests and the flat flame burner are not as great as for the Ar-broadened samples. In addition the difference between the static cell tests and the flowing gas heater tests not as apparent for N_2-broadened samples.

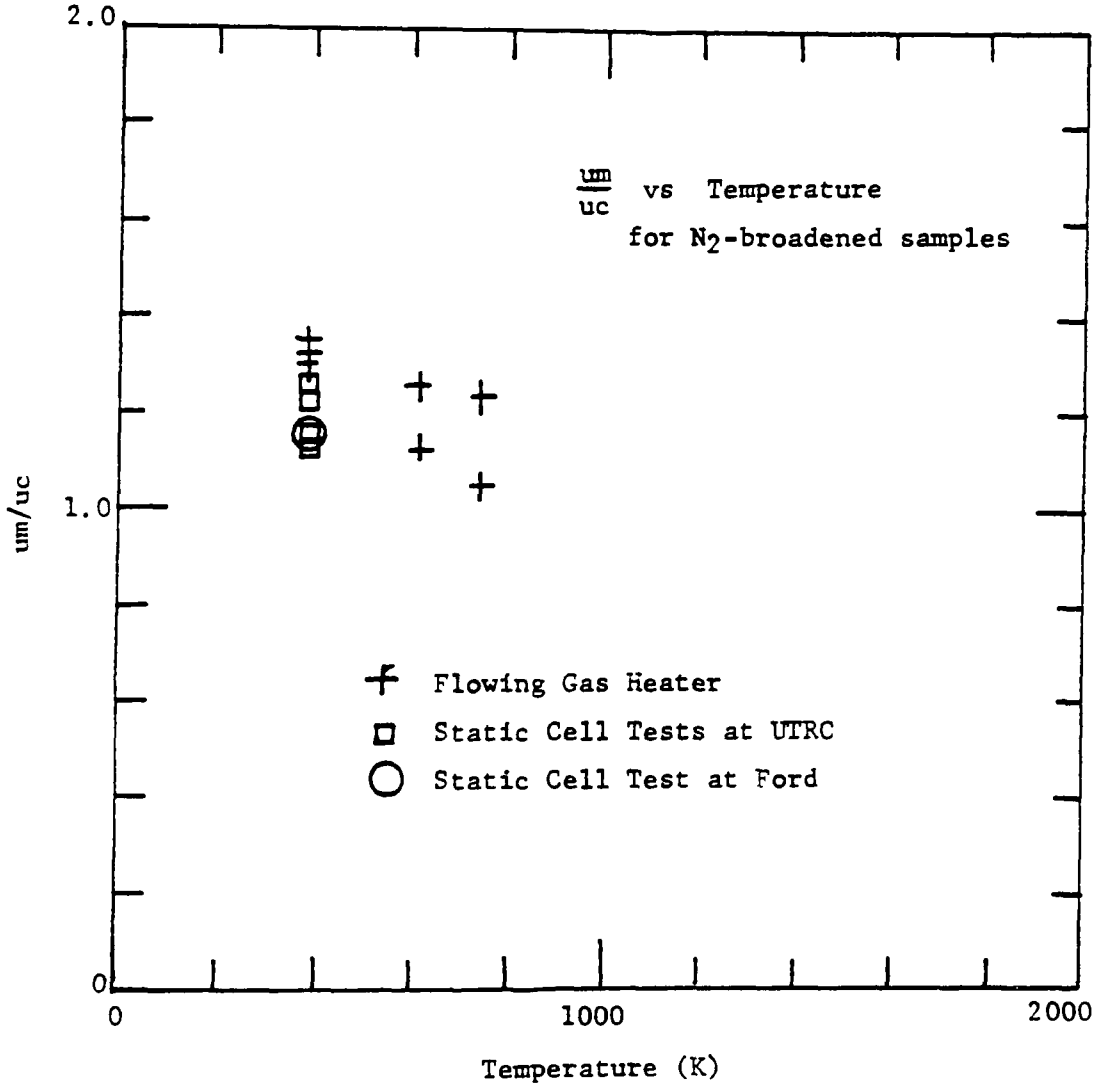

Figure 9. Plot of um/uc vs Temperature for N_2-broadened samples.

REFERENCES:

(1) Gryvnak, D.A. and Burch, D.E., "Monitoring NO and CO in Aircraft Jet Exhausts by Gas-filter Correlation Technique" prepared by Ford Aerospace and Communications Corp for the Air Force Aero-Propulsion Laboratory under contract F33615-75-C-2038, Air Force report AFAPL-TR-75-101, January 1976.

(2) Burch, D. E. and Gryvnak, D.A.,"Infrared Gas Filter Correlation Instrument for Insitu Measurement of Gaseous Polutants," prepared Ford Aerospace and Communications Corp. for EPA under contract No. 68-02-0575, EPA Report No. 650/2-74-094,December 1974.

(3) Burch D. E. and Williams D., "Infrared Absorption by Minor Atmospheric Constituents" Sci. Report 1, Contract No. AF 19(604)-2633 the Ohio State Univ. Res. Fn.(1960)

APPENDIX B

COMMENTS ON THE PROBLEMS IN THE PREVIOUSLY REPORTED SPECTRAL MODEL

The review of the spectroscopic model developed by ARO/AEDC revealed the following major problems:

1. There is an error in equation 18 of Ref. B3 (the same error is reflected in Refs. B3-B8) relating $f_{J'J''}$ to $f_{v'v''}$, which is off by a factor of 4.

2. There is an error in equation 17 of Ref. B3 (and the other reports) giving the ratio N_J''/N_o, which is off by a factor of about 2.

3. In Ref. B1 there was no distinction in population between the $^2\pi_{1/2}$ and $^2\pi_{3/2}$ states (i.e., Hund's case (b) was assumed) although this was partially corrected in Ref. B3 and the computer program delivered to UTRC, but without the correct normalization in the denominator.

4. An error exists in the equation for the Hönl-London factor for Q_{11} lines. This error can be found in the text of a 1973 report (B1), the text of a 1976 report (Ref. B3), and the computer program delivered to UTRC in 1978. ARO personnel have stated that this error was not always present, but they are uncertain as to when it first appeared. The error results in a miscalculation of NO concentration by about 15% when considered alone, and an incorrect temperature dependence for the absorption.

5. An error exists in Eq. 24 of Ref. B3 which relates the measured broadening parameter to the collision cross section. This error does not affect the predicted NO values from the model, but does result in a factor of 10 error in the collision cross section reported in Ref. B7.

In addition to the major problems listed above, a number of minor problems were discovered in the model delivered to UTRC which do not have much numerical significance, but which should be corrected.

6. The Q_{22} (30.5) and R_{12} (30.5) lines were incorrectly labeled.

7. The lines Q_{12} (3.5), R_{21} (36.5), P_{12} (31.5) and P_{12} (34.5) through P_{12} (40.5) should be added.

8. There is an error in the equation for B_v in subroutine HONNUM (Hönl-London factor computation).

Finally UTRC has shown that the use of theoretically generated line locations offers an improvement in the model when compared with the experimental line locations as given by Deezsi (Ref. B9). This does not represent an error in the earlier model, but does represent a considerable improvement, particularly at low pressures or elevated temperatures.

References:

B1 McGregor, W. K., J. D. Few, and C. D. Litton, Resonance Line Absorption Method for Determination of Nitric Oxide Concentration, Report AEDC-TR-73-182, December, 1973.

B2 Davis, M. G., W. K. McGregor, and J. D. Few, Spectral Simulation of Resonance Band Transmission Profiles for Species Concentration Measurements: NO γ-bands as an Example, Report AEDC-74-124, January 1975.

B3 Davis, M. G., W. K. McGregor, J. D. Few, and H. N. Glassman, Transmission of Doppler Broadened Resonance Radiation Through Absorbing Media with Combined Doppler and Pressure Broadening (Nitric Oxide γ-Bands as an Example), Report AEDC-TR-76-12, February 1976.

B4 Few, J. D., R. J. Bryson, and W. K. McGregor, Evaluation of Probe Sampling Versus Optical in Situ Measurements of Nitric Oxide Concentrations in a Jet Engine Combustor Exhaust, Report AEDC-TR-76-180, January 1977.

B5 Few, J. D., R. J. Bryson, W. K. McGregor, and M. G. Davis, Evaluation of Probe Sampling Versus an In Situ Optical Technique for Nitric Oxide Concentration Measurement in Combustion Gas Streams, Proceedings of the International Conference on Environmental Sensing and Assessment, Las Vegas, Nevada, September 1975.

B6 Few, J. D., W. K. McGregor, and H. N. Glassman, Ultraviolet Spectral Absorption Measurements of Nitric Oxide Concentration in T-56 Combustor Exhaust, AIAA Paper No. 76-109, AIAA 14th Aerospace Sciences Meeting, Washington, DC, January 26-28, 1976.

B7 Davis, M. G., W. K. McGregor, and J. D. Few, J. Quant. Spectrosc. Radiat. Transfer, 16, 1109 (1976).

B8 Few, J. D., W. K. McGregor, and H. N. Glassman, Resonance Absorption Measurements of NO Concentration in Combustor Exhaust, in Experimental Diagnostics in Gas Phase Combustion Systems, edited by B. T. Zinn, p. 187, published by AIAA, 1977.

B9 Deezsi, I., Acta Physica, 9, 125 (1958).

APPENDIX C

COMMENTS ON THE EXPERIMENTAL TECHNIQUE OF WISE AND FRECH

Wise and Frech observed the amount of NO decomposition by measuring the formation of the assumed products, N_2 and O_2. Molecular nitrogen was measured by trapping the remaining NO in liquid nitrogen and using 'manometric' techniques. Oxygen was allowed to react according to

$$NO + NO + O_2 \rightarrow 2\ NO_2 \qquad (1c)$$

The nitrogen dioxide was measured via optical absorption techniques. Several problems with their paper and experimental procedure may be found. First of all, no comparison is made between the N_2 and NO_2 data. Secondly, no allowance is made for alternative reactions or their products. For example, consider the overall reactions

$$4NO \rightarrow 2\ N_2 + 2\ NO_2 \qquad (2c)$$

or

$$2NO \rightarrow N_2O + 1/2\ O_2 \qquad (3c)$$

for which experimental data must be interpreted differently. Finally, and quite importantly, their pressure measurement of the product N_2 appears to be at best extremely difficult. Since very low levels of conversion were examined (usually about 0.5 percent), very small pressures of N_2 are expected, typically about one torr. In order for their technique to be useful, the nitrogen pressure must be measured accurately in a background of approximately one torr nitric oxide (vapor pressure at liquid nitrogen temperatures), one torr of oxygen (if a product), and about 1/4 torr impurity (likely to be nitrogen). Certainly, a measurement of one torr nitrogen with these other gases present would not be an easy task. If the dominant impurity in the initial NO is NO_2 rather than N_2 or N_2O (stated purity is 99.93 percent NO), then a measurement of 0.5 percent decomposition would be in error by (.07 percent) x 2/.5 percent = 28 percent when the NO_2 data is interpreted.

APPENDIX D

UTRC SPECTRAL COMPUTER PROGRAM DESCRIPTION AND LISTING

D.I. Program Description of NO Absorption of Continuum Radiation

D.I.a. Introduction

Several different versions of the NO spectral model have been developed. All of these are based on the model developed by Davis et al (1976)a and supplied to us, with corrections and additions made by us as noted in Appendix B. The plot routines are substantially different. The corrections made to the original program developed by Davis et al (1976a) make a significant difference in the amount of NO necessary to produce a given amount of absorption - about a factor of 2 at room temperature and atmospheric pressure.

The different versions of the NO spectral model may be summarized as follows. The absorption of continuum radiation by a homogeneous, isothermal layer of NO diluted in a foreign gas is modeled by the program (DUSEK*)NO-ABS (described in D.I.), in conjunction with the plot routine (DUSEK*)PLOT. PLOT5 (detailed in D.IV.) and the data file (DUSEK*)DATA-2. or (DUSEK*)DATAENG. The similar problem for absorption of continuum radiation by multiple zones, each of which is homogeneous and isothermal, is treated with two programs not described here, (PAGE*)NO-ABS. and (PAGE*)PLOT., along with the data file (PAGE*) DATA-2. The multiple zone includes the proper accounting of the complete line profile through the different absorbing layers before convolving the resultant with the slit function. The model describing the absorption of narrow-line radiation is called (DUSEK*) NO-SPECT. (described in D.II.), with the same plot routine and data files as for (DUSEK*)NO-ABS.

The program NO-ABS. predicts the transmission as a function of wavelength of incident continuum radiation by a known optical depth of nitric oxide at a given temperature and pressure. This program was written specifically for predicting transmission in high resolution over a narrow wavelength region. An additional program, PLOT., convolves this predicted transmission with a spectrometer slit function and displays the results graphically for comparison with experimental spectra.

The program NO-ABS. is composed of a main program, four subroutines, and a block data file. The program elements for the main body and the block data are NO-ABS.MAIN and NO-ABS.BLOCK-DATA, respectively. The element names of the subroutines are FUPPER, FLOWER, HONNUN, AND WFUNC. Each of these names is preceded by the file name NO-ABS, as before. A definition of variables for each element of NO-ABS. and a listing of the elements are included at the end of the program description section.

D.I.b. Main

The main program is divided into four parts. A description of the function of each part follows.

D.I.b.1. Main, Part 1

Part One reads parameters such as the optical depth, temperature, pressure, broadening information, options for line location, region of interest and a code that describes the version of the program presently in use. The options available for line location include either a theoretical calculation of line center or the use of experimentally determined line center wavenumbers. The experimental values for the line center wavenumbers were obtained from Engleman et al (1970). Theoretical line locations using spectroscopic equations and constants for NO (Engleman) yield predicted locations that differ from experimental observation by less than the room temperature Doppler width of NO (.005 Å or .0005 nm) for almost all lines. The wavenumber region of interest is defined by the first and last line numbers of that region. The present version of the program reads 474 lines. Normally, 1 to 30 of these lines are examined in a given run. Also contained in Part One of the main program is the assignment routine for the f-number of the transition. Since experimental evidence indicates that transitions originating in the $^2\pi_{1/2}$ state have a larger f-number than those originating in the $^2\pi_{3/2}$ state, provision has been made for a spin dependent f number.

D.I.b.2. Main, Part 2

Part Two of the main program reads and decodes the input line designation. The line designation consists of the branch of the transition (P, Q, R for $J'-J'' = -1, 0, +1$), upper spin state, lower spin state, and the rotational level in the lower state. The upper electronic state is slightly split (spin split) into two levels by a weak interaction of the electron spin with the magnetic field generated by the spinning molecule (and other effects, Ref. Herzberg 1939). Absorption transitions terminating in the $J = K - 1/2$ level are designated with a 2, while those terminating in the $J = K + 1/2$ level are assigned a 1. A similar system is used to define the level of the lower electronic state in which a transition originates. The lower state ($^2\pi$) is strongly split by spin-orbit coupling. The separation of the spin 1/2 and spin 3/2 levels is $\sim$120 cm^{-1}. Transitions originating in the lower energy $^2\pi_{1/2}$ state are assigned the value 1, while those originating in the higher energy $^2\pi_{3/2}$ state are assigned a 2.

Thus a line with $J = 10.5$ and $K = 11$ in the upper electronic state and with $J = 11.5$ in the lower spin energy level of the lower electronic state (i.e. $^2\pi_{1/2}$) would be labelled P21 (11.5). From the above discussion it can be seen that in general an absorption transition originating from a given J value can terminate in any one of twelve possible systems, since there are three branches and four possible combinations of levels for each branch.

Also found in Part Two is the calculation for the line center absorption coefficient, KO(I). The variable I is incremented by 1 as each line center absorption coefficient is calculated. (At this stage, KO(I) does not contain the path length over which the absorption takes place). In determining this coefficient the three subroutines FUPPER, FLOWER, and HONNUM are accessed to determine the upper state energy, lower state energy, and the Hönl-London factors, respectively, for the transition. Also at this time, the line location option is queried. If the theoretical line option was selected, the line center transition wavenumber (WO(I)) will be given by the difference of the upper and lower state energies resulting from FUPPER and FLOWER. If the experimental line location option was requested, then the wavenumber read with the line designation is used for WO(I).

D.I.b.3. Main, Part 3

Part Three of the program establishes the wavenumber region in which the transmission calculations are done. The wavenumber region will begin 2.0 Lorentz widths and 2.4 Doppler widths (DELTAW) before the line center wavenumber of the first line selected and will end an equal amount, DELTAW, after the line center wavenumber of the last line selected. The region defined by these start and stop wavenumbers is divided into 499 panels. The transmission is calculated at the wavenumber of each of these panels. The transmission is obtained for a panel from Beer's Law, $I = I_o e^{-k_\nu d}$. The absorption coefficient k_ν is determined by summing the absorption coefficients at the panel from all spectral lines which contribute significantly to the transmission at that panel's wavenumber. To determine if the absorption at a panel from a given line is significant, its contributrion to k_ν is divided by the total absorption coefficient determined from all lines previously examined at that panel. If this quotient is less than a value given to the variable ALLOW, a counter (NHOLDER, NHOLDL) is indexed. This counter is reset to zero if the quotient becomes greater than allow. When the counter value increases to three (indicating that the Allow condition has been met three times consecutively) the transmission calculation will advance to the next panel. The consecutive stipulation reduces the chances of exiting the coefficient loop when encountering an isolated weak line. In addition to the ALLOW check for the absorption contribution, the loop cannot be terminated if the absorbing line's center wavenumber is within DELTAW from the panel being examined. The absorption coefficient must frequently be evaluated at some distance from line center. For the Voight profile used, this value (k_{ν_i}) is related to the line center absorption coefficient k_{ν_i} by the expression

$$k_{\nu_i} = k_{\nu_i^o} \, \mathrm{Re} \left\{ \exp(-(\omega_i + ia')^2) \, \mathrm{erfc}(-i\omega_i + a') \right\} \qquad \text{D1}$$

where

Re = Real Part

$$\omega_i = \frac{2\,(\nu_i - \nu_i^o)}{\Delta\nu_D}\sqrt{\ln 2} \qquad \text{D2}$$

ν_i^o = line center wavenumber

ν_i = wavenumber

$\Delta\nu_D$ = Doppler width of the line

$$a' = \frac{\Delta\nu_L}{\Delta\nu_D}\sqrt{\ln 2}$$

$\Delta\nu_L$ = Lorentz width of the line

$i = \sqrt{-1}$

erfc = complementary error function

The expression for $k_{\nu i}$ is evaluated in the subroutine WFUNC.

When the transmission calculation has been completed for all 499 panels the program advances to Part Four.

D.I.b.4. Main, Part 4

The function of Part Four of the main program is to record the inputs of Part One and each panel transmission and wavenumber on a temporary file for later use by another program (PLOT.). The entire program MAIN will be repeated for each NO concentration. When an end-of-file is detected in the input data file DATA-2, the main program will terminate.

D.I.c. Input File DATA-2

In order to facilitate changes in the input parameters such as path-length, gas temperature, and NO concentration, these values are placed in a data file named DATA-2. This file also contains the spectral line information and selections for the various options. Since DATA-2. is also used as an input to a resonance absorption program (NO-SPECT.), some of the entries in DATA-2. do not apply to NO-ABS. A partial list of DATA-2. with appropriate definitions follows in Table D-I.

More concentrations can be added to the end of DATA-2 if desired. The numbers appearing after the spectral line designation are the center wavenumber of the transition as reported by Deezsi (1958). Many of these lines were not

TABLE D-I

1	2	3	4	5	6	7	8	9	10	11	12	13	14	15	16	17	18	column	Variable	Comments
0	4	5																	LINST	Integer
1	0	0																	LINEND	Integer
0	0	1																	NWOTHE	1, Theoretical Lines 0, Experimental Lines
4	5	1	0	0	.					1	.	6	3	0	6				-	Does Not Apply
4	5	4	7	8	.					.	6	9	4	4					-	
4	8	5	0	0	.					-	1	.	8	4	3				-	
																				Blank line
*		F	=	3	.	3	0	5	+	H	+	C							HEADS	Version Code
6	.																		-	Does Not Apply
1	.	6																	-	
2	.	5	9	5															APRIME	Function of pressure, temperature, broadening constant
8	0	0																	TA	Degrees K
6	0	0																	-	Does Not Apply
1	8	.	6																EL	Path Length (cm)
1	0	.																	-	Does Not Apply
0																				
0																				
		1	P	1	2	(	1	0	.	5	)		4	4	0	5	2	.	0	3	First Spectral Line
		2	P	1	2	(	1	1	.	5	)		4	4	0	5	2	.	0	3	Second Spectral Line
		3	P	1	2	(		9	.	5	)		4	4	0	5	2	.	0	3	Third Spectral Line
		4	P	1	2	(	1	2	.	5	)		4	4	0	5	2	.	7	8	Fourth Spectral Line
		5	P	1	2	(		8	.	5	)		4	4	0	5	2	.	7	8	Fifth Spectral Line
		-	-	-	-	-	-	-	-	-	-	-	-	-	-	-	-	-	-	-	-	-
4	7	4	R	2	1	(	3	9	.	5	)		4	4	9	3	4	.	5	1	474th Spectral Line
																				Blank line
0	.																			No Nitric Oxide
4	.	6	9	5	3			1	5											1st Nitric Oxide Concentration

resolved by the instrument used; hence several different lines may appear at an identical wavenumber. More highly resolved values for the line center wavenumbers are available in Engleman et al (1970). Another input data file with Engleman's experimental line locations exists in file DATAENG. This list does not contain nearly as many lines as DATA-2. and is only a partial tabulation of all the lines listed in Engleman et al. Choosing the theoretical line locations (i.e. placing 001 in line 3 of DATA-2.), while using DATA-2. will very nearly reproduce all of the experimental values available in Engleman, et al. A partial list of the difference between Engleman's experimentally measured line center values and those derived theoretically can be found in Fig. D1. The differences are generally less than the room temperature Doppler width of NO (.055 $\mathring{A}$ or .0005 nm). At high rotational values, the theoretical locations for the P_{22} lines systematically diverged from the experimentally measured values. For highest accuracy, lines should be arranged from lowest to highest energy (increasing wavenumber).

D.I.d. NO-ABS. FUPPER

The purpose of this subroutine is to calculate the upper state energy of the $\gamma(0,0)$ transition. The equations and constants used are the same as those described in the text see Section III-B.6.d.

D.I.e. NO-ABS. FLOWER

This subroutine calculates the lower state energy for a $\gamma(0,0)$ transition. The equations and constants used are the same as those described in the text see Section II-B.6.c.

D.I.f. NO-ABS.WFUNC

Subroutine WFUNC calculates the off-line center fractional absorption coefficient ($k_{\nu j}/k_{\nu j}^{o}$) for a particular spectral line. This is accomplished by determining the real part (W1) of the function.

$$W(z) = \exp(-z^2)\ \mathrm{erfc}(-iz)$$

where $i = \sqrt{-1}$

$z = \omega_j + ia'$ (See NO-ABS Main, Part 3).

The technique for evaluating this function is taken from Abramowitz et al. NBS Handbook of Mathematical Functions. There are basically two methods used to determine W1. If either ω_j or a' are in the intervals

$$0 \le \omega_j \le 3.9$$

or

$$0 \le a' \le 3.0,$$

FIG. D1

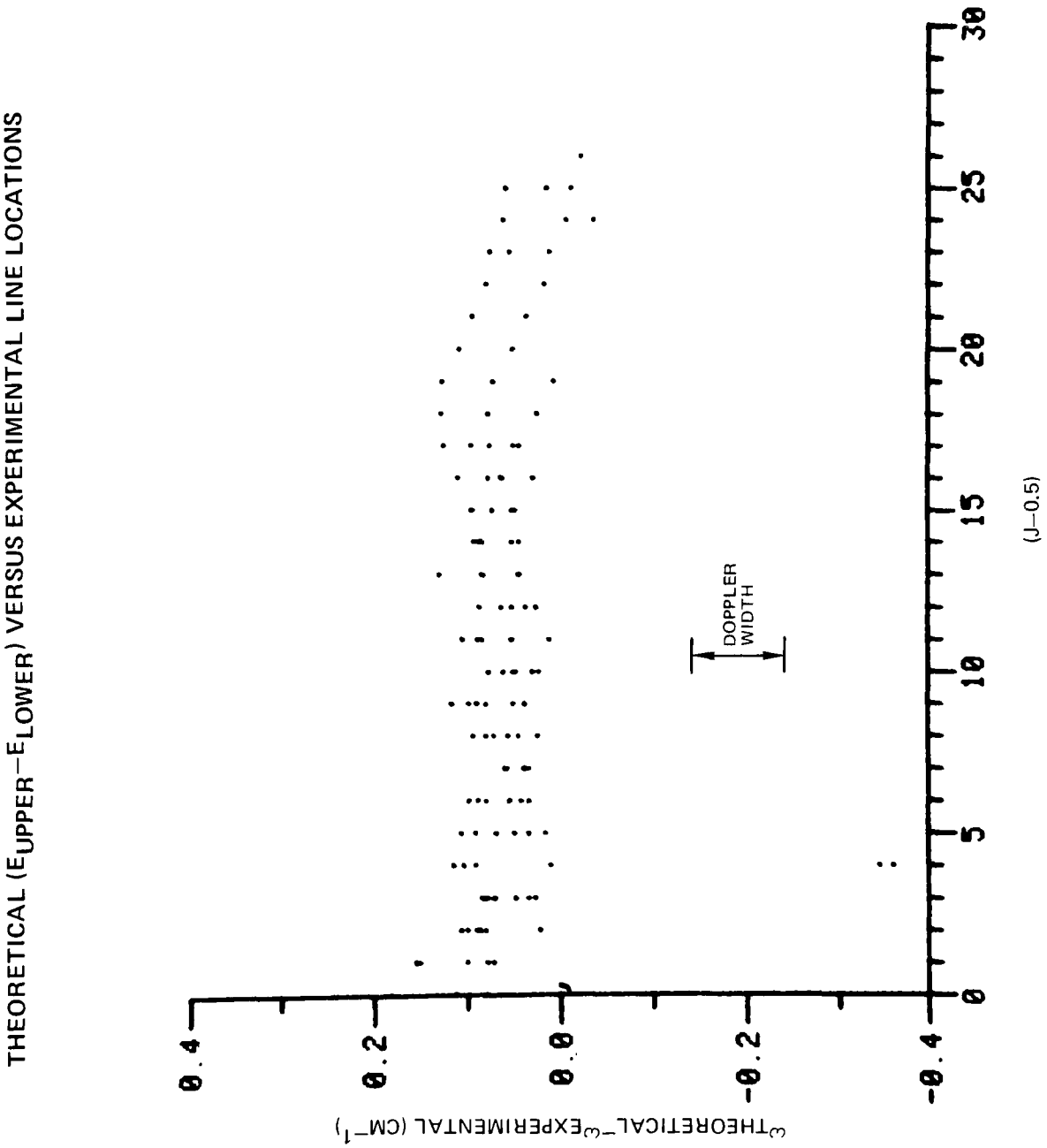

79—04—93—23

the value W1 is obtained by a two-dimensional linear interpolation from the nearest ω_j and a' values found in the block data table BLOCK-DATA (see Davis, et al (1976) for listing). This table consists of a 31 by 40 by 2 array whose elements are labeled by z(A1, B1, C1) where A1 corresponds to a', B1 corresponds to ω_j, and C1 corresponds to the real or imaginery part of W(z) i.e., W1 or W2.

The element z(11, 3, 1) is the real part of the function $\omega(z)$ evaluated for z = 0.2 + 1.0 i, while the element z(11, 3, 2) is the imaginery part of the same function and argument. Conversion of the arguments of z to a table element is accomplished by taking the integer portion of ten times the argument value plus one. This procedure yields 31 real values for a', and 40 real values for ω_j since each is evaluated in increments of 0.1 over the regions previously defined. For example, to locate the real part of $\omega(z)$ for z = 0.2 + 1.0 i, the element A1 is found by multiplying 1.0 by ten, adding 1 and taking the integer portion of this sum. Thus A1 for a' equal to 1.0 is 11, and similarly B1 for ω_j equal to 0.2 is 3. Therefore the real part of W(z) will be found in the table element z(11, 3, 1). When the arguments of $z = \omega_j + a'i$ are nonzero beyond the first decimal place, this technique automatically results in the nearest table element less than the desired value. The nearest table element greater than the desired value is obtained by adding one to the values A1 and B1 just found. From the table elements found at these element locations, the two-dimension linear interpolation approximates the desired value of W(z).

For values of ω_j and a' greater than 3.9 and 3.0 respectively, polynomial approximations for W(z) are used. For ω_j and a' in the intervals

$$3.9 < \omega_j \leq 6.0$$

or

$$3.0 < a' \leq 6.0$$

W(z) is given by

$$W(z) = i\bar{z}\,(T_1 + T_2 + T_3) + e(z)$$

where

$$T_1 = .4613135/(z^2 - .1901635)$$

$$T_2 = .09999216/(z^2 - 1.7844927)$$

$$T_3 = .002883894/(z^2 - 5.5253437)$$

and

$$|e(z)| < 2 \times 10^{-6}.$$

When either ω_j or a' is greater than 6.0, W(z) is given by

$$W(z) = iz\,(T1 + T2) + \eta(z)$$

where

$$T1 = .5124242/(z^2 - .2752551)$$

$$T2 = .05176536/(z^2 - 2.724745)$$

and

$$|\eta(z)| < 10^{-6}.$$

The last part of this subroutine is devoted to evaluating W(z) when either or both arguments of z are negative. In practice, the evaluation for negative argument is not needed. Likewise, for this application all the elements of the block data table labeled z(A1, B1, 2) are never used since these correspond to the imaginary part of W(z).

D.I.g. NO-ABS. HONNUM

Subroutine HONNUM calculates the normalized Honl-London factor for determining the intensity of a given transition. The equations are normalized such that the summation of the Honl-London factors over all the upper state J values (J') for a given lower state J value (J") equals 4(2J"+1). In general, intensities of absorption transitions originating in the J = 1/2 rotational level must be considered separately (Earls (1935)). These intensities are

$$Q_{21} = Q_{11} = 4/3$$

$$R_{21} = R_{11} = 2/3$$

All other branches are identically zero. In nitric oxide, the spin-orbit coupling constant is so large that the intensities of lines connected to the J = 1/2 level are correctly predicted to at least eight significant digits by the general expressions given.

D.II. Program Description of Resonant Absorption of NO Radiation

The program NO-SPECT.predicts the fractional transmission of radiation through a gas mixture containing a known amount of nitric oxide. The incident radiation is obtained from excited nitric oxide molecules at low pressure. The program construction and description of NO-SPECT.is very similar to the program NO-ABS.previously discussed. The differences are contained

mainly in defining the spectral distribution of the incident radiation. For NO-SPECT. the incident intensity is obtained from an experimental measurement of individual spectral lines emitted by the source and from an assumed Doppler broadened line shape. The transmission is calculated on a line by line basis. Each source spectral line in the selected wavelength region is divided into 100 panels starting 2.3 Doppler widths (DELTAW) before line center and ending an equal amount beyond line center. The incident intensity at a given panel is found by assuming a Gaussian lineshape of known full width at half maximum (FWHM) centered on the center wavenumber of the transition. The relative maximum intensity of the source line is obtained by linear interpolation from a table of experimentally derived intensities that have been normalized by the respective Hönl-London factor of the measured line. This table is contained in the data file DATA-2 in lines 4, 5, and 6. See discussion of FUNC for more information on source line strength. The absorbing line's strength at each panel is determined in a manner identical to that described in the discussion of NO-ABS.

At the completion of NO-SPECT., the integrated intensity of each lime leaving the absorbing gas is recorded on a temporary data file. The line intensities are recorded with each line's center wavenumber in groups for each concentration of NO listed at the end of the data input file DATA-2. This information is read into another program, PLOT, that convolves these lines with a spectrometer slit function and displays the results graphically.

An additional section exists at the end of NO-SPECT.MAIN Part Three that outputs the integrated fractional transmission of very closely spaced line groups. This option cannot be accessed by the input data file DATA-2. To obtain output from this option the mandatory GO TO statement (GO TO 560) must be removed from the program. These cluster transmissions are required for determining source characteristics.

All subroutines used for NO-SPECT. are identical with those described in NO-ABS. An additional subroutine (NO-SPECT. FUNC) is required for source line intensities (see D.II.a below).

Additional variable definitions for variables found only in NO-SPECT. and a figure (Fig. D-2) further describing the model's operation are found in the variable definition section.

D.I.f. NO-ABS FUNC

To predict the amount of transmission of resonant radiation through a gas, the relative source intensity at each line must be known. Many times there are overlapped lines or lines which cannot be resolved by the spectrometer and whose intensities are not directly measurable. This subroutine linearly interpolates all line intensities from a least squares fit of normalized resolved lines whose intensities can be directly measured. For electrical discharge lamps, a log-linear plot of the measured spectral line intensities divided by their respective Hönl-London factors versus the line's upper state energy will typically result in a curve shown in Fig. 20. For our purposes this curve was fit with two straight lines. The intensity of any spectral line can now be approximated from these two straight lines once the upper state energy and the Hönl-London factor for the trasition are known.

CONVOLUTION SYMBOL DEFINITIONS

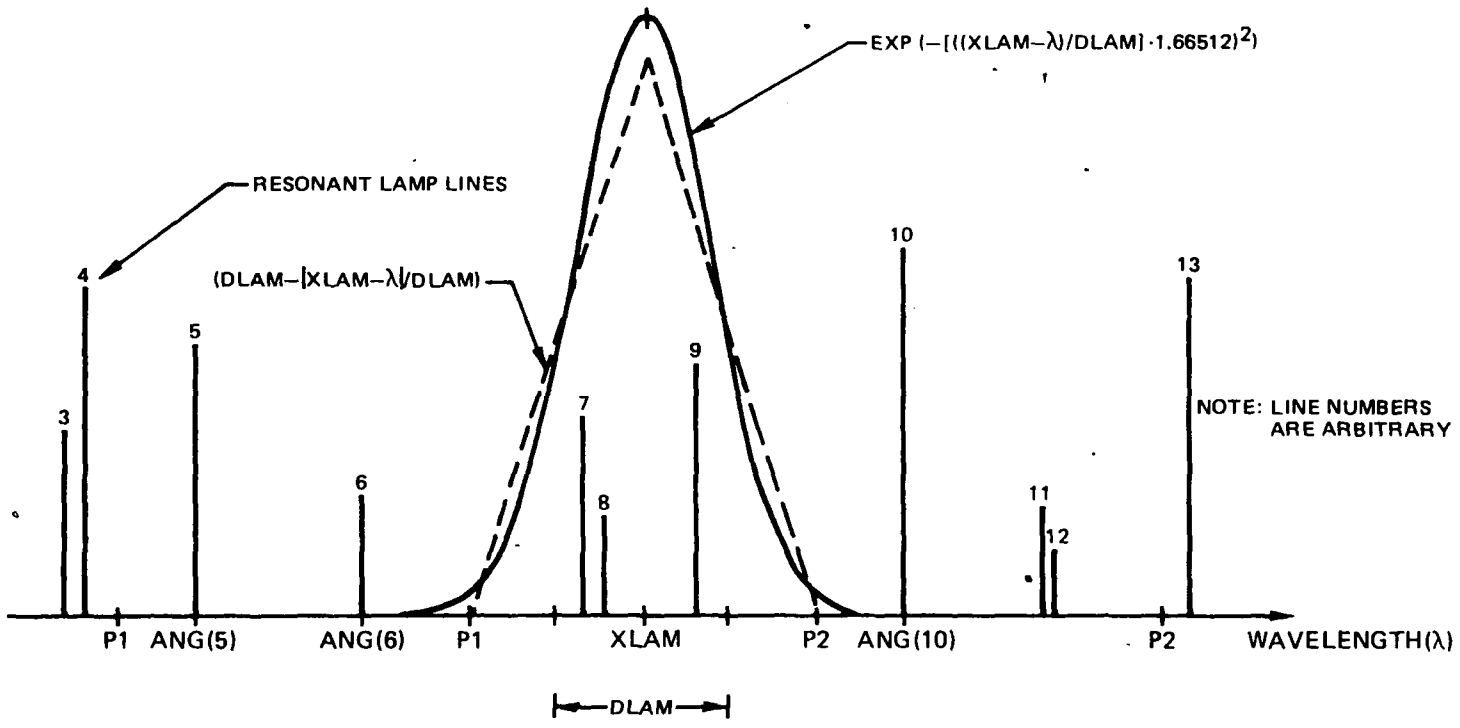

SLIT FUNCTION

GAUSSIAN (——)	TRIANGULAR (— —)
ISTART = 5 NOPTS= 8	ISTART = 7 NOPTS = 3

FIG. D2

D.III. List of Symbols

MAIN (NO-ABS)

G(n) - Vibrational energy of nth vibrational level

QVIB - Vibrational partition function

ALLOW - Ratio of absorption coefficient for a given line to total absorption coefficient from all previous lines at a particular wavenumber

LINST - Line number of first spectral line defining start of interval to be examined

LINEND - Line number of last spectral line to be examined

NWOTHE - Conditional branch variable to select theoretically-computed line locations (=1), or use experimentally-determined line locations (=0)

XDATA(I) - Wavenumber array of resolved upper level ($^2\Sigma$) source spectral lines

YDATA(I) - Normalized logarithmic intensity array of resolved source spectral lines

NP - Number of source lines used to characterize source output

HEADS - Version label

AP - Broadening parameter (a')

TA - Absorber temperature

TE - Emitter temperature (applies only to NO-SPECT.)

EL - Path length of absorption

YHGT - Records option taken for variable NWOTHE

BVEØØ - Spectroscopic constant for the zero vibrational state

AFL - Spin orbit coupling constant for lower level

C1S12 - f number for transitions connected to the $^2\pi_{1/2}$ level

C1S32 - f number for transitions connected to the $^2\pi_{3/2}$ level

C2 - hc/kT_A

CONST1 - $-2\sqrt{\ell n(2)}$

CONST2 - Doppler width of source divided by line wavenumber $(2\sqrt{2(\ell n2)}\ kT_E/m_sC^2)$

CONST3 - Doppler width of absorber divided by line wavenumber $(\sqrt{2(\ell n2)}\ kT_A/m_sC^2)$

CONST4 - 2.3 · (CONST2)

J - Spectral line position in array of spectral lines input, (not the rotational level)

RJPP - Rotational level (truncated integer)

JPP - Rotational level (truncated integer)

BRANCH - Rotational branch (P,Q,R)

ICODE - Rotational branch (=1, P, branch, = 2 Q branch, = 3 R branch)

NUP - Spin split state in upper level ($^2\Sigma$)

NLO - Spin state in lower level ($^2\pi$)

WO(J) - Line center wavenumber of line number J

ISPIN(J) - Array of lower spin states for all spectral lines in input list

S(J) - Hönl-London factor of the Jth line

NLINES - Total number of spectral lines read from input list

ENO - Nitric oxide concentration (molecules/cm^3)

KO(I) - Line center absorption coefficient of Ith lines

NINT - Wavenumber range of interest is divided into this many panels (max. 499)

DWJ - Doppler width of source

DWL - Doppler width of absorber

DELTAW - 2 Lorentz widths + 2.4 Doppler widths absorber (cm^{-1})

WST - Wavenumber at beginning interval of interest

WND - Wavenumber at ending interval of interest

AZJ - Lower wavenumber limit of mandatory computation for given spectral line

BZJ - Upper wavenumber limit of mandatory computation for a given spectral line

DEL - Incremental wavenumber of panels in region of interest

W(I) - Center wavenumber of Ith panel

E(I) - Source intensity of Ith panel (constant)

JLEFT - ϕ when examining lines of larger wavenumber than present panel; = 1 when examining smaller

SUML - Total absorption coefficient from all lines of wavenumber greater than, or equal to, nearest spectral line

SUMR - Total absorption coefficient from all lines of wavenumber less than, or equal to, nearest spectral line

NHOLDR - Number of consecutive lines whose contribution to the total absorption coefficient is less than minimum required

NHOLDL - Number of consecutive lines whose contribution to the total absorption coefficient is less than minimum required

NLESR - Number of consecutive lines whose contribution to the total absorption coefficient is less than minimum required

NLESL - Number of consecutive lines whose contribution to the total absorption coefficient is less than minimum required

BETA - $2\sqrt{\ell n 2}\ (\nu_j - \nu_j')$/(Doppler width of absorber)

WFUNC - Complex complementary error function to determine absorption coefficient at arbitrary distance from given spectral line (fraction of line center absorption coefficient)

TERM - Absorption coefficient at arbitrary distance from given spectral line (fraction of line center absorption coefficient)

TNEW - Absorption coefficient at arbitrary distance from given spectral line

II - Rotational level

CAY(I) - Total absorption coefficient for the Ith panel from all spectral lines considered

DAT(I) - Intensity of Ith panel after passing thru absorbing gas

TAUTOP - Total transmitted intensity

TAUBOT - Total incident intensity

TAU - Ratio of transmitted intensity incident intensity

ALPHA - Ratio of absorbed intensity to incident intensity

WO2(I) - Reordered panel wavenumber, largest to smallest

TJ2(I) - Reordered panel transmissions (see WO2(I))

FUPPER

V - Vibrational level

J - Rotational level

M - Spin split level in upper state ($^2\Sigma$ level)

T - Term value of electronic level

G - Term value of vibrational level

WE - ω_e

WEXE - $\omega_e\chi_e$

BE - B_e

ALPHAE - α_e

DV - D_v

BV - B_v

GAMA - γ

FN - Term value of rotational level

F - Term value of upper state ($^2\Sigma$ level)

FLOWER

V - Vibrational level

J - Rotational level

M - Lower spin state ($^2\pi$ level)

USS - Spin split level of upper state ($^2\Sigma$ level)

T - Term value of electronic level

G - Term value of vibrational level

DV - D_V

A - Lower state spin-splitting constant ($^2\pi$ level)

BE - B_E

BV - B_v

WE - W_e

WEXE - $\omega_e\chi_e$

IB - Rotational branch

NSIGN - Direction of lambda doubling shift

LMDADB - Magnitude of lambda doubling term in lower state ($^2\pi$ level)

F - Term value of lower level ($^2\pi$)

WFUNC

XF - Same as BETA (MAIN.NO-ABS)

YF - a' (Broadening parameter)

W1 - Interpolated real part of the complex function W(z) where z = XF + YF i

WZ - Interpolated imaginary part of the complex function W(z)

Z(DUM1,DUM2, 1) - Real part (W(DUM2 + (DUM1)i))

Z(DUM1,DUM2, 2) - Imaginary part (W(DUM2 + (DUM1)i))

X(DUM) - Real Part of W(z) (Table Value)

Y(DUM) - Imaginary part of W(z) (Table Value)

IFLAG - Conditional branch variable whose value is
$\phi \rightarrow$ when $\rightarrow$ XF $\geq$ YF $> \phi$
1 when XF $< \phi$, YF $> \phi$
4 when XF $< \phi$, YF $< \phi$

II - Converts YF into an integer $\geq$ 1 (Lower bound in table look-up for YF)

JJ - Converts XF into an integer $\geq$ 1 (Lower bound in table look-up for XF)

II1 - II+1 upper bound in table look-up for YF interpolation

JJ1 - JJ+1 upper bound in table look-up for YF interpolation

Z1 - Linearly interpolated value for XF with Y=CONST=II

Z2 - Linearly interpolated value for XF with Y=CONST=II1

W(1) - Interpolated real value of W(XF+YF i)

W(2) - Interpolated imaginary value of W(XF+YF i)

ZC - z = XF+ YFi (complex) = argument of W function

HONNUM

NUP - Upper vibrational state (v')

NUPP - Lower vibrational state (v")

MEGAN - Upper spin state

MEGAM - Lower spin state

IB - Rotational branch

J - Lower rotational level

A - Lower state spin-splitting constant

BE - B_e

ALPHAE - α_e

BV - B_v

RNUM - Numerator of Honl-London factor

DENOM - Denominator of Honl-London factor

HONL - Honl-London factor for transition

MAIN (NO-SPECT)

XDATA(I) - Lower state wavenumber of source spectral line

YDATA(I) - Natural logarithm of resolved source spectral line intensity normalized by the Hönl-London factor of the transition

TE - Source Temperature

CONST2 - Doppler width of source divided by line wavenumber $(2\sqrt{2(\ell n2)\kappa(TE)/mc^2})$

CONST4 - 2.3 times CONST2

EO(J) - Line intensity of Jth source spectral line

NINT - Number of calculations (panels) performed over a single source spectral line

W(I) - Wavenumber of Ith panel of a given source spectral line

E(I) - Intensity of Ith panel of a given source spectral line (Gaussian shape assumed)

DIST - 4.6 Source Doppler widths FWHM

TAUTOP - Integrated intensity of lines passing through the absorbing gas

TAUBOT - Integrated intensity of lines incident on absorbing gas

FUNC

X - Wavenumber of upper level transition of line of interest

XDATA - Wavenumber array of resolved upper level transitions for source

YDATA - Natural logarithm array of normalized resolved source line intensities

NP - Number of points used to characterize source line intensities

NP1 - NP minus 1

FUNC - Linearly interpolated normalized natural logarithm of the intensity of unresolved source line

D.IV. Program Description PLOT.PLOT5

D.IV.a. Introduction

The program PLOT.PLOT5 convolves the spectral transmission calculated in programs NO-SPECT. and NO-ABS. with a spectrometer slit function to aid in reducing experimental data. Results of the convolution are presented graphically.

The program is divided into four parts. A discussion of the function of each part is presented in the following section.

D.IV.b. Discussion

D.IV.b.1. Part One

Part One of the program reads the transmitted intensity and wavenumber at each wavelength present in the radiation source. For resonant radiation (NO-SPECT.), these wavenumbers are the center wavenumbers of each line. The transmissions at these wavenumbers are the integrated intensities of individual lines (i.e., the transmission verses wavenumber is nonzero only at the center wavenumber of the transition; no direct information on line shape is contained in these transmissions). For absorption from a continuum source (NO-ABS.), the wavenumbers read are uniformly spaced throughout the region of interest. In this case, the original lineshape of the absorbing line is retained. Original input parameters for NO-SPECT. or NO-ABS. are read for documentation purposes on the plots. Options are presented for plotting the data as read (zero slit plots) in addition to the convolution plots generated by PLOT.PLOT5. At this time, the user is also queried for the slit width of the convolution. The slit width is defined as the apparent full width at half maximum transmission (FWHM) of a resolved line in the experimental spectra. The slit width must have units of angstroms (Å). Part One continues with a conversion of the original wavenumbers to wavelengths. Since line order (increasing wavelength) is assumed in the construction of later parts of the program, Part One contains a sorting loop (ISORT) which looks twenty lines ahead of the present line location to resort lines and intensities for continually increasing wavelength.

D.IV.b.2. Part Two

Part Two produces plots of the data as received after the line sort operation described in Part One. A vertical line is drawn at the location of each wavelength initially read. The relative heights of these vertical lines are proportional to the spectral intensity read at each wavelength. These plots are referred to as zero slit plots, since no instrument broadening has been included. It should be reemphasized that plots for resonant absorption (NO-SPECT.) do not retain line shape information. Zero slit

plots for resonant absorption, and absorption of continuum radiation are shown in Figs. D3 and D4, respectively. Part Two also sets the convolution interval (WIDE) for Part Three.

D.IV.b.3.Part Three

Part Three computes the resultant intensity verses wavelength when the individual intensities are examined by a measuring intrument (spectrometer) of finite resolution. The transfer function of the spectrometer can be determined by scanning and examining the resultant profile of a spectral line whose bandwidth is very narrow relative to the spectrometer's bandpass. For the spectrometer used in our measurements, the transfer function can be approximated as a triangular function for bandpasses greater than 0.5 Å and by a Gaussian function for bandpasses less than 0.5 Å (Figs. D5 and D6). To produce the convolved spectral plots, a wavelength region starting twice the convolution interval (2·WIDE) before the wavelength of the first spectral line and ending an equal amount after the last spectral line is divided into 2499 panels. At each panel, a convolution interval is defined (WIDE) whose width is twice the spectrometer slit function for the triangular case and six times the slit function for the Gaussian case. This convolution interval is centered on the panel at which the calculation is being performed. Beyond this interval, the contribution to the convolution is considered to be zero. A loop is set up to determine the first spectral line number (ISAVE) and total number of spectral lines (NOPTS) within the convolution interval. Starting at spectral line number ISAVE, the intensity of each of the next NOPTS lines is weighted with a Gaussian or triangular function according to the relation.

$$\text{TRIADD} = \text{HT(JBL)} \exp\left(-\left[(\text{XLAM} - \text{ANG(JBL)})/\text{DLAM} \cdot 1.66512\right]^2\right)$$

or

$$\text{TRIADD} = \text{HT(JBL)} \left[\text{DLAM} - \left|\text{xLAM} - \text{ANG(JBL)}\right|\right] / \text{DLAM}$$

where TRIADD is the weighted intensity, HT(JBL) is the original line intensity, DLAM is the FWHM of the spectrometer in angstroms, XLAM is the panel wavelength at which the convolution is taking place and ANG(JBL) is the wavelength of the spectral line being weighted. Figure D2 presents symbol definitions graphically. Weighted intensities at the edge of the convolution interval for the Gaussian case are down by more than 10^{-11} relative to the same intensity at the center of the interval. The weighted intensities over the entire convolution interval are summed under the variable name SUMMER. When the sum is completed, the value of SUMMER is placed in the array PLOTY (KKOUNT) and the center wavelength of the convolution interval is placed in the array PLOTX (KKOUNT) where KKOUNT is the panel number at

ZERO SLIT WIDTH PLOT FOR RESONANT LINE SOURCE

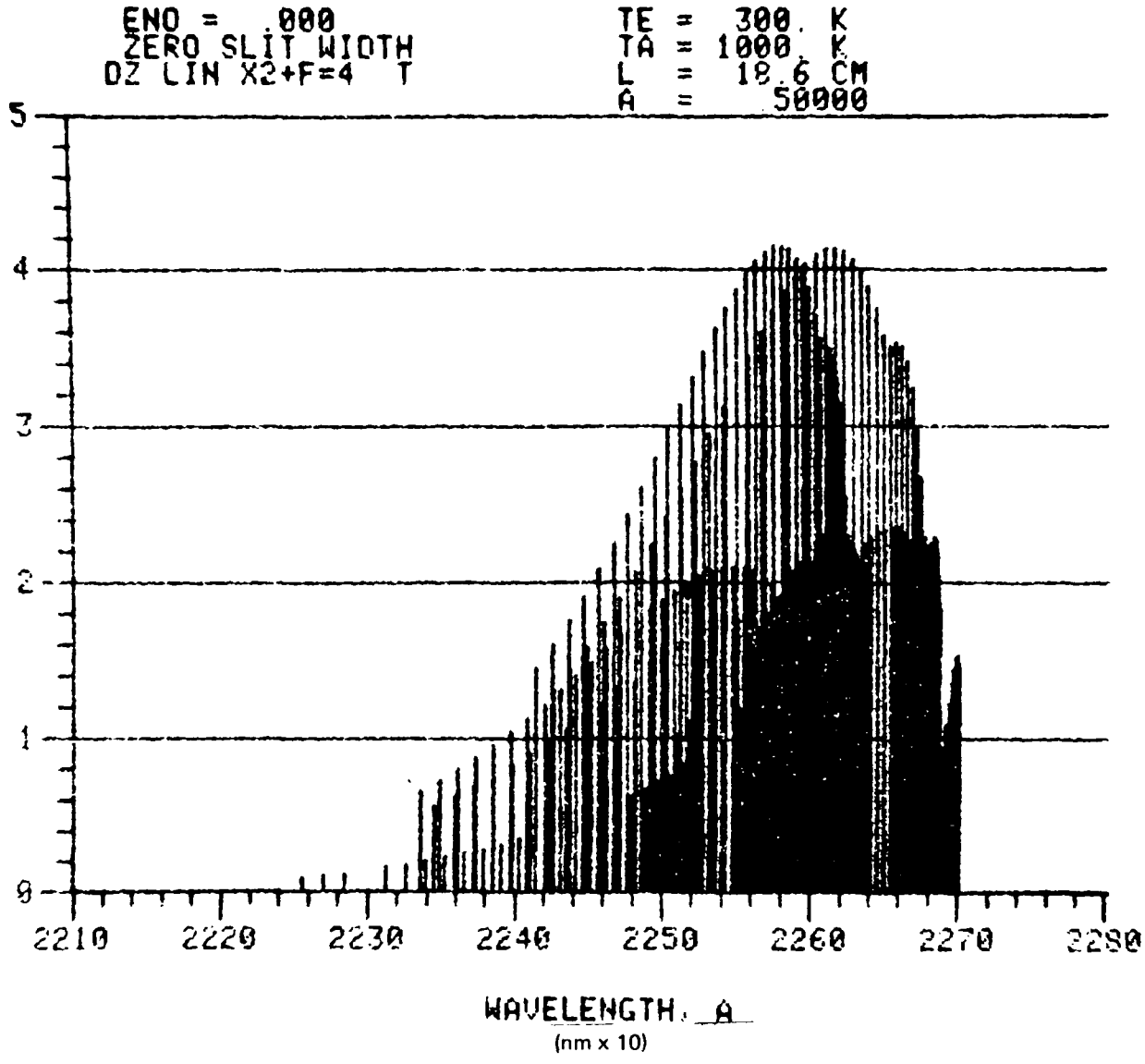

FIG. D3

79-04-93-2

ZERO SLIT WIDTH FOR CONTINUUM SOURCE

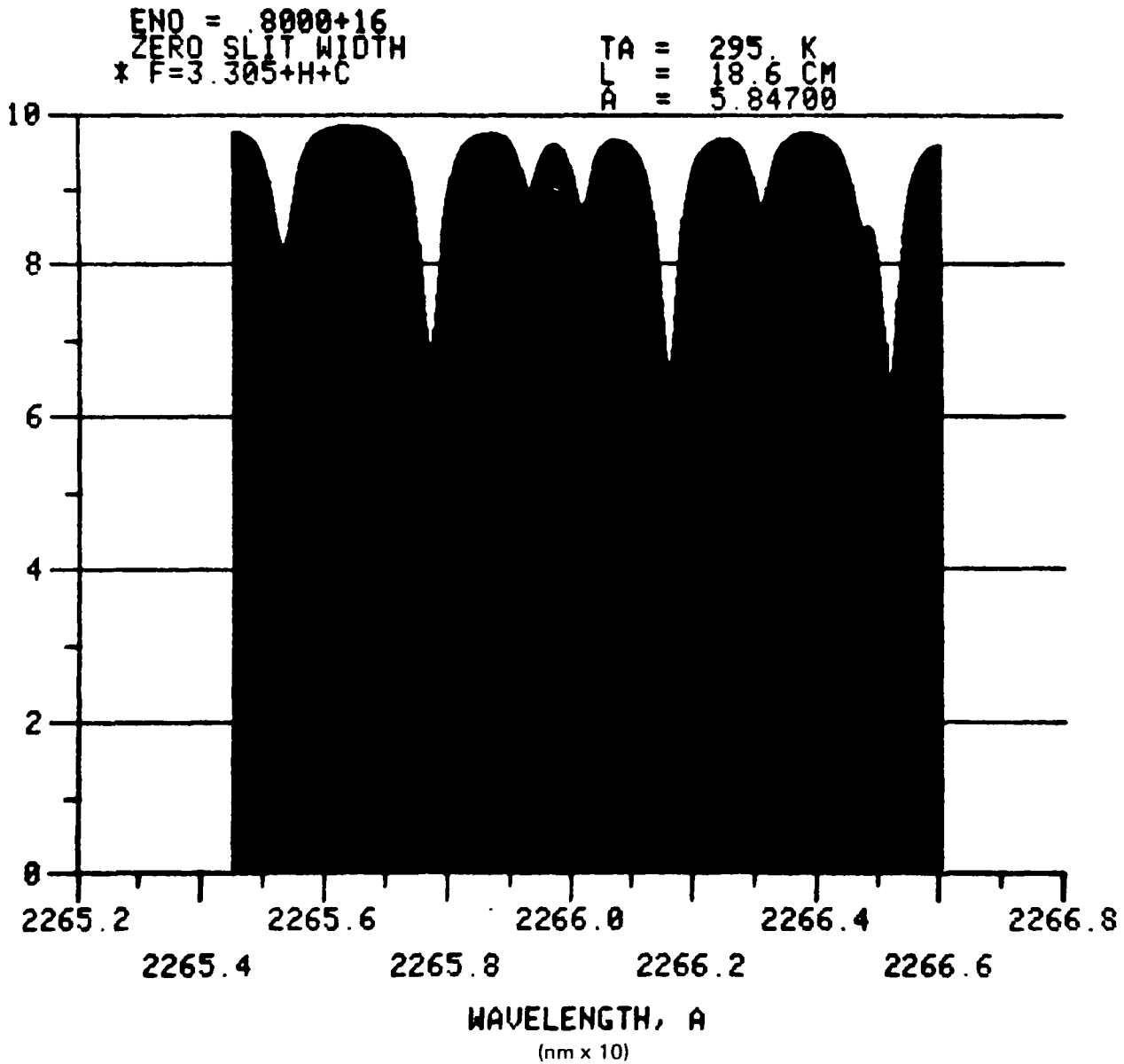

FIG. D4

79-04-93-1

SPECTROMETER TRANSFER FUNCTION, 1000μm SLITS

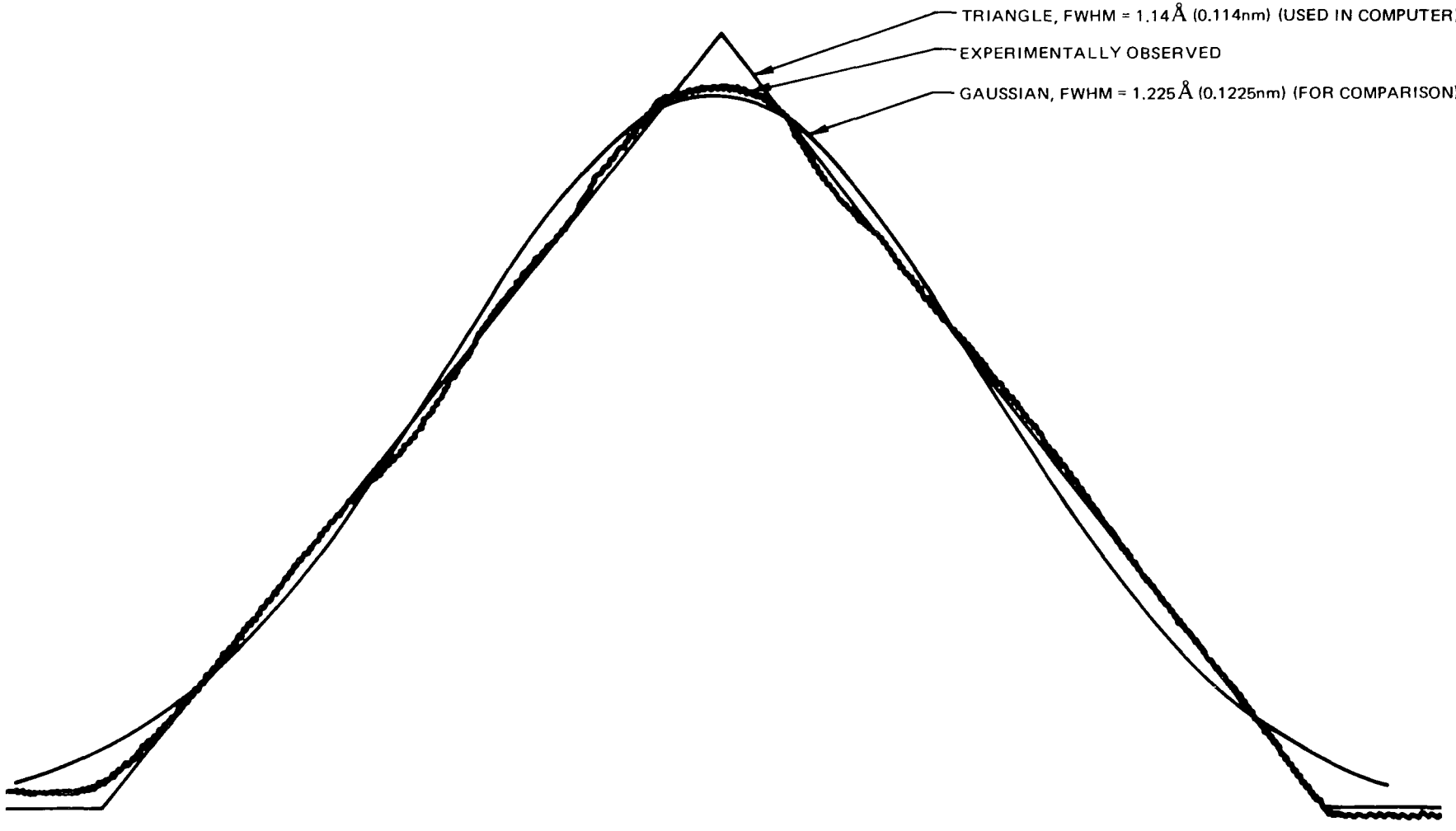

FIG. D5

79-04-93-3

SPECTROMETER TRANSFER FUNCTION, 100μm SLITS

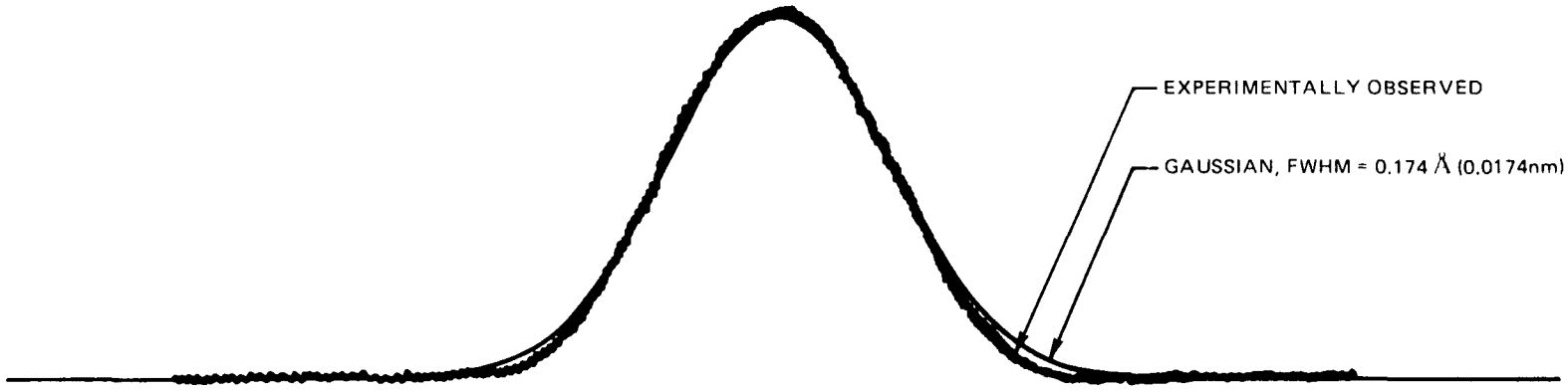

FIG. D6

79-04-93 4

which the calculation was performed. The weighting and summing process is repeated for all 2499 panels. The maximum value in PLOTY (KKOUNT) is assigned to the variable SPMAX and the first value of SPMAX (no nitric oxide) is assigned to the variable DIV. The variable DIV is divided into the intensities of each panel for each concentration to normalize the maximum peak height to unity for plotting purposes. The remaining sections of Part Three write the values of PLOTX and PLOTY into a temporary storage file and reread this file for display purposes when all spectra for each nitric oxide concentration have been calculated. This file is also used for wavelength scale expansions; no new calculations are done when a scale expansion is requested. Sample convolved outputs for a continuum and a resonant absorption case are shown in Figs. D7 and D8. Numerical values for features in the convolved spectra can be obtained utilizing Part Four of PLOT.PLOT5.

D.IV.b.4.Part Four

Part Four produces the numerical value of extrema on each concentration curve for a given wavelength range. This option is accessed by a carriage return after the completion of the convolution plots. The wavelength of the start of the extrema interval is assigned to the variable XSTR and the end to XSTP. The minimum and maximum values and their wavelengths within this interval are determined. The extrema of the first case (no nitric oxide) are used to normalize the extrema of following cases. This results in the fractional value of the extrema for each curve in the specified interval. The extrema, fractional extrema, extrema wavelengths, and concentrations are presented followed by a request to determine if another region is to be examined. A response of ' NO' (include blank before word NO) will terminate the program. A sample of this option is included in Fig. D9.

CONVOLUTED SPECTRUM FOR CONTINUUM LAMP, SLIT FUNCTION FWHM = 0.020Å

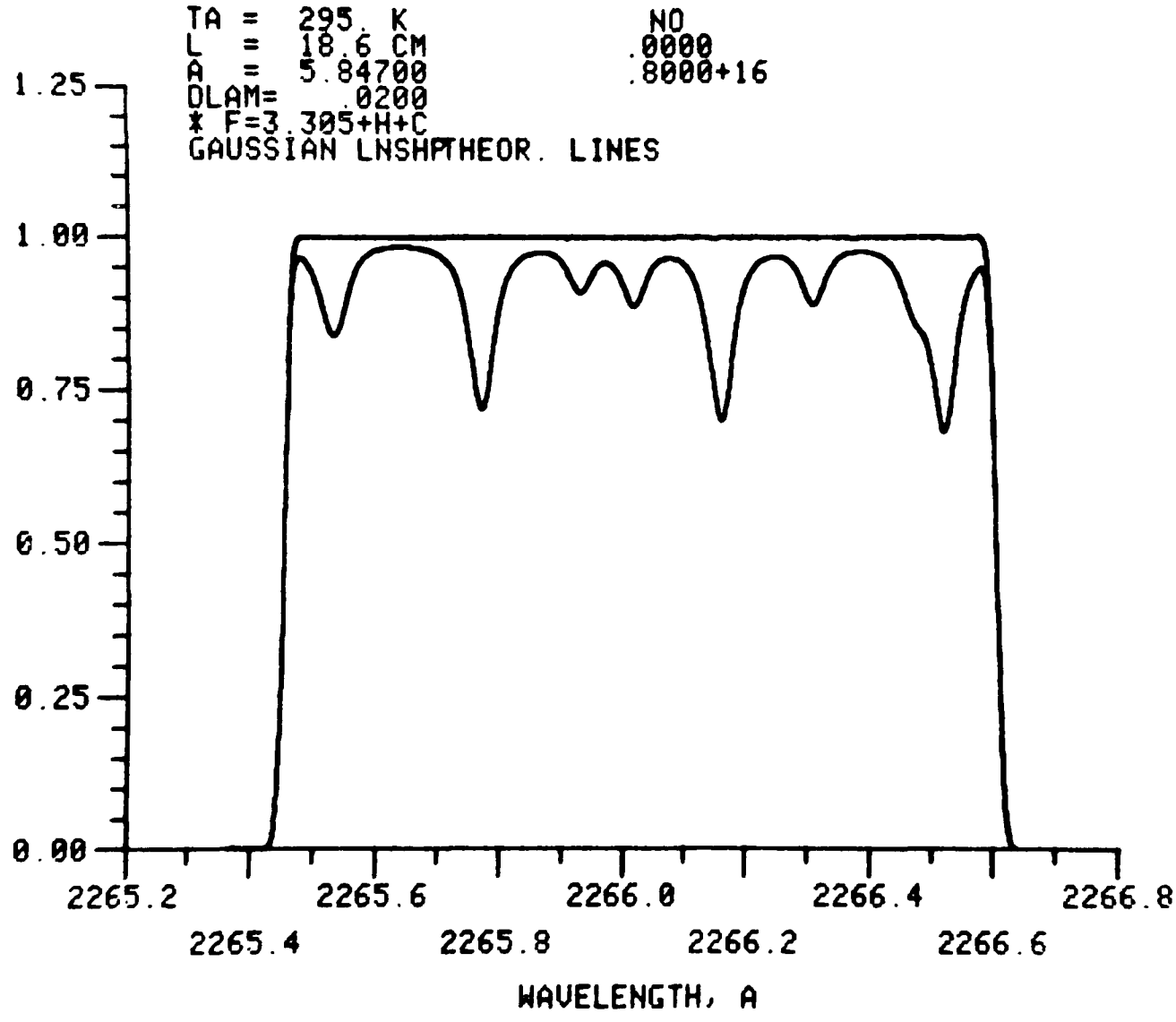

79-04-93-6

FIG. D7

CONVOLUTED SPECTRUM FOR RESONANT LINE SOURCE, SLIT FUNCTION FWHM = 1.60Å (0.16nm)

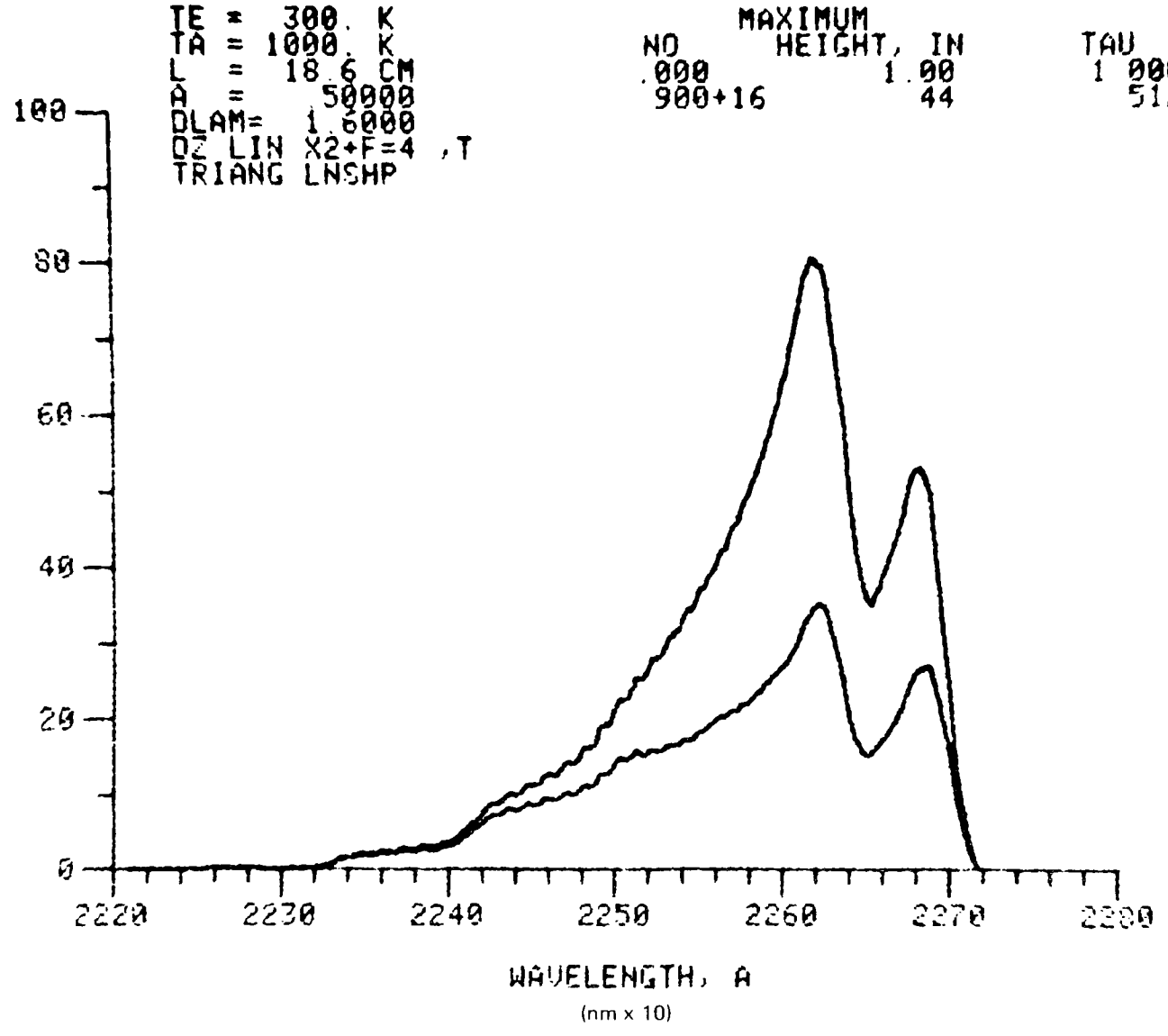

79-04-93-7

FIG. D8

EXTREMA DISPLAY

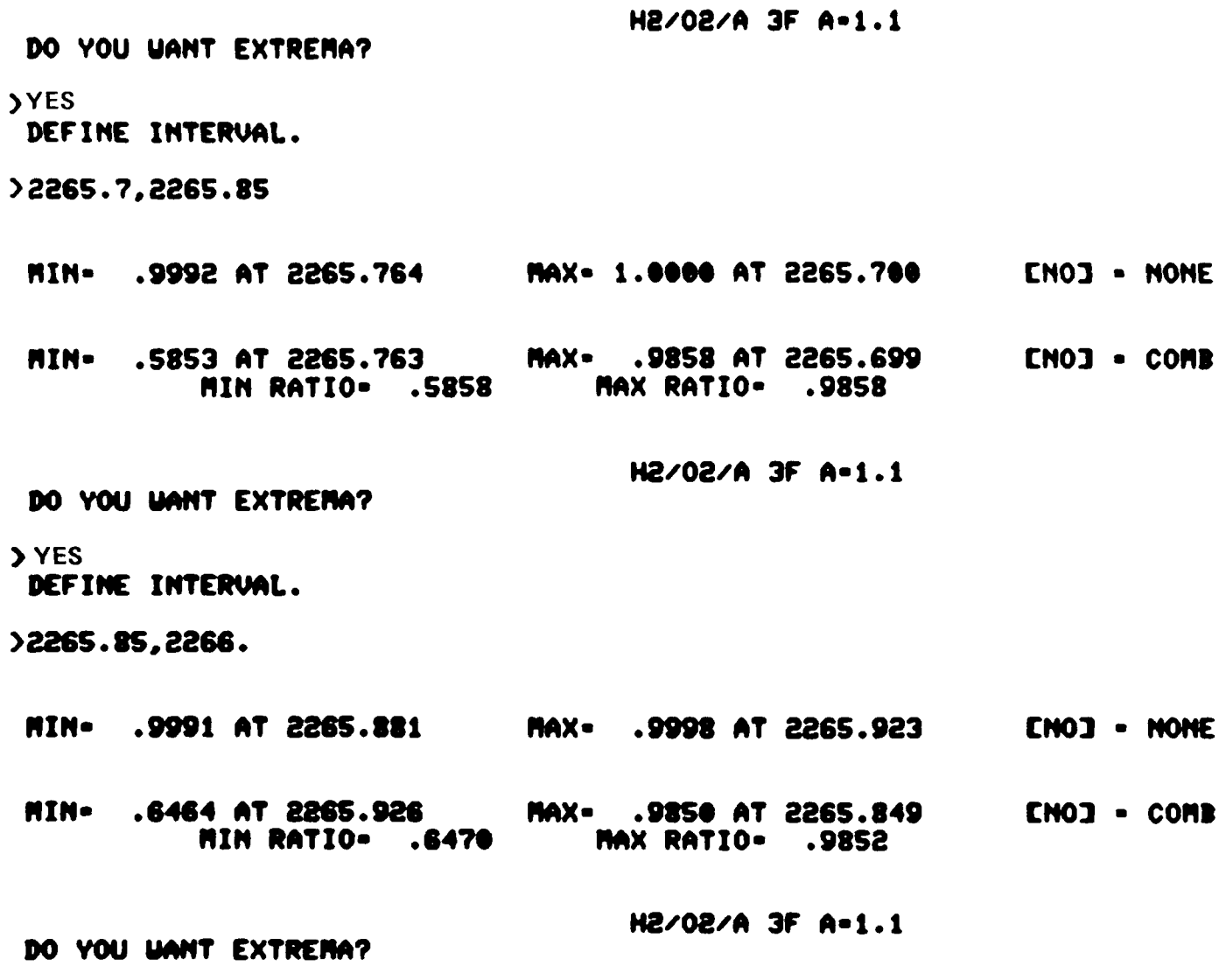

79-04-93-8

FIG. D9

NCASE	counter for concentration case
ISTART	flag for no NO concentration (equals 1 for NO = Ø. Ø for NO ≠ Ø.)
DATE1	date of run
TIME1	time of run
STMAX	maximum line intensity
XMIN	minimum wavelength to be plotted
XMAX	maximum wavelength to be plotted
DLAM2	slit function of spectrometer in angstroms (FWHM)
IPLT1I	option for plots, 1 for zero slit plots Ø to delete zero slit plots
PLTMIN	same as LINST
PLTMAX	same as LINEND
YHGT	indicates method of obtaining line locations for data (YHGT equals 1 for theoretically computed line locations and Ø for experimentally measured line locations)
NLINES	total number of spectral locations read
ENO	NO concentration (molecules/cm^3)
TE	Source temperature (Kelvin)
TA	absorber temperature (Kelvin)
EL	path length of absorption (cm)
APRIME	gas broadening constant
TAU	integrated fractional transmission
HEADS	program version code

IPLOT1	same as IPLT1I
DLAM	same as DLAM2
LINST	starting spectral line number
LINEND	final spectral line number
LINT	total number of spectral lines read
ANG(I)	wavenumber of Ith spectral line (later converted to wavelength)
HT(I)	intensity of Ith spectral line
IS1	line number of start of wavelength sort
IS2	line number of end of wavelength sort (IS1 + 20)
WIDE	width in angstroms of spectral region to be convolved at a given wavelength
II	same as LINT
XPLT(1)	line center wavelength
XPLT(2)	same as XPLT(1)
YPLT(1)	Ø
YPLT(2)	integrated intensity of line at XPLT(2)
ISAVE	line number of first spectral line in convolution interval
KKOUNT	panel counter (1-2499)
DELLAM	total wavelength interval divided by 2499
PP1	wavelength of first panel

SPMAX	maximum convolved intensity for a given concentration
P1	wavelength of start of individual convolution interval
P2	wavelength of end of individual convolution interval
XLAM	center wavelength of convolution interval
I	counter to determine which spectral lines lie within the convolution interval
NOPTS	same as KOUNT
IPN1	line number of last spectral line in convolution interval
JBL	counter for lines within convolution interval
SUMMER	integrated intensity of all lines within the convolution interval
TRIADD	line intensity weighted by slit function
PLOTX(I)	wavelength of convolved line transmissions (Ith panel)
PLOTY(I)	intensity of convolved line transmissions (Ith panel)
DIV	maximum convolved intensity for no NO present
TRNCAS (NCASE,I)	array of intensities for each concentration (NCASE) at Ith panel
DECIS	option for extrema in wavelength region specified
XSTR	starting wavelength for extrema option
XSTP	ending wavelength for extrema option
J1	counter for concentration case
STLOOK	XSTR minus one percent of extrema interval

SMALL	minimum transmission over extrema interval
BIG	maximum transmission over extrema interval
DIF1	minima check
DIF2	maxima check
LAMIN	wavelength of minimum transmission
LAMAX	wavelength of maximum transmission
MINSAV	minimum transmission with no NO present
MAXSAV	maximum transmission with no NO present
MINRAT	minimum fractional transmission
MAXRAT	maximum fractional transmission

```
C
C*************************************************************************
C PART1    PART1    PART1    PART1    PART1    PART1    PART1    PART1
C*************************************************************************
C
      REAL*4 KO
      INTEGER*4 P,Q,R,BLANK
      INTEGER*4 BRANCH
      DIMENSION S(500),FL(500),WO(500)
        DIMENSION WO2(500),TJ2(500)
      DIMENSION HEADS(20)
      DIMENSION KO(500),ISPIN(500)
      DATA BLANK/' '/, P/'P'/,Q/'Q'/,R/'R'/
      COMMON/PAREM/CONST1,CONST2,CONST3,WO,KO,NLINES
       DIMENSION XDATA(100),YDATA(100)
      DIMENSION W(500),E(500),CAY(500),DAT(500)
      G(LEV)=1904.405*(LEV+.5)-14.187*(LEV+.5)**2
      ALLOW=.01
      READ(5,4) LINST
      READ(5,4) LINEND
      READ(5,4) NWOTHE
    4 FORMAT(I3)
    8 DO 12  I=1,1000
      READ (5,10 )XDATA(I),YDATA(I)
   10 FORMAT(8F10.0)
      IF (XDATA(I).EQ.0.D0) GO TO 14
   12 CONTINUE
   14 CONTINUE
      NP=I-1
      NP1=NP-1
      L1R2=2
      IWW=0
      IWL=0
      READ (5,20)HEADS
   20 FORMAT(20A4)
      READ (5,140)DELPLT
      READ (5,140)SLIT
      DLAM=SLIT
      READ (5,140)AP
      READ (5,140)TA
      READ (5,140)TE
      READ (5,140)EL
      READ (5,140)YHGT
      READ (5,40)IPLOT1
      READ (5,40)IPLOT2
   40 FORMAT(2I1)
   60 FORMAT(I1,2F10.0)
      WRITE (6,590)TA,TE,EMO,EL,TAU,ALPHA
C
C     BVE00 IS THE SPECTROSCOPIC CONSTANT FOR THE ZERO VIB. STATE
      BVE00=1.69562
C
C       AFL IS THE LOWER STATE SPIN SPLITTING
      AFL=123.18
54:)
```

```
C
C         INCLUDE TEMP. CORRECTION TO POP. DIST. FOR PARTITION FUNCTION
      C1=3.7796E-14*BVE00/(TA**(3.D0/2.D0)*(1+EXP(-1.43836*
     X(AFL-2.*BVE00)/TA)))
C
C       INSERT SPIN DEPENDENT F-NUMBERS
       C1S32=C1/3.64*3.57
       C1S12=C1/3.64*3.78
       C2=-1.43836D0/TA
       CONST1=-2.D0*DSQRT(DLOG(2.D0))
       CONST2=1.307D-7* SQRT(TE)
       CONST3=1.307D-7* SQRT(TA)
       CONST4=3.E-7*SQRT(TE)
       WRITE (6,80)HEADS,AP
   80 FORMAT(1H1,20X,20A4,10X,3HA'=,F7.4)
C
C*****************************************************************************
C PART2    PART2    PART2    PART2    PART2    PART2    PART2    PART2
C*****************************************************************************
C
       J=1
  100 READ (5,120)BRANCH,NUP,NLO,RJPP,UO(J)
       ISPIN(J)=NLO
  120 FORMAT(3X,A1,I1,I1,1X,F4.0,1X,F11.0)
       IF (BRANCH.EQ.BLANK) GO TO 240
       JPP=RJPP
       IF (BRANCH.EQ.P) GO TO 180
       ICODE=3
       IF (BRANCH.EQ.Q) GO TO 160
       CALL FUPPER(IUU,NUP,JPP+1,FU)
       CALL HONNUM(IUU,IUL,NUP,NLO,JPP+1,JPP,3,S(J))
       GO TO 200
  140 FORMAT(4F10.0)
  160 CALL FUPPER(IUU,NUP,JPP  ,FU)
       CALL HONNUM(IUU,IUL,NUP,NLO,JPP,JPP,2,S(J))
       ICODE=2
       GO TO 200
  180 CALL FUPPER(IUU,NUP,JPP-1,FU)
       CALL HONNUM(IUU,IUL,NUP,NLO,JPP-1,JPP,1,S(J))
       ICODE=1
  200 CALL FLOWER(IUL,NLO,ICODE,NUP,JPP,FL(J))
       IF (NWOTHE.EQ.0) GOTO 210
       UO(J)=FU-FL(J)
  210 CONTINUE
       J=J+1
       GO TO 100
  240 CONTINUE
       NLINES=J-1
  260 READ (5,140,END=680)ENO
       QUIB=0.
       IZ=0
       DO 280 IVEE=IZ,5
  280 QUIB=QUIB+EXP(C2*EO(IVEE))
       DO 300 I=1,NLINES
        C1=C1S12
       IF (ISPIN(I).EQ.2) C1=C1S32
```

```
      B=C1*S(I)/QUIB*EXP(C2*FL(I))
      KO(I)=B*ENO
  300 CONTINUE
C
C*****************************************************************************
C PART3    PART3    PART3    PART3    PART3    PART3    PART3    PART3
C*****************************************************************************
C
      UHOLD=UO(LINST-1)
      LINTOT=0
      ISAVE=1
      NINT=499
      NP2=NINT+1
      TAUTOP=0.D0
      TAUBOT=0.D0
       J=LINST
      DO 500 I=1,NP2
      DUJ=CONST2*UO(J)
      DELTAU=CONST3*UO(J)*2.39*(AP+1)
      UST=UO(LINST)-CONST3*UO(LINST)*2.39*(AP+1)
      UND=UO(LINEND)+CONST3*UO(LINEND)*2.39*(AP+1)
      AZJ=UO(J)-DELTAU
      BZJ=UO(J)+DELTAU
      DIST=BZJ-AZJ
      DEL=(UND-UST)/NINT
      U(I)=UST+(I-1)*DEL
      E(I)=10.
       IF (U(I).GT.(UO(J)+DELTAU)) J=J+1
      IF (ENO.EQ.0.) GO TO 480
       IF (J.GT.LINEND) GOTO 500
      JLEFT=0
      SUML=0.
      SUMR=0.
      II=J
      NHOLDR=0
      NHOLDL=0
      NLESR=0
      NLESL=0
  320 DUL=CONST3*UO(II)
      IF (AP.EQ.0.) GO TO 340
      BETA=-CONST1*(U(I)-UO(II))/DUL
      CALL UFUNC(BETA,AP,TERM,DUMS)
      GO TO 360
  340 TERM=EXP(-((U(I)-UO(II))*CONST1/DUL)**2)
  360 CONTINUE
      TNEU=KO(II)*TERM
      IF (JLEFT.EQ.1) GO TO 420
      SUMR=SUMR+TNEU
      IF (UO(II).GT.U(I).AND.TNEU.EQ.0.) GO TO 400
      IF (II.EQ.MLINES) GO TO 400
      IF (UO(II).LT.BZJ) GO TO 380
      IF (ABS(TNEU/SUMR).LE.ALLOU) NLESR=NLESR+1
      IF(NHOLDR.EQ.NLESR) NLESR=0
      NHOLDR=NLESR
      IF(NLESR.EQ.3) GOTO 400
  380 CONTINUE
166:)
```

```
      II=II+1
      GO TO 320
  400 JLEFT=1
      II=J-1
      IF (J.EQ.1) GO TO 460
      GO TO 320
  420 CONTINUE
      SUML=SUML+TNEU
      IF (UO(II).LT.U(I).AND.TNEU.EQ.0.) GOTO 460
      IF (II.EQ.1) GO TO 460
      IF (UO(II).GT.AZJ) GO TO 440
      IF (ABS(TNEU/SUML).LE.ALLOW) NLESL=NLESL+1
      IF(NHOLDL.EQ.NLESL) NLESL=0
      NHOLDL=NLESL
      IF (NLESL.EQ.3) GOTO 460
  440 CONTINUE
      II=II-1
      GO TO 320
  460 CONTINUE
      GO TO 500
  480 SUML=0.
      SUMR=0.
  500 CAY(I)=SUML+SUMR
      SUM1=0.D0
      SUM2=0.D0
      DEL2=DEL/2.D0
      DO 520 I=1,NP2
  520 DAT(I)=E(I)* EXP(-CAY(I)*EL)
      WRITE(21,1000)(DAT(I),U(I),I=1,NP2)
 1000 FORMAT(' ',2(G16.8,3X))
      DO 540 I=1,NINT
      SUM1=SUM1+DEL2*(DAT(I)+DAT(I+1))
  540 SUM2=SUM2+DEL2*(E(I)+E(I+1))
      TAUTOP=SUM1
      TAUBOT=SUM2
C
C*************************************************************************
C PART4    PART4    PART4    PART4    PART4    PART4    PART4    PART4
C*************************************************************************
C
      TAU=TAUTOP/TAUBOT
      ALPHA=1.D0-TAU
      WRITE (6,580)TA,TE,ENO,EL,TAU,ALPHA
  580 FORMAT(//,5X,'TA=',E16.8,5X,'TE=',E16.8,5X,'NO=',E16.8,5X,'L=',
     1E16.8,5X,/,5X,'TAU=',E16.8,5X,'ALPHA=',E16.8)
      PLTMIN=1.
      PLTMAX=500.
      YHGT=NWOTHE
      WRITE(20)SLIT,PLTMIN,PLTMAX,DELPLT,DLAM,YHGT,NLINES,ENO,
     1TE,TA,EL,IPLOT1,IPLOT2
     2,LIN2,AP
     3,TAU
     4,HEADS
      LINT=NINT+1
      )
```

```
      DO 600 I=1,LINT
      LKT=LINT+1-I
      U02(I)=U(LKT)
      TJ2(I)=DAT(LKT)
600   CONTINUE
        WRITE (20) (U02(I),TJ2(I),I=1,LINT)
      GO TO 260
620    CONTINUE
      STOP
      END
)
```

```
      1:      SUBROUTINE FUPPER(V,M,JINDEX,F)
      2:C
      3:C     SUBROUTINE FUPPER CALCULATES THE ROTATIONAL ENERGY OF THE UPPER
      4:C     ELECTRON STATE FOR A GIVEN VIBRATIONAL STATE(V), A GIVEN SPIN
      5:C     STATE(M), AND A GIVEN ROTATIONAL STATE(J)
      6:C
      7:      INTEGER V
      8:      REAL*4 J
      9:      J=JINDEX+.5
     10:      T=43966.2643
     11:      WE=2374.307
     12:      WEXE=16.106
     13:      BE=1.9977
     14:      ALPHAE=.0198
     15:      DV=4.6D-6
     16:      BV=1.98576
     17:      GAMA=.00276
     18:      GO TO (20,40),M
     19:   20 FN=BV*(J+.5)*(J-.5)+.5*GAMA*(J-.5)-DV*(J+.5)**2*(J-.5)**2
     20:      GO TO 60
     21:   40 FN=BV*(J+.5)*(J+1.5)-.5*GAMA*(J+1.5)-DV*(J+.5)**2*(J+1.5)**2
     22:   60 CONTINUE
     23:      G=WE*(V+.5)-WEXE*(V+.5)**2
     24:      F=T+G+FN
     25:      RETURN
     26:      END
EOF:26
0:>
```

```
      SUBROUTINE FLOWER(V,M,IB,USS,JINDEX,F)
C     SUBROUTINE FLOWER CALCULATES THE ROTATIONAL ENERGY OF A GIVEN
C     ROTATIONAL STATE(J), VIBRATIONAL STATE(V), AND SPIN STATE(M)
C      USS=UPPER SPIN STATE
C      IB=1 FOR P,2 FOR Q,3 FOR R
C
      INTEGER V,USS
      REAL*4 J,MU,JBAR,LMDADB
      J=JINDEX+.5
      JBAR=J+.5
      P=-1.17E-2
      Q=+7.8E-5
      T=0.
      G=0.
      DV=4.5E-6
      A=123.19
      BE=1.70427
      ALPHAE=.01728
      BV=BE-ALPHAE*(V+.5)
      BV=1.69568
      C=-5.8E-4
      YV=(A+C*(J-.5)**2)/BV
      WE=1904.405
      WEXE=14.187
      MU=DV/BV
      ALPHA=(YV-2.)**2/4.+(JBAR**2-1.)*(1.+2.*MU*(2.*JBAR**2-YV)
     X+MU**2*((2.*JBAR**2-1.)**2-1.))
      FN=BV*(JBAR**2-1.)-DV*(JBAR**4-JBAR**2+1.)
      G=WE*(V+.5)-WEXE*(V+.5)**2
      NSIGN=1
      IF(USS.EQ.M) GOTO 5
      IF(IB.NE.2) GOTO 10
      NSIGN=-1
      GOTO 10
    5 IF(IB.EQ.2)GOTO 10
      NSIGN=-1
   10 CONTINUE
      GO TO (20,40),M
C
C           SPIN 1/2 STATE
   20 FN=FN-SQRT(ALPHA)*BV
      LMDADB=(((2.-YV)/(2.*SQRT(ALPHA))-1.)*(.5*P+Q)+Q/SQRT(ALPHA)
     X*(JBAR**2-1.))*JBAR/2.
      GO TO 60
C
C             SPIN 3/2 STATE
   40 FN=FN+SQRT(ALPHA)*BV
      LMDADB=(((2.-YV)/(2.*SQRT(ALPHA))+1.)*(.5*P+Q)+Q/SQRT(ALPHA)
     X*(JBAR**2-1.))*JBAR/2.
   60 F=FN+NSIGN*LMDADB+T+G+A/2.
      RETURN
      END
EOF:52
0:)
```

```
      1:       FUNCTION FUNC(X,XDATA,YDATA,NP,NP1)
      2:       DIMENSION XDATA(100),YDATA(100)
      3:       IF (X.LT.XDATA(1)) GO TO 60
      4:       DO 20 I=1,NP1
      5:       IF (XDATA(I).LE.X.AND.XDATA(I+1).GE.X) GO TO 40
      6:    20 CONTINUE
      7:       FUNC=(YDATA(NP)-YDATA(NP1))*(X-XDATA(NP))/(XDATA(NP)-XDATA(NP1))+Y
      8:      1DATA(NP)
      9:       RETURN
     10:    40 FUNC=(YDATA(I+1)-YDATA(I))/(XDATA(I+1)-XDATA(I))*(X-XDATA(I))
     11:      1+YDATA(I)
     12:       RETURN
     13:    60 FUNC=(YDATA(2)-YDATA(1))*(X-XDATA(1))/(XDATA(2)-XDATA(1))+YDATA(1)
     14:       RETURN
     15:       END
EOF:15
0:)
```

```
      SUBROUTINE WFUNC(XF,YF,U1,U2)
C
C     XF,YF ARE THE REAL AND IMAGINARY PARTS OF THE ARGUMENT
C     U1,U2 ARE THE REAL AND IMAGINARY PARTS OF THE FUNCTION
C     W(Z)=EXP(-Z**2)ERFC(-IZ)  (SEE NATIONAL BUREAU OF STANDARDS
C     HANDBOOK OF MATHEMATICAL FUNCTIONS, PAGE 297)
C
      IMPLICIT REAL*8(A-H,O-Z)
      REAL XF,YF,U1,U2
      COMPLEX ZC,WC,J,ZS,T1,T2,T3
      COMMON/TABLE/Z(31,40,2),X(40),Y(31)
      DIMENSION W(2)
      IFLAG=0
      IF(XF.LT.0.)IFLAG=IFLAG+1
      IF(YF.LT.0.)IFLAG=IFLAG+3
      XI=ABS(XF)
      YI=ABS(YF)
      IF (XI.GE.3.90.OR.YI.GE.3.0) GO TO 40
      II=10*YI+1
      JJ=10*XI+1
      II1=II+1
      JJ1=JJ+1
      DO 20 K=1,2
      Z1=(Z(II,JJ,K)-Z(II,JJ1,K))*(XI-X(JJ1))/(X(JJ)-X(JJ1))+Z(II,JJ1,K)
      Z2=(Z(II1,JJ,K)-Z(II1,JJ1,K))*(XI-X(JJ1))/(X(JJ)-X(JJ1))
     1+Z(II1,JJ1,K)
   20 W(K)=(Z1-Z2)*(YI-Y(II1))/(Y(II)-Y(II1))+Z2
      U1=W(1)
      U2=W(2)
      IF(IFLAG.EQ.0)RETURN
      GO TO (80,100,100,120),IFLAG
   40 IF (XI.GT.6.00.OR.YI.GT.6.00) GO TO 60
      J=(0.00,1.00)
      ZC=CMPLX(XI,YI)
      ZS=ZC*ZC
      T1=.461313500/(ZS-.190163500)
      T2=.0999921600/(ZS-1.784492700)
      T3=.00288389400/(ZS-5.525343700)
      WC=J*ZC*(T1+T2+T3)
      U1=(WC+CONJG(WC))*.500
      U2=(CONJG(WC)-WC)*J*.500
      IF(IFLAG.EQ.0)RETURN
      GO TO (80,100,100,120),IFLAG
   60 J=(0.00,1.00)
      ZC=CMPLX(XI,YI)
      ZS=ZC*ZC
      T1=.512424200/(ZS-.876255100)
      T2=.0517653600/(ZS-2.72474500)
      WC=J*ZC*(T1+T2)
      U1=(WC+CONJG(WC))*.500
      U2=(CONJG(WC)-WC)*J*.500
      IF(IFLAG.EQ.0)RETURN
      GO TO (80,100,100,120),IFLAG
   70  FORMAT (// '** IFLAG IN WFUNC=',I3//)
   80 U2=-U2
      RETURN
      END
```

```
      56:       RETURN
      57:  100 G=2.00*EXP(YI*YI-XI*XI)
      58:       GG=2.00*XI*YI
      59:       U1=G*COS(GG)-U1
      60:       U2=G*SIN(GG)+U2
      61:        WRITE (6,70) IFLAG
      62:       RETURN
      63:  120 G=2.00*EXP(YI*YI-XI*XI)
      64:       GG=2.00*XI*YI
      65:       U1=G*COS(GG)-U1
      66:       U2=-G*SIN(GG)-U2
      67:        WRITE(6,70) IFLAG
      68:       RETURN
      69:       END
69:)
```

```
      SUBROUTINE HONNUM(MUP,MUPP,MEGAN,MEGAM,JP,JPP,IB,HONL)
C     SUBROUTINE HONNUM CALCULATES THE HONL-LONDON FACTOR WHERE
C     MUP=UPPER VIBRATIONAL STATE
C     MUPP=LOWER VIBRATIONAL STATE
C     MEGAN=UPPER SPIN STATE
C     MEGAM=LOWER SPIN STATE
C     J=J''
C     IB=1 FOR P BRANCH, =2 FOR Q BRANCH, =3 FOR R BRANCH
C
      REAL*4 J
      J=JPP+.5
      A=123.18
      BE=1.70427
      ALPHAE=.01728
      BV=BE-ALPHAE*(MUPP +.5)
      YU=A/BV
      T1=2.*J+1.
      T2=T1*T1
      T3=1./SQRT(YU*(YU-4.)+T2)
      JB=IB+1
      GO TO (20,20,160,300),JB
   20 CONTINUE
      GO TO (40,100),MEGAN
   40 CONTINUE
      GO TO (60,80),MEGAM
   60 RNUM=T2+T1*T3*(4.*J**2+4.*J+1.-2.*YU)
      DENOM=8.*J
      GO TO 440
   80 RNUM=T2-T1*T3*(4.*J**2+4.*J+1.-2.*YU)
      DENOM=8.*J
      GO TO 440
  100 CONTINUE
      GO TO (120,140),MEGAM
  120 RNUM=T2-T1*T3*(4.*J**2+4.*J-7.+2.*YU)
      DENOM=8.*J
      GO TO 440
  140 RNUM=T2+T1*T3*(4.*J**2+4.*J-7.+2.*YU)
      DENOM=8.*J
      GO TO 440
  160 CONTINUE
      GO TO (180,240),MEGAN
  180 CONTINUE
      GO TO (200,220),MEGAM
  200 RNUM=T1*((4.*J**2+4.*J-1.)+T3*(8.*J**3+12.*J**2-2.*J-7.+2.*YU))
      DENOM=8.*J*(J+1.)
      GO TO 440
  220 RNUM=T1*(4.*J**2+4.*J-1.-T3*(8.*J**3+12.*J**2-2.*J-7.+2.*YU))
      DENOM=8.*J*(J+1.)
      GO TO 440
  240 CONTINUE
      GO TO (260,280),MEGAM
  260 RNUM=T1*((4.*J**2+4.*J-1.)-T3*(8.*J**3+12.*J**2-2.*J+1.-2.*YU))
      DENOM=8.*J*(J+1.)
      GO TO 440
  280 RNUM=T1*((4.*J*J+4.*J-1.)+T3*(8.*J**3+12.*J*J-2.*J+1.-2.*YU))
>
```

```
      DENOM=8.*J*(J+1.)
      GO TO 440
  300 CONTINUE
      GO TO (320,380),MEGAM
  320 CONTINUE
      GO TO (340,360),MEGAM
  340 RNUM=T2+T1*T3*(4.*J*J+4.*J-7.+2.*YU)
      DENOM=8.*(J+1.)
      GO TO 440
  360 RNUM=T2-T1*T3*(4.*J**2+4.*J-7.+2.*YU)
      DENOM=8.*(J+1)
      GO TO 440
  380 CONTINUE
      GO TO (400,420),MEGAM
  400 RNUM=T2-T1*T3*(4.*J**2+4.*J+1.-2.*YU)
      DENOM=8.*(J+1.)
      GO TO 440
  420 RNUM=T2+T1*T3*(4.*J**2+4.*J+1.-2.*YU)
      DENOM=8.*(J+1.)
  440 CONTINUE
      IF (DENOM.EQ.0) GO TO 460
      HONL=RNUM/DENOM
      RETURN
  460 HONL=0.
      RETURN
      END
81:)
```

```
C
C*************************************************************************
C PART1    PART1    PART1    PART1    PART1    PART1    PART1    PART1
C*************************************************************************
C
      REAL*4 KO
      INTEGER*4 P,Q,R,BLANK
      INTEGER*4 BRANCH
      DIMENSION S(500),FL(500),WO(500),EO(500)
        DIMENSION WO2(500),TJ2(500)
      DIMENSION HEADS(20)
      DIMENSION KO(500),ISPIN(500)
      DATA BLANK/' '/, P/'P'/,Q/'Q'/,R/'R'/
      COMMON/PAREM/CONST1,CONST2,CONST3,WO,EO,KO,NLINES
       DIMENSION XDATA(100),YDATA(100)
      DIMENSION W(500),E(500),CAY(500),DAT(500),EJ(500),TJ(500)
      G(LEV)=1904.405*(LEV+.5)-14.187*(LEV+.5)**2
      ALLOW=.01
       READ(5,4) LINST
       READ(5,4) LINEND
      READ(5,4) NWOTHE
    4  FORMAT(I3)
    8  DO 12  I=1,1000
       READ (5,10 )XDATA(I),YDATA(I)
   10  FORMAT(8F10.0)
       IF (XDATA(I).EQ.0.D0) GO TO 14
   12  CONTINUE
   14  CONTINUE
       NP=I-1
       NP1=NP-1
       L1R2=2
       IVU=0
       IVL=0
       READ (5,20)HEADS
   20  FORMAT(20A4)
       READ (5,140)DELPLT
       READ (5,140)SLIT
       DLAM=SLIT
       READ (5,140)AP
       READ (5,140)TA
       READ (5,140)TE
       READ (5,140)EL
       READ (5,140)YHGT
       READ (5,40)IPLOT1
       READ (5,40)IPLOT2
   40  FORMAT(2I1)
   60  FORMAT(I1,2F10.0)
       WRITE (6,580)TA,TE,EMO,EL,TAU,ALPHA
C
C        BVE00 IS THE SPECTROSCOPIC CONSTANT FOR THE ZERO VIB. STATE
       BVE00=1.69562
C
C          AFL IS THE LOWER STATE SPIN SPLITTING
       AFL=123.18
C
55:)
```

```
C          TEMP CORRECTION FOR POPULATION DISTRIBUTION
      C1=3.7796D-14*DVE00/(TA**(3.D0/2.D0)*(1+EXP(-1.43836*
     X(AFL-2.*DVE00)/TA)))
C
C     INSERT SPIN DEPENDENT F NUMBER
      C1S32=C1/3.64*3.20
      C1S12=C1/3.64*3.53
      C2=-1.43836D0/TA
      CONST1=-2.D0*DSQRT(DLOG(2.D0))
      CONST2=1.307D-7* SQRT(TE)
      CONST3=1.307D-7* SQRT(TA)
      CONST4=3.E-7*SQRT(TE)
      WRITE (6,80)HEADS,AP
   80 FORMAT(1H1,20X,20A4,10X,3HA'=,F7.4)
C
C*****************************************************************************
C PART2    PART2    PART2    PART2    PART2    PART2    PART2    PART2
C*****************************************************************************
C
      J=1
  100 READ (5,120)BRANCH,NUP,NLO,RJPP,WO(J)
      ISPIN(J)=NLO
  120 FORMAT(3X,A1,I1,I1,1X,F4.0,1X,F11.0)
      IF (BRANCH.EQ.BLANK) GO TO 240
      JPP=RJPP
      IF (BRANCH.EQ.P) GO TO 180
      IF (BRANCH.EQ.Q) GO TO 160
       ICODE=3
      CALL FUPPER(IUU,NUP,JPP+1,FU)
      CALL HONNUM(IUU,IUL,NUP,NLO,JPP+1,JPP,3,S(J))
      GO TO 200
  140 FORMAT(4F10.0)
  160 CALL FUPPER(IUU,NUP,JPP   ,FU)
      CALL HONNUM(IUU,IUL,NUP,NLO,JPP,JPP,2,S(J))
      ICODE=2
      GO TO 200
  180 CALL FUPPER(IUU,NUP,JPP-1,FU)
      CALL HONNUM(IUU,IUL,NUP,NLO,JPP-1,JPP,1,S(J))
      ICODE=1
  200 CALL FLOWER(IUL,NLO,ICODE,NUP,JPP,FL(J))
      IF (NUOTHE.EQ.0) GOTO 210
      WO(J)=FU-FL(J)
  210 CONTINUE
      EO(J)=S(J)*EXP(FUNC(FU,XDATA,YDATA,NP,NP1))
C
C  REMOVE MANDATORY GOTO 222 TO PRINT LINE PROPERTIES
C
      GOTO 222
      WRITE (6,220)J,BRANCH,NUP,NLO,JPP,FU,FL(J),WO(J),S(J),EO(J)
  220 FORMAT(2X,I3,2X,A1,I1,I1,'(',I2,')','FU=',E16.8,5X,'FL=',E16.8,
     15X,'WO=',E16.8,5X,'SJ=',E16.8,5X,'EOJ=',E16.8)
  222  CONTINUE
      J=J+1
      GO TO 100
  240 CONTINUE
      )
```

```
      NLINES=J-1
  260 READ (5,140,END=620)ENO
      QVIB=0.
      IZ=0
      DO 280 IVEE=IZ,5
  280 QVIB=QVIB+EXP(C2*G(IVEE))
      DO 300 I=1,NLINES
      C1=C1S12
      IF(ISPIN(I).EQ.2) C1=C1S32
      B=C1*S(I)/QVIB*EXP(C2*FL(I))
      KO(I)=B*ENO
  300 CONTINUE
C
C*************************************************************************
C PART3    PART3    PART3    PART3    PART3    PART3    PART3    PART3
C*************************************************************************
C
      WHOLD=WO(LINST-1)
      LINTOT=0
      ISAVE=1
      NINT=100
      NP2=NINT+1
      TAUTOP=0.D0
      TAUBOT=0.D0
      DO 560 J=LINST,LINEND
      DWJ=CONST2*WO(J)
      DELTAW=CONST4*WO(J)
      AZJ=WO(J)-DELTAW
      BZJ=WO(J)+DELTAW
      DIST=BZJ-AZJ
      DEL=DIST/NINT
      DO 500 I=1,NP2
      W(I)=AZJ+(I-1)*DEL
      E(I)=EO(J)* EXP(-((W(I)-WO(J))*CONST1/DWJ)**2)
      IF (ENO.EQ.0.) GO TO 480
      JLEFT=0
      SUML=0.
      SUMR=0.
      II=J
      NHOLDR=0
      NHOLDL=0
      NLESR=0
      NLESL=0
  320 DWL=CONST3*WO(II)
      IF (AP.EQ.0.) GO TO 340
      BETA=-CONST1*(W(I)-WO(II))/DWL
      CALL WFUNC(BETA,AP,TERM,DUMS)
      GO TO 360
  340 TERM=EXP(-((W(I)-WO(II))*CONST1/DWL)**2)
  360 CONTINUE
      TNEW=KO(II)*TERM
      IF (JLEFT.EQ.1) GO TO 420
      SUMR=SUMR+TNEW
      IF (WO(II).GT.W(I).AND.TNEW.EQ.0.) GO TO 400
      IF (II.EQ.NLINES) GO TO 400
165:)
```

```
      IF (UO(II).LT.BZJ) GO TO 380
      IF (ABS(TNEW/SUMR).LE.ALLOW) NLESR=NLESR+1
      IF (NHOLDR.EQ.NLESR) NLESR=0
      NHOLDR=NLESR
      IF (NLESR.EQ.3) GOTO 400
380   CONTINUE
      II=II+1
      GO TO 320
400   JLEFT=1
      II=J-1
      IF (J.EQ.1) GO TO 460
      GO TO 320
420   CONTINUE
      SUML=SUML+TNEW
      IF (UO(II).LT.U(I).AND.TNEW.EQ.0.) GO TO 460
      IF (II.EQ.1) GO TO 460
      IF (UO(II).GT.AZJ) GO TO 440
      IF (ABS(TNEW/SUML).LE.ALLOW) NLESL=NLESL+1
      IF (NHOLDL.EQ.NLESL) NLESL=0
      NHOLDL=NLESL
      IF (NLESL.EQ.3) GOTO 460
440   CONTINUE
      II=II-1
      GO TO 320
460   CONTINUE
      GO TO 500
480   SUML=0.
      SUMR=0.
500   CAY(I)=SUML+SUMR
      SUM1=0.D0
      SUM2=0.D0
      DEL2=DEL/2.D0
      DO 520 I=1,NP2
520   DAT(I)=E(I)* EXP(-CAY(I)*EL)
      DO 540 I=1,NINT
      SUM1=SUM1+DEL2*(DAT(I)+DAT(I+1))
540   SUM2=SUM2+DEL2*(E(I)+E(I+1))
      EJ(J)=SUM2
      TJ(J)=SUM1
      TAUTOP=TAUTOP+TJ(J)
      TAUBOT=TAUBOT+EJ(J)
C
C  REMOVE MANDATORY GOTO 560 TO OBTAIN INDIVIDUAL
C   LINE BUNDLE TRANSMISSIONS
C
      GOTO 500
       IF (ENO.EQ.0.) GOTO 560
      SUMT=SUMT+TJ(J)
      SUME=SUME+EJ(J)
      LINTOT=LINTOT+1
      TRNSLN=SUMT/SUME
      DOPCK=(UHOLD-UO(J)*(1.-1.5*CONST3))*(UHOLD-UO(J)*(1.+1.5*CONST3))
      IF (DOPCK.LT.0.) GOTO 557
      IF (LINTOT.NE.1) GOTO 542
      WRITE (6,555) LINTOT,TRNSLN
      )
```

```
      GOTO 544
  542 CONTINUE
      WRITE(6,555) LINTOT,TRNLN2
  544 CONTINUE
      LINTOT=0
      SUMT=0.
      SUME=0.
      GOTO 559
  557 CONTINUE
  555  FORMAT (10X,I2,2X,E16.6)
      TRNLN2=TRNSLN
  559 CONTINUE
       WOINV=1.E+08/WO(J)
      WRITE (6,550) J,TJ(J),EJ(J),WO(J),WOINV
      WHOLD=WO(J)
  550  FORMAT(1X,I3,2X,4E16.6)
  560 CONTINUE
C
C*****************************************************************************
C PART4    PART4    PART4    PART4    PART4    PART4    PART4    PART4
C*****************************************************************************
C
      TAU=TAUTOP/TAUBOT
      ALPHA=1.D0-TAU
      WRITE (6,580)TA,TE,ENO,EL,TAU,ALPHA
  580 FORMAT(//,5X,'TA=',E16.8,5X,'TE=',E16.8,5X,'NO=',E16.8,5X,'L=',
     1E16.8,5X,/,5X,'TAU=',E16.8,5X,'ALPHA=',E16.8)
      PLTMIN=LINST
      PLTMAX=LINEND
      YHGT=NWOTHE
      WRITE(20)SLIT,PLTMIN,PLTMAX,DELPLT,DLAM,YHGT,NLINES,ENO,
     1TE,TA,EL,IPLOT1,IPLOT2
     2,L1R2,AP
     3,TAU
     4,HEADS
      LINT=LINEND-LINST+1
      DO 600 I=1,LINT
      LKT=LINEND-I+1
       WO2(I)=WO(LKT)
       TJ2(I) = TJ(LKT)
  600 CONTINUE
       WRITE (20) (WO2(I),TJ2(I),I=1,LINT)
      GO TO 260
  620  CONTINUE
      STOP
      END
)
```

```
      REAL*4 LAMIN,LAMAX,MINSAV,MAXSAV,MINRAT,MAXRAT
      DATA NO''NO''/
      DIMENSION HEADS(20),HDUR(20),TRNCAS(3,2500)
      DIMENSION HTSTOR(30),ENSTOR(30),TAUSTR(30)
      DIMENSION ANG(2500),HT(2500),PLOTX(2500),PLOTY(2500)
     X ,XPLT(4),YPLT(4)
       DIMENSION ENSTUR(2),APUR(2)
C
C ******************************
C PART 1     PART 1     PART1
C ******************************
C
      NCASE=0
      ISTART=1
      CALL DATE (DATE1)
      CALL TIME(TIME1)
      STMAX=-1000.
C
C     READ IN CONTROL PARAMETERS
C
       CALL INITT(240)
       WRITE (6,25)
   25  FORMAT (' FOR DEFAULT SCALES INPUT 0.,0.' /
     X     ' TO BLOW UP SCALE, INPUT MIN AND MAX FOR ABSCISSA'/)
       READ (5,30) XMIN,XMAX
   30  FORMAT( )
      IF(XMIN.NE.XMAX) GOTO 36
       WRITE(6,32)
   32  FORMAT(' INPUT FWHM'/)
       READ(5,30) DLAM2
      WRITE (6,34)
   34 FORMAT(' TYPE 1 FOR ZERO WIDTH PLOTS'/
     X     ' TYPE 0 TO DELETE ZERO WIDTH PLOTS'/)
      READ (5,30) IPLT1I
   36 CONTINUE
       CALL ERASE
C  IF VALUES NOT BOTH ZERO WANT TO BLOW UP SECTION OF PLOT FROM XMIN TO XMAX.
C  VALUES WILL BE AVAILABLE ON 28 SO WILL NOT REDO CALC.
       IF (XMIN .NE. XMAX) GO TO 415
       ISKIP=8
   40 READ (20,END=400)SLIT,PLTMIN,PLTMAX,DELPLT,DLAM,YHGT,NLINES,ENO,TE
     1,TA,EL,IPLOT1,IPLOT2,L1R2,APRIME,TAU,HEADS
       IPLOT1= IPLT1I
       LINST=PLTMIN
       LINEND=PLTMAX
       DLAM=DLAM2
       IF (ISKIP .EQ. 8) GO TO 45
       NUMPLT = IPLOT2
       IF (NUMPLT .NE. 0) NUMPLT =1
       ISKIP = 8
   45  CONTINUE
C
C     READ IN WAVENUMBER, TRANSMISSION PAIRS, CONVERT WAVENUMBERS
C     TO WAVELENGTH AND DETERMINE MAXIMUM TRANSMISSION
C
55:>
```

```
      LINT=LINEND-LINST+1
       READ (20) (ANG(ICARD),HT(ICARD),ICARD=1,LINT        )
      DO 60 ICARD=1,LINT
      IF(HT(ICARD).LT.0.)HT(ICARD)=0.
      STMAX=AMAX1(STMAX,HT(ICARD))
      ANG(ICARD)=(1.E+08)/ANG(ICARD)
   60 CONTINUE
      DO 65 ICARD=1,LINT
      IS1=ICARD+1
      IS2=ICARD+21
      DO 65 ISORT=IS1,IS2
      IF (ISORT.GT.LINT) GOTO 65
      IF (ANG(ICARD).LE.ANG(ISORT)) GOTO 65
      TEMP1=ANG(ICARD)
      TEMP2=HT(ICARD)
      ANG(ICARD)=ANG(ISORT)
      HT(ICARD)=HT(ISORT)
      ANG(ISORT)=TEMP1
      HT(ISORT)=TEMP2
   65 CONTINUE
C
C ******************************
C PART 2     PART 2     PART 2
C ******************************
C
      NCASE=NCASE+1
      II=LINT
      PLTMIN=ANG(1)
      PLTMAX=ANG(LINT  )
      IF (DLAM.GT..5) GOTO 70
C  SET CONVOLUTION INTERVAL FOR GAUSSIAN SLIT FUNCTION
      WIDE=6.*DLAM
      GOTO 74
C  SET CONVOLUTION INTERVAL FOR TRIANGULAR SLIT FUNCTION
   70 WIDE=2.*DLAM
   74 PLTMIN=PLTMIN-2.*WIDE
      PLTMAX=PLTMAX+2.*WIDE
      DELTA=STMAX
   80 CONTINUE
C
C     PRODUCE THE ZERO SLIT WIDTH PLOTS WHEN IPLOT1=1
C
      IF (IPLOT1.EQ.0) GO TO 120
      XPLT(3)=PLTMIN
C     XPLT(4)=DELPLT
       XPLT(4)=PLTMAX
      YPLT(3)=0.
      YPLT(4)=DELTA
      BOOZE=YPLT(4)
      YPLT(1)=0.
       XPLT(1)=0.
       CALL BINITT
C  SUPPRESS X GRID
       CALL XFRM(2)
       CALL DLIMX(PLTMIN,PLTMAX)
)
```

```
      CALL DLIMY(0.,DELTA)
      CALL CHECK (XPLT,YPLT)
      CALL DSPLAY (XPLT,YPLT)
      LABPRT = 88
      IX=550
      IY=765
     ENCODE (421,HDUR) HEADS
421  FORMAT (5A4)
      ENCODE(426,ENSTWR)ENO
      CALL MOVABS(180,IY)
      CALL AOUTST(7,' ENO = ')
      CALL AOUTST(8,ENSTWR)
     CALL MOVABS(180,745)
     CALL AOUTST(16,' ZERO SLIT WIDTH')
     CALL MOVABS(180,725)
     CALL AOUTST(20,HDUR)
      GO TO 429
 88   CONTINUE
     DO 100 I=1,II
     RLAM=ANG(I)
      IF (I .GT. 500) GO TO 95
 95   CONTINUE
     IF (PLTMIN.GT.RLAM.OR.PLTMAX.LT.RLAM) GO TO 100
C  DRAW INDIVIDUAL LINES
     YPLT(2)=AMIN1(HT(I),BOOZE)
     XPLT(1)=RLAM
     XPLT(2)=XPLT(1)
      CALL MOVEA (XPLT(1),YPLT(1) )
      CALL DRAWA (XPLT(2),YPLT(2) )
100  CONTINUE
       CALL TSEND
      CALL TIMPUT(1)
      CALL ERASE
120  CONTINUE
C
C ******************************
C PART 3     PART 3     PART 3
C ******************************
C
C     PRODUCE THE ACTUAL SPECTRA PLOT
C
      ISAVE=1
      KKOUNT=1
      DELLAM=(PLTMAX-PLTMIN)/2499
      PP1=PLTMIN-DELLAM
       SPMAX=-100.
140  LOOK=ISAVE-1
     IF(LOOK.LE.0)LOOK=1
C
C     CHOOSE A POINT ALONG THE PLOT AXIS AND SET AN INTERVAL OF WIDTH
C     EQUAL TO HALF THE CONVOLUTION WIDTH ON EITHER SIDE
C
      P1=PP1+KKOUNT*DELLAM
      P2=P1+WIDE
      XLAM=(P1+P2)*.5
)
```

```
      KOUNT=1
C
C     THIS LOOP DETERMINES WHICH LINES LIE IN THE CHOSEN INTERVAL
C
      DO 160 I=1,II
      IF (ANG(I).GT.P2) GO TO 180
      IF (ANG(I).LT.P1) GO TO 160
      IF(KOUNT.EQ.1)ISAVE=I
      KOUNT=KOUNT+1
  160 CONTINUE
  180 NOPTS=KOUNT-1
C
C     THE FOLLOWING STATEMENTS SIMULATE THE  SLIT FUNCTION
C     BY SUMMING THE CONTRIBUTIONS OF ALL THE LINES IN THE INTERVAL
C
      IF (NOPTS.EQ.0) GO TO 220
      SUMMER=0.
      IPN1=ISAVE+NOPTS-1
      DO 200 JBL=ISAVE,IPN1
      IF (DLAM.GT..5) GO TO 190
C  WEIGHTING FACTOR FOR GAUSSIAN SLIT FUNCTION
      TRIADD=HT(JBL)*EXP(-(ABS(XLAM-ANG(JBL))/DLAM*1.66512)**2)
      GOTO 200
C  WEIGHTING FACTOR FOR TRIANGULAR SLIT FUNCTION
  190    TRIADD=HT(JBL)*(DLAM-ABS(XLAM-ANG(JBL)))/DLAM
  200 SUMMER=SUMMER+AMAX1(0.,TRIADD)
      PLOTX(KKOUNT)=XLAM
      PLOTY(KKOUNT)=SUMMER
       IF (PLOTY(KKOUNT) .GT. SPMAX) SPMAX=PLOTY(KKOUNT)
  218  CONTINUE
      KKOUNT=KKOUNT+1
      IF (KKOUNT.EQ.2501) GO TO 240
      GO TO 140
  220 PLOTX(KKOUNT)=XLAM
      PLOTY(KKOUNT)=0.
      KKOUNT=KKOUNT+1
      IF (ANG(II).LT.P1) GO TO 240
      IF (KKOUNT.EQ.2501) GO TO 240
      GO TO 140
  240 II=KKOUNT-1
      N=II
      IF(ISTART.EQ.1) DIV=SPMAX
      DO 260 I=1,N
      PLOTY(I)=PLOTY(I)/DIV
  260 CONTINUE
C
C     DETERMINE THE MAXIMUM VALUE OF THE SPECTRAL CURVE AND IF THIS
C     IS THE FIRST CURVE COMPUTED, THE Y AXIS SCALE FACTOR IS CALCULATED
C
      IF(ISTART.EQ.1)DELYP=SPMAX
  300 PLOTY(N+1)=0.
      PLOTY(N+2)=DELYP
      PLOTX(N+1)=PLTMIN
      PLOTX(N+2)=DELPLT
      NP2=N+2
)
```

```
      ISTART=0
      TAUSTR(NCASE)=TAU
      HTSTOR(NCASE)=SPMAX/DELYP
      ENSTOR(NCASE)=ENO
       URITE(28)NP2,ENSTOR(NCASE),HTSTOR(NCASE),TAUSTR(NCASE),
     X  TA,TE,EL,APRIME,DELYP,HEADS,YHGT,(PLOTX(L),PLOTY(L),L=1,NP2),
     X  DLAM2
       GO TO 40
360 CONTINUE
C
C     PRODUCE THE FINAL SPECTRA PLOT
C
380 FORMAT(5X,'N=',E16.8,5X,'HT=',E16.8)
400 CONTINUE
       END FILE 28
       LABPRT=0
       REWIND 28
415 CONTINUE
       NCASE=0
420  CONTINUE
       NCASE=NCASE+1
       READ(28,END=460)NP2,ENSTOR(NCASE),HTSTOR(NCASE),TAUSTR(NCASE),
     X  TA,TE,EL,APRIME,DELYP,HEADS,YHGT,(PLOTX(L),PLOTY(L),L=1,NP2),
     X  DLAM2
418  CONTINUE
      N=NP2-2
      DO 419 J2=1,N
      TRNCAS(NCASE,J2)=PLOTY(J2)
419 CONTINUE
       IF (NUMPLT .EQ. 8) GO TO 430
       CALL BINITT
       IF (XMIN .NE. XMAX) CALL DLIMX (XMIN,XMAX)
       CALL DLIMY (0.,1.06)
      IF(XMIN.EQ.XMAX) CALL DLIMX(PLOTX(1),PLOTX(N))
C NO Y LABELS
C      CALL YLAB(0)
C SUPPRESS Y AXIS
       CALL YFRM(2)
C PUT IN X TICS BUT NOT  X GRID
       CALL XFRM(2)
       CALL CHECK(PLOTX,PLOTY)
       IF (NUMPLT .NE. 1) NUMPLT=8
C  PUT IN LABELS FOR SCALE AND OTHER GENERAL ONES HERE
422 FORMAT (F5.0)
423 FORMAT (F5.1)
424 FORMAT (F8.5)
426 FORMAT (E8.4)
427 FORMAT(F7.4)
428 FORMAT(A6)
       IX=200
       IY=765
429  CONTINUE
      ENCODE (421,HOUR) HEADS
       ENCODE (422,TEUR) TE
       ENCODE (422,TAUR) TA
)
```

```
      ENCODE (423,ELWR) EL
      ENCODE (424,APWR) APRIME
     ENCODE(428,DATWR) DATE1
     ENCODE(428,TIMWR) TIME1
      CALL MOVABS(450,5)
      CALL AOUTST (13,'WAVELENGTH, A')
     CALL MOVABS(750,25)
     CALL AOUTST(6,DATWR)
     CALL MOVABS(750,5)
     CALL AOUTST(6,TIMWR)
      CALL MOVABS(IX,IY)
      CALL AOUTST(5,'TE = ')
      CALL AOUTST (5,TEWR)
      CALL AOUTST (2,' K')
      IY=IY-20
      CALL MOVABS (IX,IY)
      CALL AOUTST (5,'TA = ')
      CALL AOUTST (5,TAWR)
      CALL AOUTST (2,' K')
      IY=IY-20
      CALL MOVABS(IX,IY)
      CALL AOUTST (5,'L  = ')
      CALL AOUTST (5,ELWR)
      CALL AOUTST (3,' CM')
      IY=IY-20
      CALL MOVABS(IX,IY)
      CALL AOUTST(5,'A  = ')
      CALL AOUTST (8,APWR)
      IF (LABPRT .EQ. 88) GO TO 88
      IY =IY - 20
     ENCODE (427,DLWR)DLAM2
     CALL MOVABS(IX,IY)
     CALL AOUTST(6,'DLAM= ')
     CALL AOUTST(7,DLWR)
     IY=IY-20
     CALL MOVABS(IX,IY)
     CALL AOUTST(20,HDWR)
     IY=IY-20
     CALL MOVABS(IX,IY)
     IF (DLAM2.GT..5) GOTO 4290
     CALL AOUTST(14,'GAUSSIAN LNSHP')
      GOTO 4300
4290  CALL AOUTST(12,'TRIANG LNSHP')
4300 CONTINUE
     CALL MOVABS(405,IY)
     IF (YHGT.EQ.1) GOTO 4310
     CALL AOUTST (12,'EXPER. LINES')
     GOTO 4320
4310 CALL AOUTST (12,'THEOR. LINES')
4320 CONTINUE
     IX=550
     IY=765
      CALL MOVABS(690,IY)
      CALL AOUTST (7,'MAXIMUM')
      IY = IY -20
)
```

```
      CALL MOVABS(IX,IY)
      CALL AOUTST(26,'NO          HEIGHT     TAU')
      CALL NPTS (N)
      CALL DSPLAY (PLOTX,PLOTY)
      GO TO 431
430   CONTINUE
      CALL NPTS (N)
      CALL CPLOT (PLOTX,PLOTY)
431   CONTINUE
C  PUT IN LABELS FOR PARTICULAR CURVE
      ENCODE(426,ENSTUR)ENSTOR(NCASE)
432   FORMAT (F6.3)
433 FORMAT (F6.3)
      ENCODE(432,HTSTUR)HTSTOR(NCASE)
      ENCODE(433,TAUUR)TAUSTR(NCASE)
      IY=IY-20
      CALL MOVABS(530,IY)
      CALL AOUTST(12,ENSTUR)
      CALL AOUTST(6,HTSTUR)
      CALL AOUTST(6,'      ')
      CALL AOUTST(6,TAUUR)
      GO TO 420
460   CONTINUE
C
C ******************************
C PART 4     PART 4     PART 4
C ******************************
C
      NCASE=NCASE-1
       CALL TSEND
       CALL TINPUT(1)
      CALL ERASE
       CALL MOVABS (0,700)
470 CONTINUE
      WRITE (6,480)
480 FORMAT (' DO YOU WANT EXTREMA?')
      READ (5,495) DECIS
495 FORMAT(1X,A2)
      IF (DECIS.EQ.'NO') GOTO 560
      WRITE (6,500)
500 FORMAT (' DEFINE INTERVAL.')
      READ (5,30) XSTR,XSTP
      STLOOK=XSTR-(XSTP-XSTR)*.01
      DO 530 J1=1,NCASE
      SMALL=1.
      BIG=0.
      DO 520 IDUM=1,N
      IF (PLOTX(IDUM).LT.STLOOK.OR.PLOTX(IDUM).GT.XSTP) GOTO 520
      DIF1=SMALL-TRNCAS(J1,IDUM)
      DIF2=TRNCAS(J1,IDUM)-BIG
      IF (DIF1.LE.0.) GOTO 505
      SMALL=TRNCAS(J1,IDUM)
      LAMIN=PLOTX(IDUM)
505 IF (DIF2.LE.0.) GOTO 520
      BIG=TRNCAS(J1,IDUM)
)
```

```
      LAMAX=PLOTX(IDUM)
  520 CONTINUE
      WRITE (6,540)SMALL,LAMIN,BIG,LAMAX,ENSTOR(J1)
  540 FORMAT(//' MIN=',F7.4,' AT',F9.3,5X,' MAX=',F7.4,
     X   ' AT',F9.3,5X,' NO=',E9.4)
      IF (J1.NE.1) GOTO 527
      MINSAV=SMALL
      MAXSAV=BIG
      GOTO 530
  527 CONTINUE
      MINRAT=SMALL/MINSAV
      MAXRAT=BIG/MAXSAV
      WRITE (6,529) MINRAT,MAXRAT
  529 FORMAT(10X,' MIN RATIO=',F7.4,,5X,' MAX RATIO=',F7.4//)
  530 CONTINUE
      GOTO 470
  560 CONTINUE
      CALL ERASE
       CALL FINITT (0,700)
      STOP
      END
```


*U.S. GOVERNMENT PRINTING OFFICE 1981 0-725-404/1113